

DISSERTATION

A NUMERICAL INVESTIGATION OF FLORIDA'S  
SEA BREEZE - CUMULONIMBUS INTERACTIONS

Submitted by

Jenn-Luen Song

Department of Atmospheric Science



COLORADO STATE UNIVERSITY

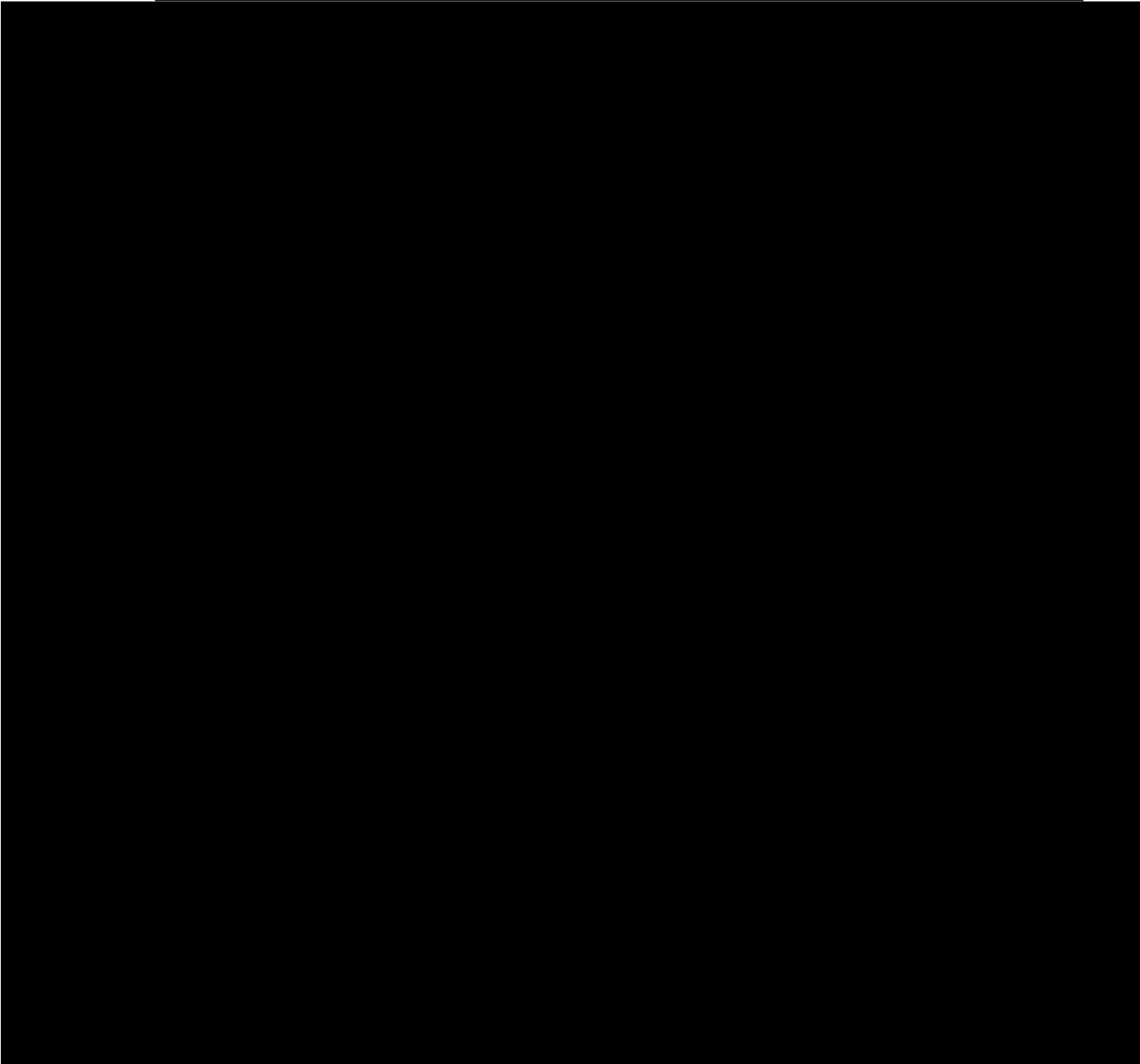
Summer 1986



ABSTRACT OF DISSERTATION  
A NUMERICAL INVESTIGATION OF FLORIDA'S  
SEA BREEZE - CUMULONIMBUS INTERACTIONS

Florida State University

---



provides new favorable environments for initiating deep convection. A "four-cell" vertical circulation pattern is formed as a result of the upper tropospheric divergence, mid-tropospheric convergence and the surface divergence due to the downdraft cooling. Finally, Stage 3 (decaying stage) is associated with only mesoscale weaker upward and downward motions without new deep cumulus convective developments.

The model does not simulate properly the effect of Lake Okeechobee due to the use of 22 km as the horizontal grid spacing. On the other hand, the Florida deep convective-environmental interrelationship described above is

---

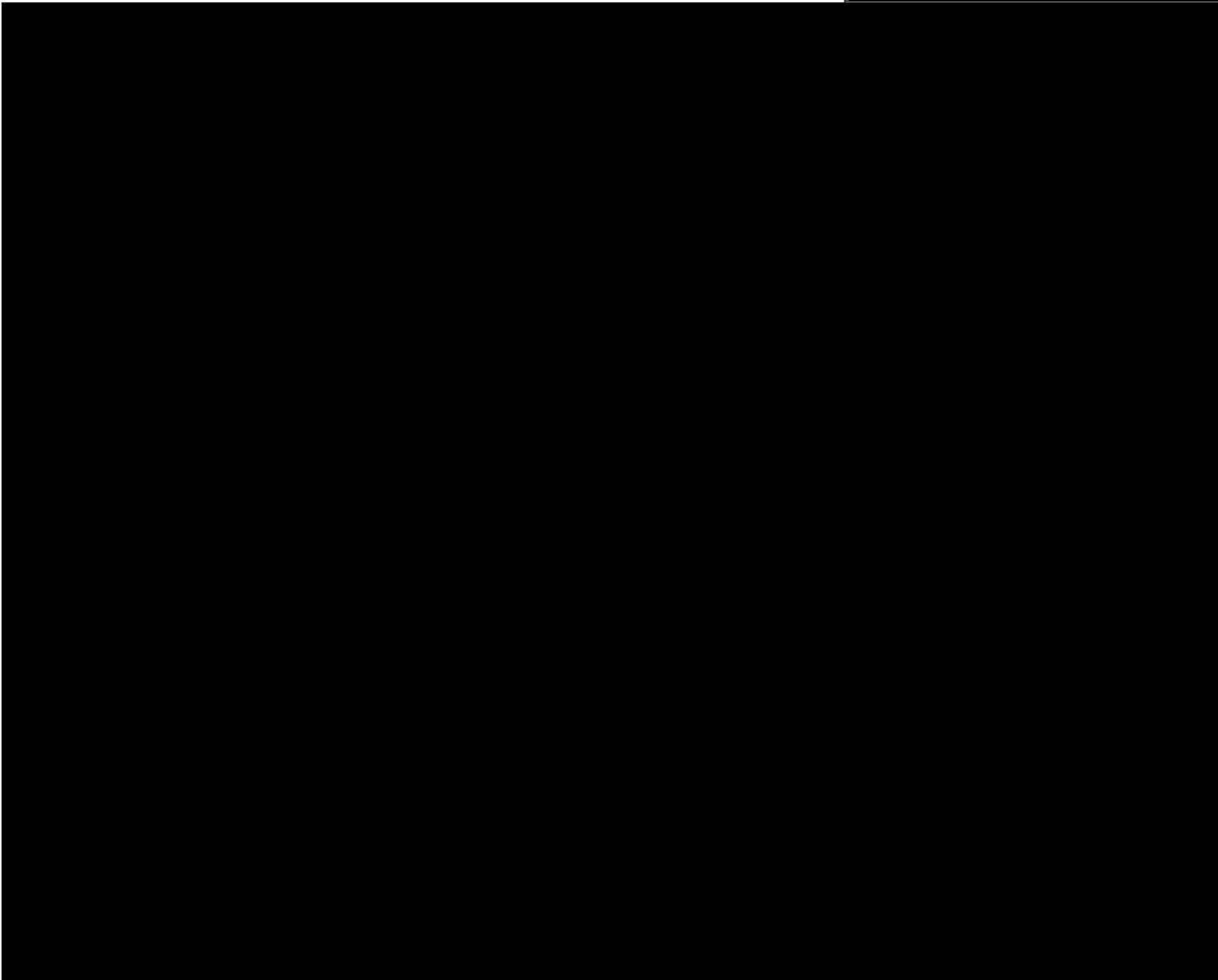
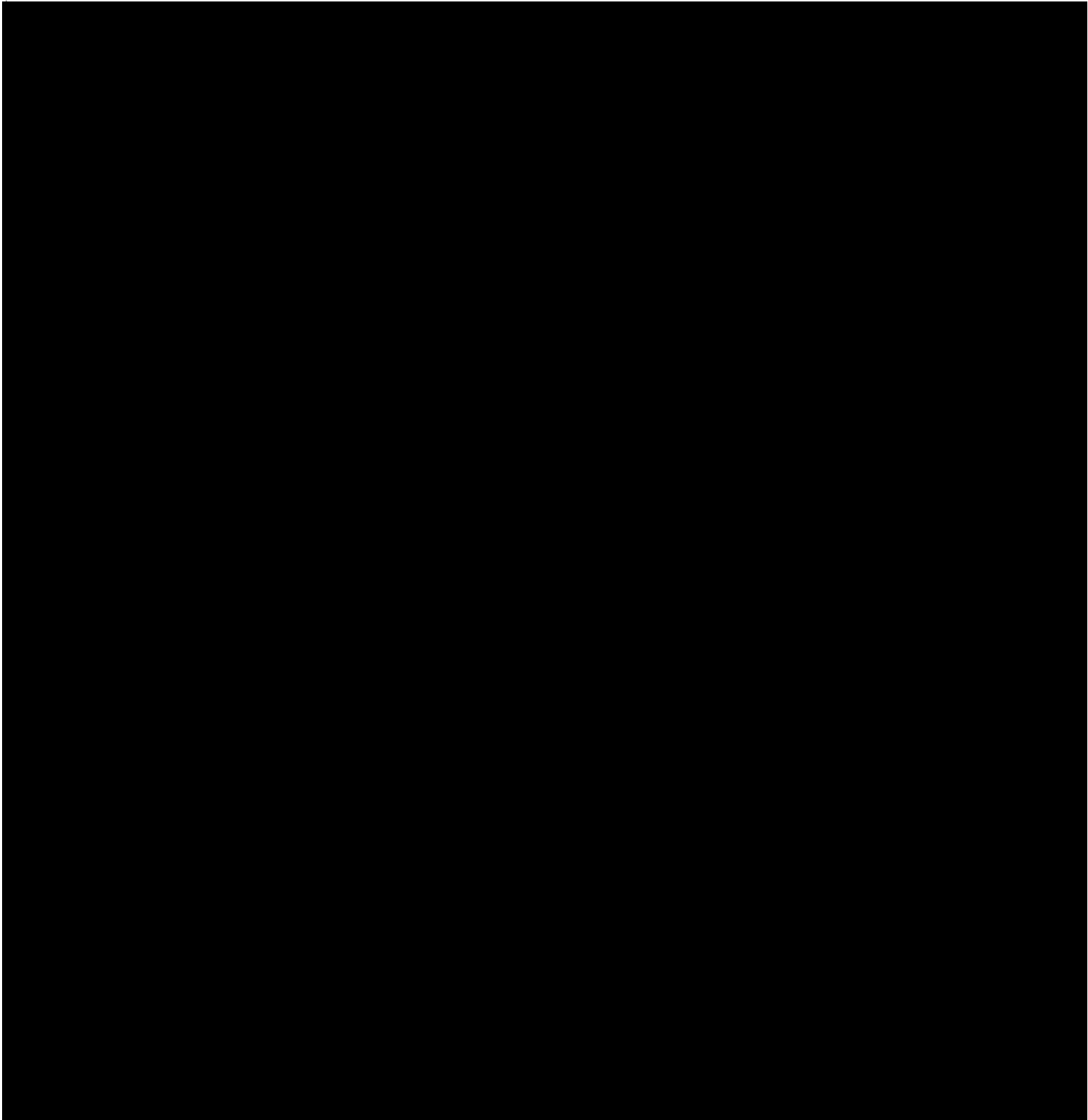
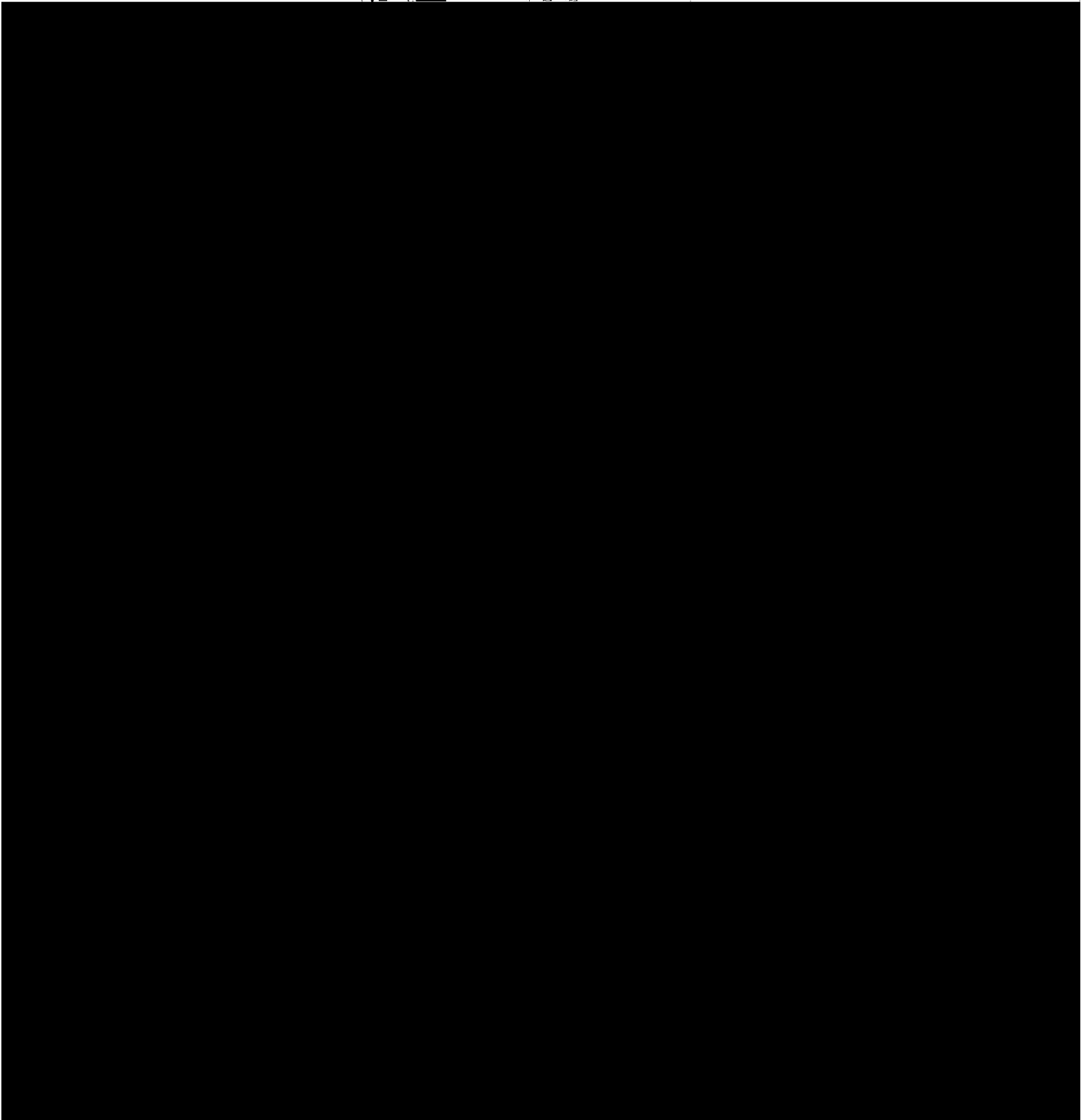


TABLE OF CONTENTS

---



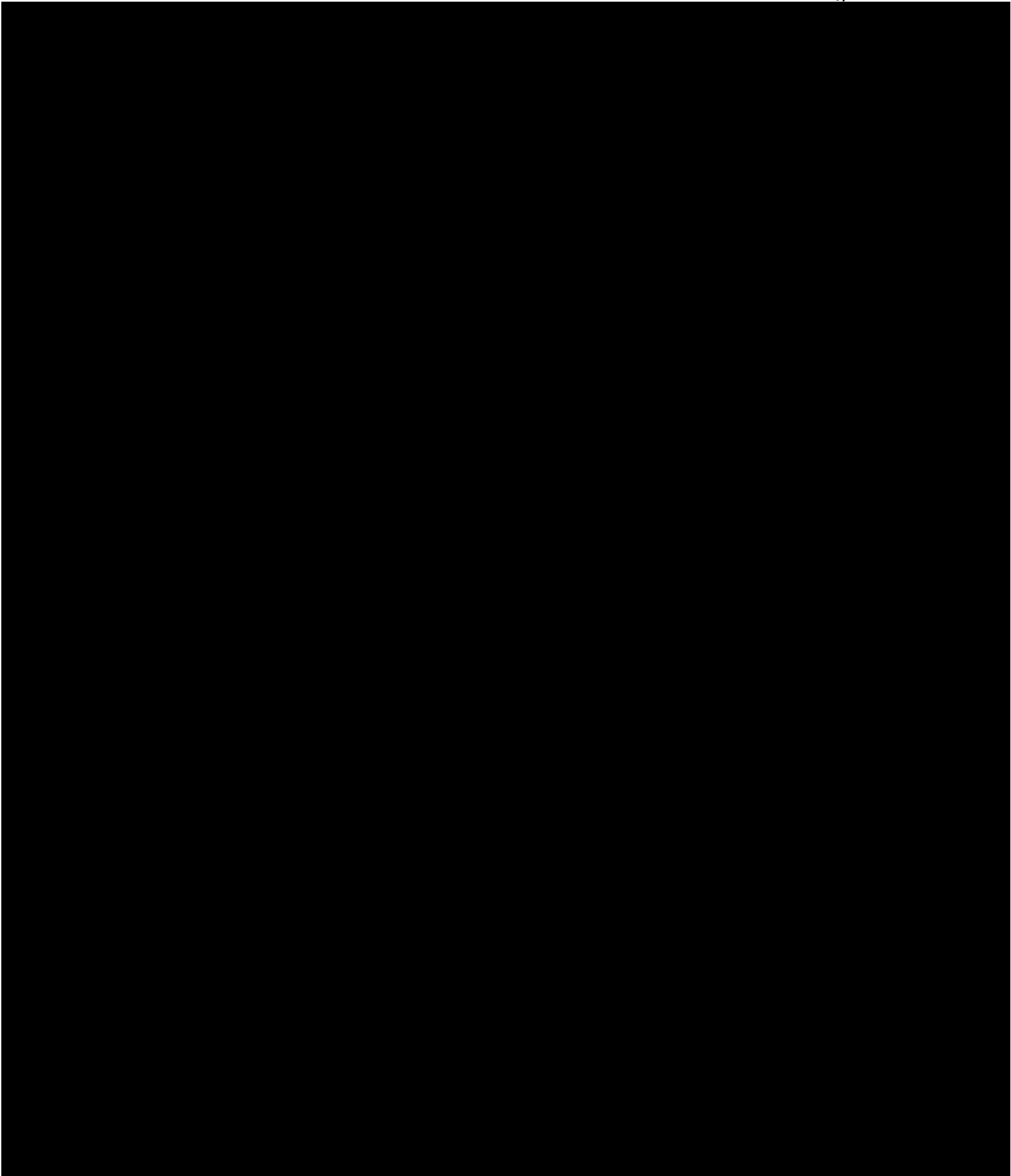
<u>Section</u>	<u>Page</u>
5-2 Weak Southeasterly Experiment . . . . .	119
5-3 Strong Southeasterly Experiment . . . . .	123
5-4 Drier-Sounding Experiment . . . . .	123
5-5 No-Downdraft Experiment . . . . .	126
6 CONCEPTUAL MODEL OF FLORIDA'S SEA BREEZE - CUMULONIMBUS	





LIST OF FIGURES

<u>Figure</u>		<u>Page</u>
3-1	Temporal development of (top) surface perturbation pressures below convective systems I and II (dashed lines) and within the meso network area (solid line); and (bottom) boundary layer mass flux for the cloud areas of systems I and II (dashed lines) and the meso network area (solid line). The mesoscale pressure perturbation is the averaged perturbation over an area of 35 km x 50 km. A constant pressure gradient of $-0.2 \text{ mb } 35 \text{ km}^{-1}$ in the absence of friction would result in a horizontal wind acceleration of $2.5 \text{ ms}^{-1}/\text{hour}$ . . . . .	26
3-2	A schematic illustration of the convective parameterization used for the moist sea breeze simulations . . . . .	29
3-3	The calculated CAPE (convective available potential	

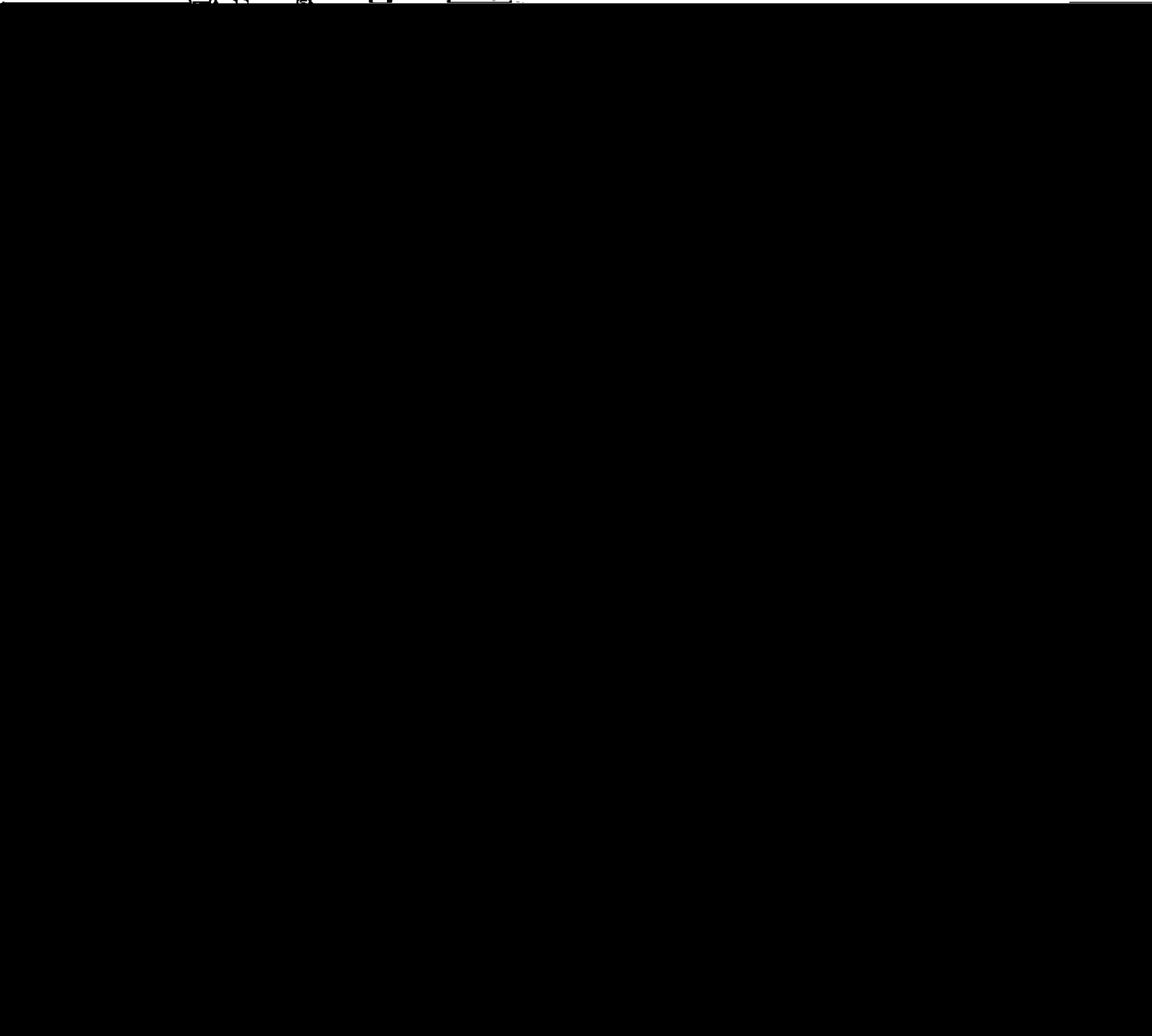


Figure

Page

4-2-9	The model produced horizontal maps of vertical velocity (cm/s) near 10 km (top) and 1 km (middle); and the model rainfall rate (mm/10 hour) (bottom), at 3 PM. The symbol "H" indicate upward motions, while "L" indicate downward motions. The contour interval for the velocities is 3 cm/s, and for the rainfall rates 2.2 mm/hour . . . . .	73
4-2-10	Surface radar rainfall map at 1500 EST over the southern Florida of July 17, 1973. Also included are the surface wind vectors (from Pielke and Cotton, 1977) . . . . .	74

4-2-11

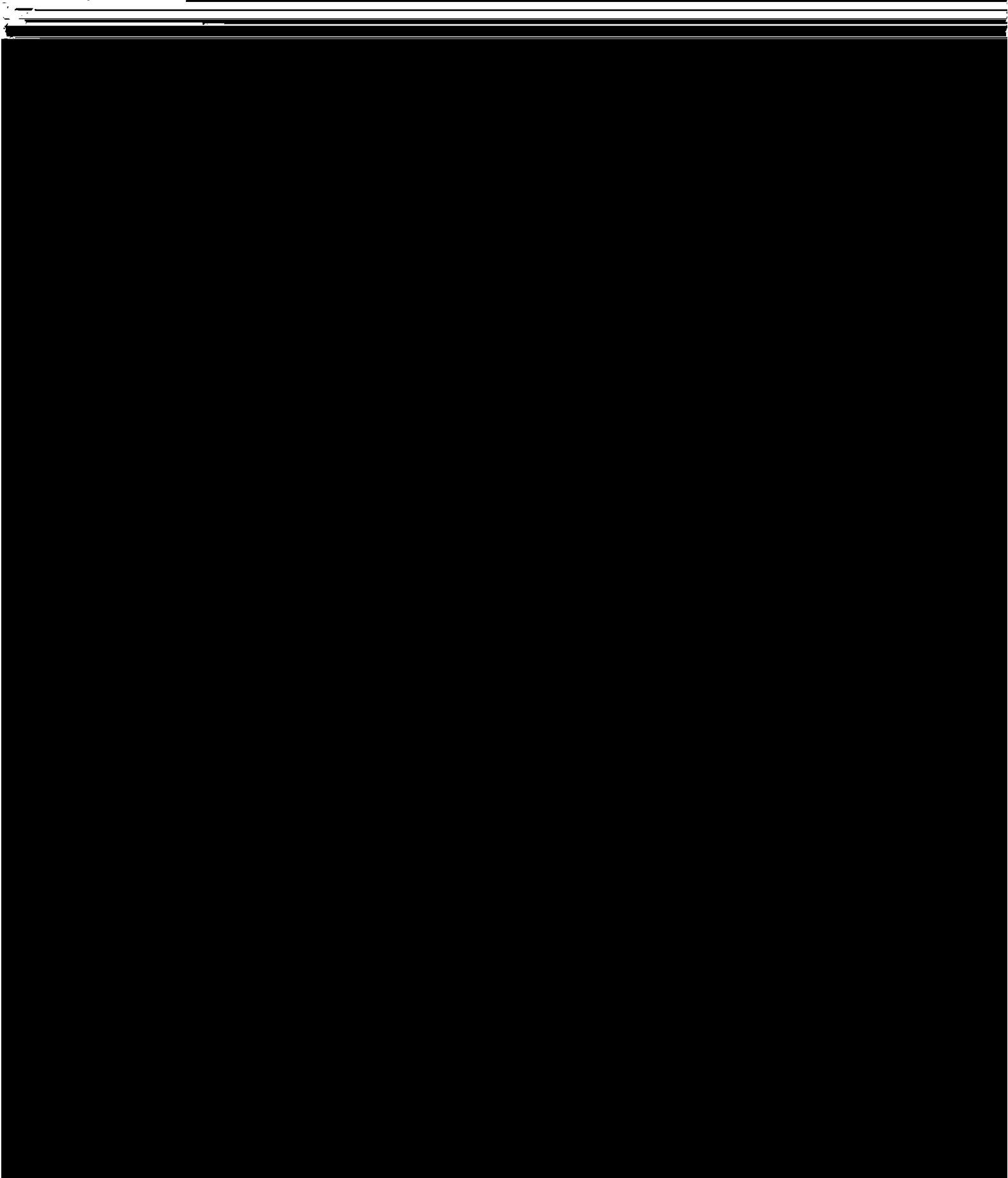


Figure

Page

4-3-2 The "total-dry" quantities at 9 m at 1 PM, including  
(a) potential temperature (note magnitudes are scaled



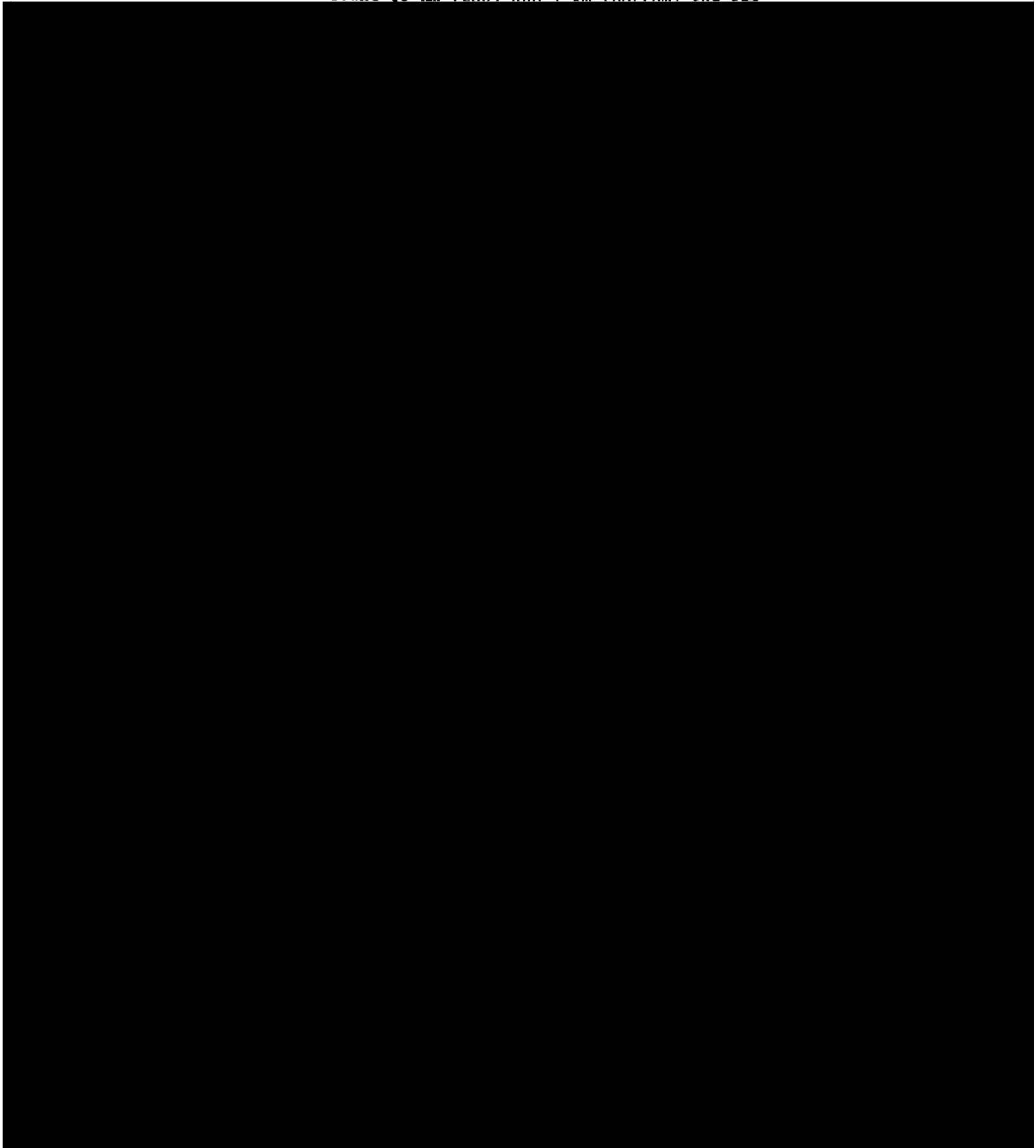


Figure

Page

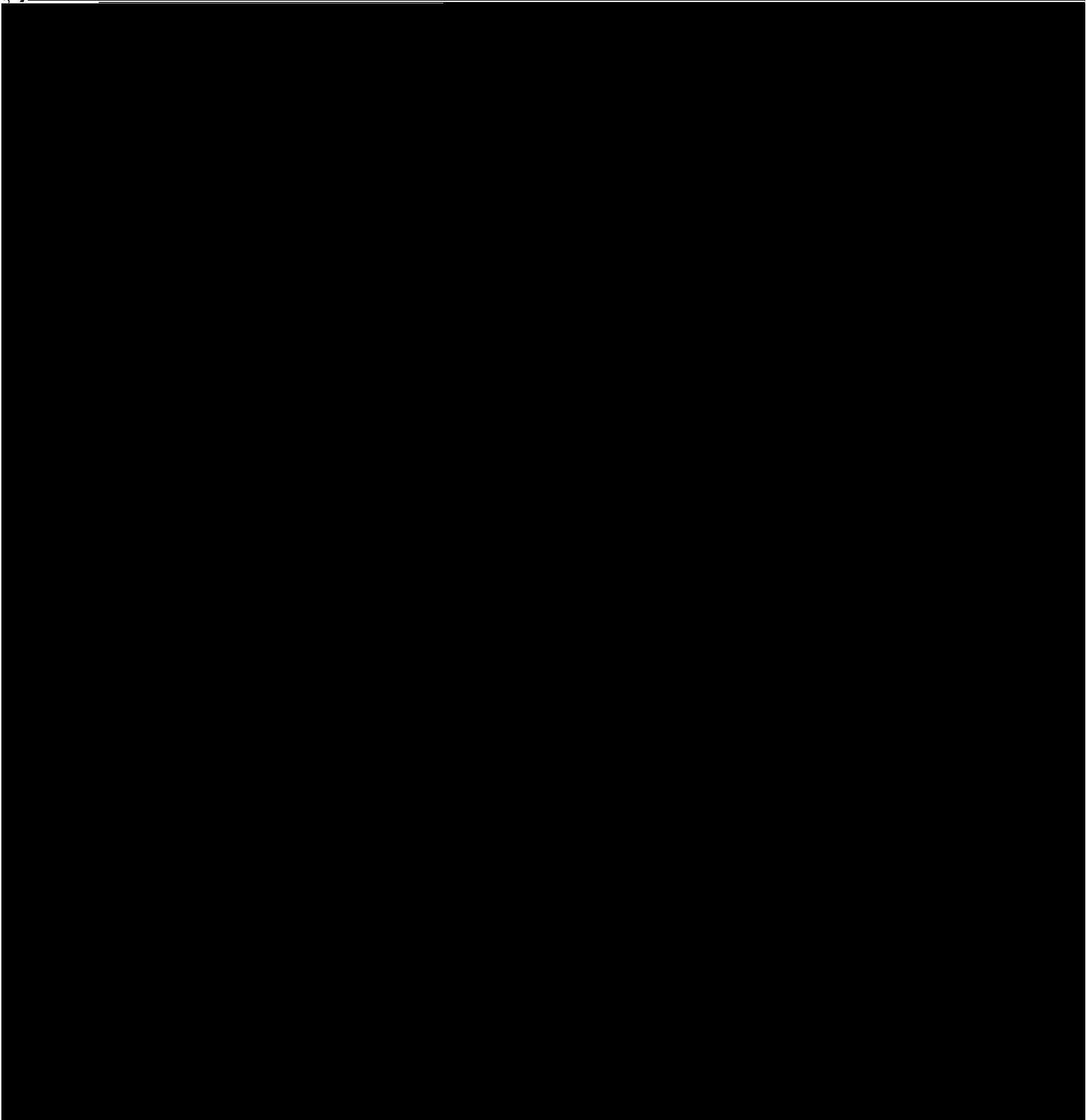
5-1

The model produced vertical velocities (cm/s) at  
4 PM around 10 km (top) and 1 km (bottom) for the



<u>Figure</u>		<u>Page</u>
6-1	The time averaged horizontal divergence ( $10^{-4} \text{ s}^{-1}$ ) on the XZ-cross section for the Stage-1 (over the time period of 1200-1400 EST) . . . . .	135
6-2	The time averaged moisture flux term (vertical	

---



<u>Figure</u>	<u>Page</u>
6-13	The time averaged vertical velocity (cm/s) on the XZ-cross section for the Stage-3 (over the time period of 1200-1400 EST) . . . . . 151
6-14	A conceptual model for the Stage-3's sea breeze-deep convective interactions over the southern Florida peninsula during synoptically undisturbed days . . . . 152
6-15	Vertical profiles of the horizontally-integrated kinetic energy budget components (watt/m <sup>2</sup> /km) at 3 PM for the dry sea breeze run (left) and the moist sea breeze run (right). The different curves are explained in the figure . . . . . 153
6-16	The horizontal pressure gradient term in the kinetic energy budget equation on the XZ-cross section for the three stages of the dry sea breeze simulation . . . 156
6-17	The horizontal pressure gradient term in the kinetic energy budget equation on the XZ-cross section for the three stages of the moist sea breeze simulation . . 157

## Chapter 1

### INTRODUCTION

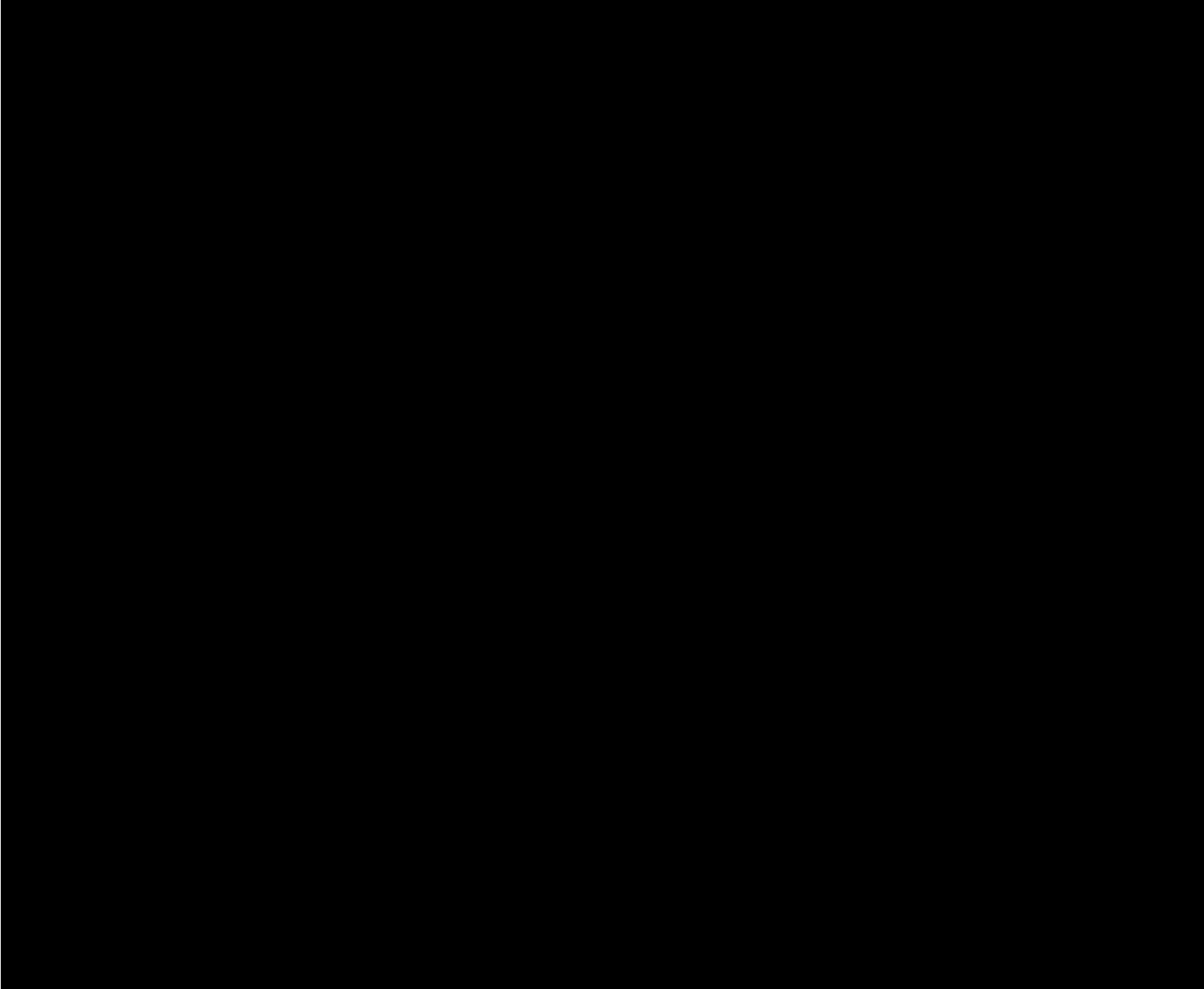
---

---

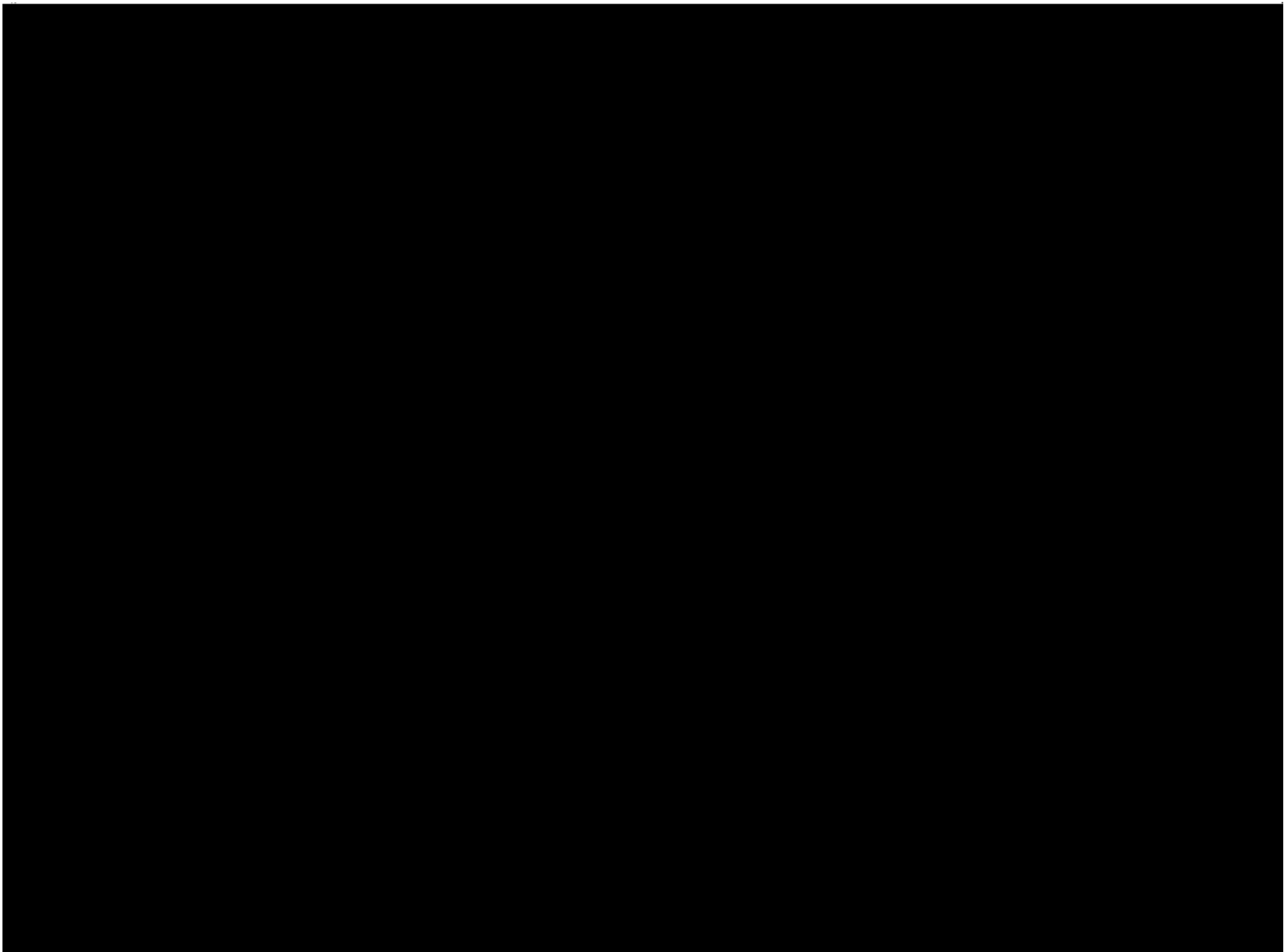


as suggested by them, is due primarily to the effect associated with downdraft outflow (or, the surface micro-cold front produced by the thunderstorm downdraft).

An important advantage provided by the summer Florida peninsula for investigating convective-environmental interaction is that there is a typically well established mesoscale sea breeze circulation during the undisturbed days. Numerous studies have indicated that the Florida deep convective activities are significantly modulated by the diurnally-varying sea breeze circulation (Pielke, 1974; Atkinson, 1980; among others). For example, Frank, Moore and Fisher (1967) showed that



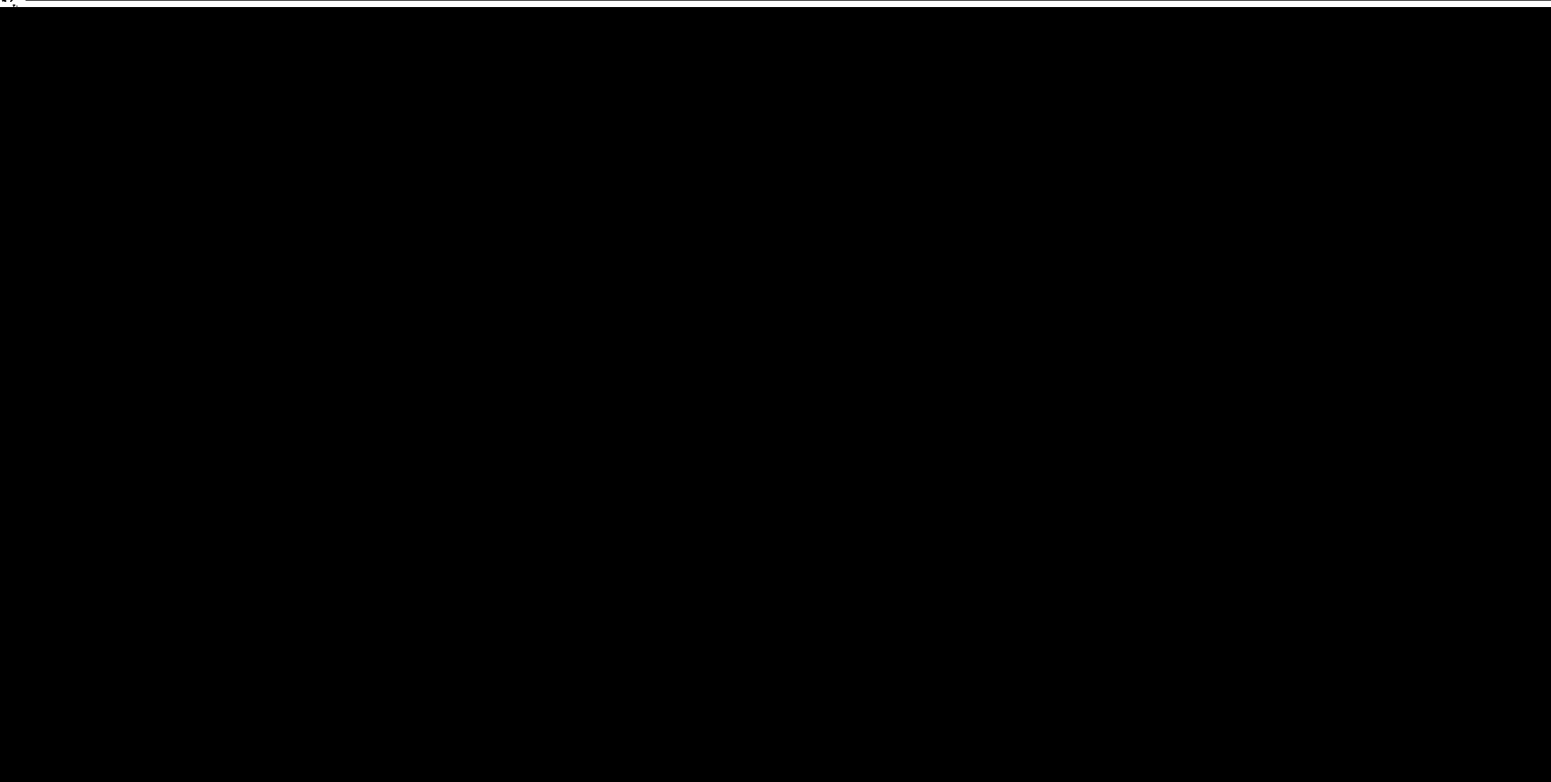
mechanisms, through which Florida convection initiates, enhances and maintains itself, have been revealed/confirmed by these studies. For example, Simpson et al. (1980) stated that one of the most important mechanisms for Florida deep convection to grow is through the surface convergence associated with storm-generated outflow at surface. The new cell growth induced by such surface convergence (or, the "bridging" between two old cells due to the outflow) was regarded by them as storm merging. This merging process has been considered as the fundamental mechanism that the Florida mesoscale convective systems (or clusters) can be formed. Ulanski and Garstang (1978) observed that a mesoscale surface convergence typically precedes a storm development (by an amount of time of about one hour).



The Florida deep convective development is also dependent on other physical factors or mechanisms, such as the surface pressure gradient in the immediate storm environment (Cunning and DeMaria, 1986); surface response due to anvil cover (Pielke and Cotton, 1977); surface properties (Gannon, 1978); etc.

Recently, Van De Berg and Oerlemans (1985) simulated the dependence of sea breeze front propagation upon non-precipitating cloud formation, using a non-hydrostatic 2-D model. They hypothesized that the coupling of the convective heating over land and the evaporative cooling over sea produces an additional horizontal thermal gradient, thereby enhancing the intensity and inland propagation of the sea breeze front. In a similar sea breeze front simulation performed by Gross (1985), however, the above described cloud effect was not found. Rather, cloud formation appeared to affect only the intensity of sea breeze circulation and not the sea breeze front propagation. Briere (1986) studied the 2-D energetics of dry sea breeze circulations using a third-order turbulence closure model. This study differs from the

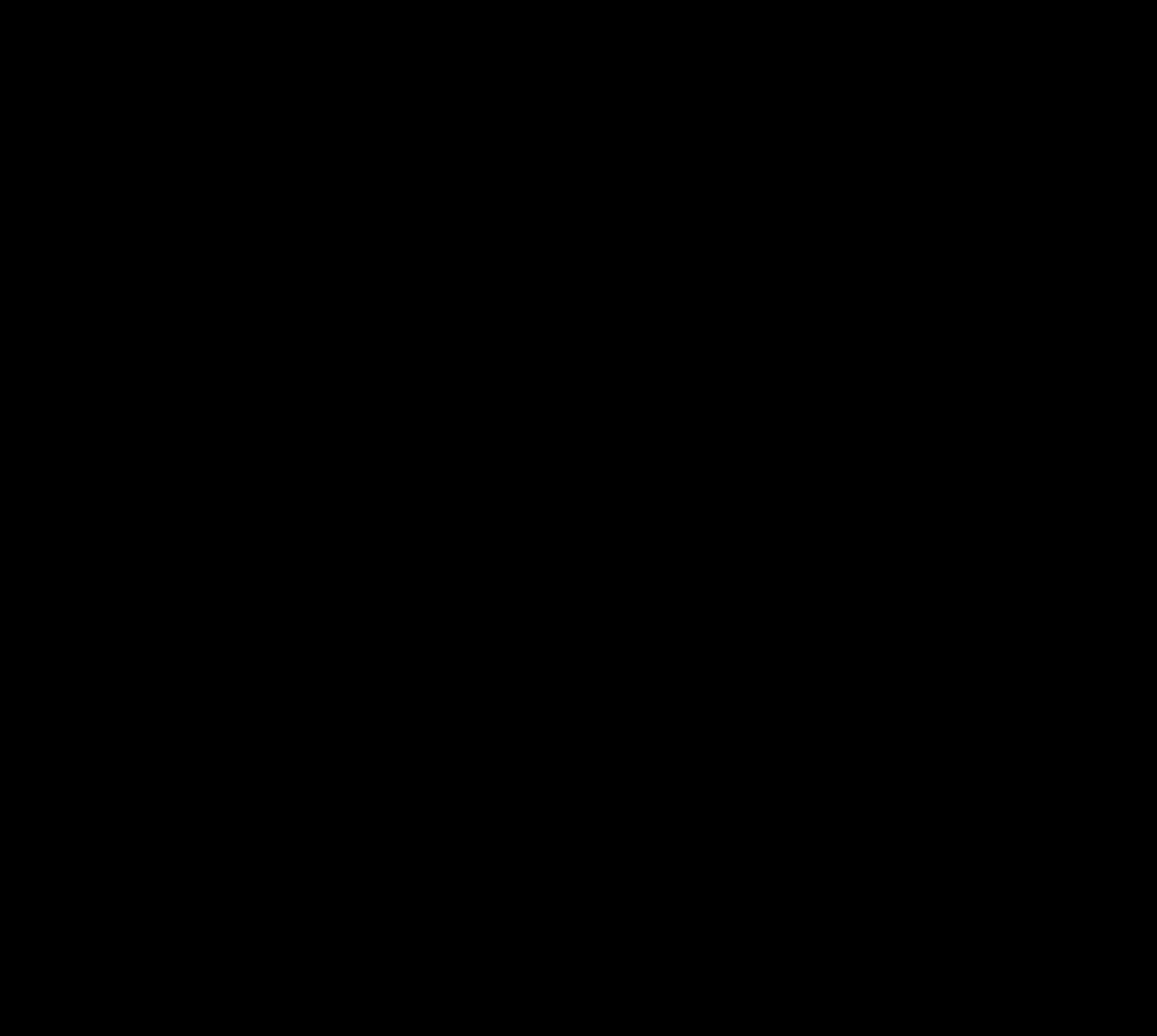
---



appear to be closely related to both the sea breeze circulation and the convective-generated downdraft. The majority of the organized convection is found to be produced by the merging process, which is associated with the diurnally-varying sea breeze convergence zone and the locally enhanced downdraft effect on surface.

1-2. Motivation of the Study

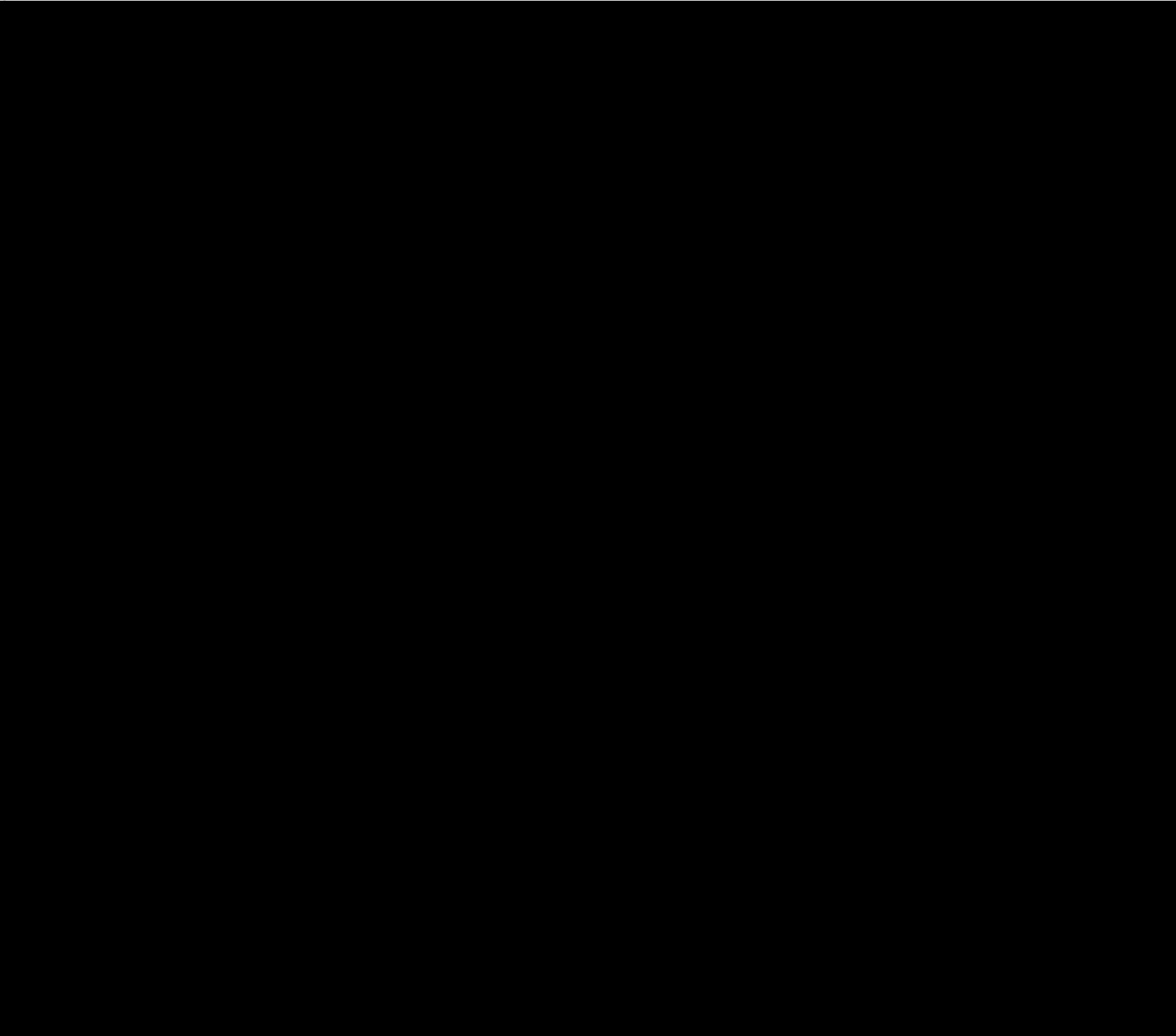
Although the aforementioned investigations on Florida convection have revealed some of the most important mechanisms concerning the deep



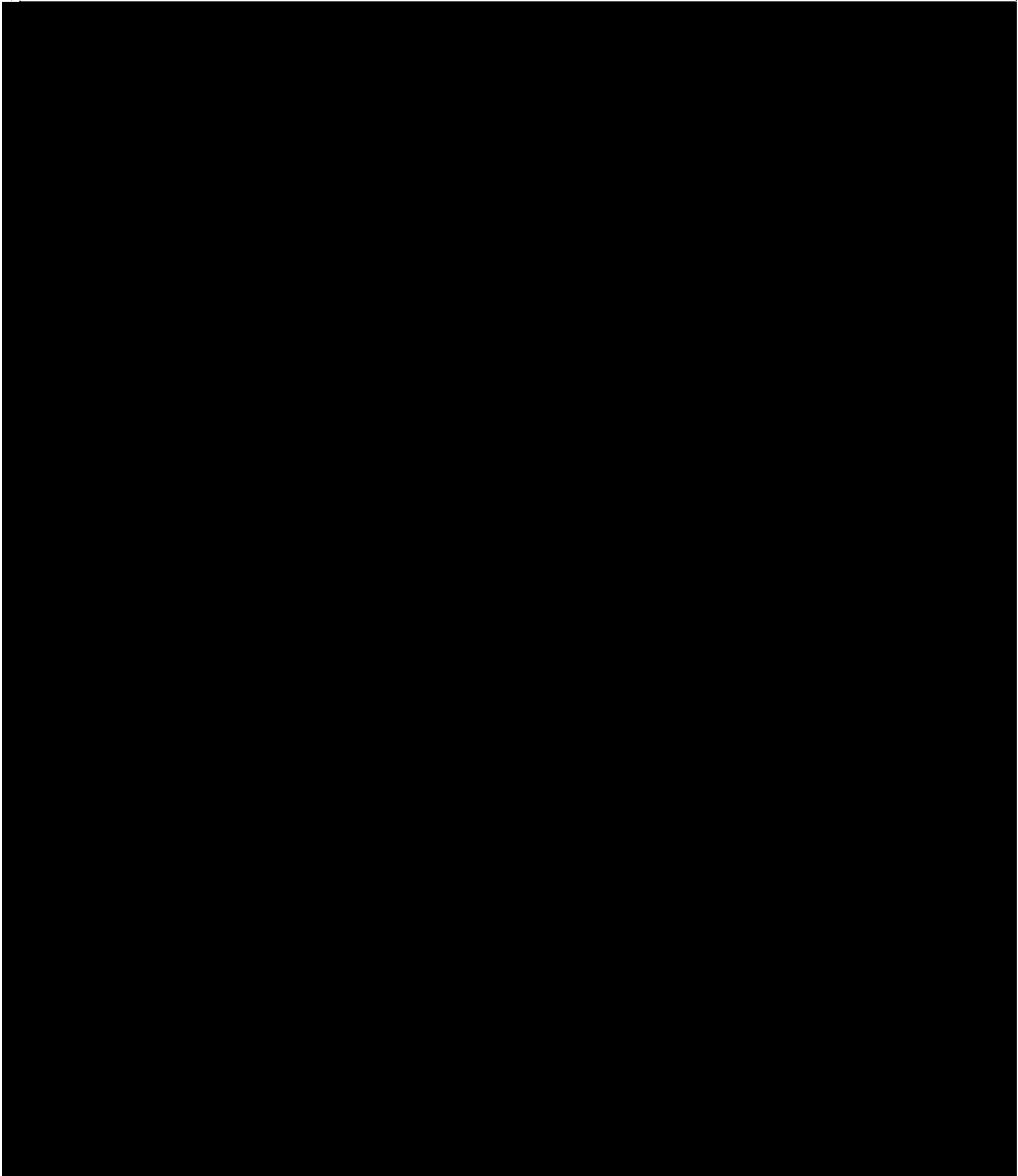
least cover spatial scales of about 300 km x 300 km and time scale about 10 hours. Such domain sizes are currently impossible to be considered for the explicit convective simulations (such as that performed by Tripoli and Cotton, 1980).

To circumvent the difficulty associated with computational resource limitations, it is felt in this study that a cumulus parameterization approach must be utilized. That is, it is felt that the

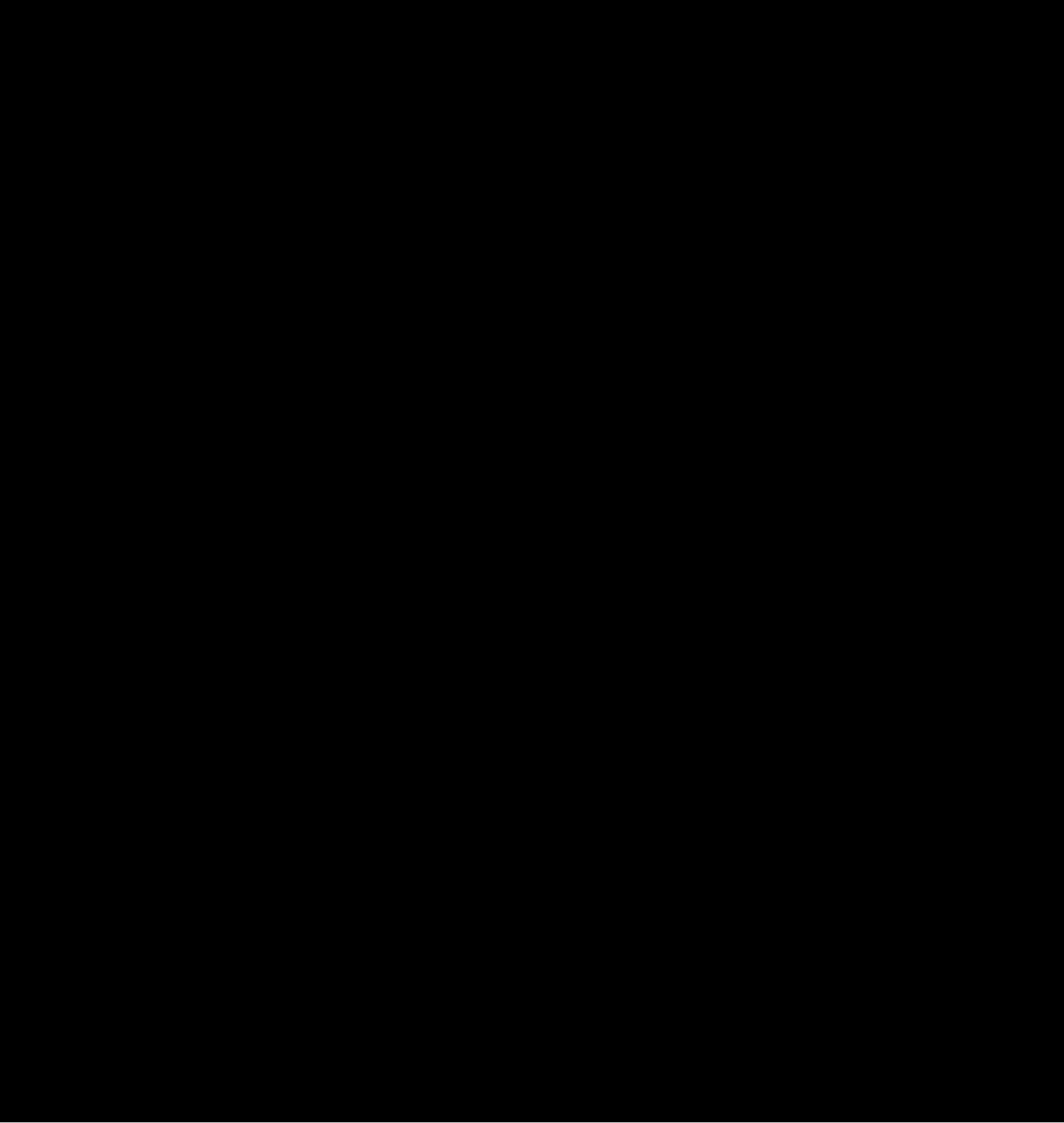
---



(3) How does the sea breeze-convective interrelationship develop?



information: available observation (such as that documented in Pielke and Cotton, 1977); previous parameterization logic (such as that documented in Fritsch and Chappell, 1980, and Frank and Cohen, 1984); and some diagnostic information from a cloud-scale explicit simulation



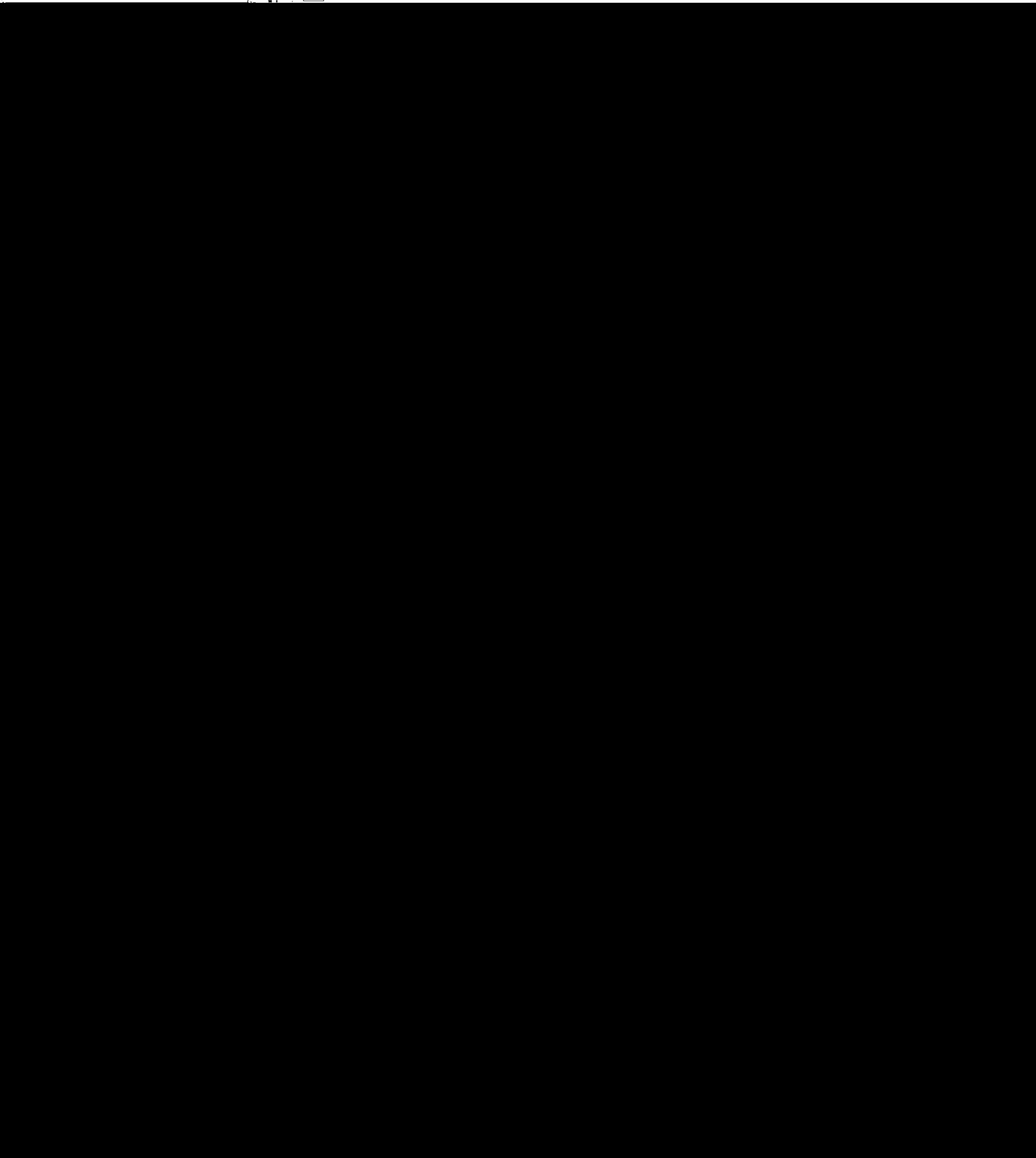
## Chapter 2

### MODEL EQUATIONS

In this chapter, the prognostic mesoscale model (into which the deep convective effects will be incorporated) will be briefly described. The computations of the model contains two main parts,

three-dimensional hydrostatic primitive equation model originally developed by Pielke (1974) in order to study the sea breezes over south.

---



"parameterization" to simulate the effects. Using 22 km, the relative contribution from subgrid-scale processes can be more realistically isolated from the total quantities, as compared with using 11 km. In the following, the governing equations will be illustrated:

2-1-a. Governing Equations

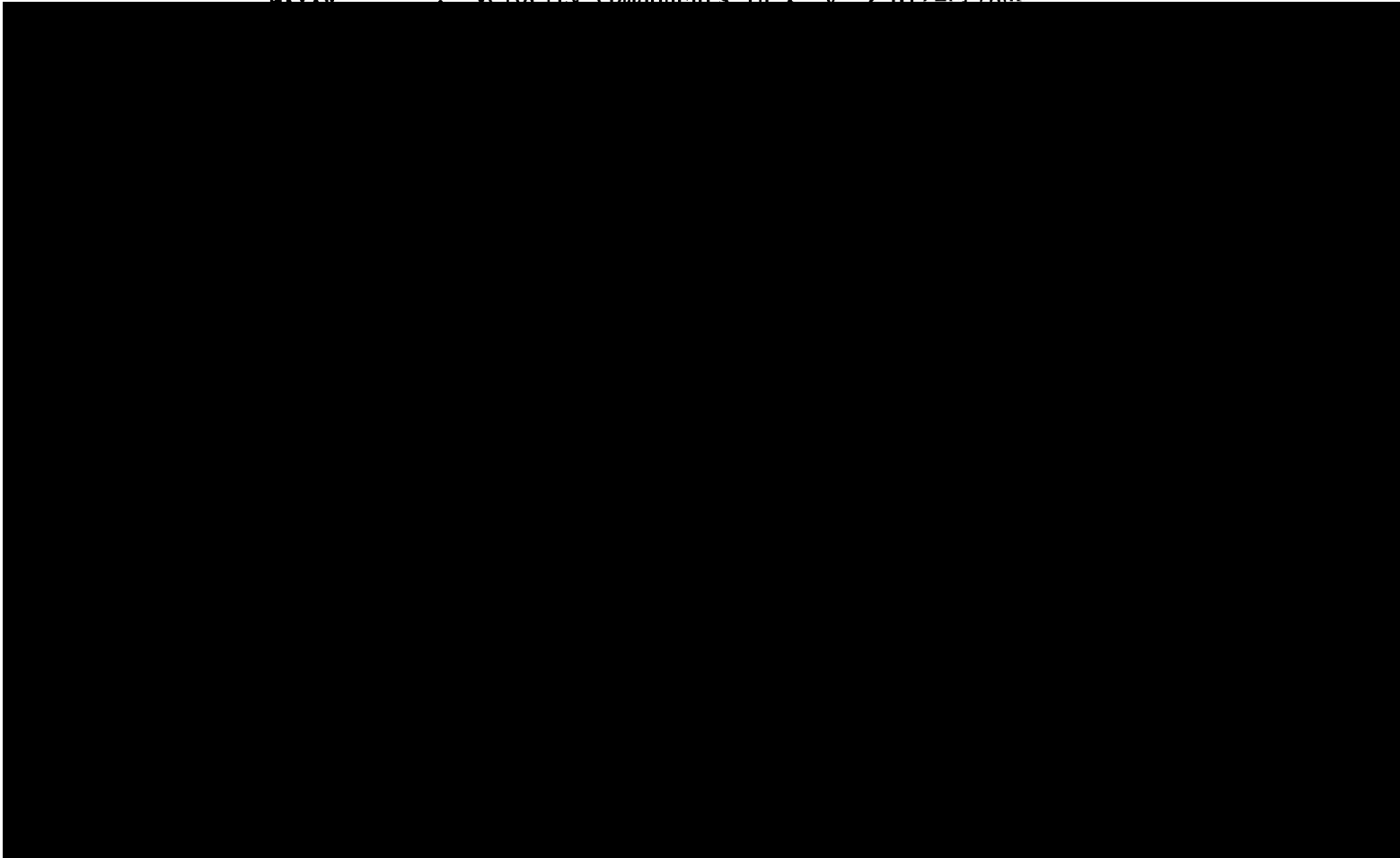
- Horizontal momentum equations

$$\begin{aligned} \frac{\partial u}{\partial t} = & -u \frac{\partial u}{\partial x} - v \frac{\partial u}{\partial y} - w \frac{\partial u}{\partial z} + f v - f v_g - \hat{f} w - \theta \frac{\partial \pi}{\partial x} + \frac{\partial}{\partial z} \left( K_z^m \frac{\partial u}{\partial z} \right) \\ & + \left. \frac{\delta u}{\delta t} \right|_{CU} + H^u \end{aligned} \quad (1)$$

$$\begin{aligned} \frac{\partial v}{\partial t} = & -u \frac{\partial v}{\partial x} - v \frac{\partial v}{\partial y} - w \frac{\partial v}{\partial z} - f u + f u_g - \theta \frac{\partial \pi}{\partial y} + \frac{\partial}{\partial z} \left( K_z^m \frac{\partial v}{\partial z} \right) \\ & + \left. \frac{\delta v}{\delta t} \right|_{CU} + H^v \end{aligned} \quad (2)$$

where

$u, v, w$  : velocity components in  $x, y, z$  directions



$\frac{\delta\theta}{\delta t}\Big|_{CU}$  : deep convective feedbacks.

$H^\theta$  : the horizontal filter effect.

- Moisture Conservation Equation

$$\frac{\partial q}{\partial t} = -u \frac{\partial q}{\partial x} - v \frac{\partial q}{\partial y} - w \frac{\partial q}{\partial z} + \frac{\partial}{\partial z} \left( \kappa_z^q \frac{\partial q}{\partial z} \right) + \frac{\delta q}{\delta t}\Big|_{CU} + H^q \quad (4)$$

Therefore, vertical velocity at each level is calculated as:

$$w_j = \frac{\rho_{oj-1}}{\rho_{oj}} w_{j-1} + \frac{\hat{\rho}_{oj}}{\rho_{oj}} (-\nabla \cdot \mathbf{v})_j \cdot \Delta z_j \quad (6b)$$

where "j" is the index of the model vertical levels. Other parameters and variables defined as:

$$\Delta z_j = z_j - z_{j-1}$$

$$\hat{\rho}_{oj} = \frac{1}{2}(\rho_{oj} + \rho_{oj-1});$$

$$\rho_o \text{ is diagnosed from: } \rho_o = \frac{P_{oo}}{R} \left( \frac{\pi_o}{C_p} \right)^{\frac{C_p}{R} - 1} \cdot \frac{1}{\theta_o} \quad (6c)$$

$P_{oo}$  : reference pressure

$\pi_o, \theta_o$  : the environmental scaled-pressure (to be defined below) and potential temperature,  $\pi_o = \pi_o(z)$ ,  $\theta_o = \theta_o(z)$ .

$R$  : gas constant for dry air

$C_p$  : specific heat a constant pressure

Vertical velocity is defined as:

- Diagnostic Hydrostatic Pressure Equation

$$\pi_{\text{top}}^{\tau} = \pi_{\text{top}}^{\tau-1} - \Delta S \frac{g}{\theta_{\text{top}}} \quad (8a)$$

$$\pi_j = \pi_{j+1} + g \cdot \int_j^{j+1} \frac{1}{\theta} dz \quad (8b)$$

- where  $\pi_{\text{top}}, \theta_{\text{top}}$  : scaled-pressure (defined below) and potential temperature at the top (i.e., the material surface)
- $\tau, \tau-1$  : index of model time step
- $g$  : acceleration of gravity
- $\pi \equiv C_p \left( \frac{P}{P_{\text{oo}}} \right)^{R/C_p}$  (9)
- $P$  : pressure

#### 2-1-b. Dry PBL Diabatic Processes

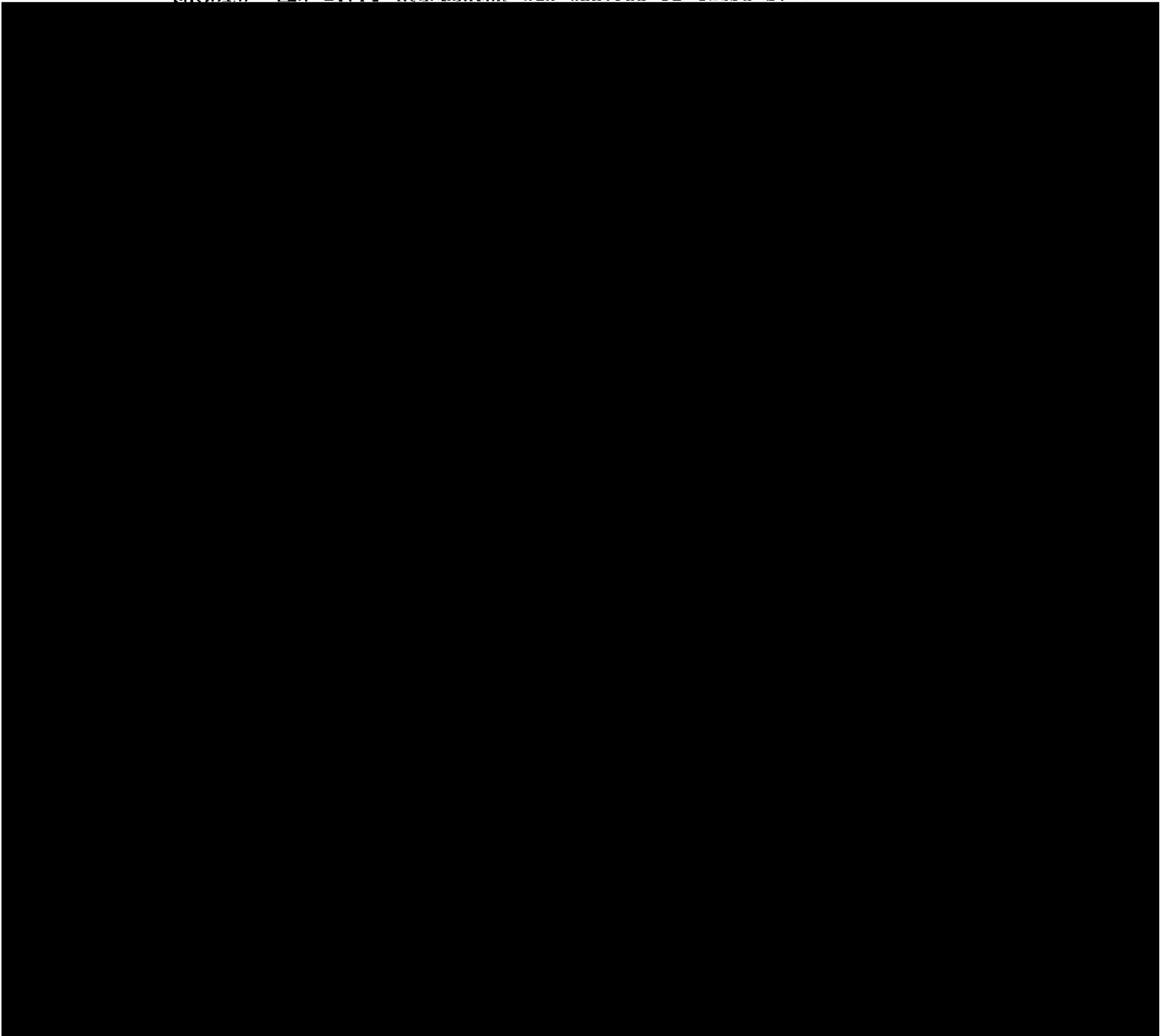
The dry surface layer fluxes of heat, moisture and momentum are based on the work of Businger (1973), while the dry turbulent mixing in the remainder of the planetary boundary layer was parameterized for an unstable surface layer using an exchange coefficient formulation as described by O'Brien (1970). The depth of the dry planetary boundary layer for this case of upward heat flux is predicted utilizing a formulation introduced by Deardorff (1974). When deep convection is produced, the PBL height calculated from this formulation is modified



longer than  $4\Delta x$  are essentially unchanged. In this study, a constant coefficient of 0.02 is used except in the absorbing layer (described in Subsection 2-1-d) of the model in the lower stratosphere when the deep convection is permitted.

2-1-d. Boundary Condition

At the lateral boundaries, a zero-gradient condition (Pielke and Mahrer, 1978) is used. When deep convective effects are incorporated, two extra procedures are applied in order to



typically deep clouds expand horizontally to larger areas (anvil cloud). Therefore, the cloud-scale pressure gradients produced by convective heating are not expected to be significant in this lower stratospheric layer.

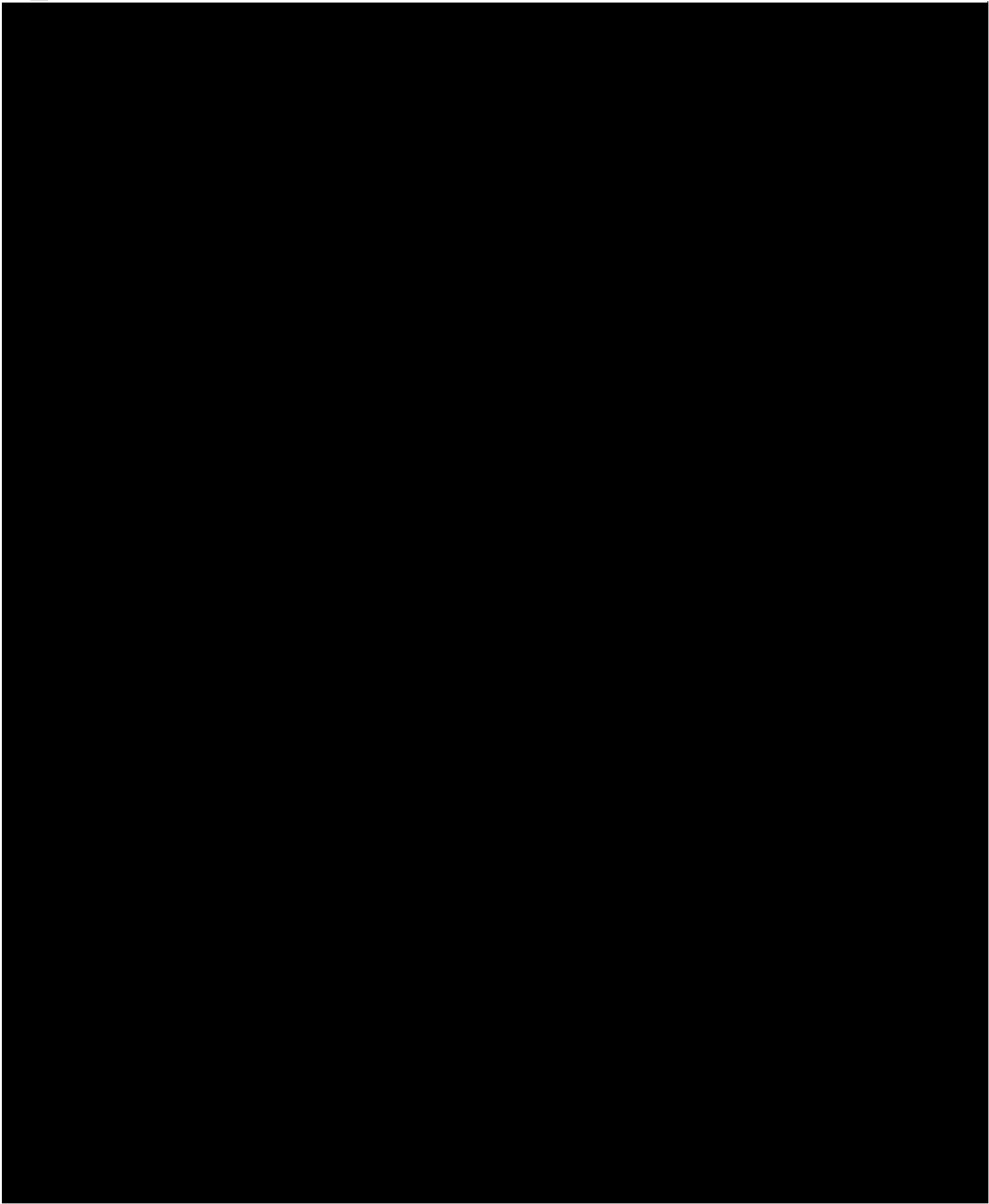
#### 2-2. Kinetic Energy Budget Equation

Following Ward and Smith (1976), Vincent and Schlatter (1979),

Further, ...

---

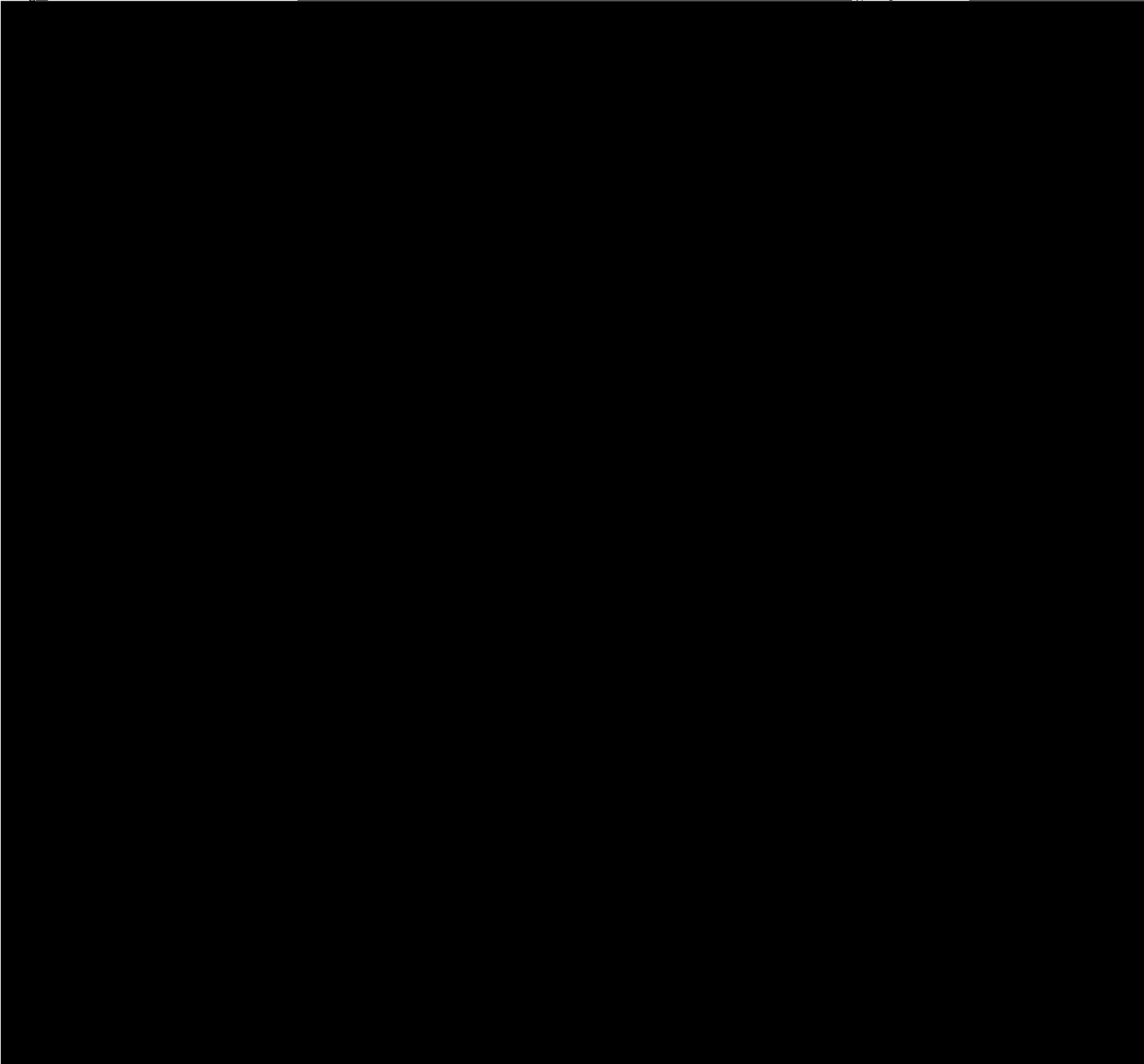




- Turbulence term = Term (d)

This term is explicitly written as:  $\rho_0 u \frac{\partial}{\partial z} (K_z^m \frac{\partial u}{\partial z})$   
 $+ \rho_0 v \frac{\partial}{\partial z} (K_z^m \frac{\partial v}{\partial z})$ .

It represents the friction effect upon the model kinetic energy. Since the eddy exchange coefficients of momentum essentially become negligible above PBL in the absence of deep cumulus convection, the



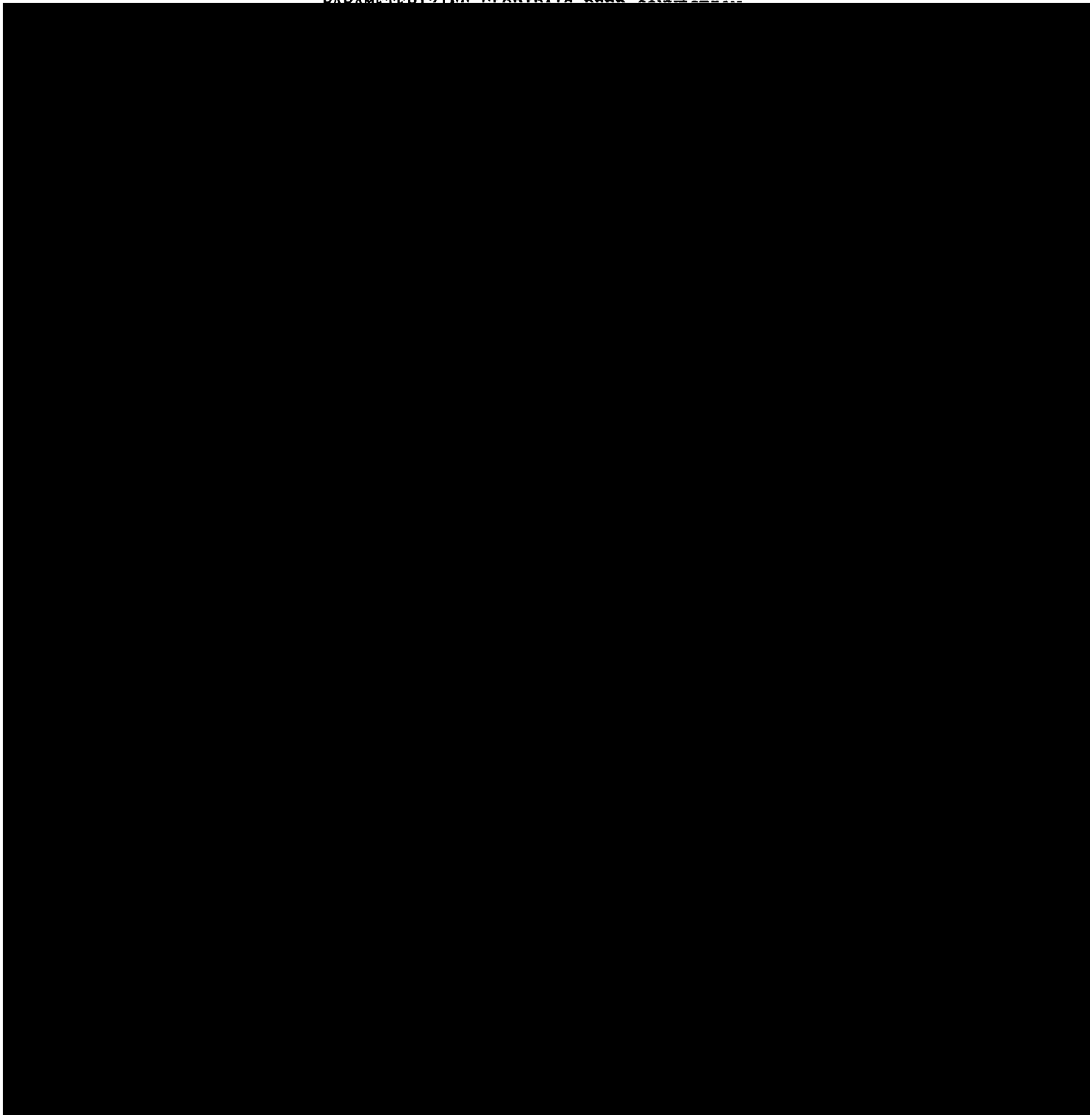
$$+ \frac{1}{L_x L_y} \int_x \int_y \int_z (\text{TUR}) \, dx dy dz$$

$$+ \frac{1}{L_x L_y} \int_x \int_y \int_z (\text{CON}) \, dx dy dz$$

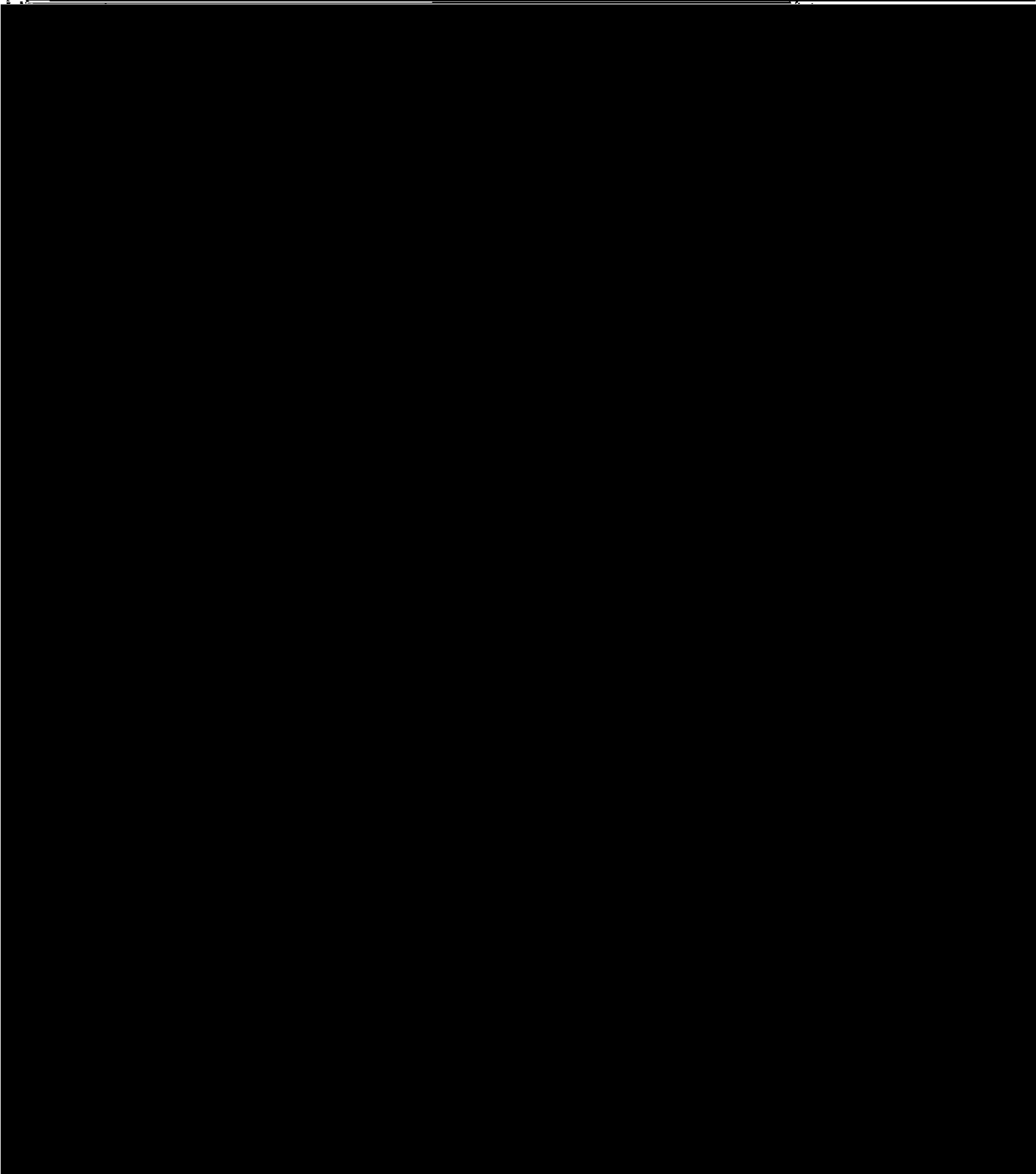
$$+ \frac{1}{V} \int \int \rho k \frac{\Delta S}{\Delta t} \, dx dv \quad (11)$$

## Chapter 3

### PARAMETERIZING FLORIDA'S BEER CONSUMPTION



(2) It develops deep connections to

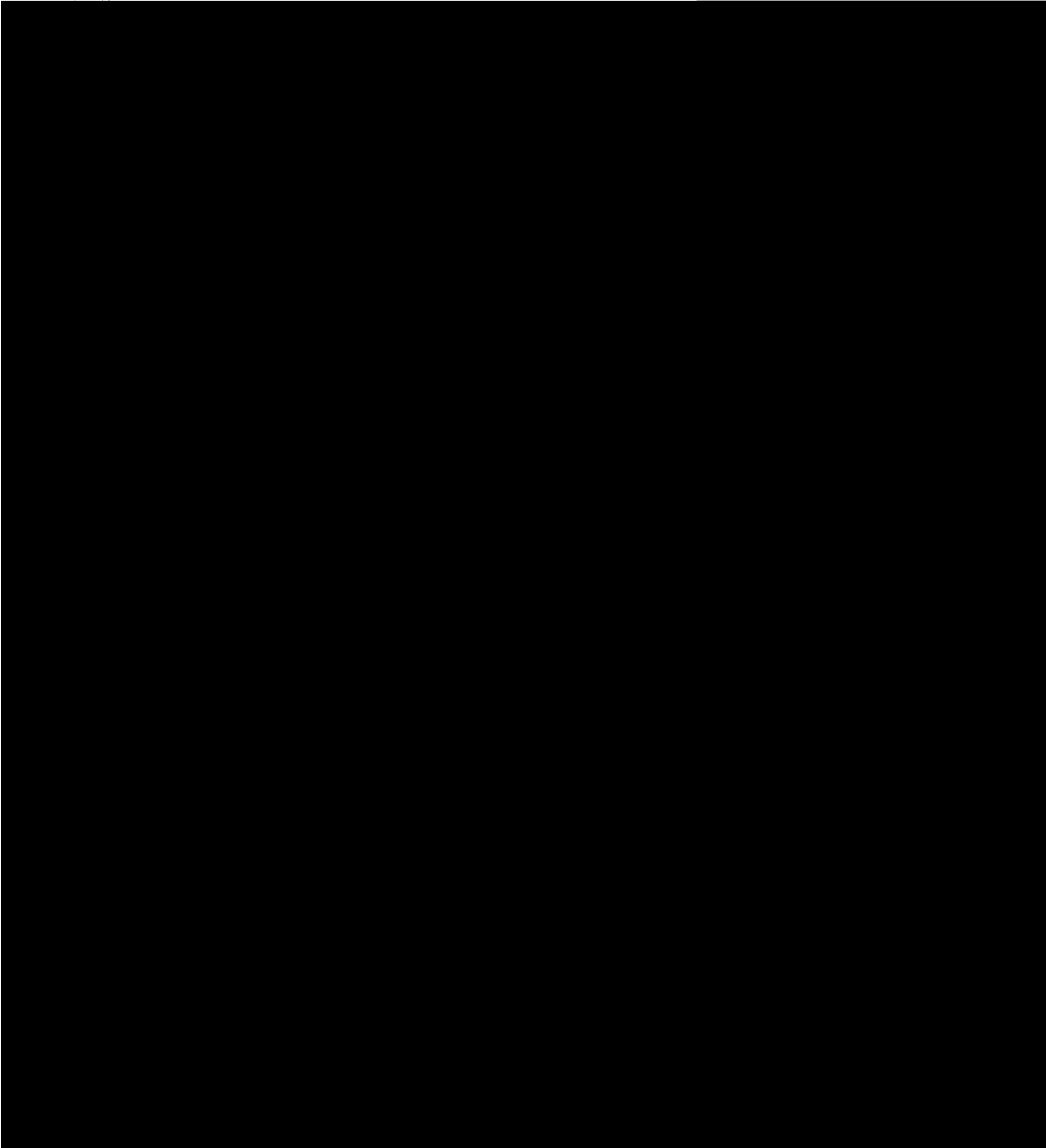


30 min to 1 hour (that is, convection must be such that it



The task of a convective parameterization can be separated into two parts: (A) the calculation of convective intensity and (B) the

---

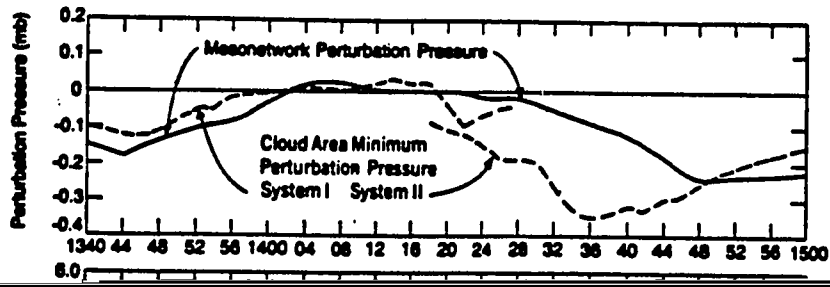


(note, the interaction is "two-way" that is every 20 min the

---

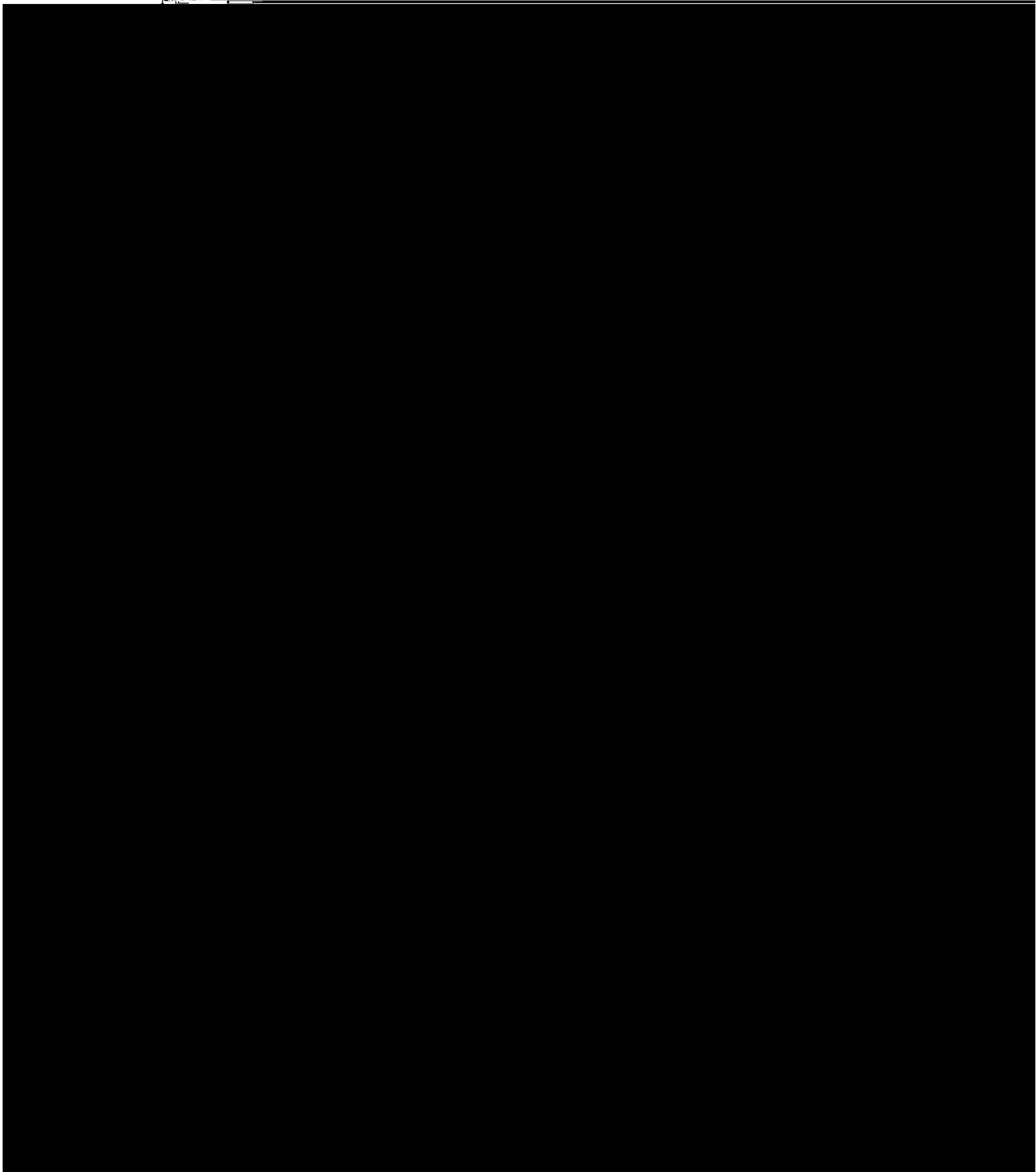
---





numerical techniques (such as model resolution, etc.). Cumulonimbus

generated by the model.

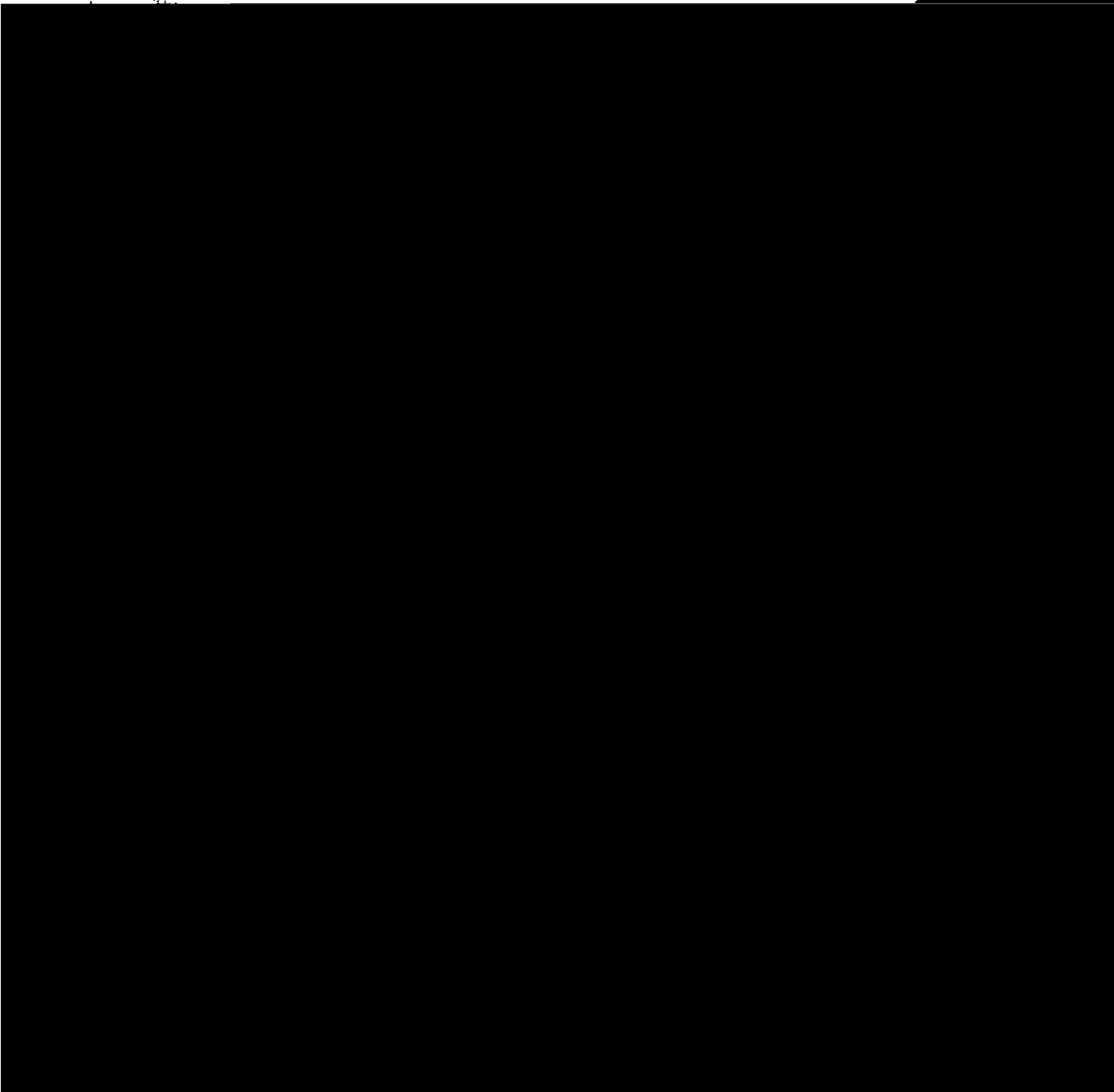


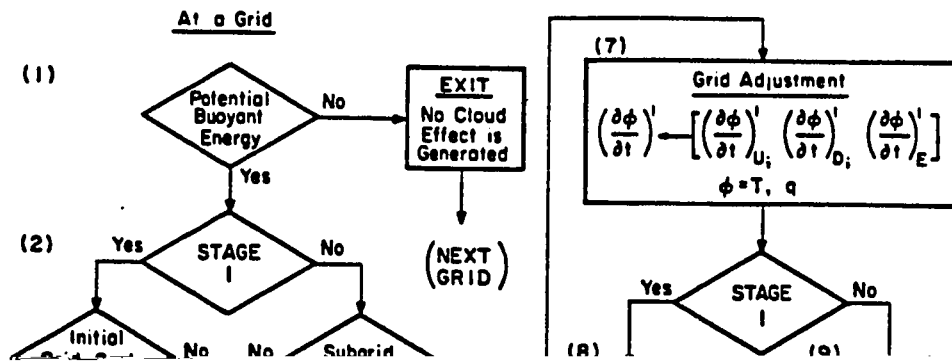
stabilizes the convection itself, while simultaneously producing enhanced convection (or convergence) in the surrounding immediate environment. The decaying stage (or Stage 3) refers to the rest of the convective lifetime excluding the above two stages. This stage may

---

---

---

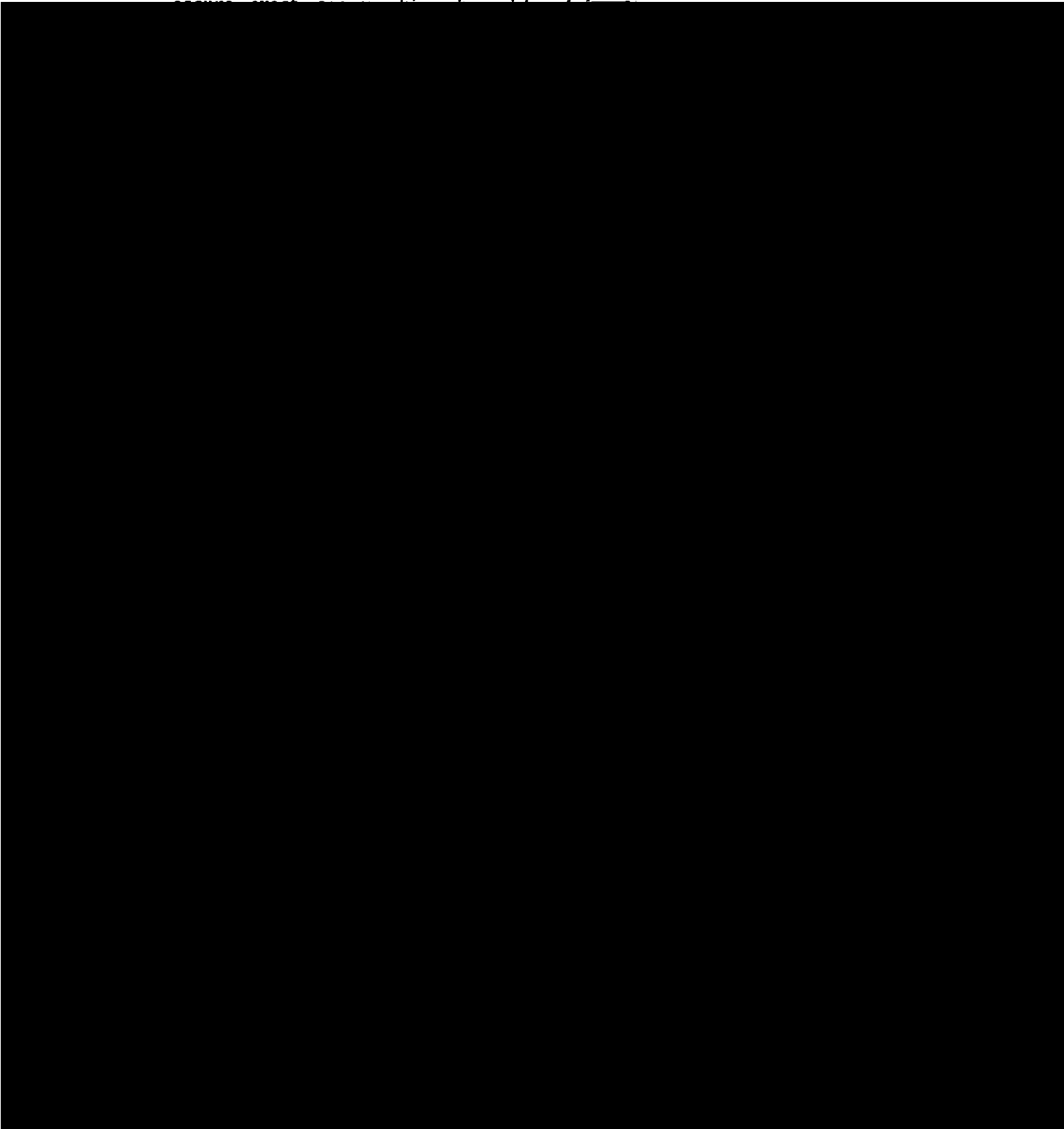




when the downdraft enters into the subcloud layer the subsequent convection is "stronger" than the initial convection by a "ratio" formulated in Fig. 3-2. Conceptually, such an assumption is consistent with the fact of considering the "three-dimensional" mass convergence in the subcloud layer (Frank, 1982; personal communication). That is, convection is developed due to both the grid-scale horizontal convergence and the vertical mass influx due to the downdrafts. Therefore, the current scheme calculates the enhanced convective effect for the mature stage by computing the ratio using the updated grid-scale mass flux at cloud base and the updated downdraft mass flux at cloud top.

indicates conservation of both the moist static energy and water substance.

After the cumulus parameterization is performed, an adjustment to



w	q <sub>old</sub>
100	.0000100
100	.0000100
461	.0000101
120	.0000100
114	.0000158
987	.0003497
321	.0014970
210	.0035780
210	.0035780
362	.0035370
903	.0072520
235	.0086340
404	.0138700
357	.0159700
357	.0163800
357	.0165900
351	.0167300

ults with the adjustments.

$\frac{g}{kg}$ 20 min)	$\theta$ new	$\theta$ old	$q$ new	$q$ old
000000	475.99	476.00	.0000100	.0000100
000000	367.06	367.28	.0000100	.0000100
051568	337.79	338.32	.0001132	.0000101
000940	335.40	335.31	.0000119	.0000100
047594	333.22	332.08	.0001110	.0000158
925844	330.70	329.06	.0002980	.0003497
033432	323.75	323.02	.0014301	.0014970
080795	316.33	315.52	.0034164	.0035780
464198	310.35	309.94	.0044654	.0035370
194398	305.37	305.20	.0076408	.0072520
194398	305.37	305.20	.0076408	.0072520
703240	303.79	303.80	.0100405	.0086340
188827	302.34	302.45	.0134923	.0138700
112987	301.96	302.63	.0157440	.0159700
317987	301.96	302.63	.0157440	.0163800
422987	301.96	302.63	.0157440	.0165900
225320	302.61	304.71	.0162794	.0167300

of both moist static energy and water substance in the parameterization, the heating/moistening are listed separately for the cases without (Table 3-2) and with (Table 3-3) the adjustment.

Comparing Table 3-2 and Table 3-3 we see that due to the

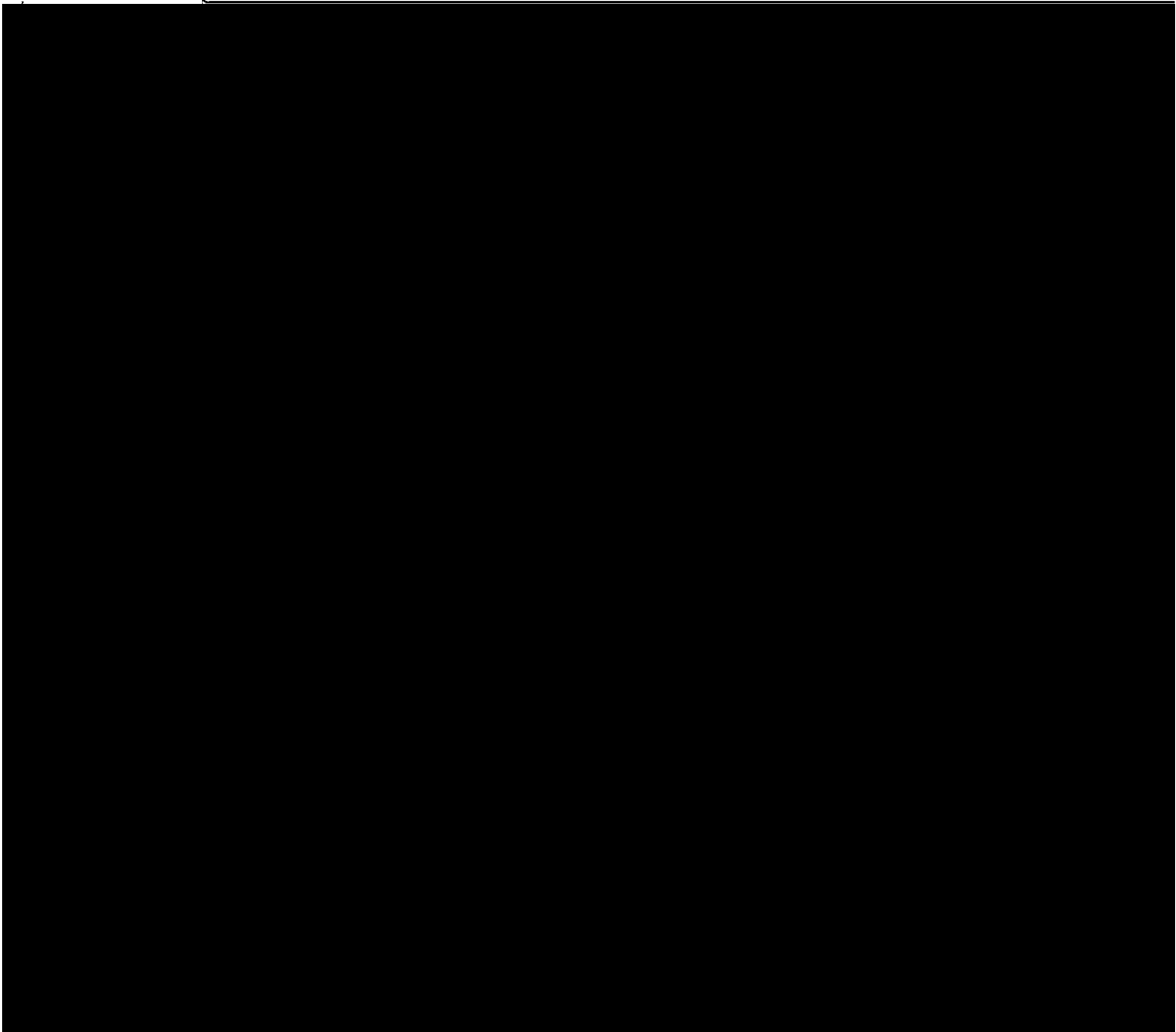


Other parameterization quantities not discussed in this section are found to be relatively insensitive to the chosen parameter.

3-4-a. Sensitivity to the Non-hydrostatic Parameter in the Vertical Equation of Motion

The  $\beta$  parameter in the vertical velocity equation is, as indicated in Kreitzberg and Perkey (1976), associated with the compensating effect of neglecting the nonhydrostatic pressure perturbation in the buoyancy equation. It is realized that there are other important terms

in the vertical velocity equation.



3-4-b. Sensitivity to Precipitation Efficiency

Table 3-11

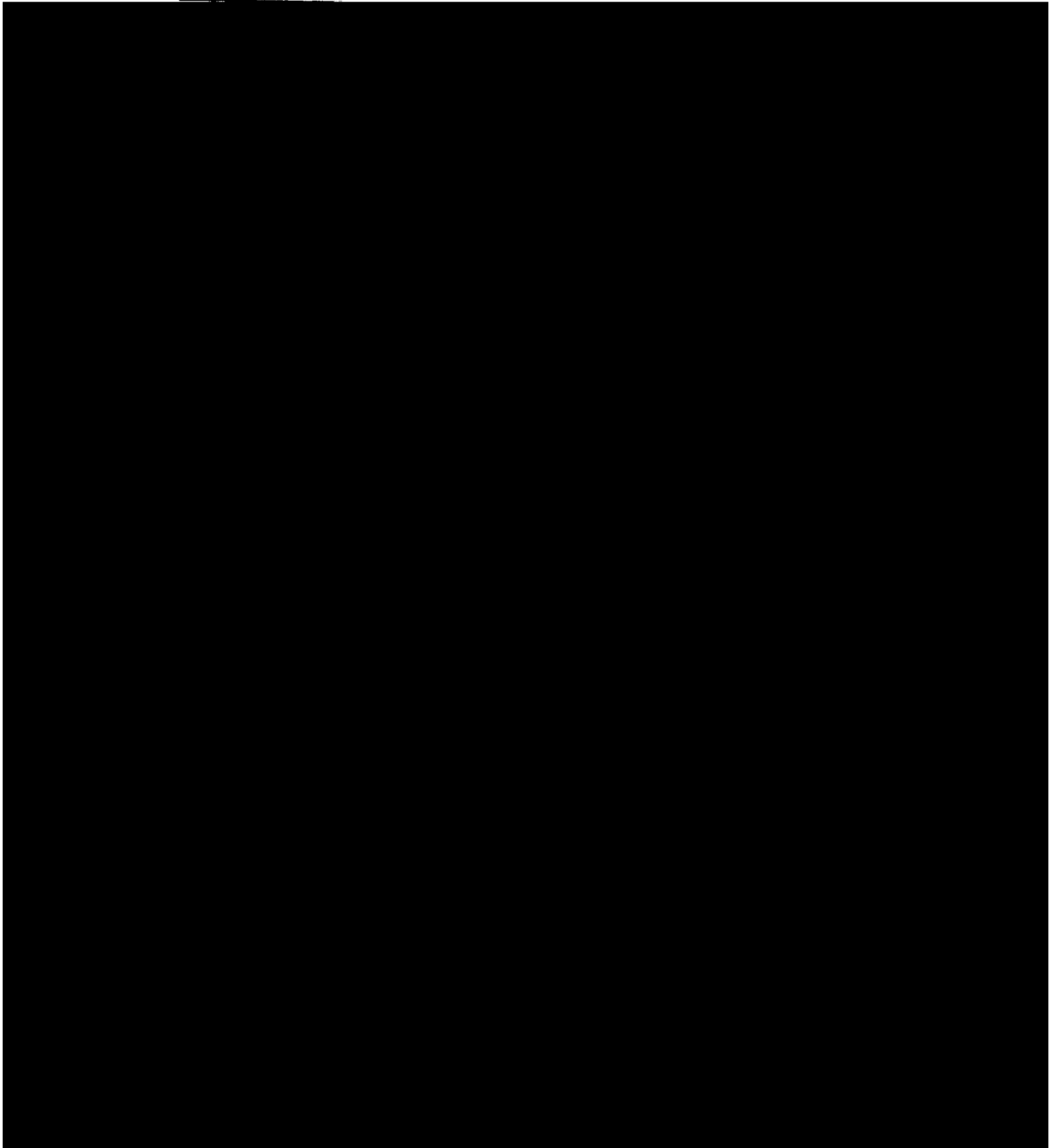


Table 3-6.

---

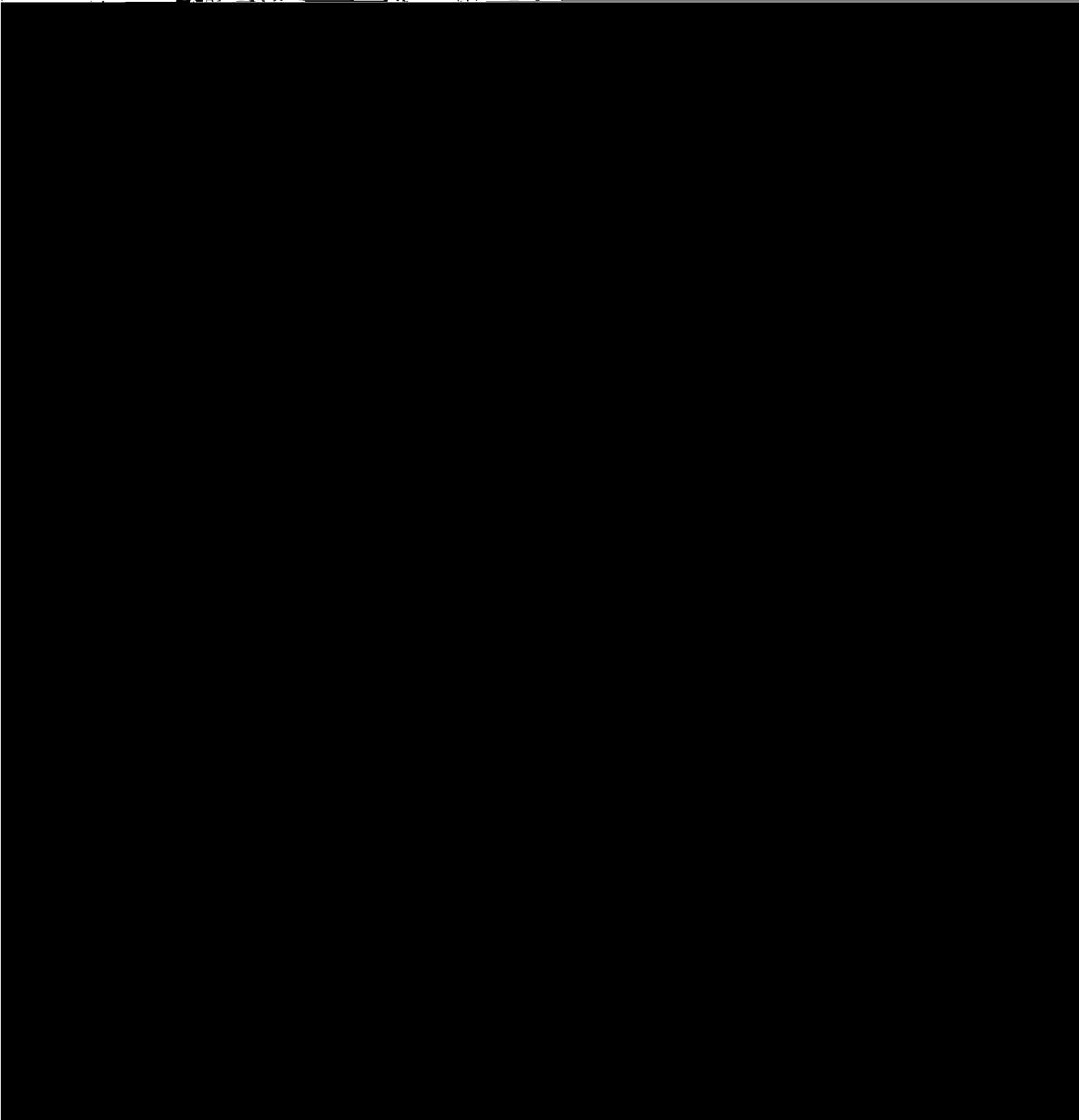
FRACI	Cloud depth (km)	Max. heating (°C)
-------	------------------	-------------------

---



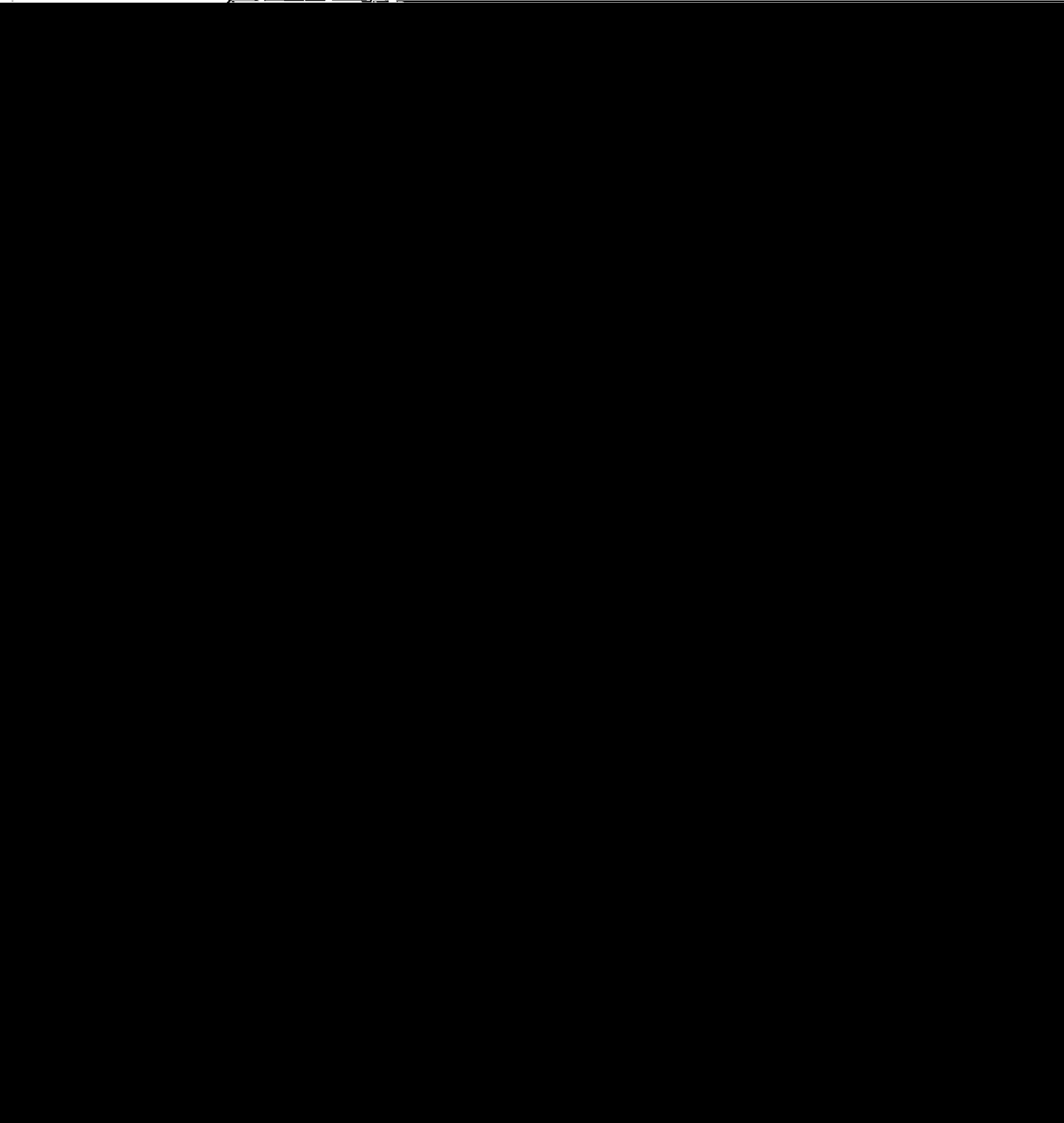
It is seen that, as expected, both updraft and downdraft intensities are rather significantly dependent upon the entrainment rate. Accordingly, cloud depth varies with the entrainment rate. The

findings are summarized in the following table.



3-4-f. Sensitivity to Initial Downdraft Massflux

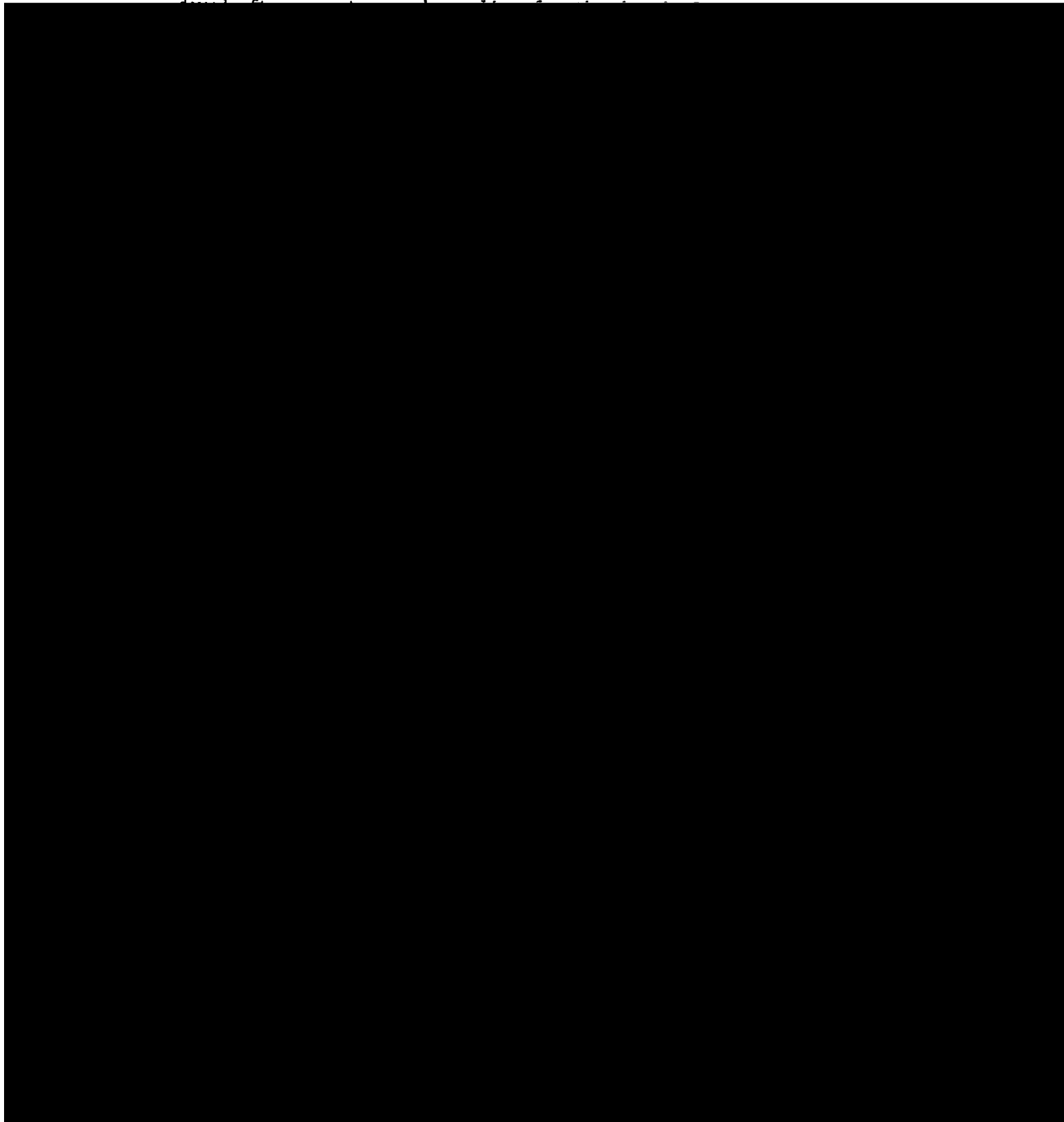
In this sensitivity experiment, the initial downdraft massflux is assumed to be the updraft massflux at cloud base multiplied by a ratio,  $\nu$ . That is,  $\text{initial downdraft massflux} = \nu \cdot \text{initial updraft}$

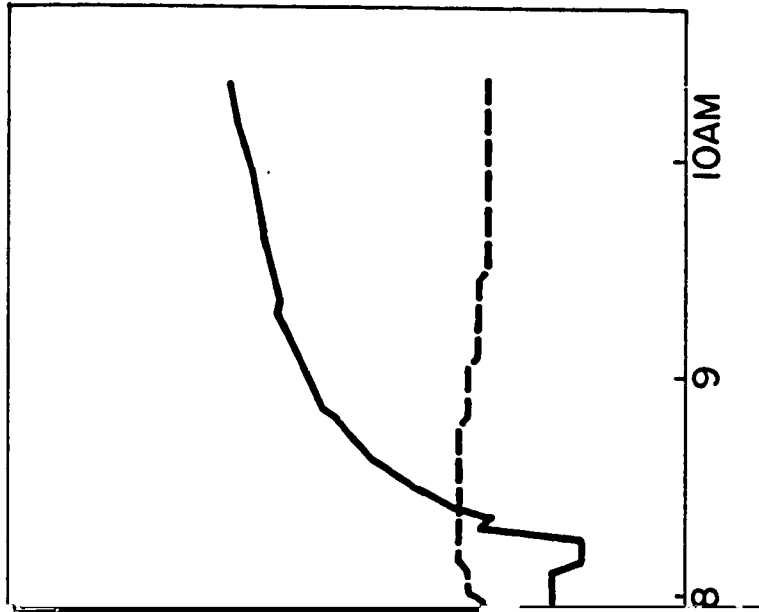


3-4-g. Sensitivity to Downdraft Relative Humidity

In this sensitivity experiment, for a downdraft relative humidity (RHD)  $\lesssim$  50 percent, there is not enough cooling to sustain the

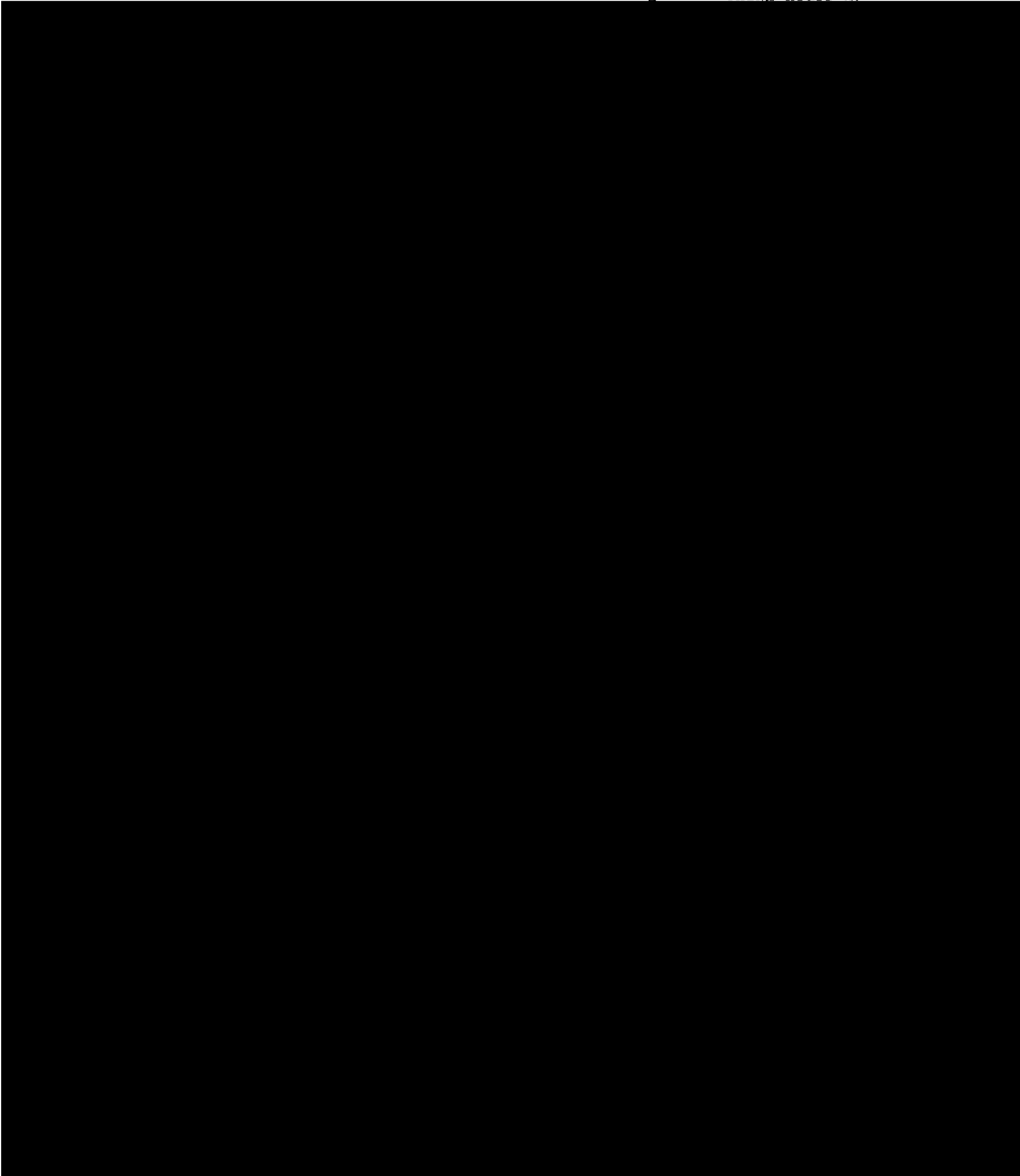
down draft. For a downdraft relative humidity of 50 percent, the



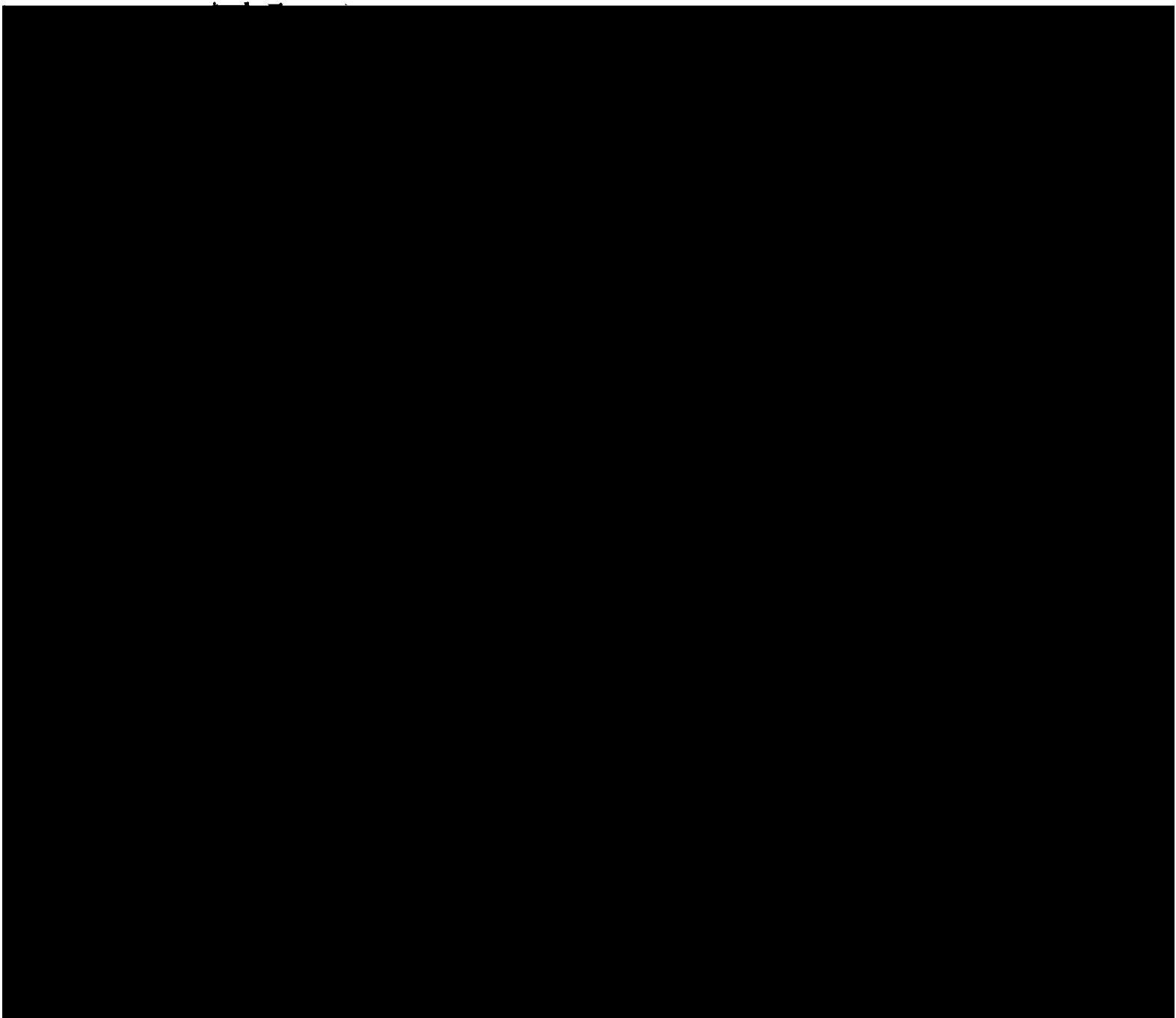


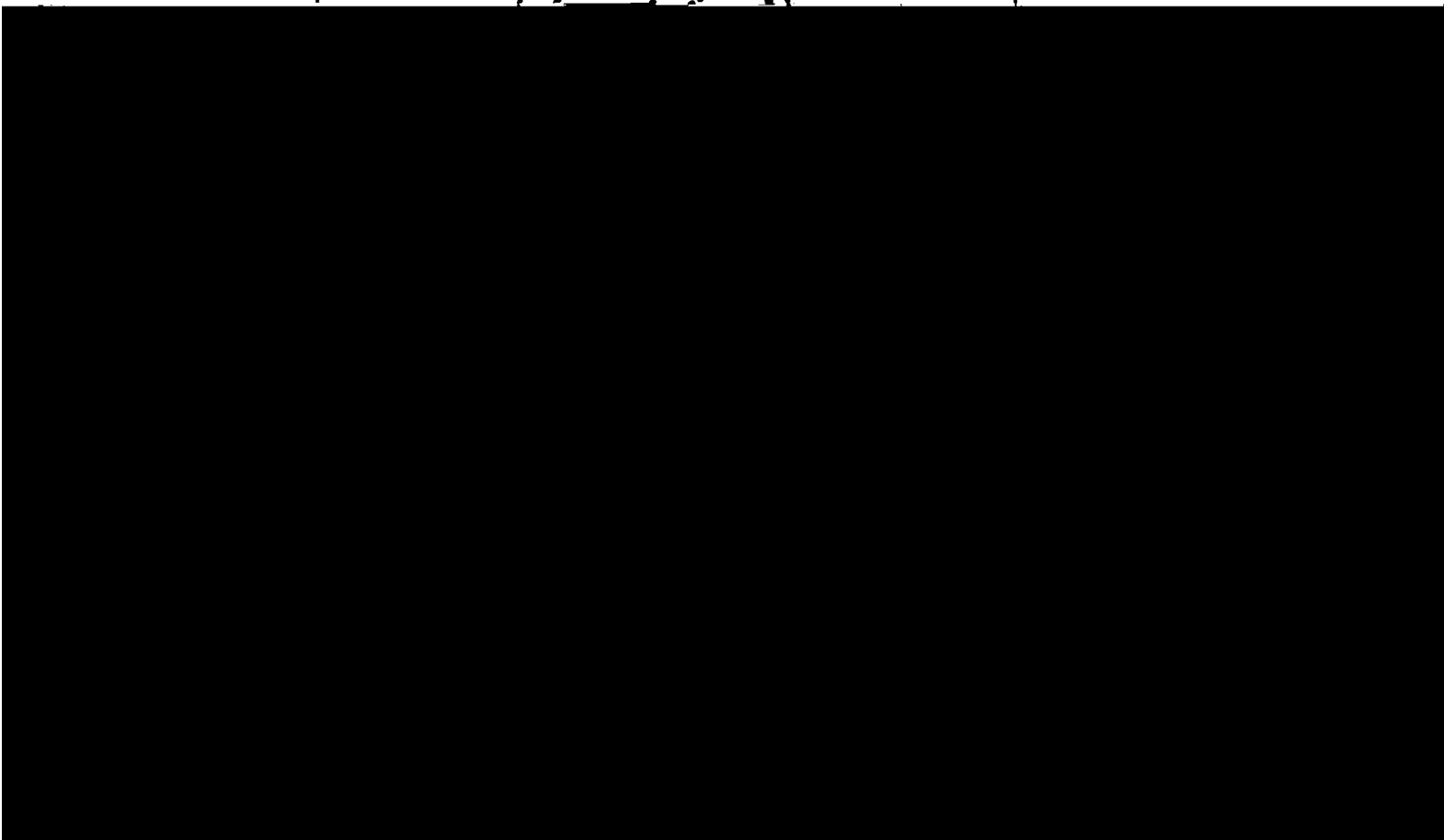
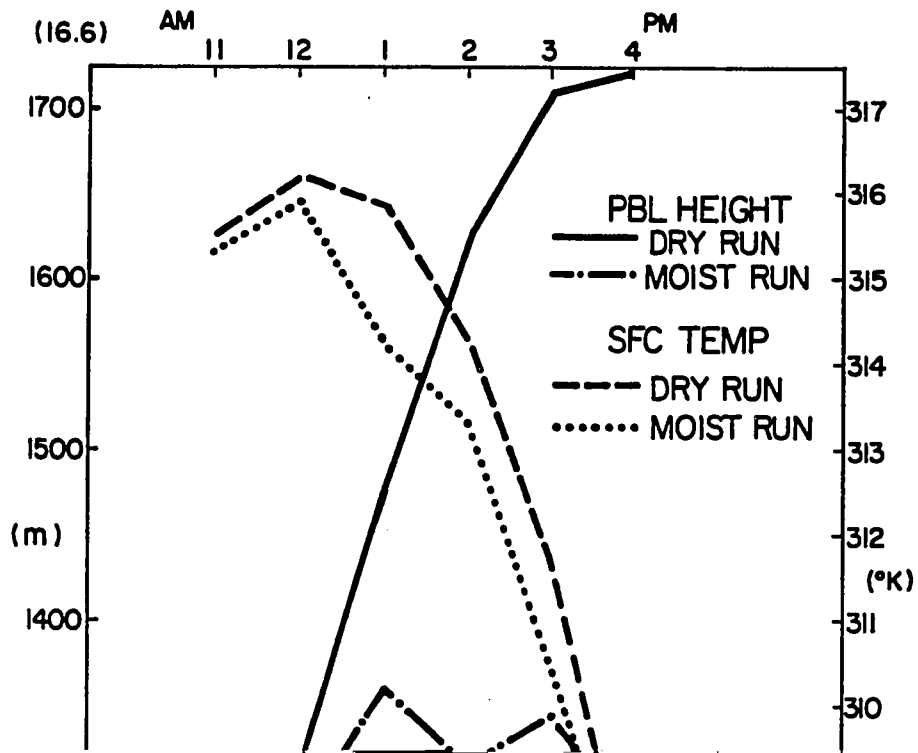
and a water grid point during the morning hours  
the control run).

land/sea difference of CAPE is established during the morning hours of



layer thickness is changed. As detailed in Appendix A, the dry boundary layer height is calculated using the formulation of Deardorff (1974). When deep convection is produced, the grid-environmental subsidence motion lowers the boundary layer height while the surface cooling reduces the surface upward heat flux. The combination of these two processes forms the modification upon Deardorff's PBL height equation due to convection. Figure 3-4 shows the surface temperature and PBL height for a dry sea breeze simulation and a moist sea breeze

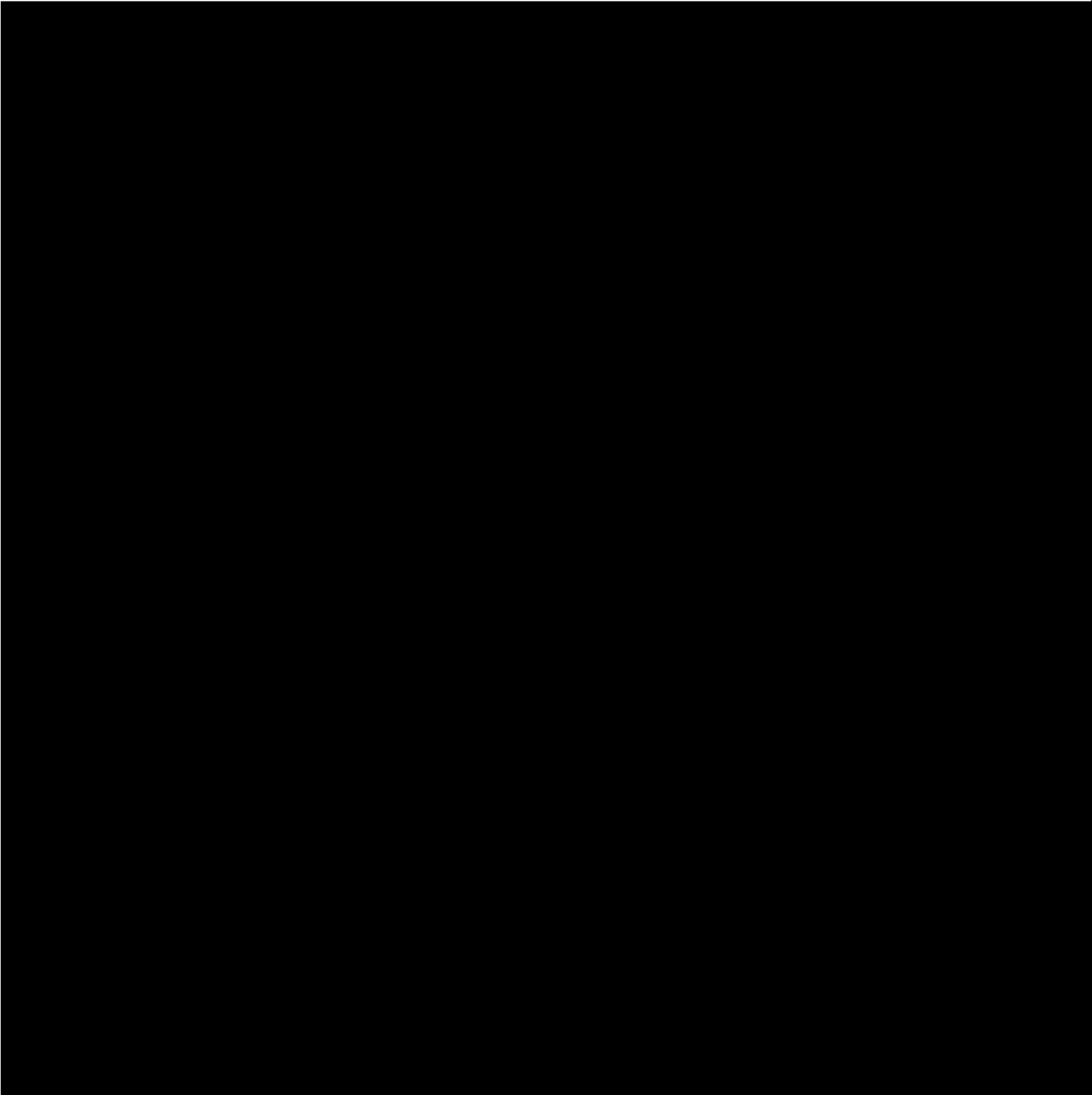




convection is regularly modulated by the lower tropospheric sea breeze



10 10 15 18 18 16 19 15 18 8 2 5 9 3 18 16 0 9 3 0 2 1 8 6 2 1 5 5



According to this analysis we see that for  $\beta = 1$  and  $\alpha = 1$

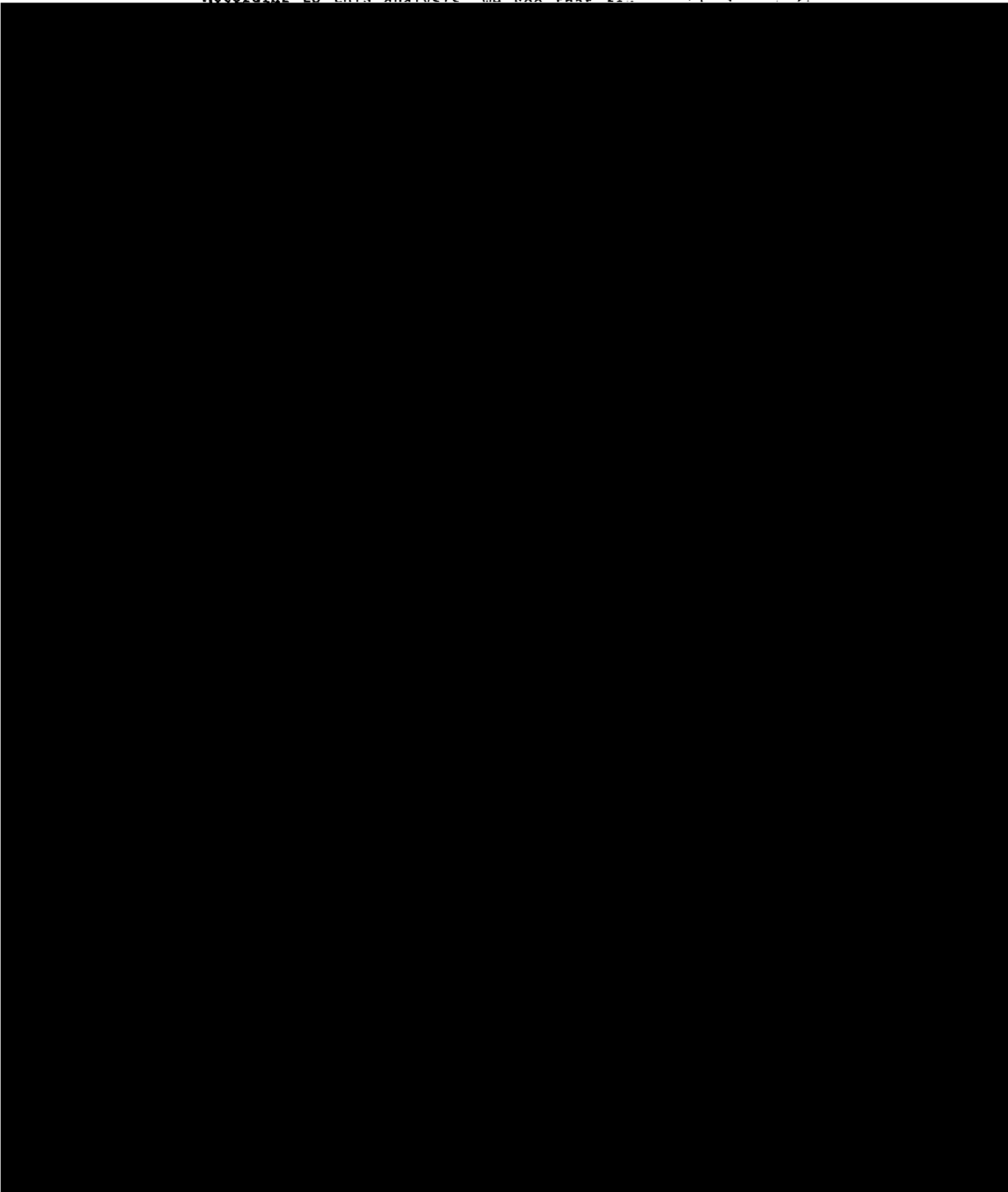
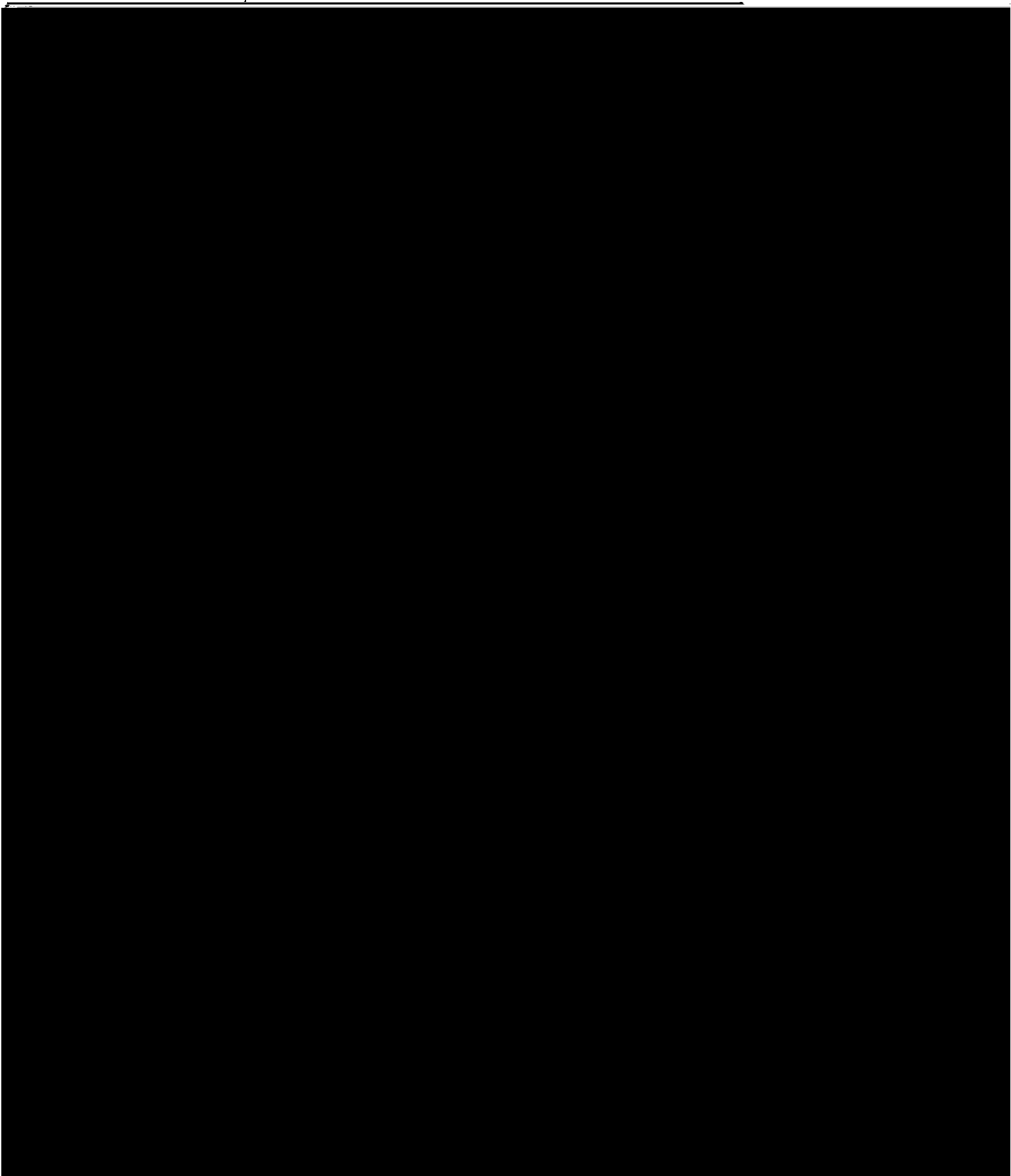


Table 3-12

Z (cm)	Ratio	$\frac{\delta K}{\delta t}$ cu ( $\frac{\text{watt}}{\text{m}^2}/\text{km}$ )
2072839.0	0.00	0.0
2001421.0	0.00	0.0
1930003.1	0.00	0.0
1858585.1	0.05	0.0
1787167.1	0.08	0.0
1715749.2	0.08	0.0
1644331.2	0.07	0.0
1572913.2	0.07	0.0
1501495.3	0.07	0.565E-11
1430077.3	0.06	0.197E-01
1358659.3	0.13	0.105E+00
1287241.4	0.20	0.237E+00
1215823.4	0.24	0.376E+00
1144405.4	0.25	0.488E+00
1072987.5	0.26	0.577E+00

In the particular point see brass simulation performed in 1991



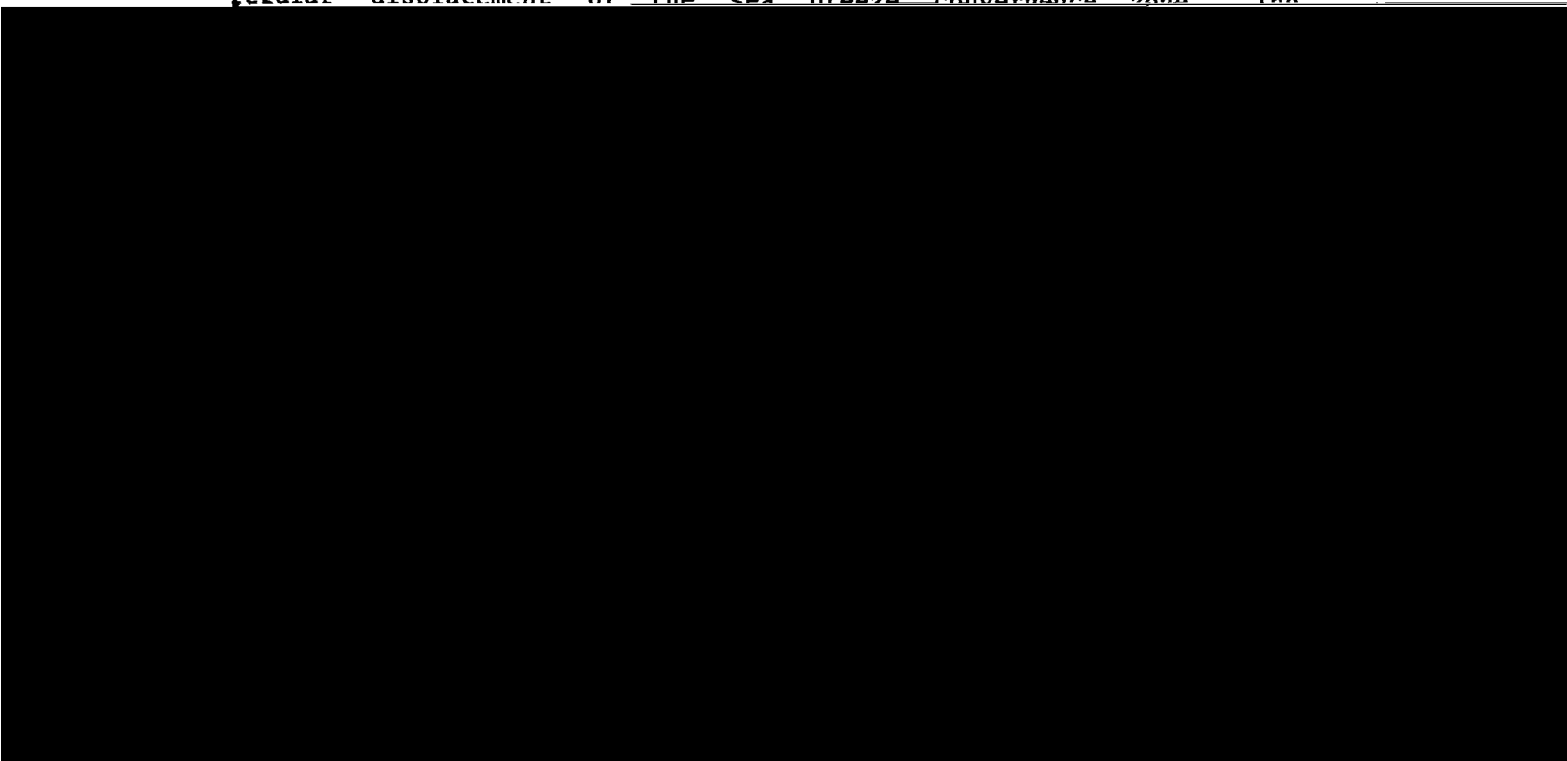
## Chapter 4

### SEA BREEZE - DEEP CUMULUS CONVECTIVE INTERACTIONS

#### 4-1. Introduction

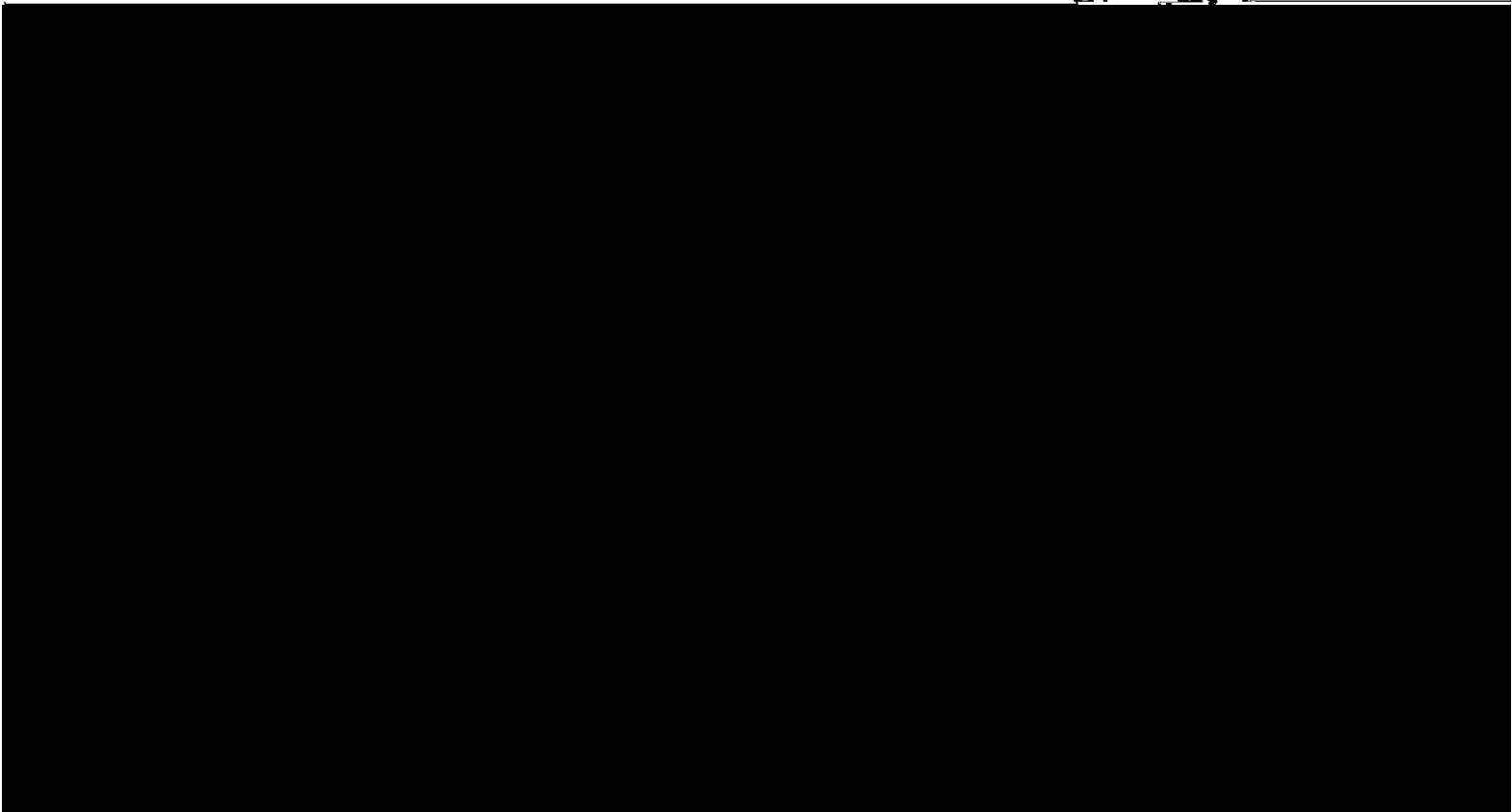
During the last decade there has been considerable interest in understanding mesoscale weather systems and their interactions with both large-scale circulations and cumulus convection. An ideal location for examining these interactions is the south Florida peninsula where mesoscale sea breeze circulations on both coasts regularly initiate deep convection on synoptically undisturbed days.

A considerable amount of observational study has been devoted to the south Florida mesoscale region bounded by the east and west coasts and Lake Okeechobee. Frank, Moore, and Fisher (1967), for example, have summarized radar analyses on the peninsula-scale convective patterns for a diurnal period, as well as related shower activity to the regular displacement of the sea breeze convergence zone. The



The relationship between convective rainfall and peninsula-scale forcing has also been investigated by Burpee (1979) and Burpee and Lahiff (1984), in which it was concluded that the mid-tropospheric moistening (due to pre-existing convection) is important for generating convective rainfall during the afternoon period. A thorough statistical analysis of Florida's convective activities performed by Lopez et al. (1984a,b) confirmed that the majority of Florida's mesoscale convective systems are mergers of smaller systems, being consistent with the earlier finding of the "tendency to form clusters" (Byers and Braham, 1949) and the merging hypothesis of Simpson et al., (1980).

However, due to the difficulties of performing a peninsula-scale observational program, investigations of the convective feedback effects upon the mesoscale sea breeze circulation and on the peninsula-scale environment have been very limited. From the point of view of understanding Florida's sea breeze-convective interactions, it is unfortunate that there have been essentially no mesoscale/peninsula-scale observations which also include



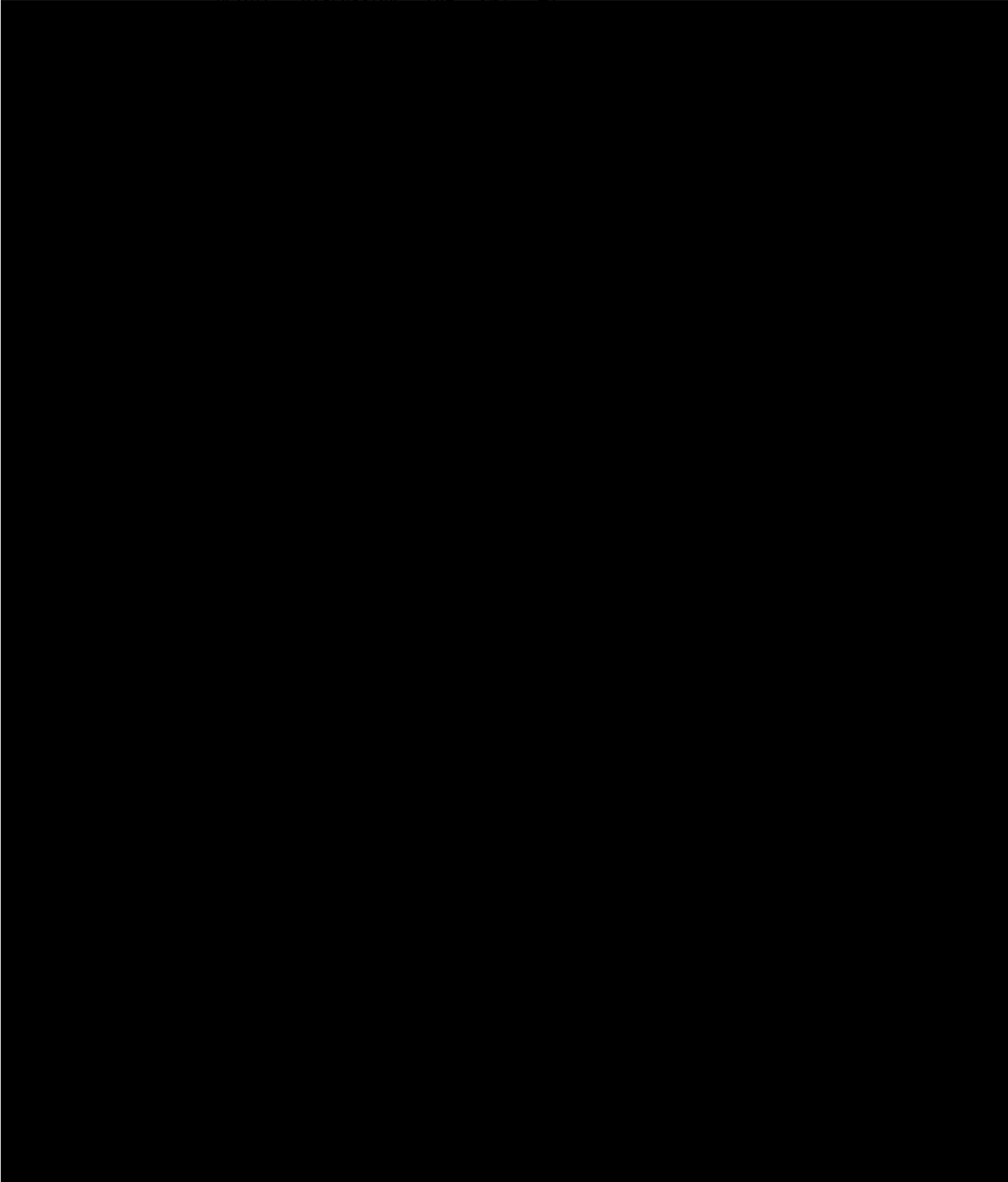
convective-environmental interaction should provide some insight concerning deep convective/large-scale interrelationships in other places.

- (2) One of the reasons that the summer Florida environment provides an excellent natural laboratory for investigating

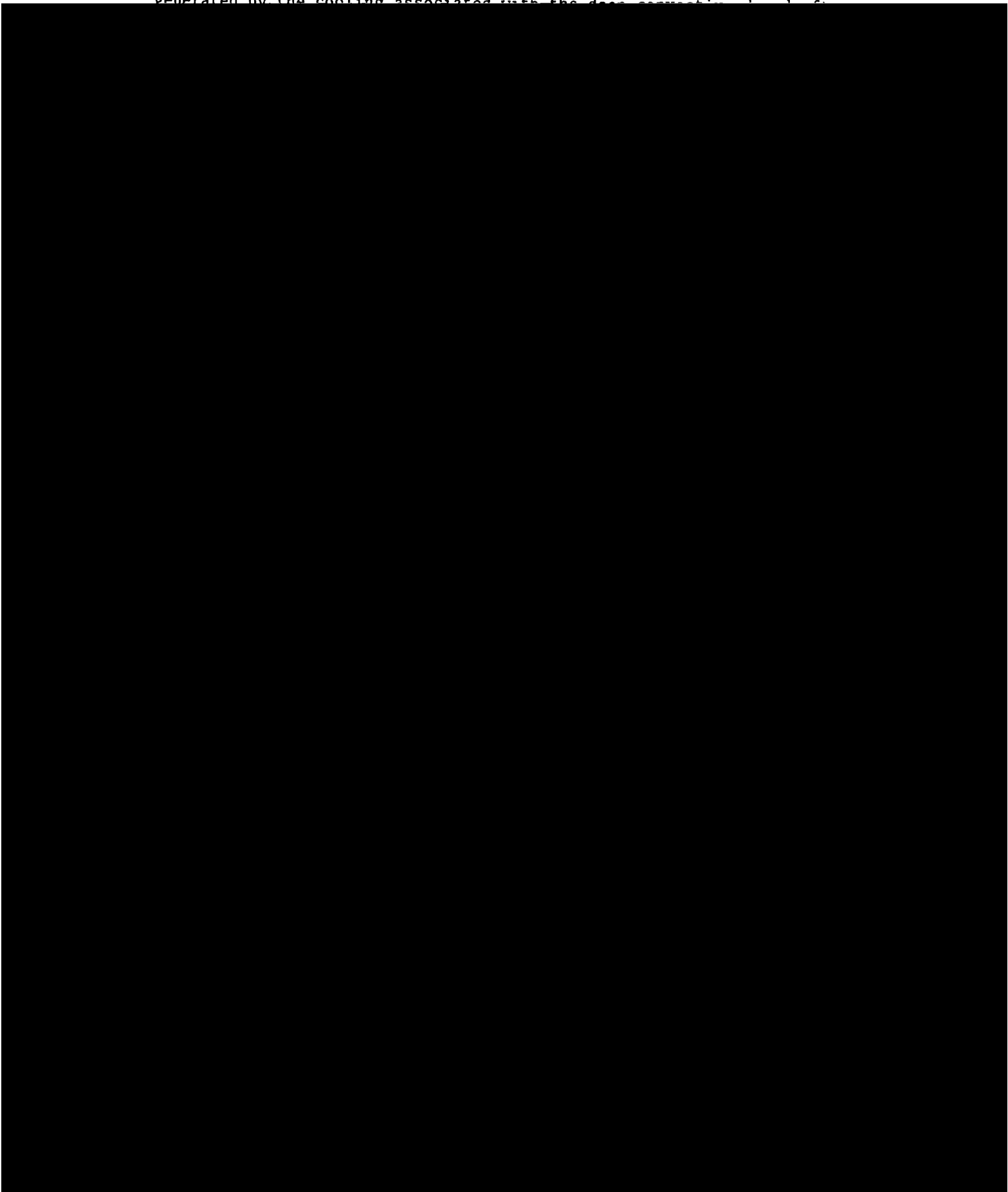
~~deep convective-environmental interactions.~~



Before discussing the case, please read carefully the following text:



generated by the cooling associated with the deep correction. In 1961, the



sounding of this day at Miami and the 0700 EST synoptic surface analysis was used for initiating the simulation (shown in Fig. 4-2-1a and b).

Model results chosen for the validation in this section include vertical velocities near 10 km and 1 km and model generated surface

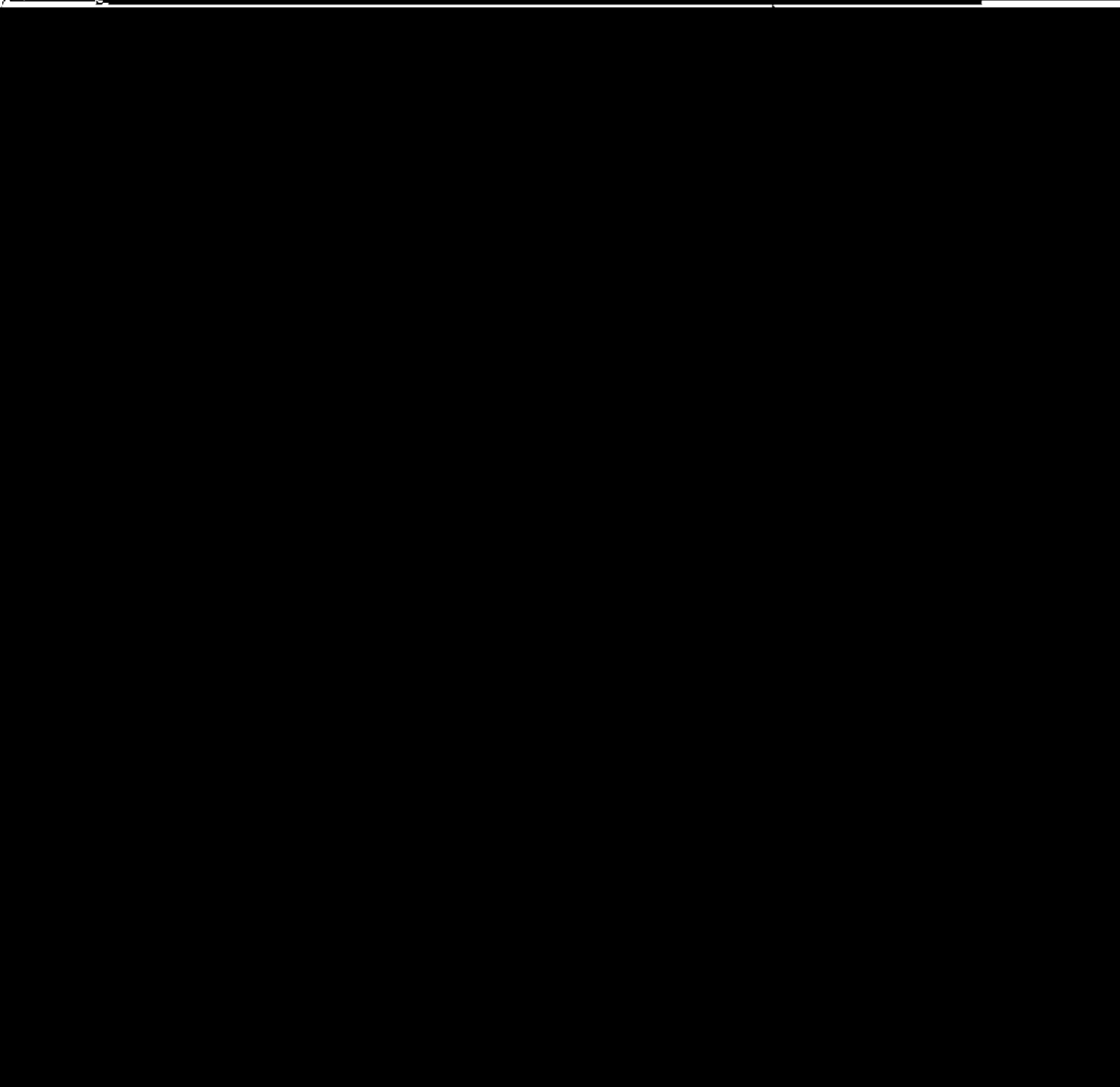
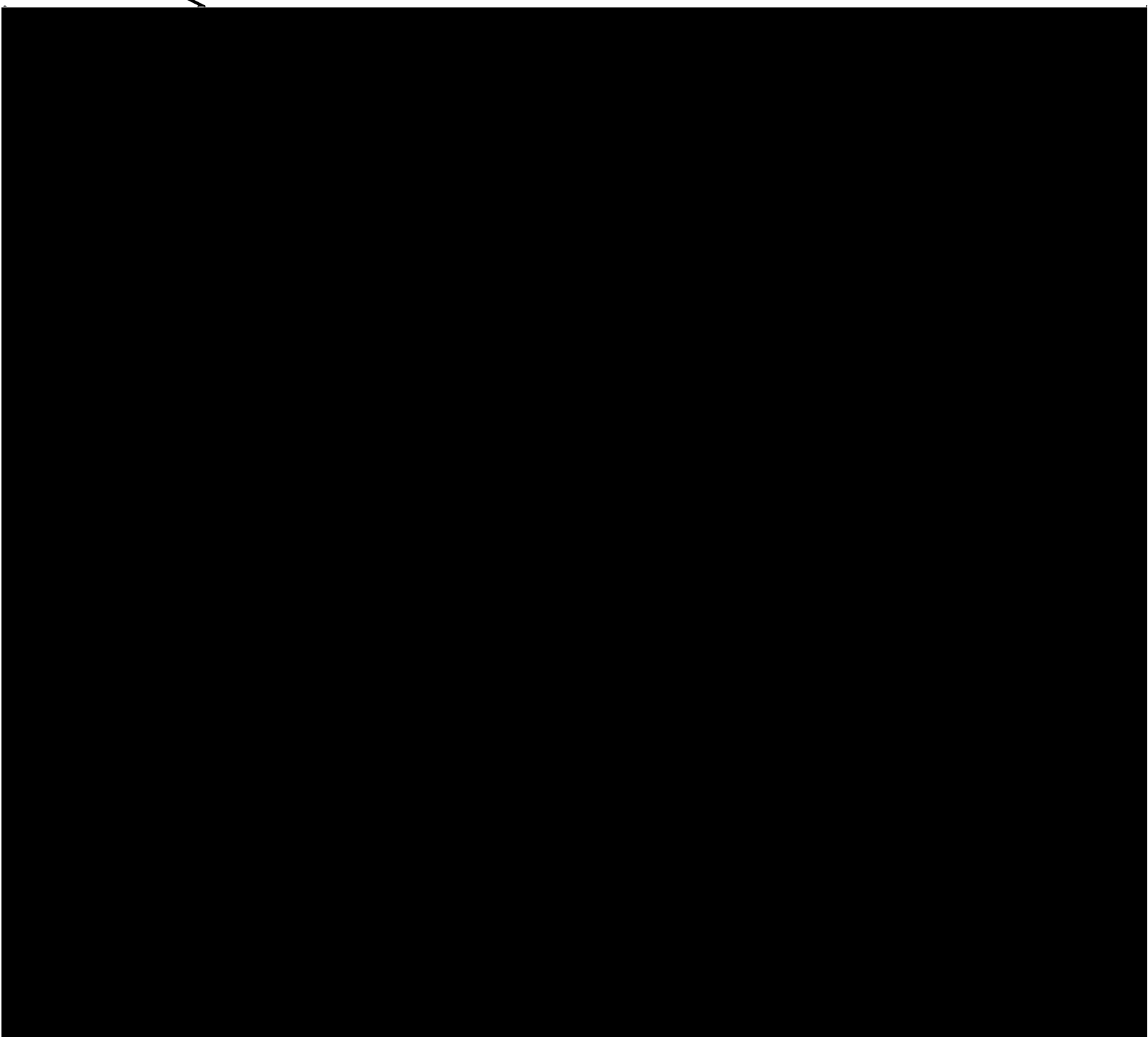
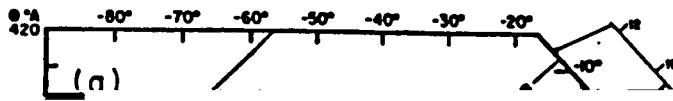


Figure 4-2-1(a). The early morning (07 EST) Miami sounding of July 17, 1973, which is used for initiating the moist sea breeze simulation (or the control run). The surface wind is seen in Fig. 4-2-1(b).

---





MIAMI SOUNDING  
17 JULY 1973

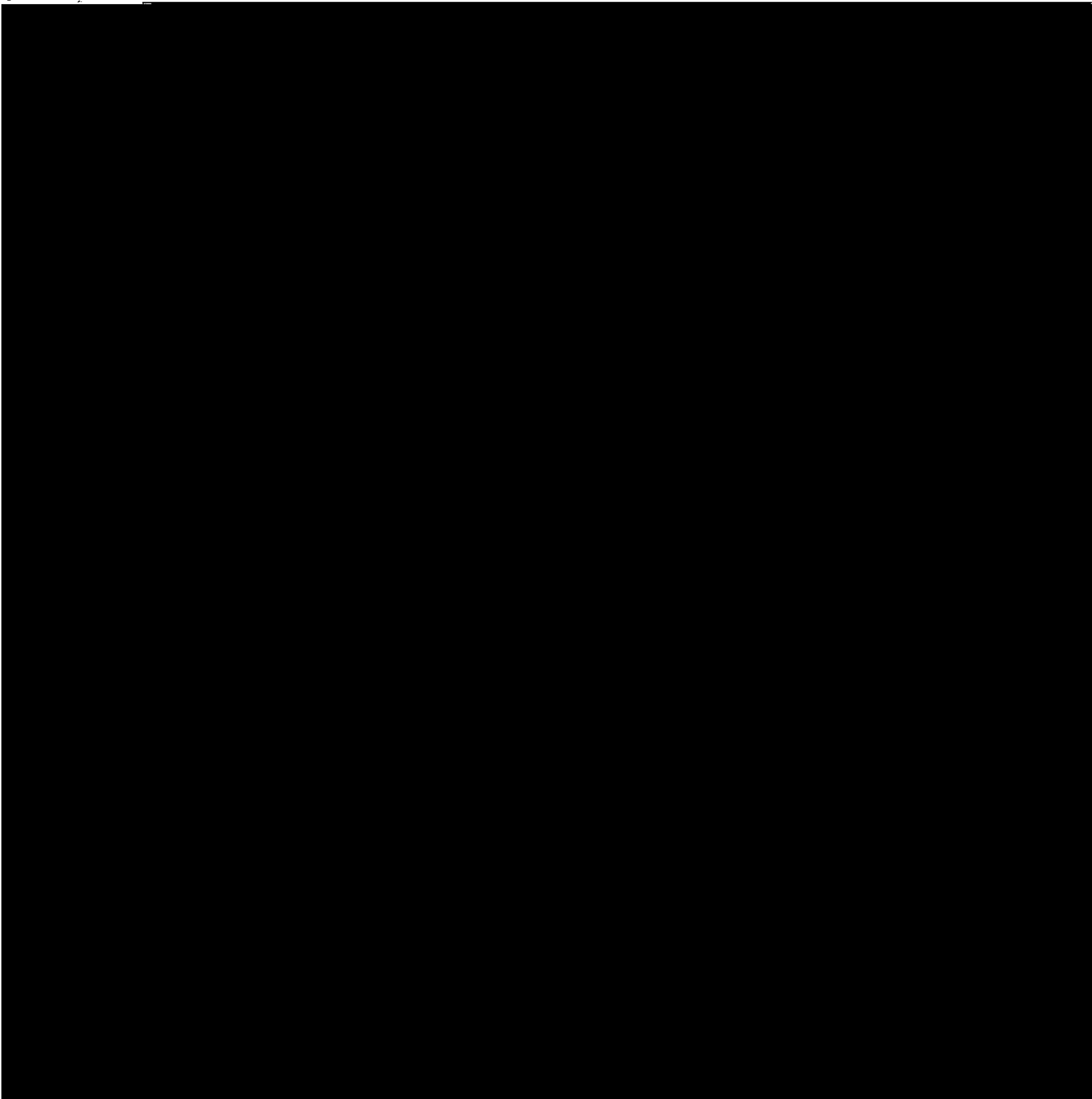
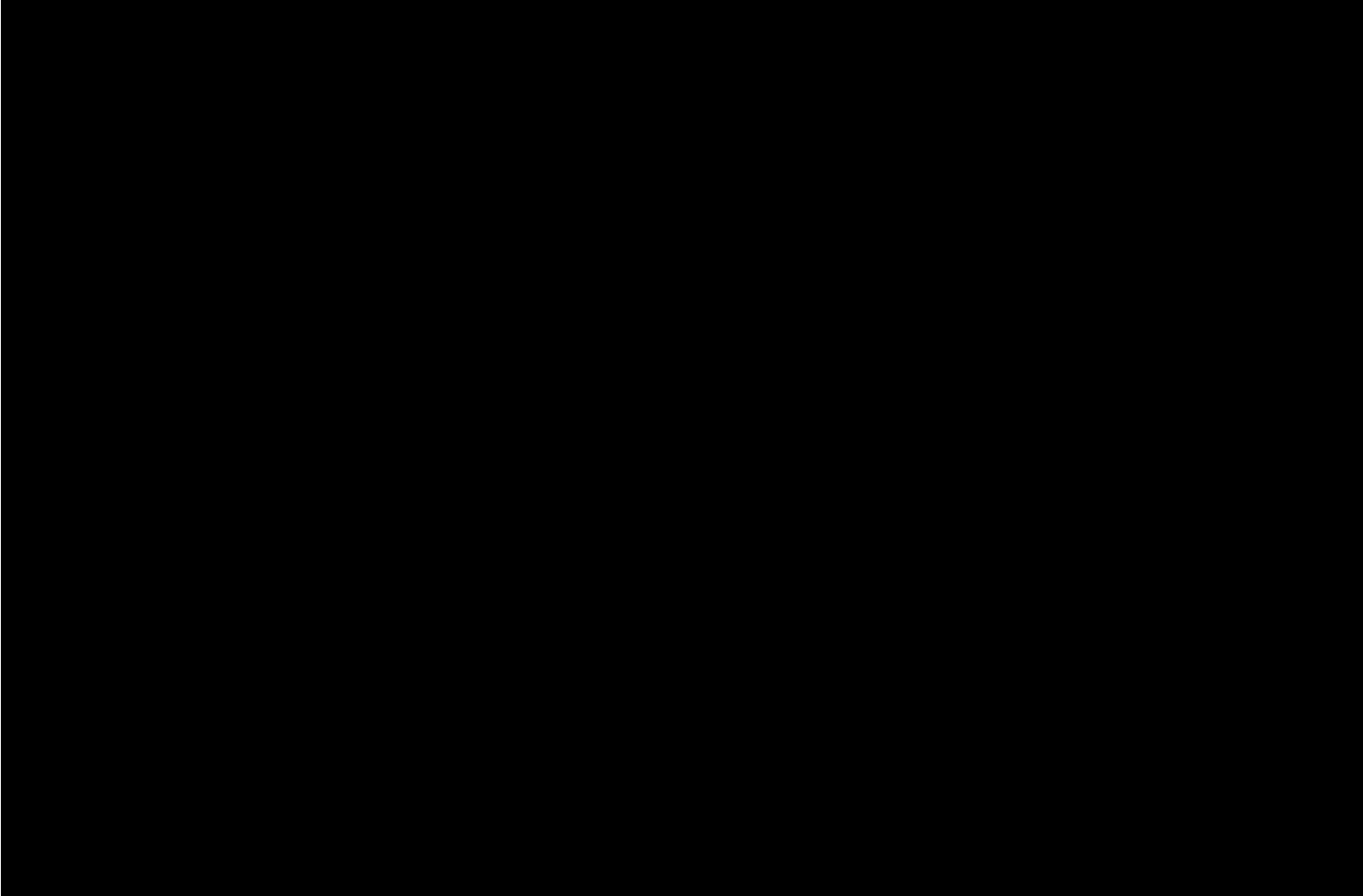
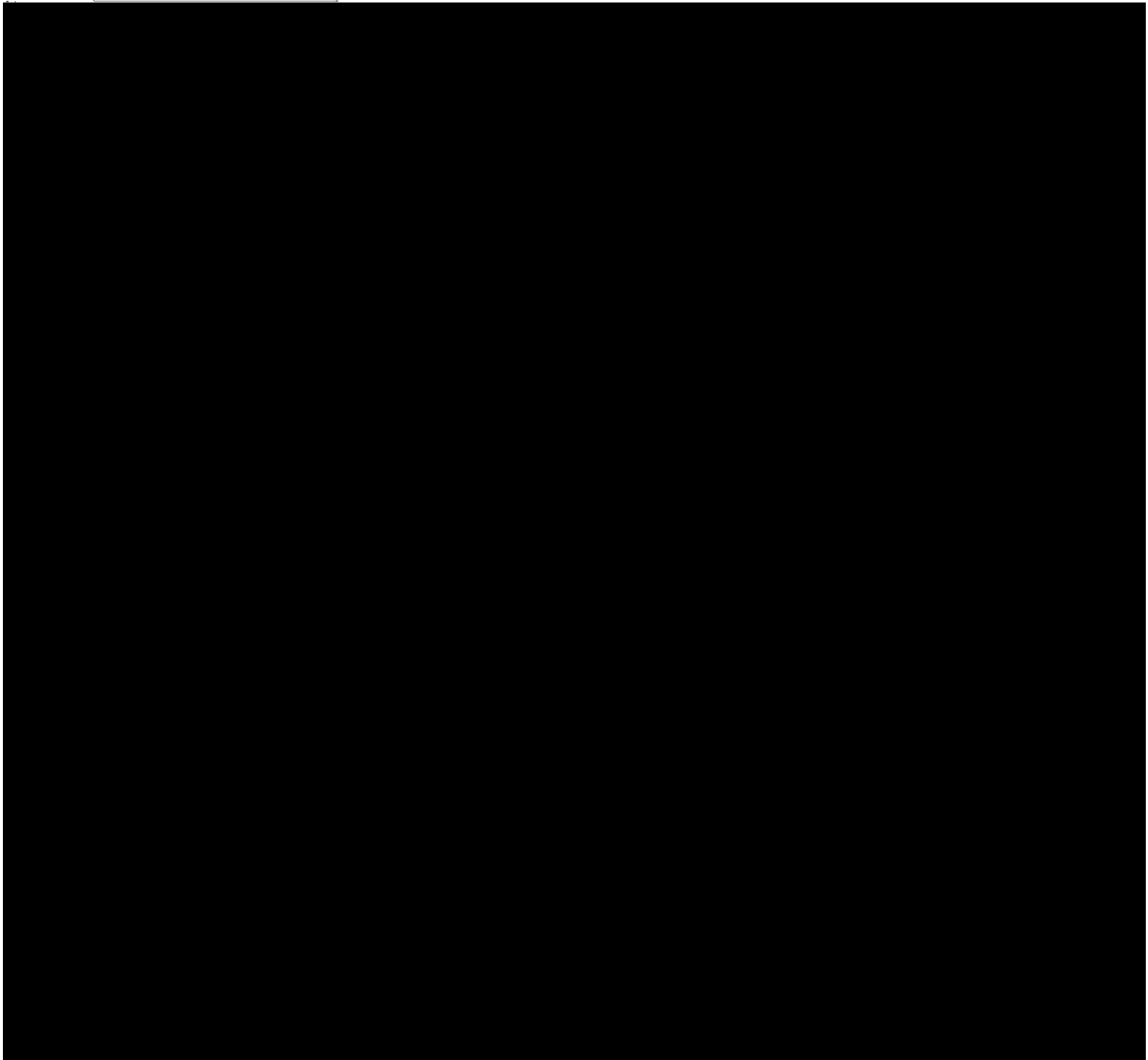
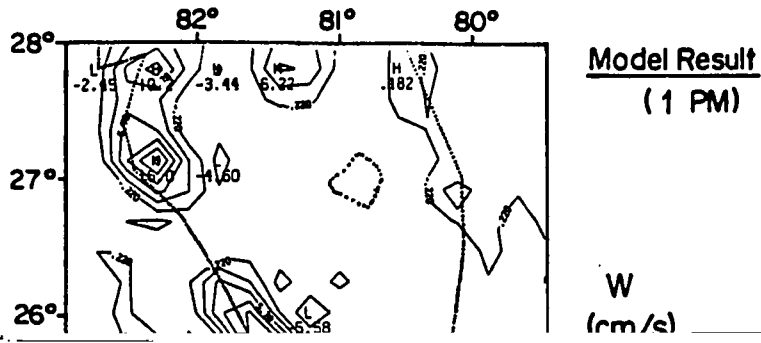
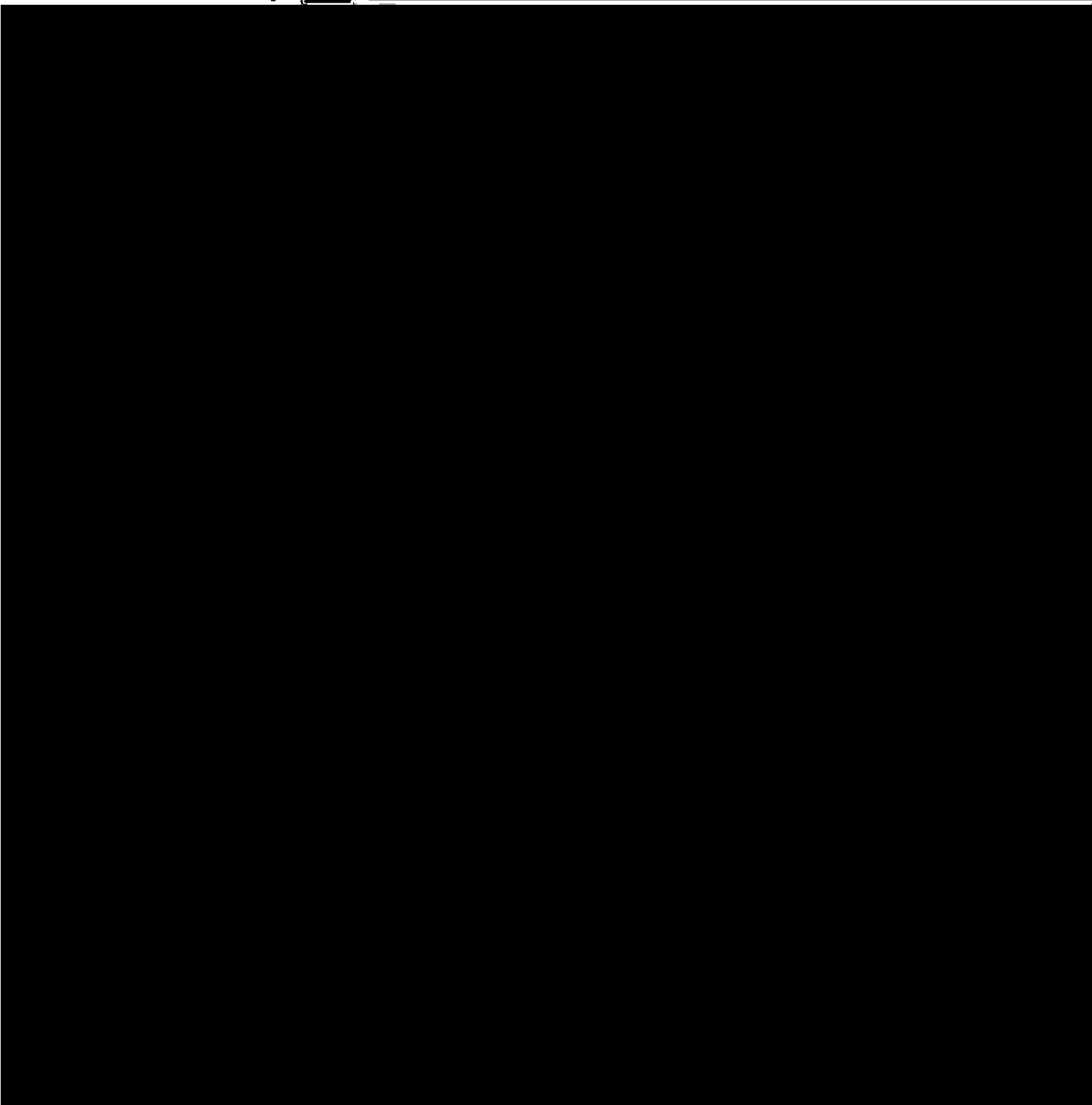
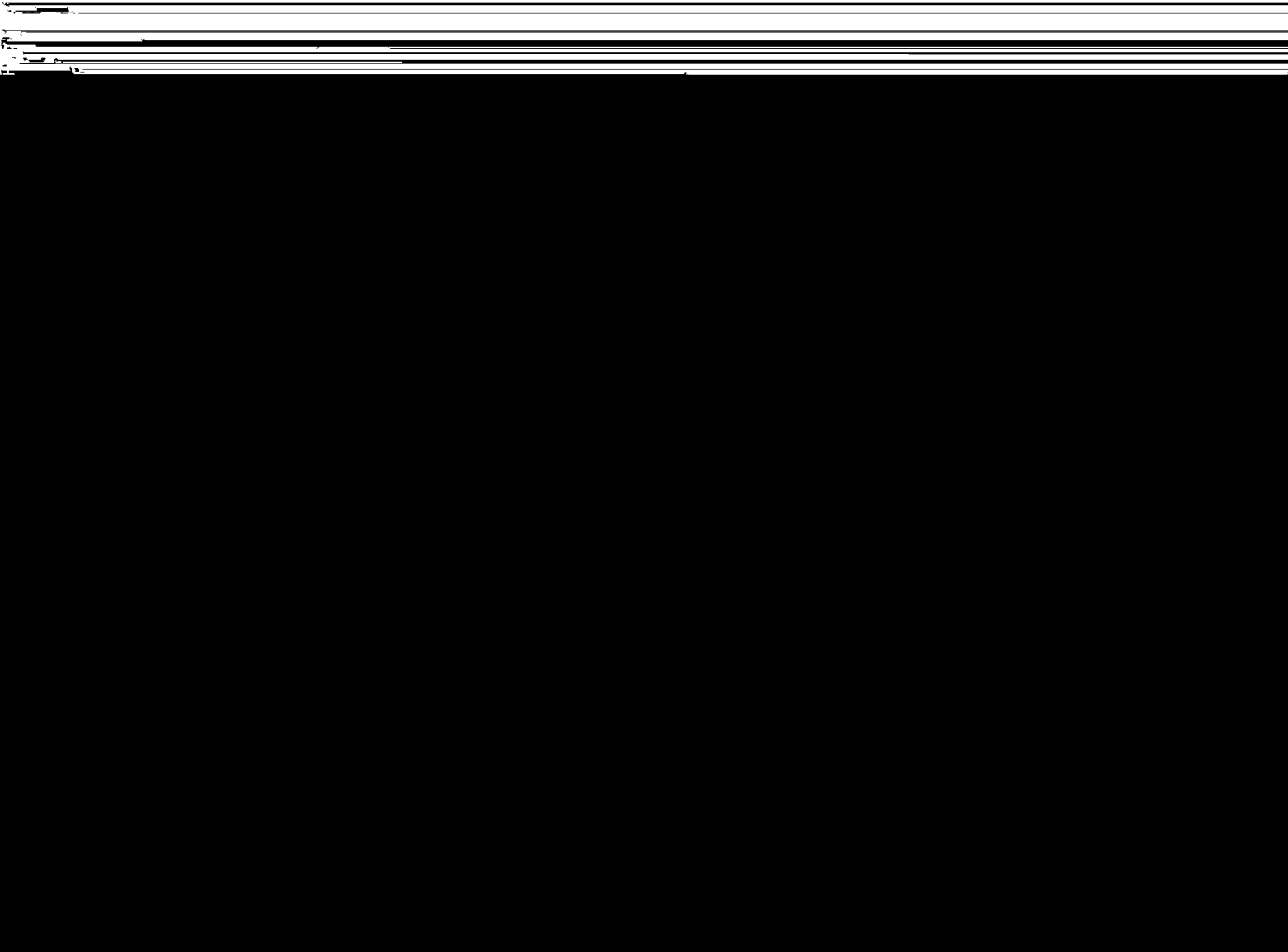
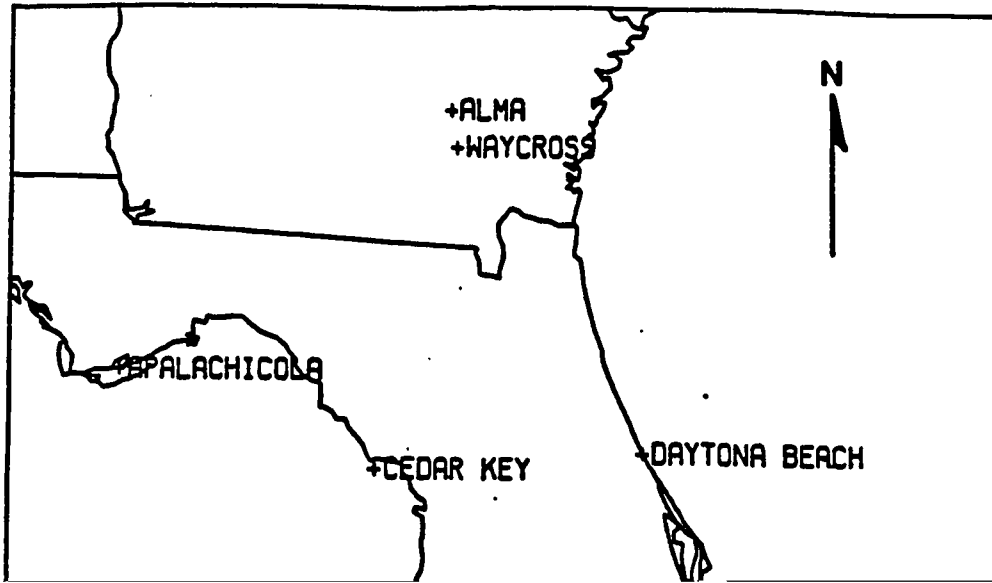


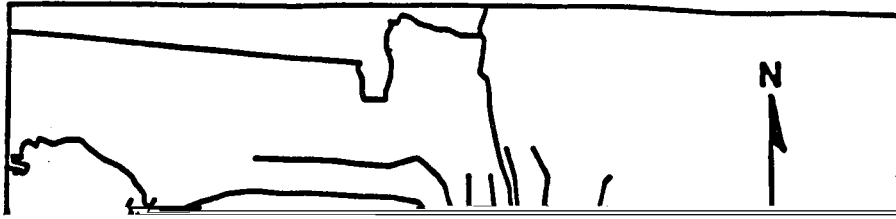
Figure 4-2-2. The model produced horizontal maps of vertical velocity (cm/s) near 10 km (top) and 1 km (middle); and the model rainfall rate (mm/10 hour) (bottom), at 1 PM. The symbol "H" indicate upward motions, while "I." indicate

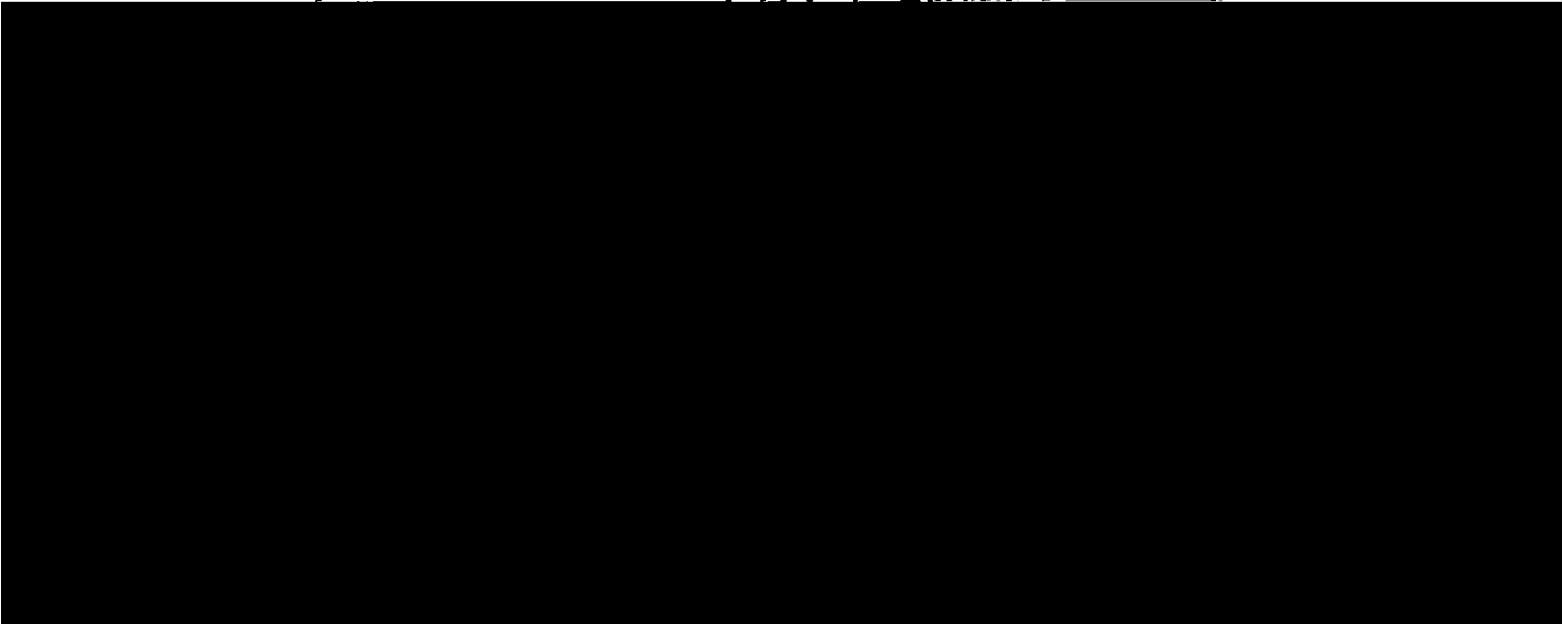
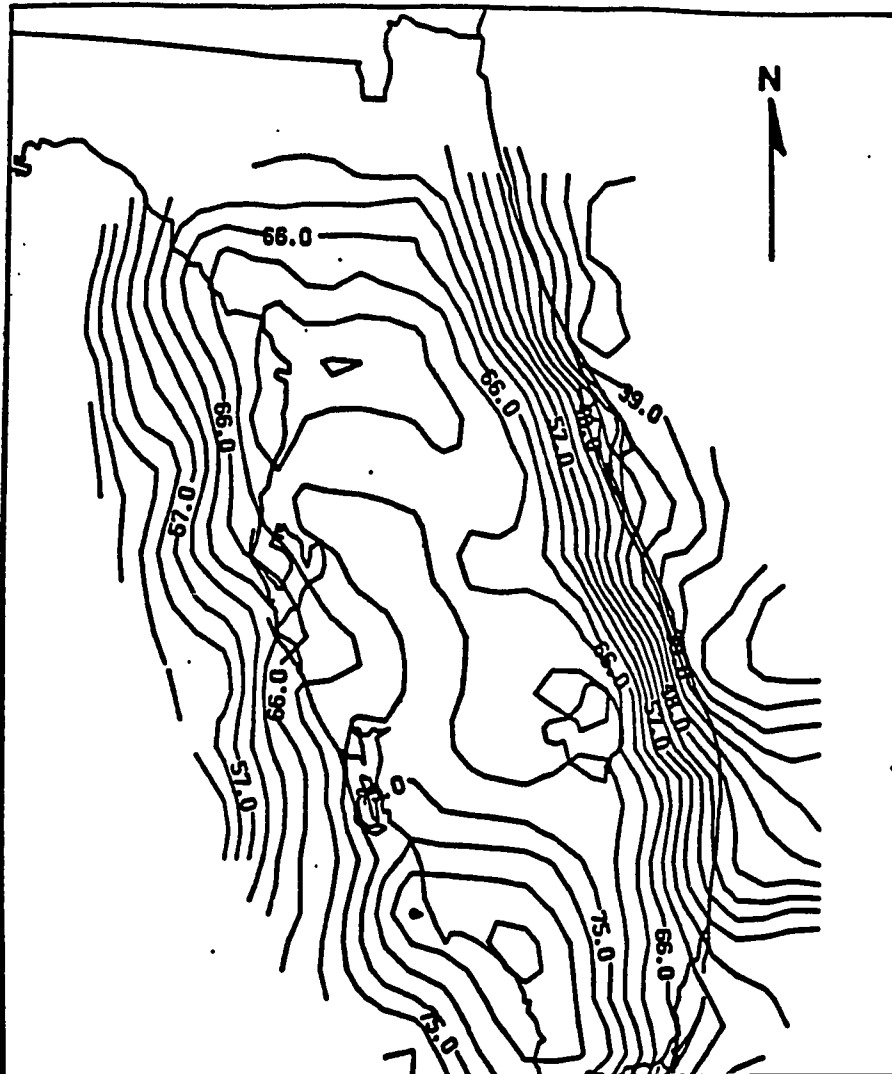






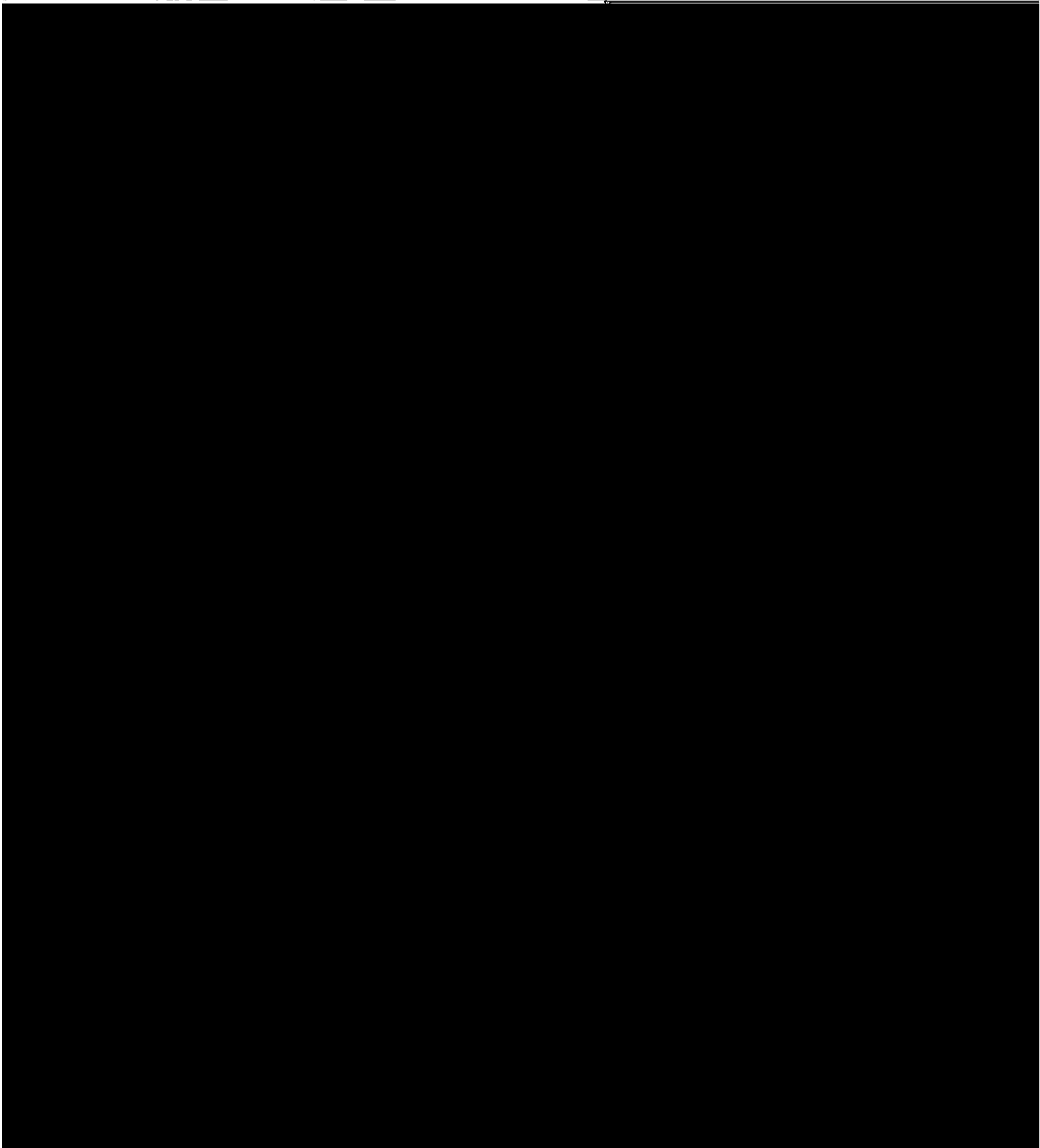




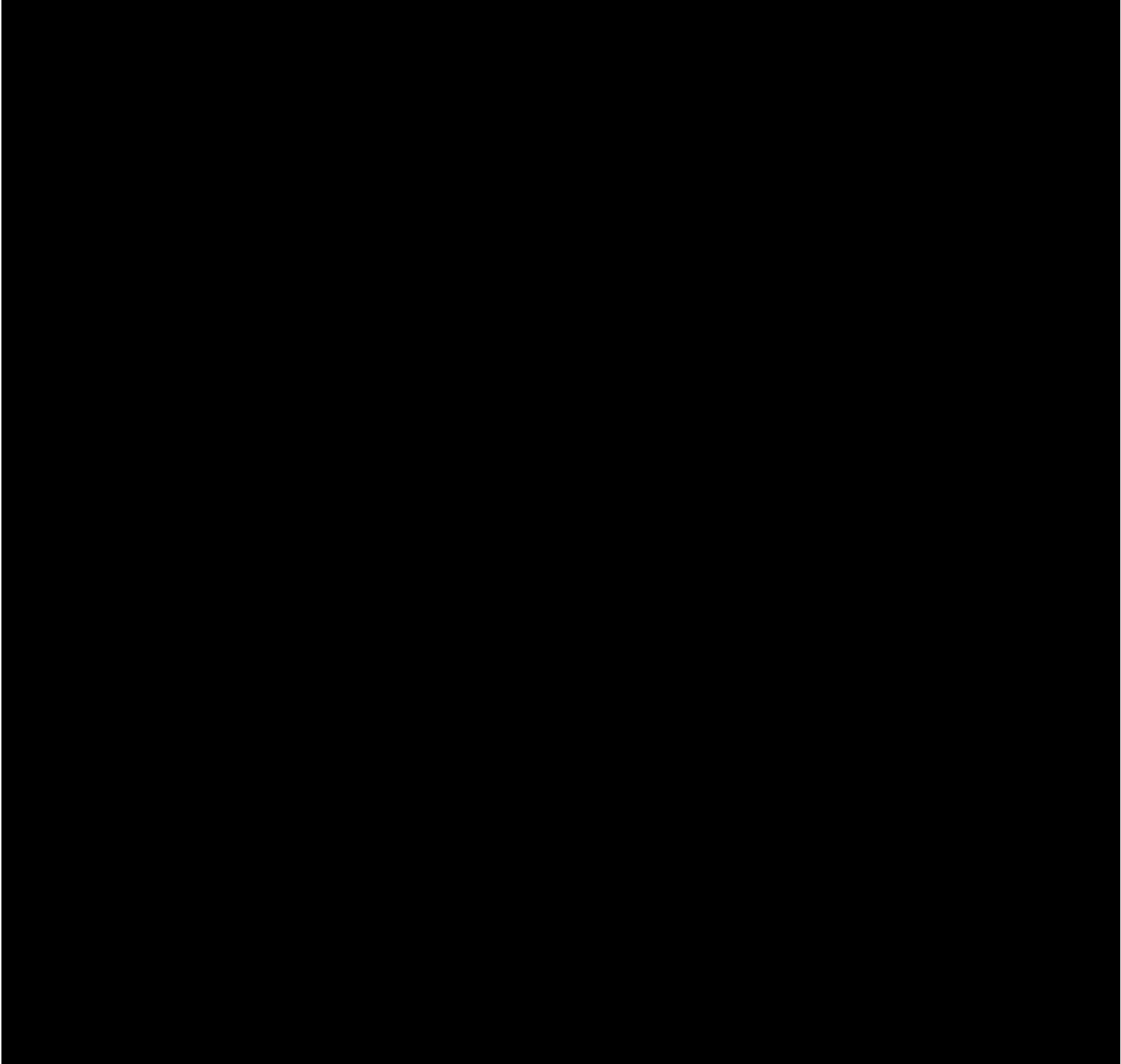


that the diurnal March of the MDR VIP region starts from the southeast corner and the southern tip of the peninsula. Figure 4-2-4(b) and (c)

(continued)



\_\_\_\_\_



4-2-(b) Results at 2 PM

Figure 4-2-6 shows two peak areas of model rainfall are produced at 2 PM: one along the west coast to the north of the lake, and the other along the southwest coast. The rain area covers a large fraction over the western part of southern Florida.

Figure 4-2-7 (reproduced from McQueen and Pielke, 1985) shows the composite satellite

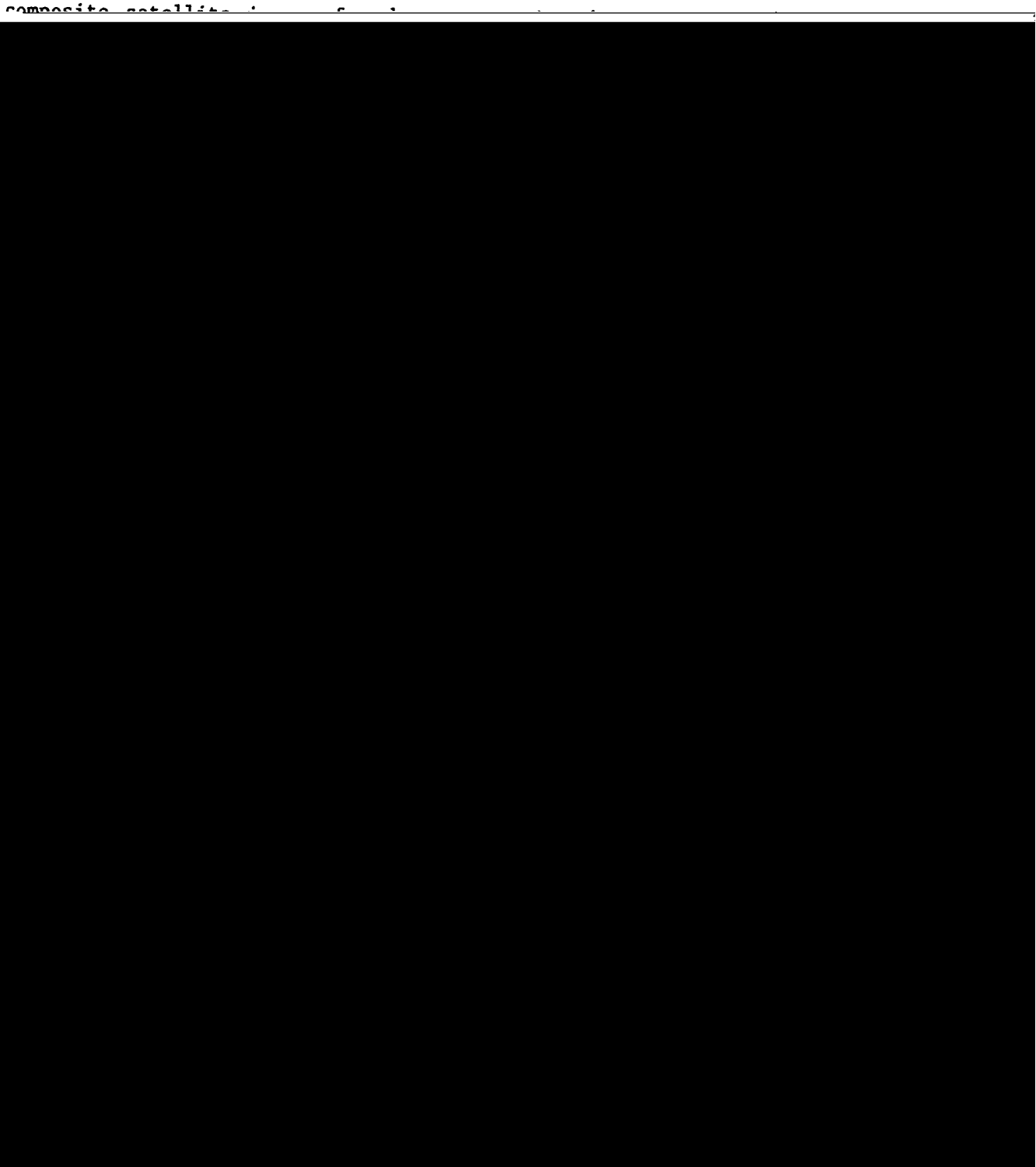
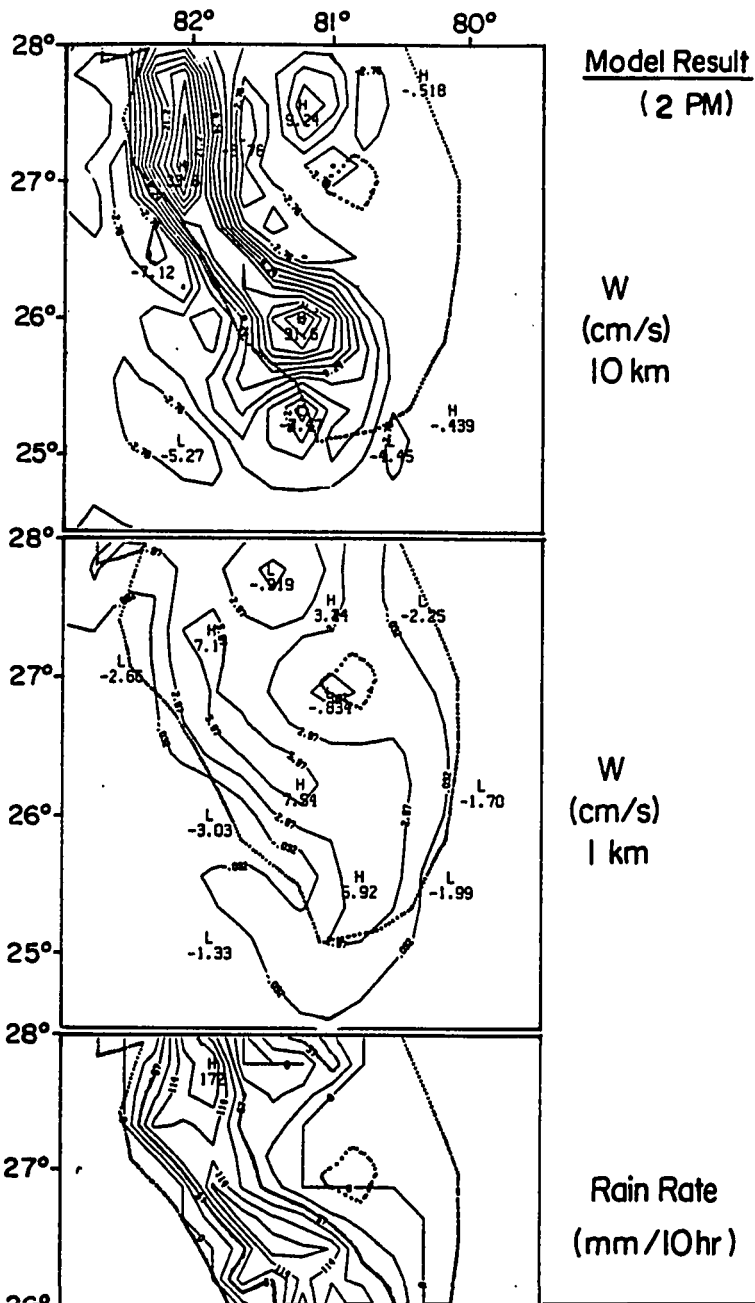
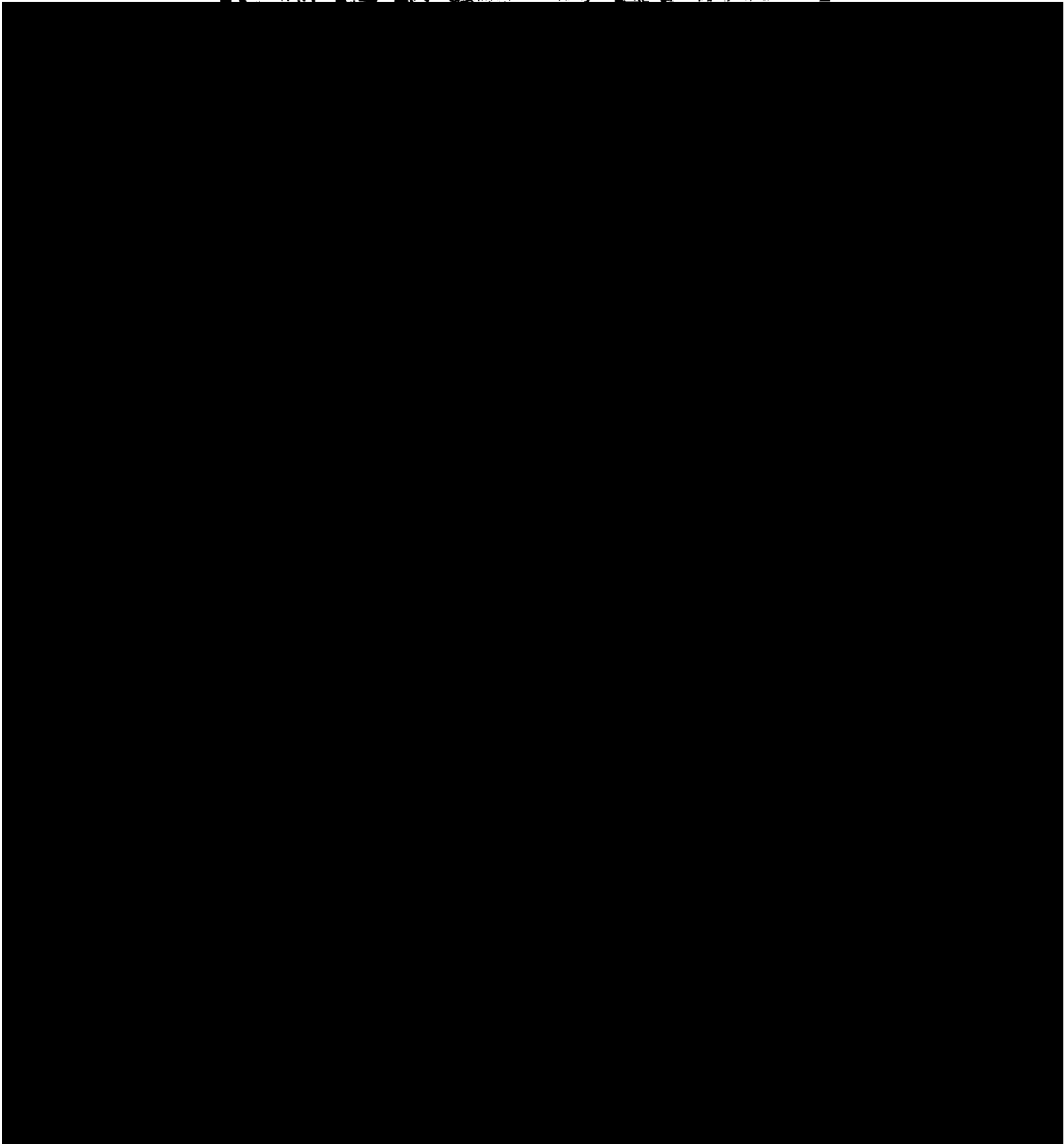
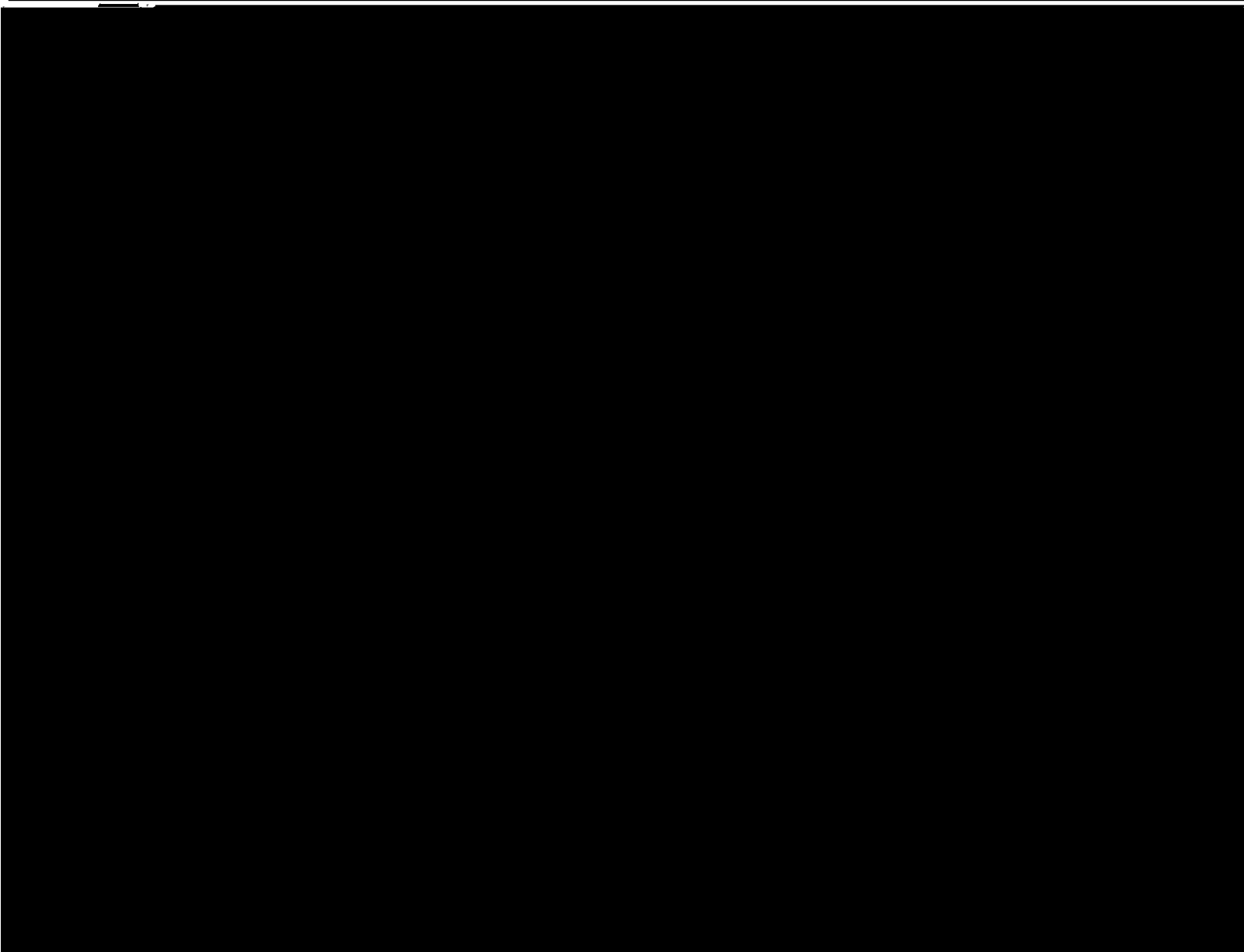
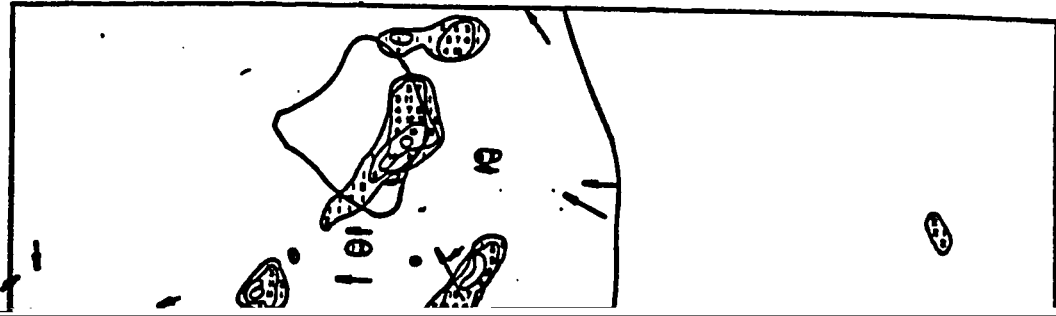


Figure 4-2-6. The model produced horizontal maps of vertical velocity (cm/s) near 10 km (top) and 1 km (middle); and the model rainfall rate (mm/10 hour) (bottom), at 2 PM. The symbol "H" indicate upward motions, while "L" indicate downward motions. The contour interval for the velocities is 3 cm/s, and for the rainfall rates 2.2 mm/hour.







lake generally occurs within the region of model predicted cumulonimbus convection. The agreement with the radar patterns is shown in

---

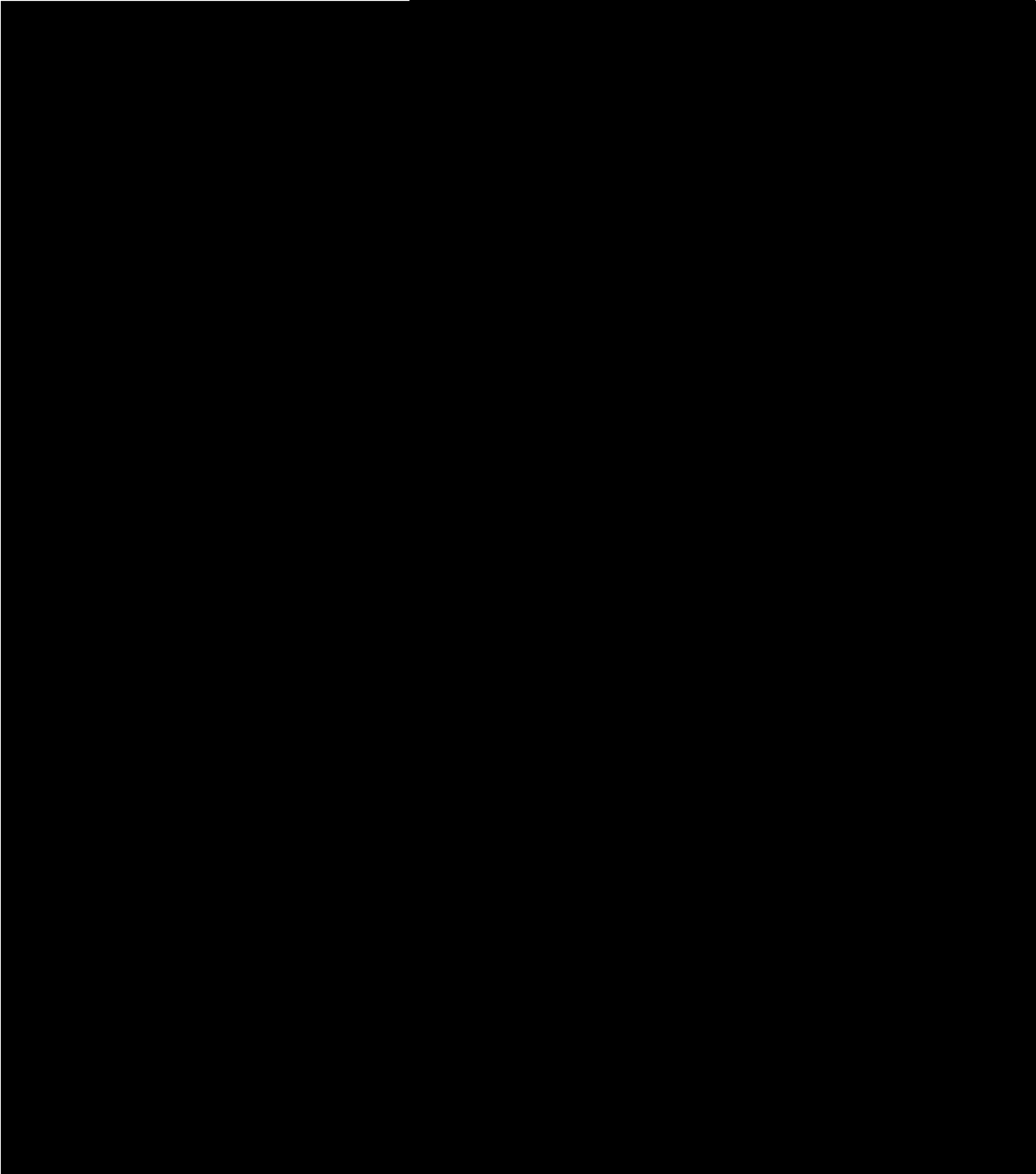
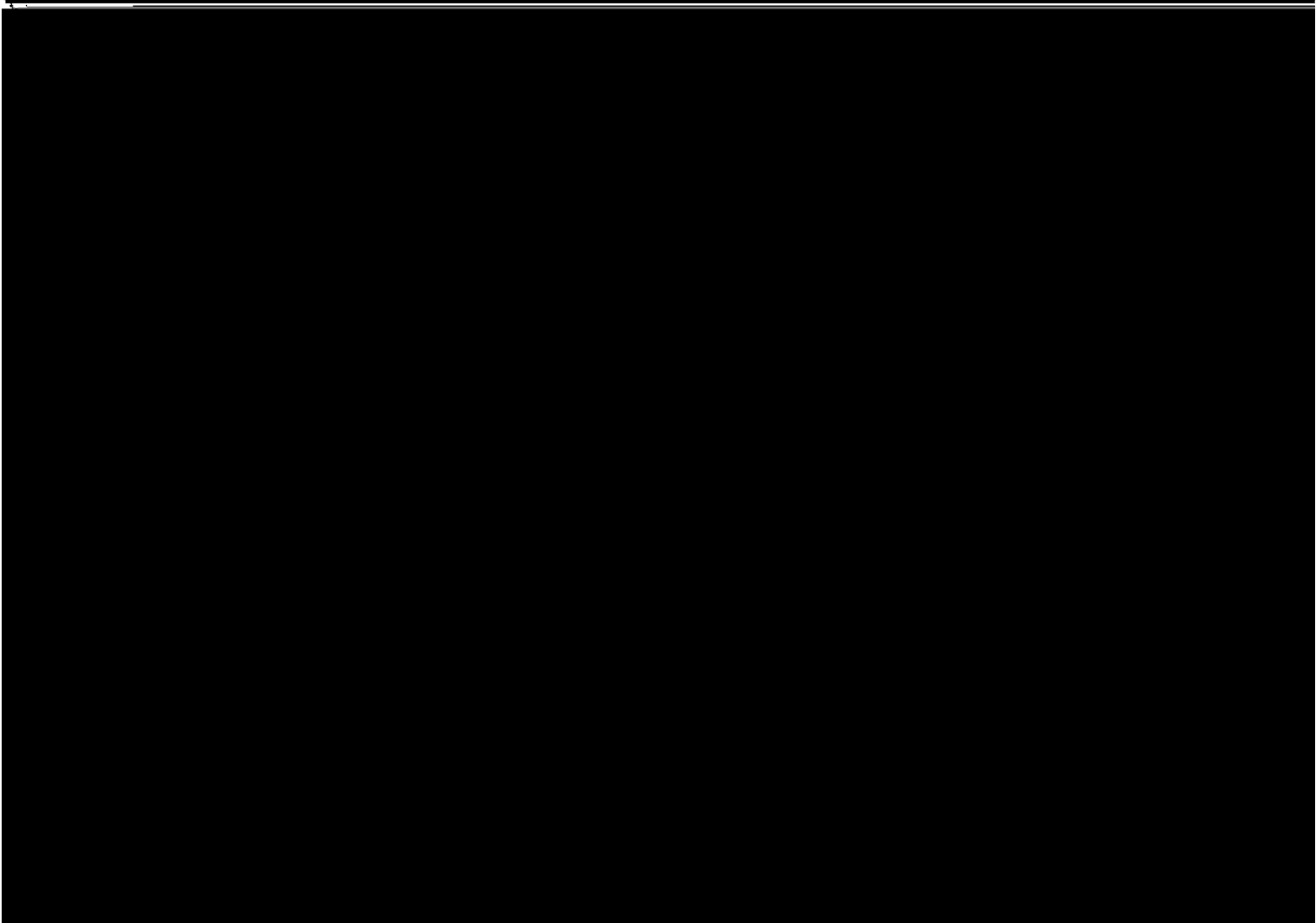
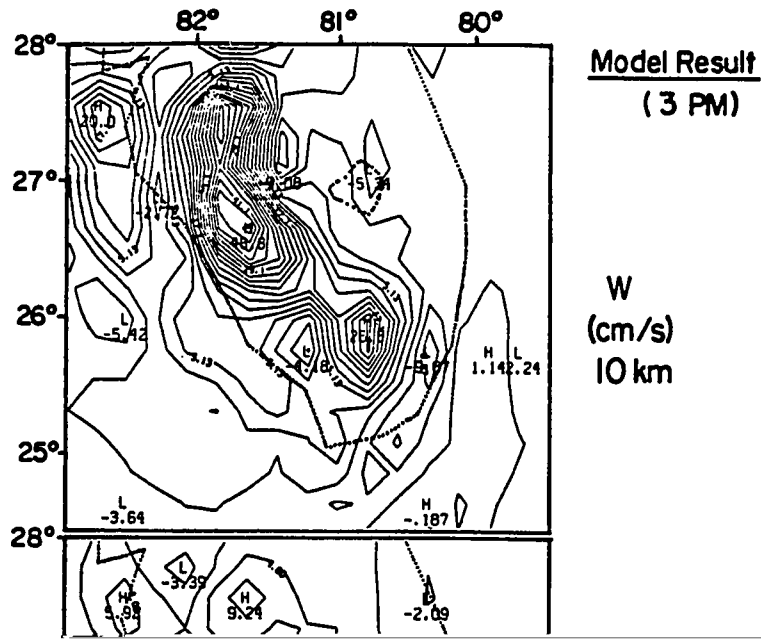
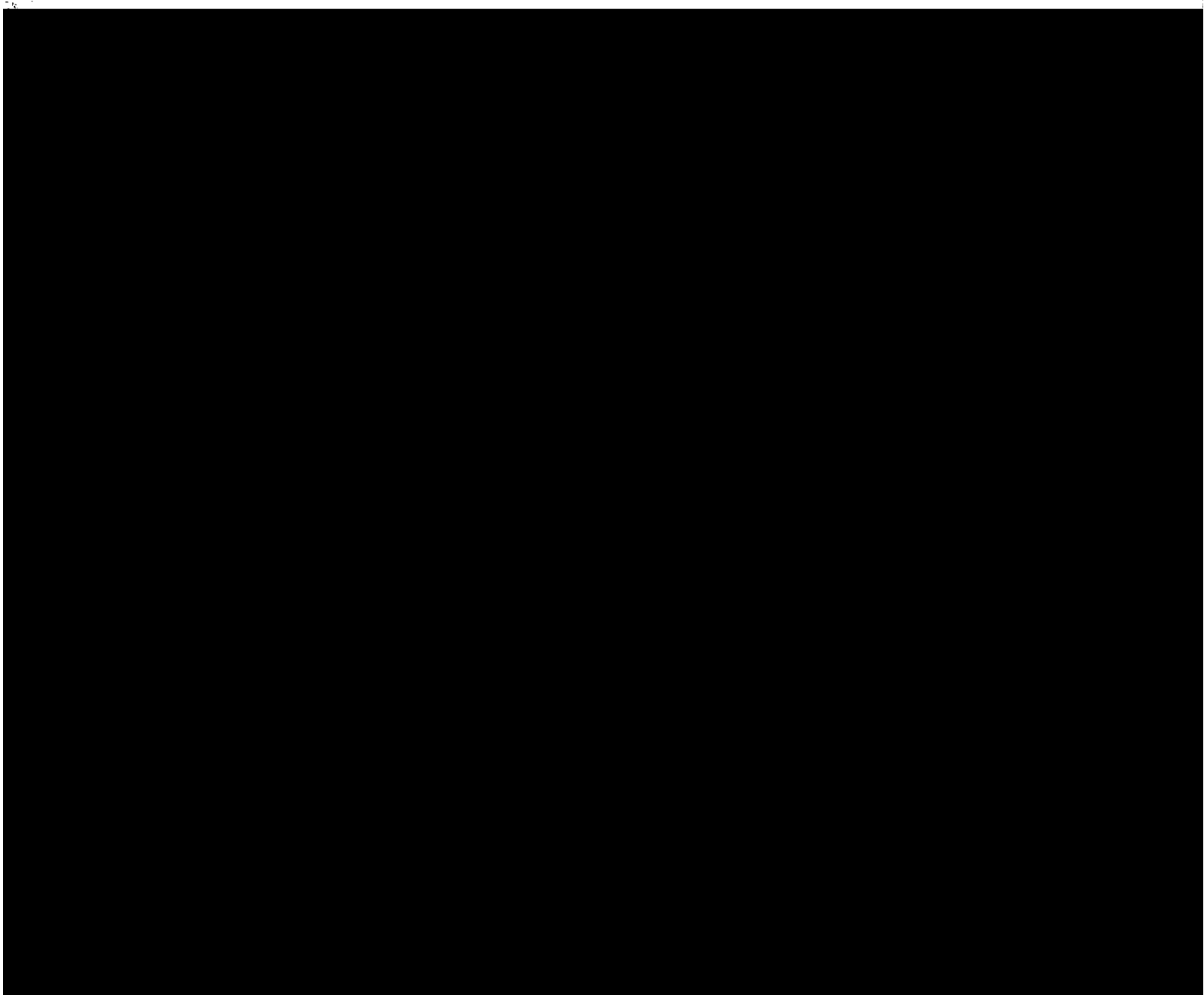
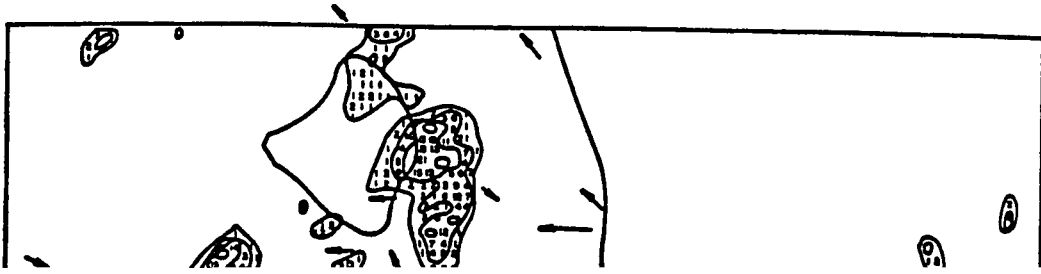


Figure 4-2-9. The model produced horizontal maps of vertical velocity  
(cm/s) near 10 km (top) and 1 km (middle) for 1000 hPa.







- convective surface outflow from nearby earlier deep convective systems to the northeast and to the southwest along the west coast.

Both of these mechanisms enhance low level convergence.

4-2-(d) Results at 4 PM

By 4 PM, Fig. 4-2-11 (top) shows that, due to surface downdraft cooling, the original sea breeze convergence zone has become associated with downward motion, while on its east and west sides upward motions are found. The simulated results at 4 PM are shown in Fig. 4-2-11 (bottom).

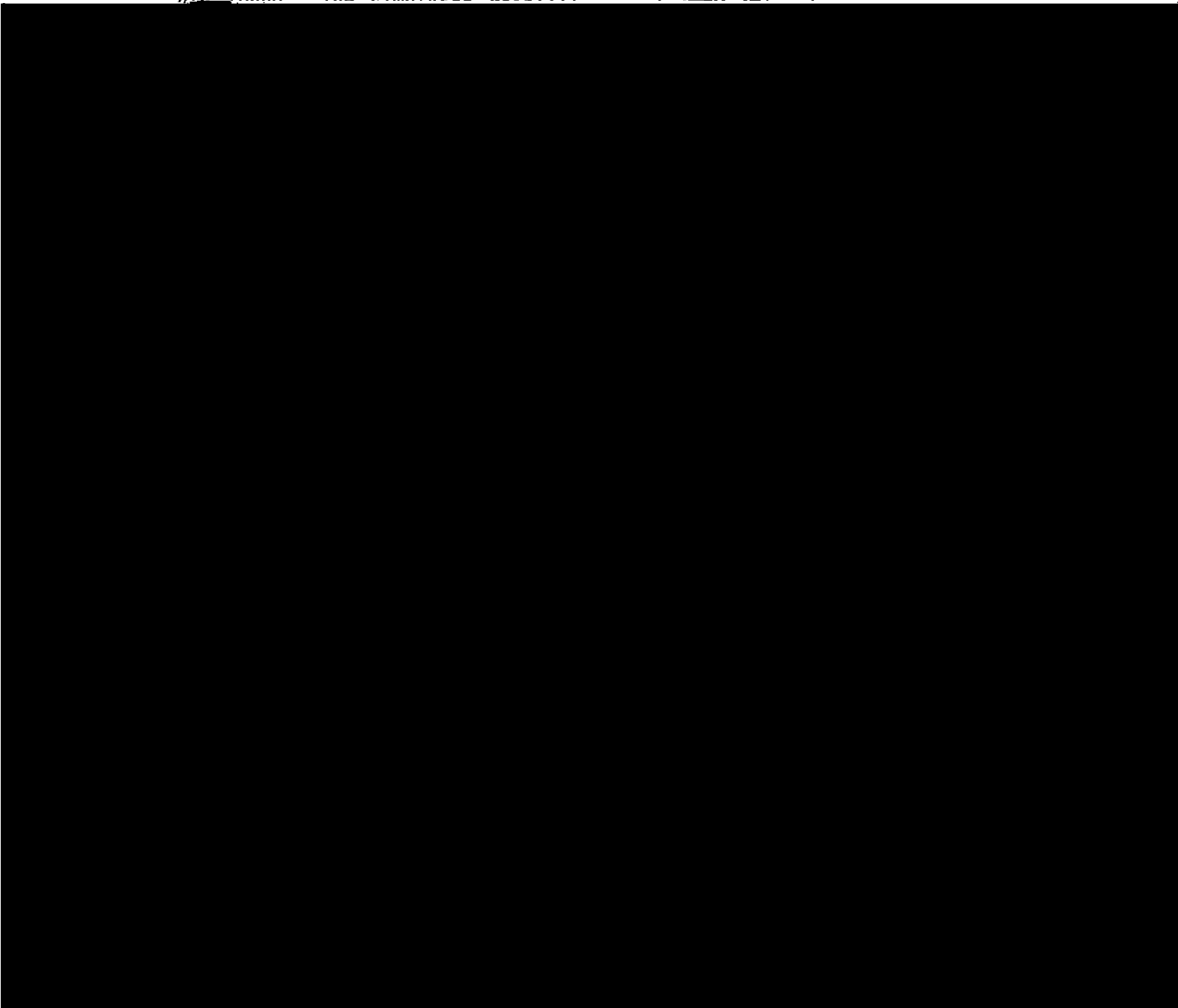
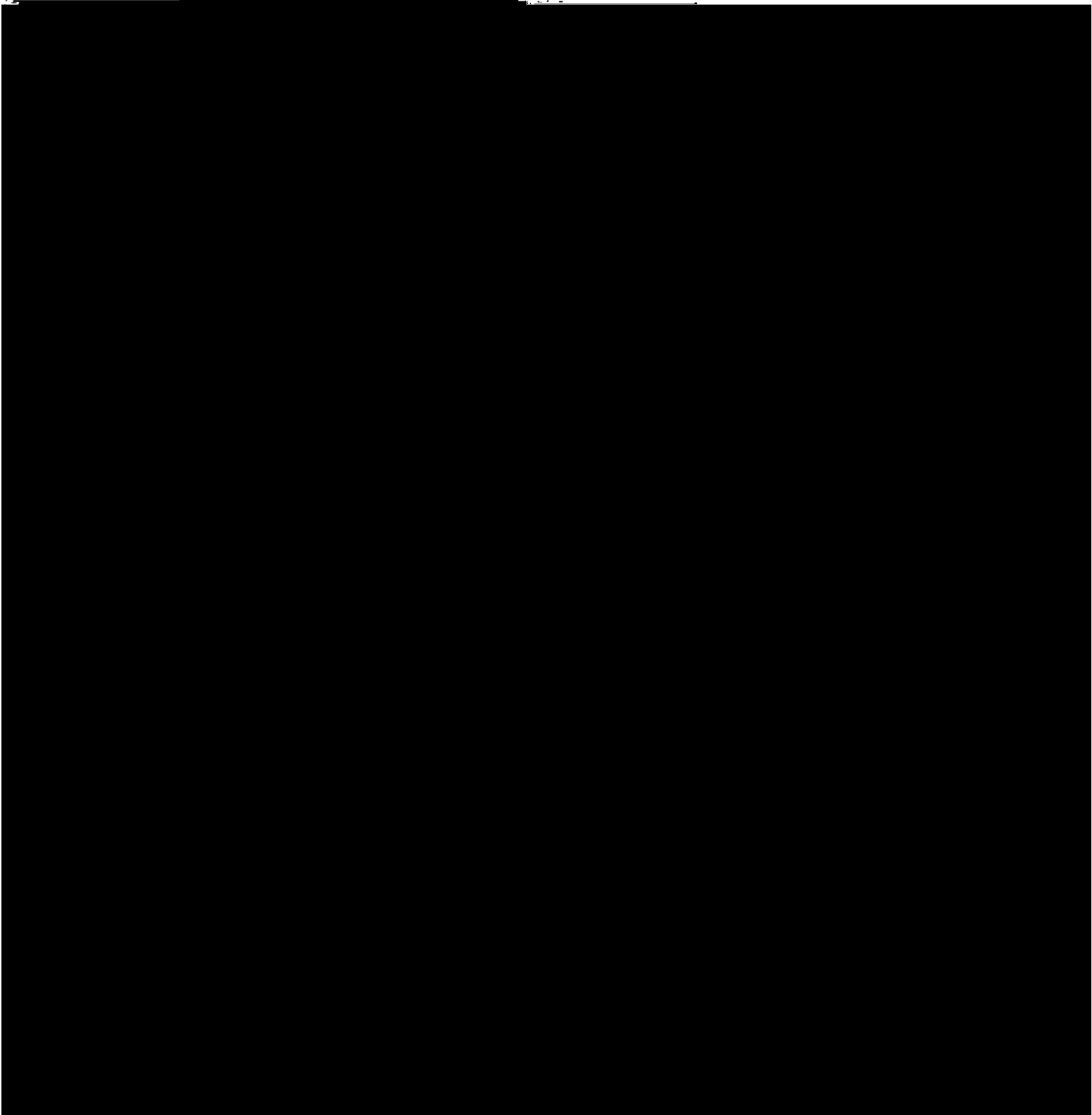
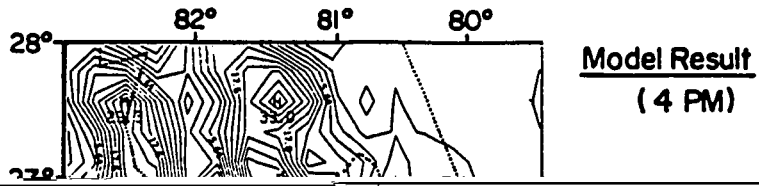
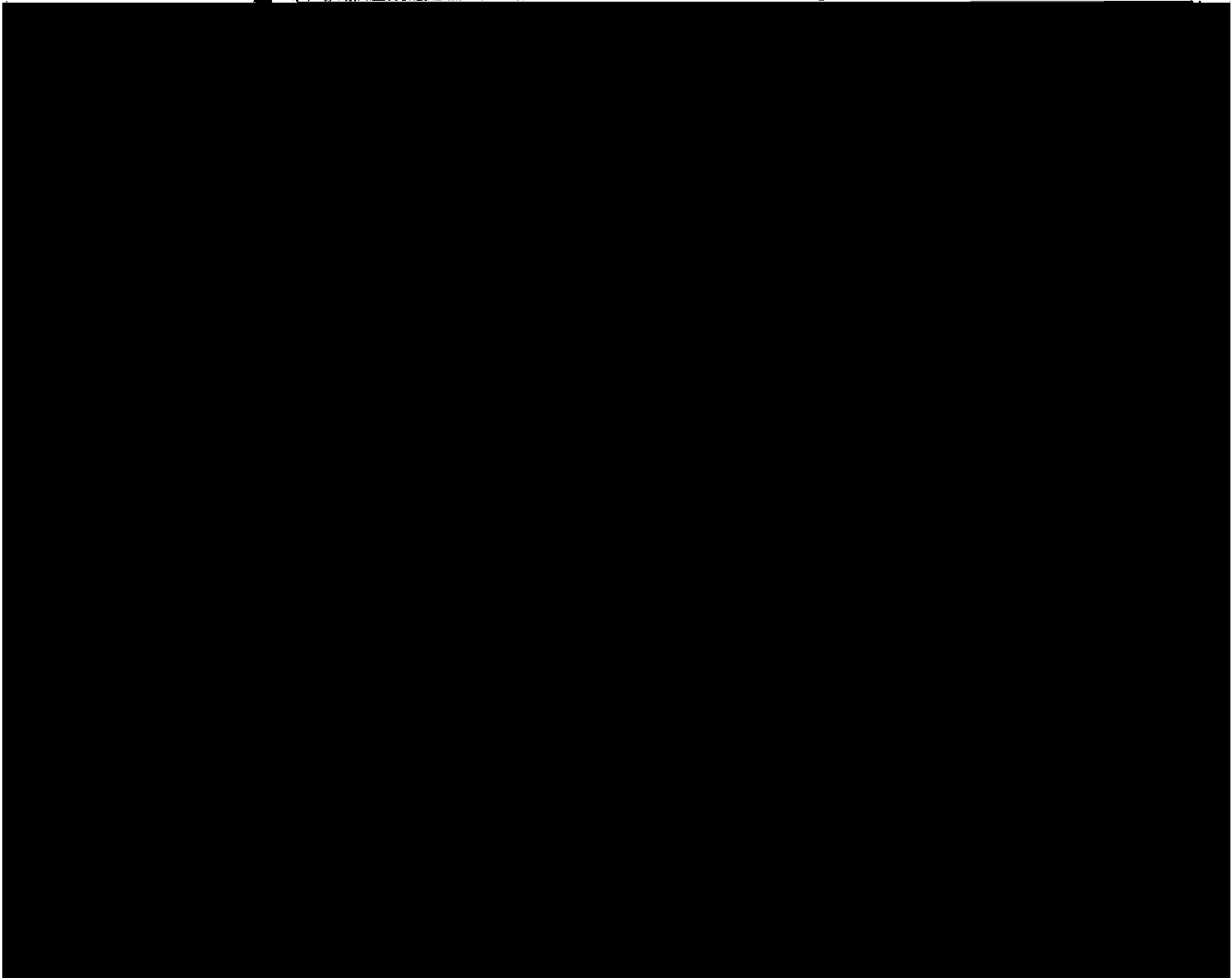
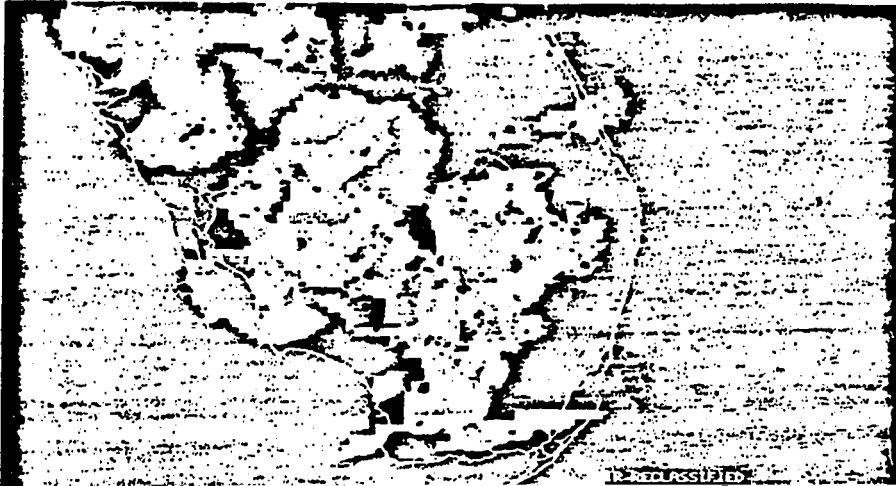


Figure 4-2-11. The model produced horizontal maps of vertical velocity (cm/s) near 10 km (top) and 1 km (middle); and the model rainfall rate (mm/10 hour) (bottom), at 4 PM. The symbol "H" indicate upward motions, while "L" indicate downward motions. The contour interval for the velocities is 3 cm/s, and for the rainfall rates 2.2 mm/hour.





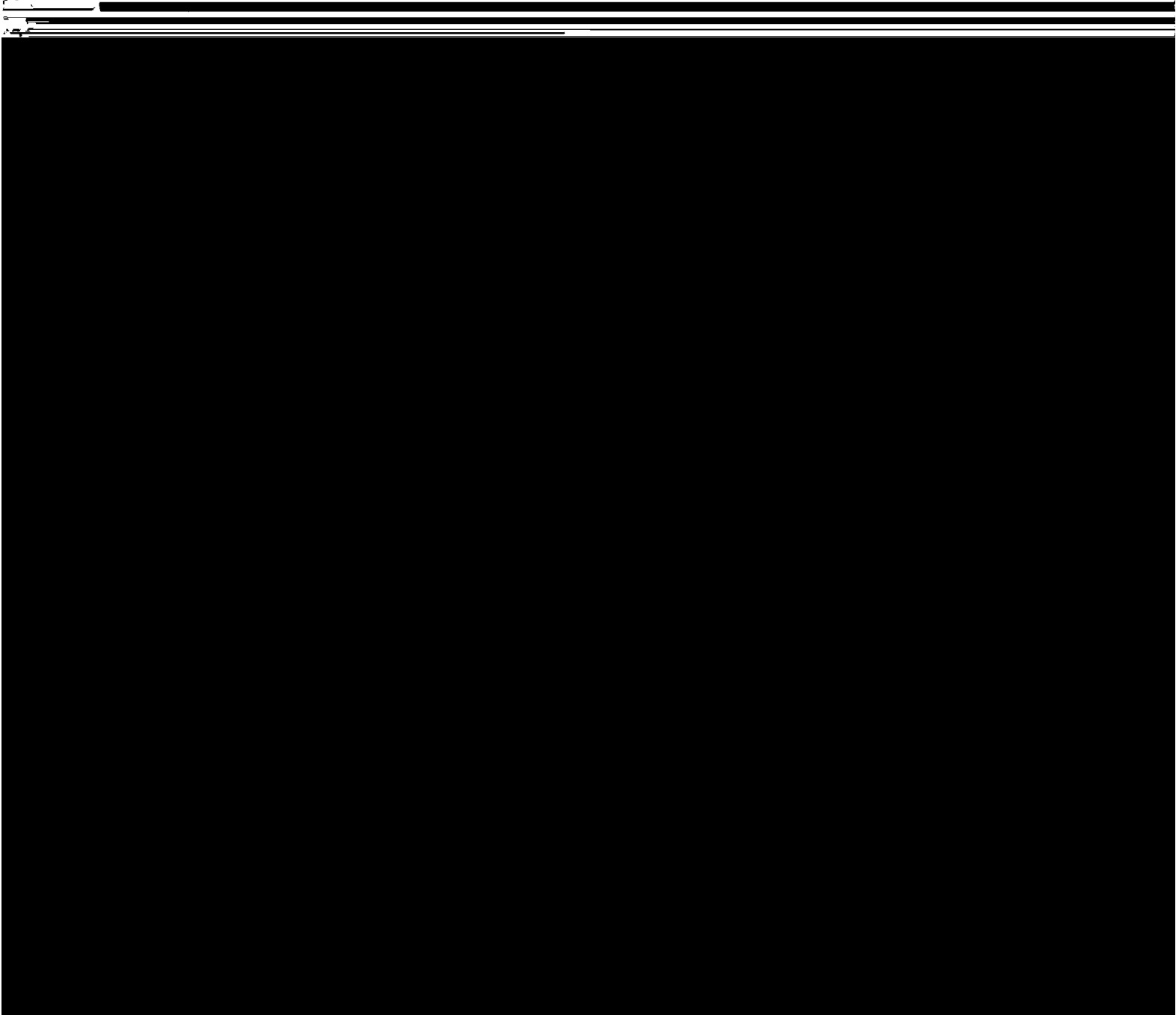
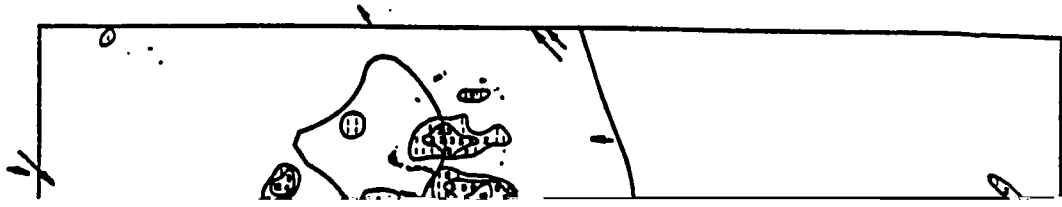


Fig. 4-2-10) that the southern part of the peninsula became essentially free of convection. The original tendency for elongated convective zones have become replaced by locally enhanced convective systems by 4 PM. This indicates the mature convective development is no longer

within the - - - - -

---

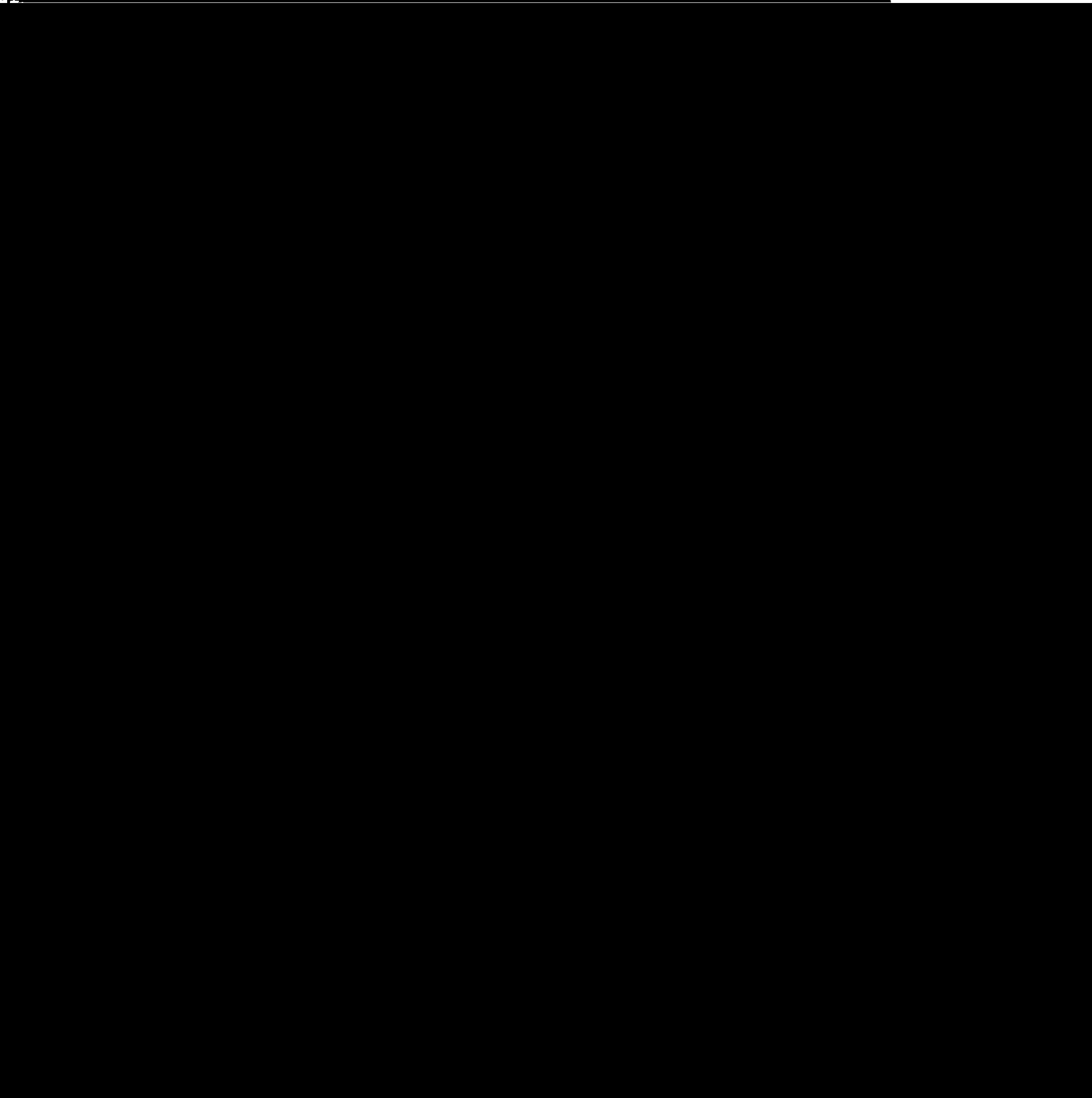
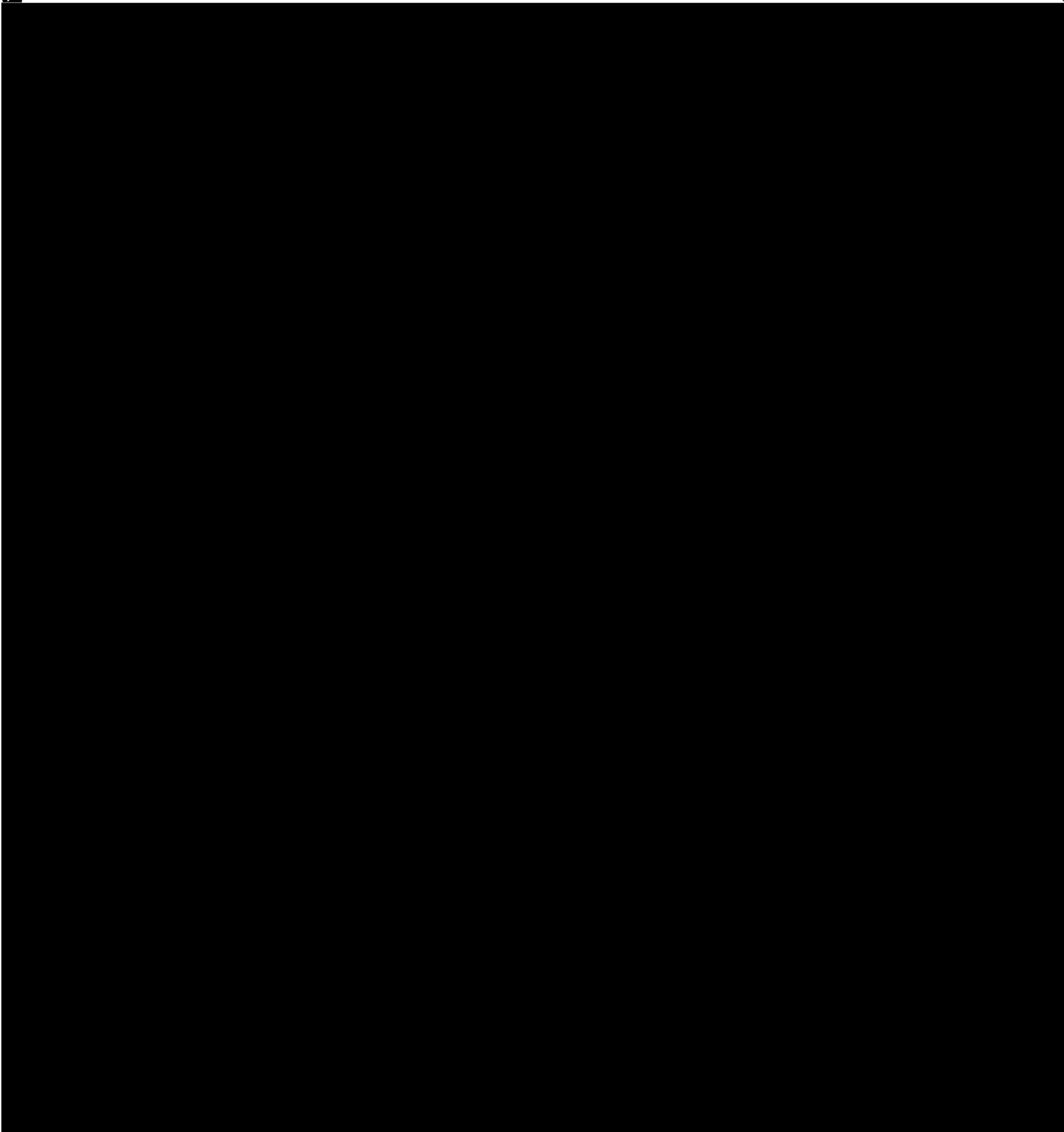
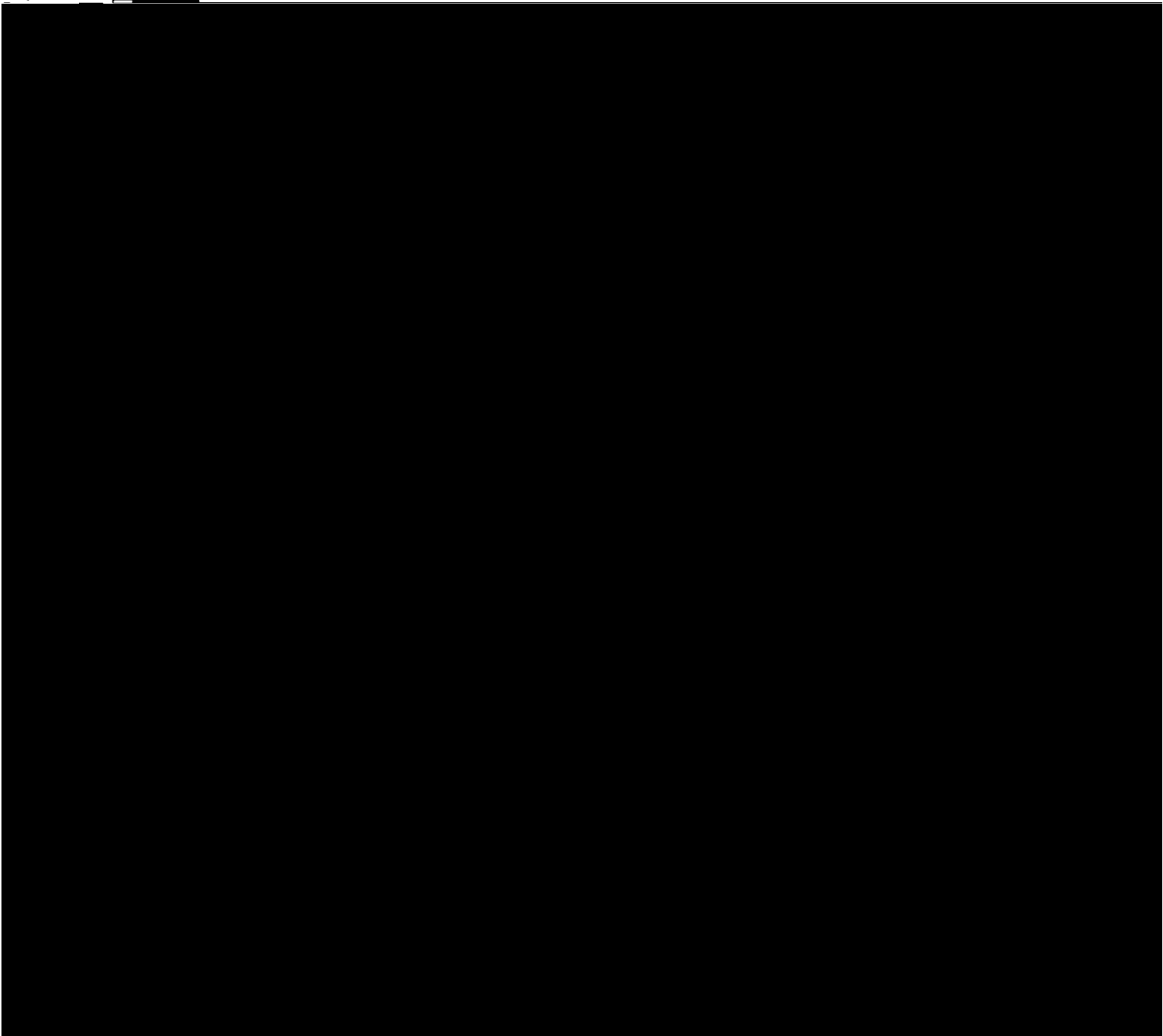
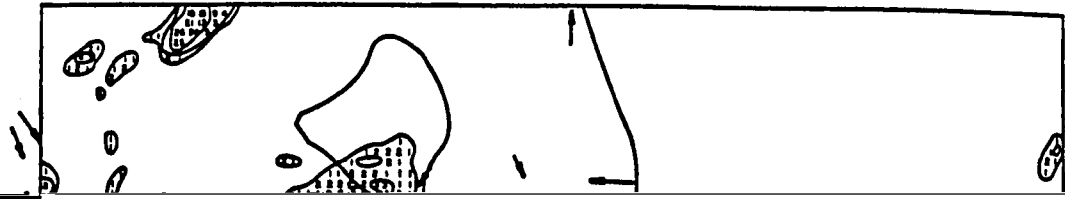
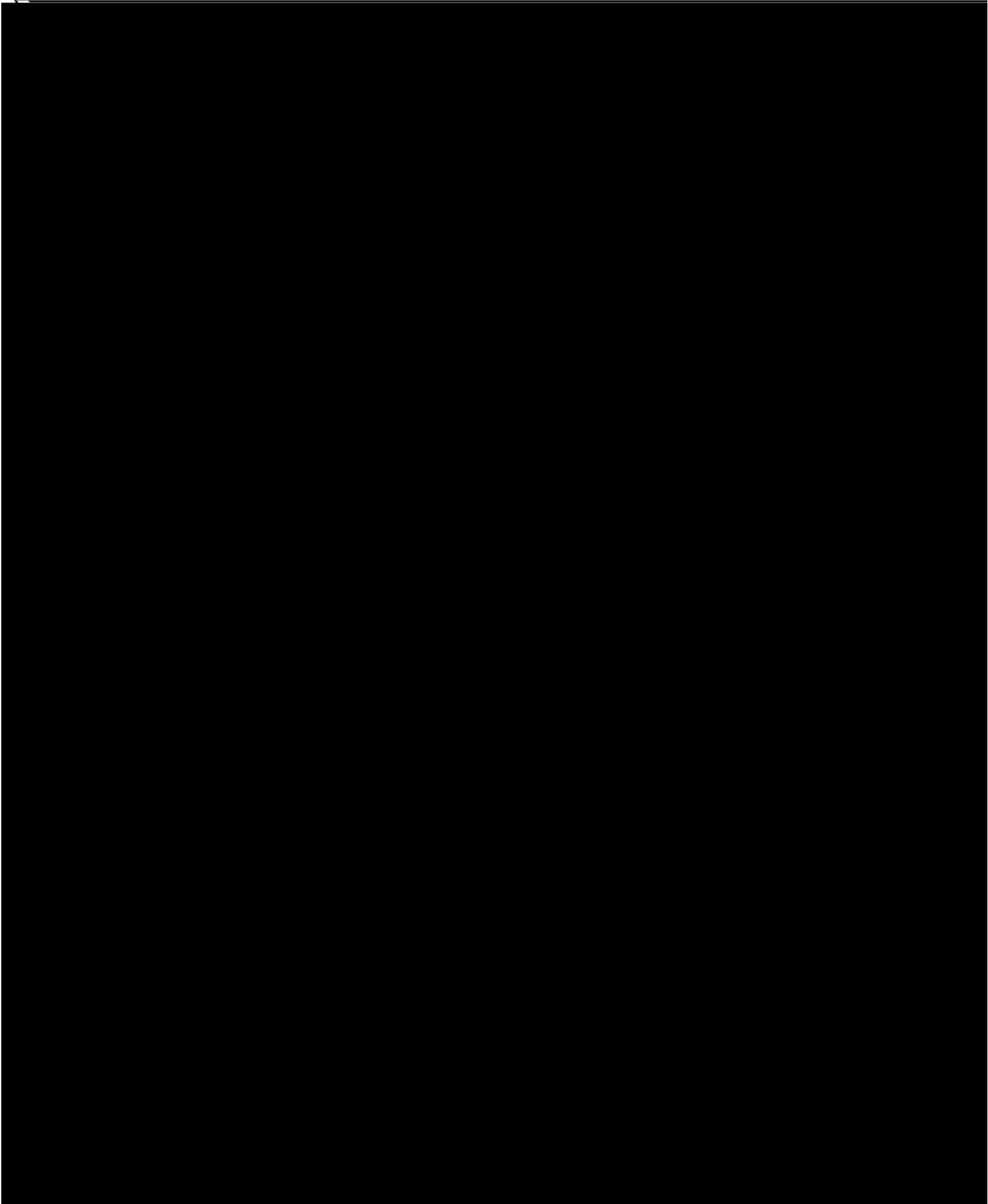


Figure 4-2-14. The model produced horizontal maps of vertical velocity (cm/s) near 10 km (top) and 1 km (middle); and the model rainfall rate (mm/10 hour) (bottom), at 5 PM. The symbol "H" indicate upward motions, while "L" indicate downward motions. The contour interval for the velocities is 3 cm/s, and for the rainfall rates 2.2 mm/hour.







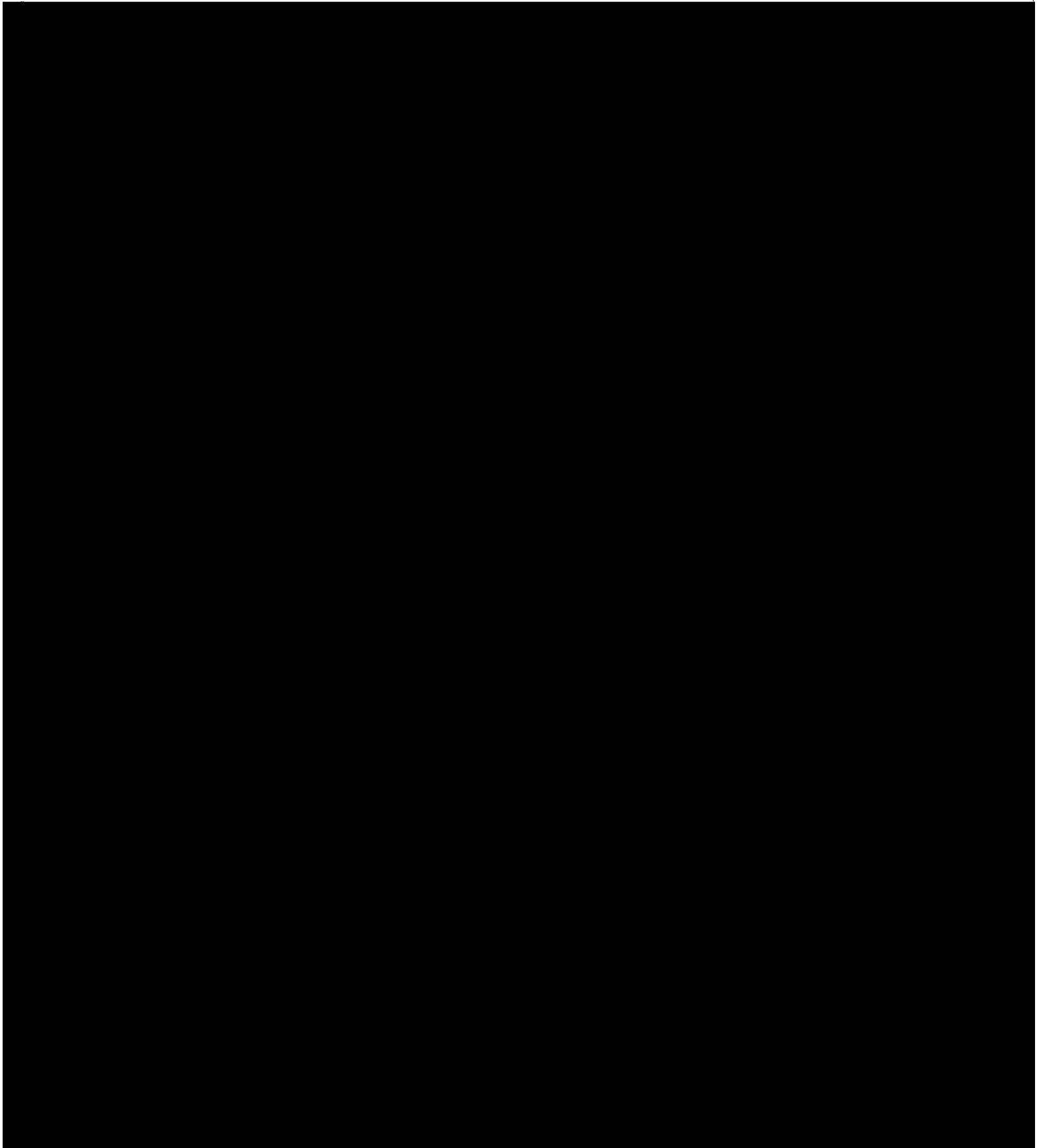
Horizontal Divergence ( $10^{-4}\text{s}^{-1}$ ) at 9m. (1 PM)

82°

81°

80°

80°

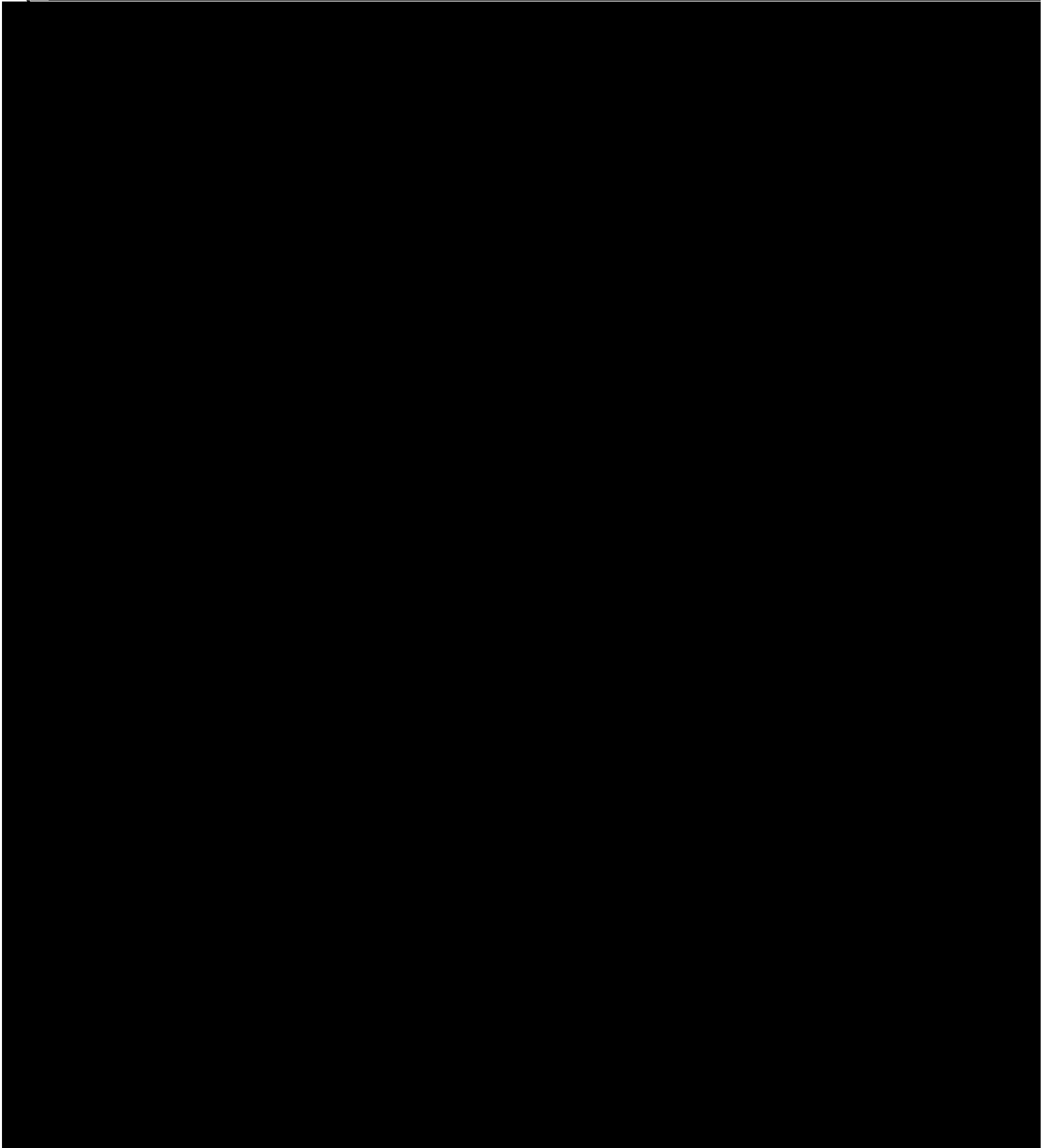


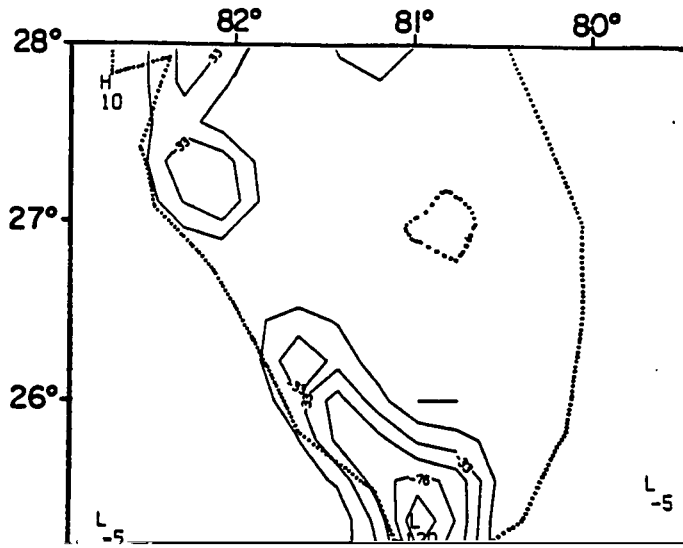
is producing a dramatically different surface divergence pattern. The

deep convection pattern is

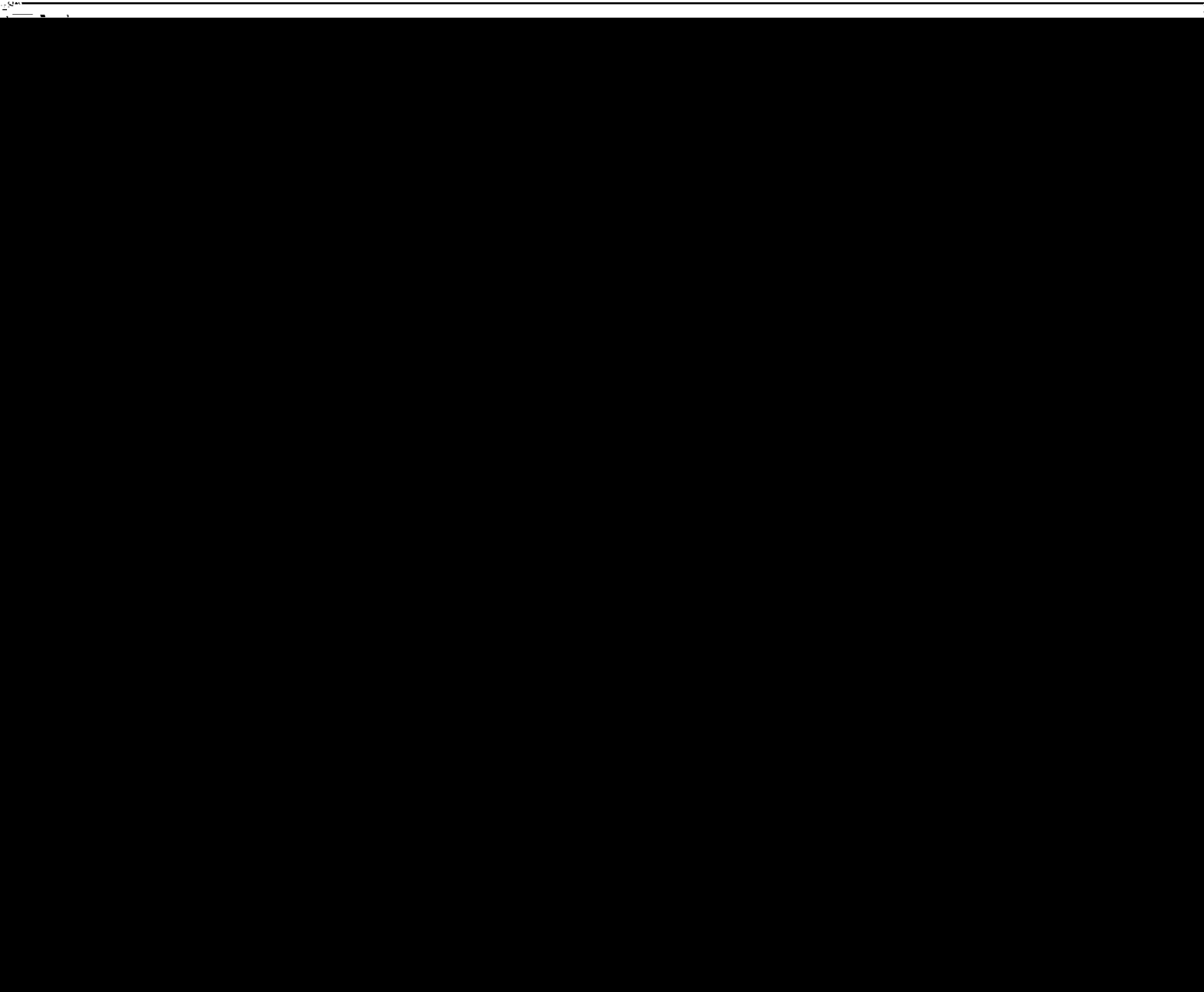
---

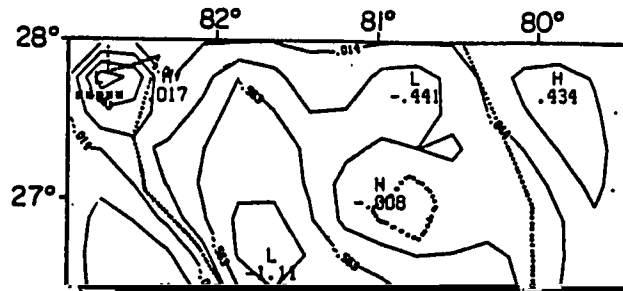
---





(a) total-dry  
( 1 PM )  
Potential  
Temperature



Horizontal Divergence ( $10^{-4} s^{-1}$ ) at 9m. (2 PM)

et al., 1980). The enlarged surface cooling is clearly seen in Fig. 4-3-4 (top). This cooling generates horizontal flows at 9 m (Fig. 4-3-4, bottom).

By 3 PM, Fig. 4-3-5 shows that due to the downdraft cooling, a continuous zone with deep cumulus convection (indicated by the surface divergence) is formed. Comparing Fig. 4-3-5 (top) with Fig. 4-3-1 (top) we see that the

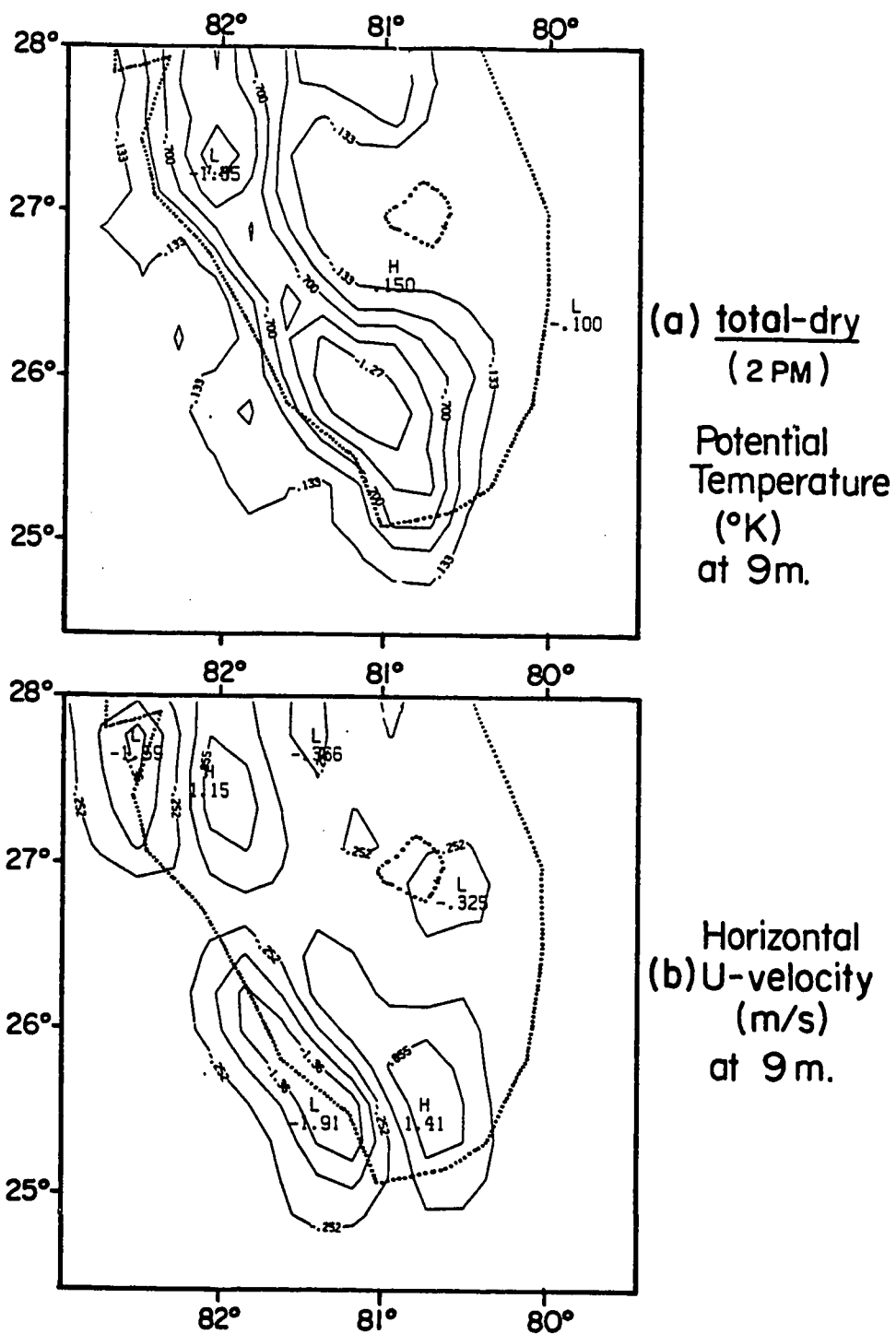
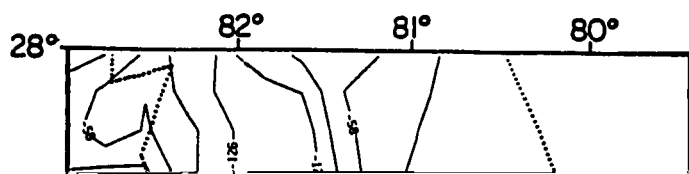


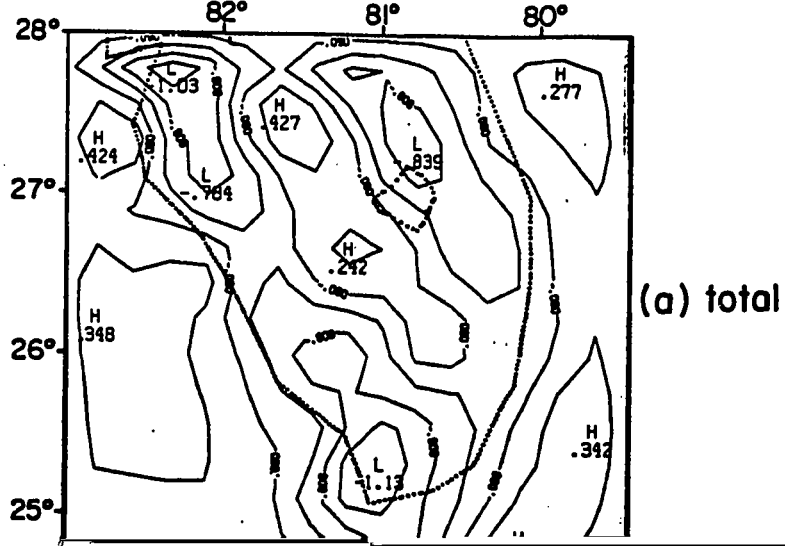
Figure 4-3-4. The "total-dry" quantities at 9 m at 2 PM, including (a) potential temperature (note magnitudes are scaled by 100) and (b) horizontal u-velocity (m/s).

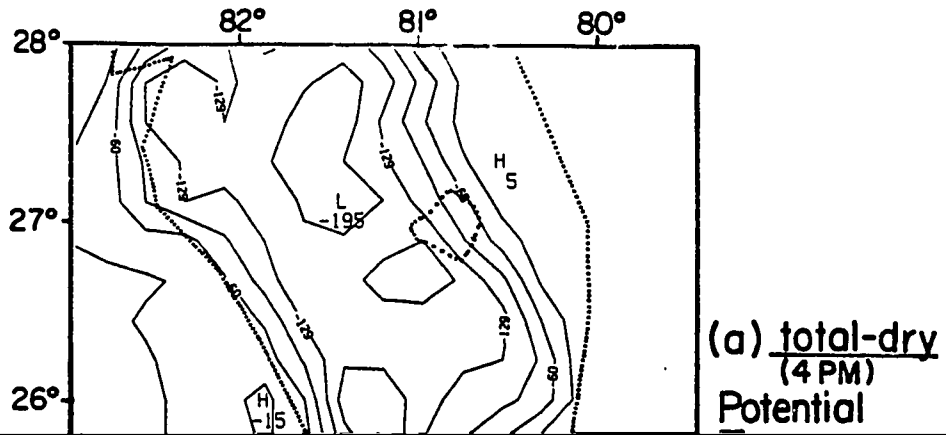
Horizontal Divergence ( $10^{-4} \text{ s}^{-1}$ ) at 9m (3PM)

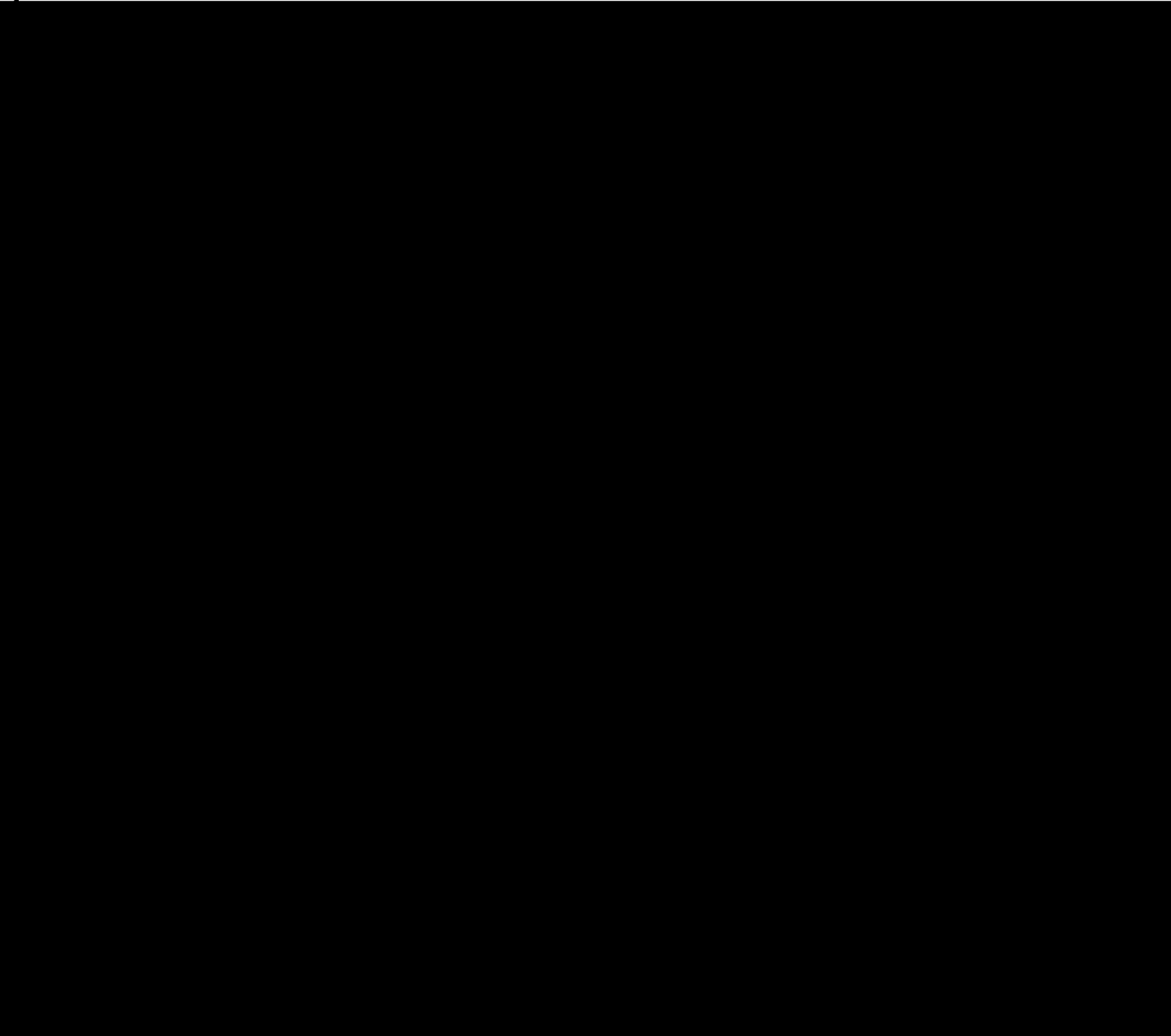




Horizontal Divergence ( $10^{-4} s^{-1}$ ) at 9m. (4PM)





- (1) The deep convective area (Fig. 4-3-5, bottom) matches well with the original sea breeze convergence zone (Fig. 4-3-1, top), suggesting clearly that the sea breeze provides the necessary favorable preconditioned environment for deep convection to grow (Pielke, 1978; Lopze et al., 1984a,b).
  - (2) The peninsular or mesoscale surface divergence pattern can be rather significantly modified on the local area due to de-
- 
- 

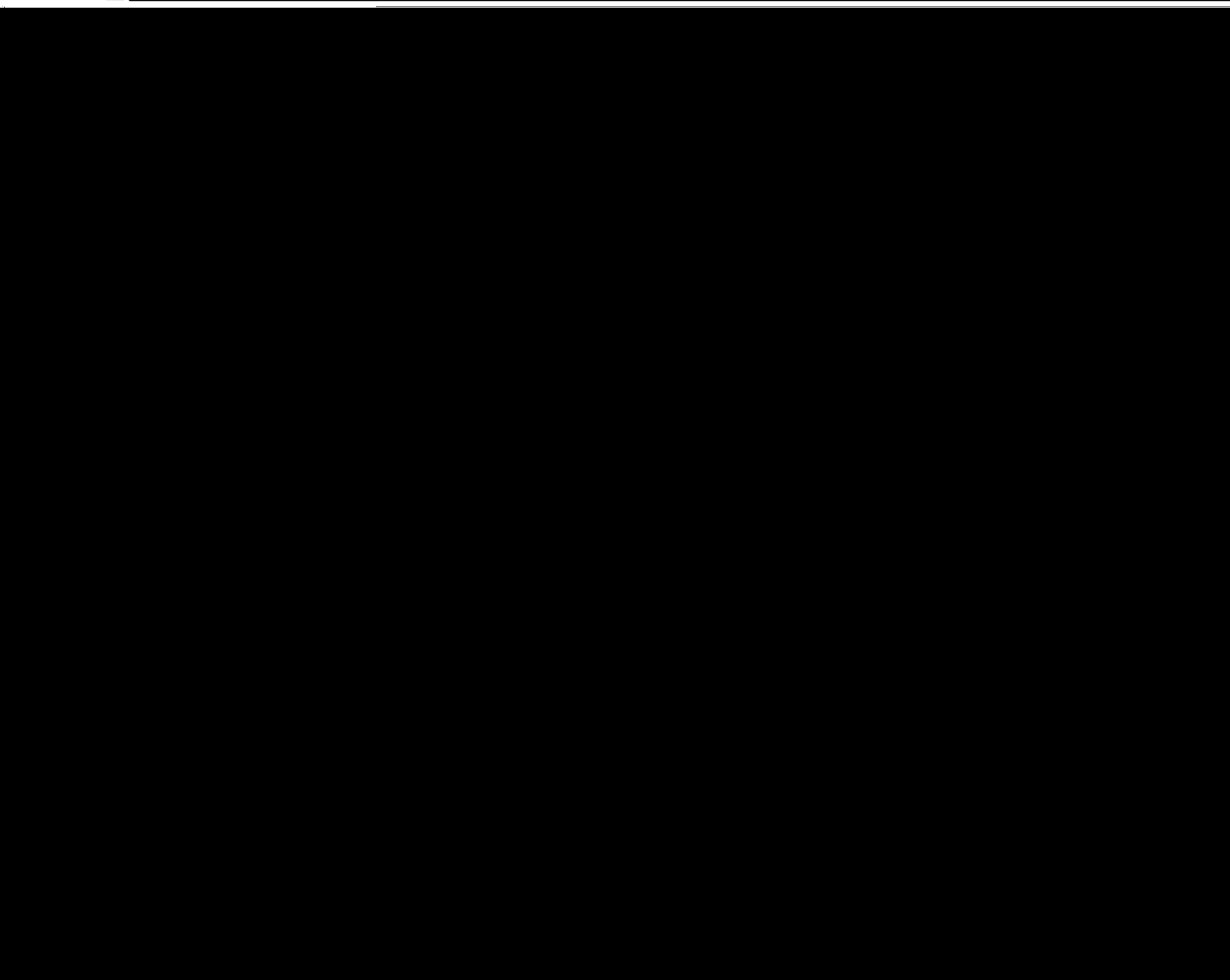


4-4 Deep Cumulus Convective Effects Upon the Peninsula-Scale Tropospheric Flow

Convective-produced effects on the surface flow have been illustrated in the previous section. The parameterized cumulonimbus effect upon the upper troposphere will be illustrated in this section.

Unfortunately, very little has been reported in the literature concerning deep convective-induced mesoscale tropospheric circulations for the Florida environment. Therefore it is necessary to compare several of the model results with observed deep convective activities in other areas. In the following figures, the pure convectively induced mesoscale circulations will be illustrated at 3 DM and 4 DM

---



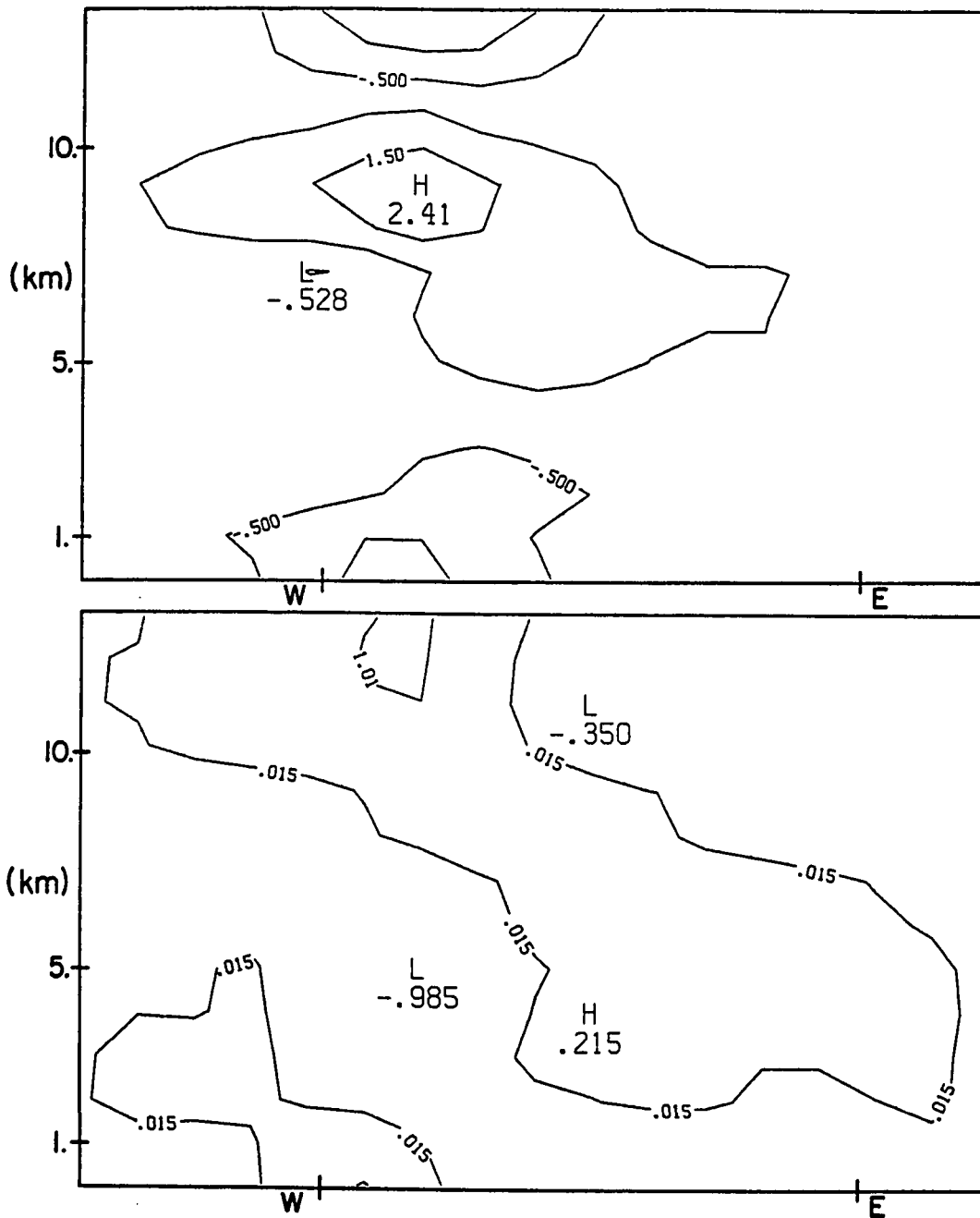
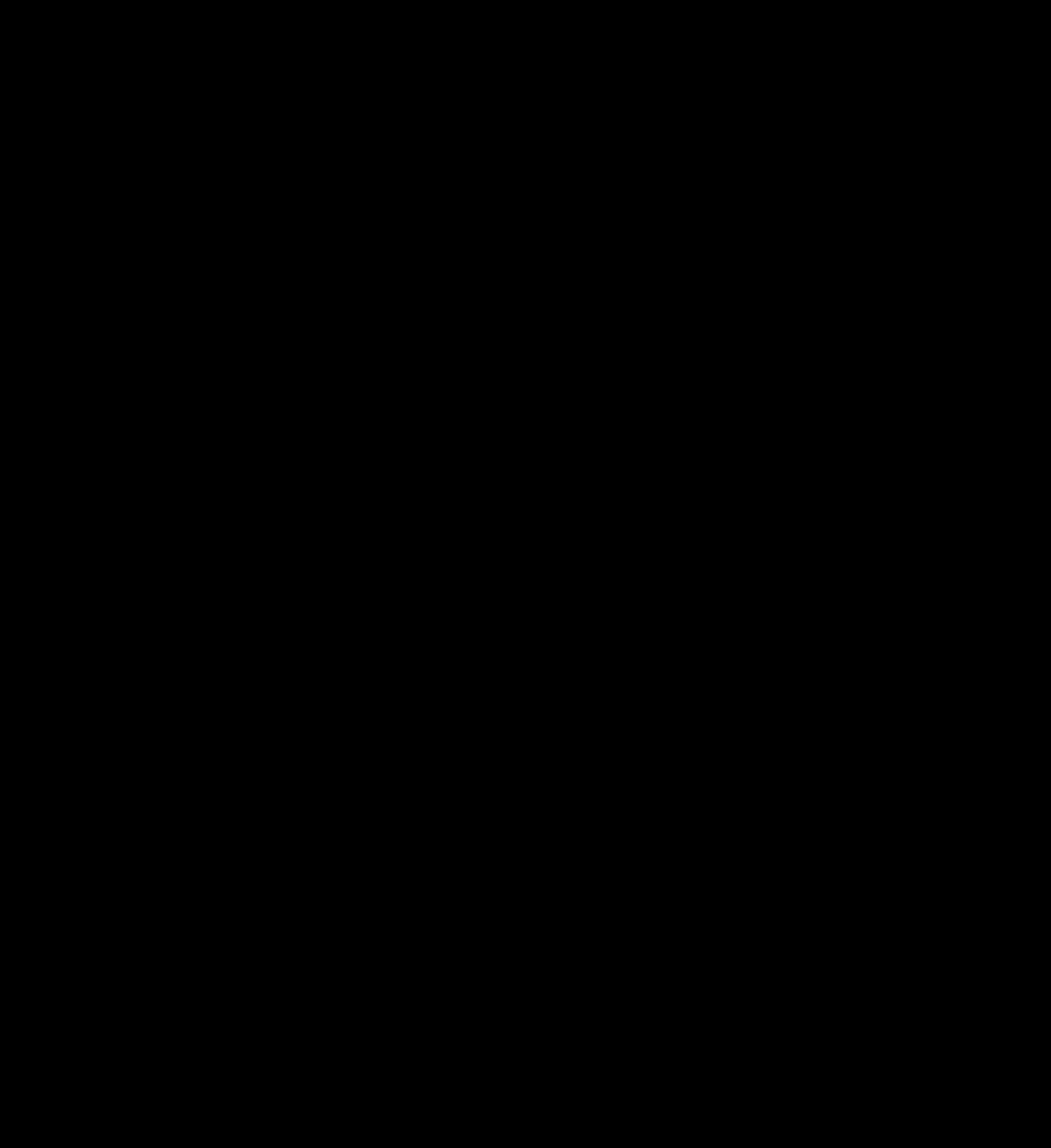
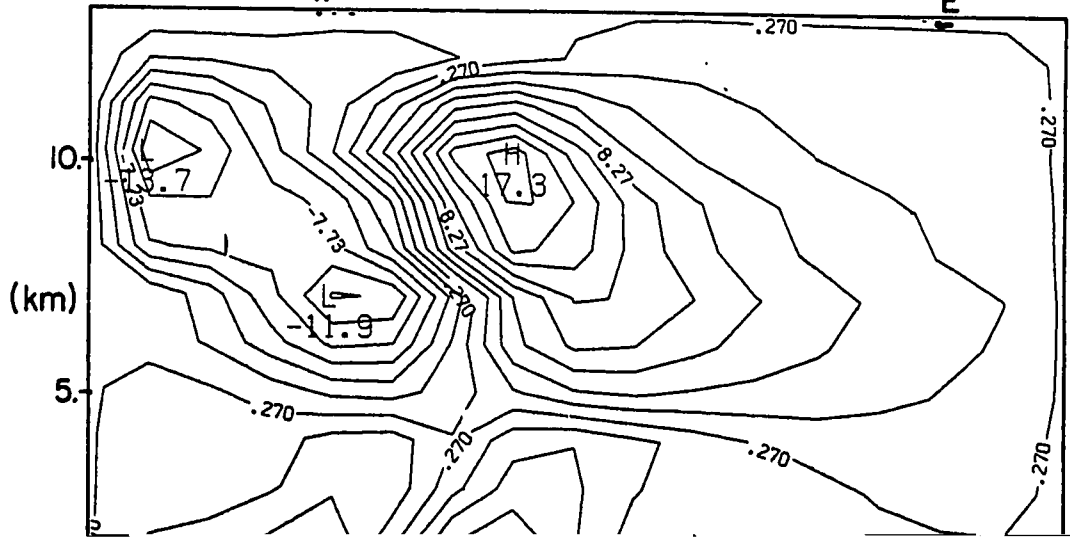
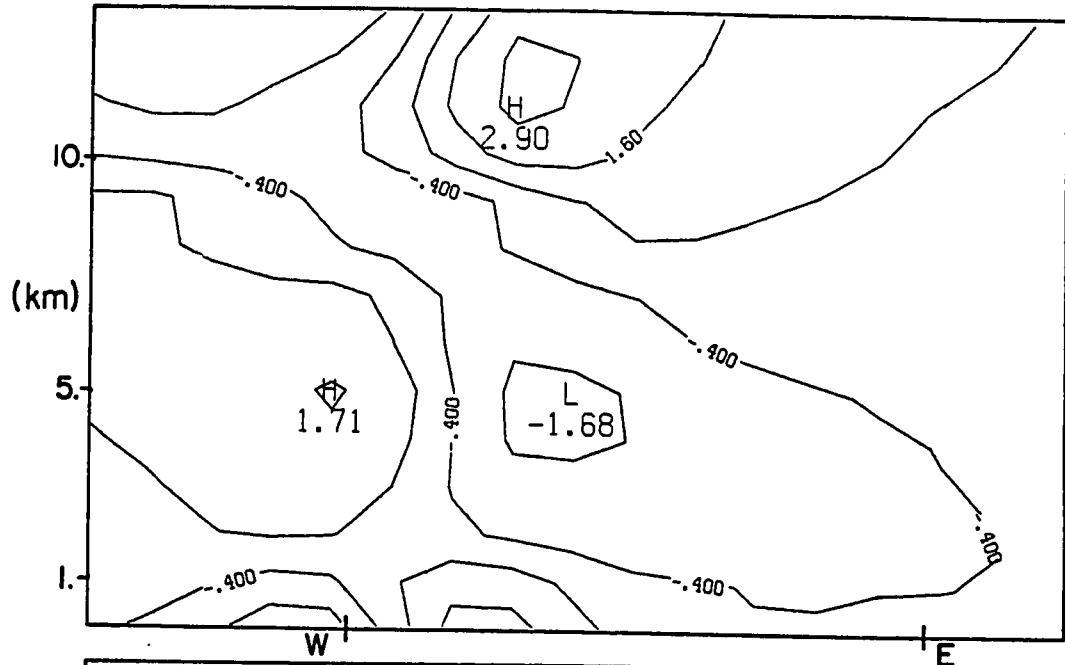
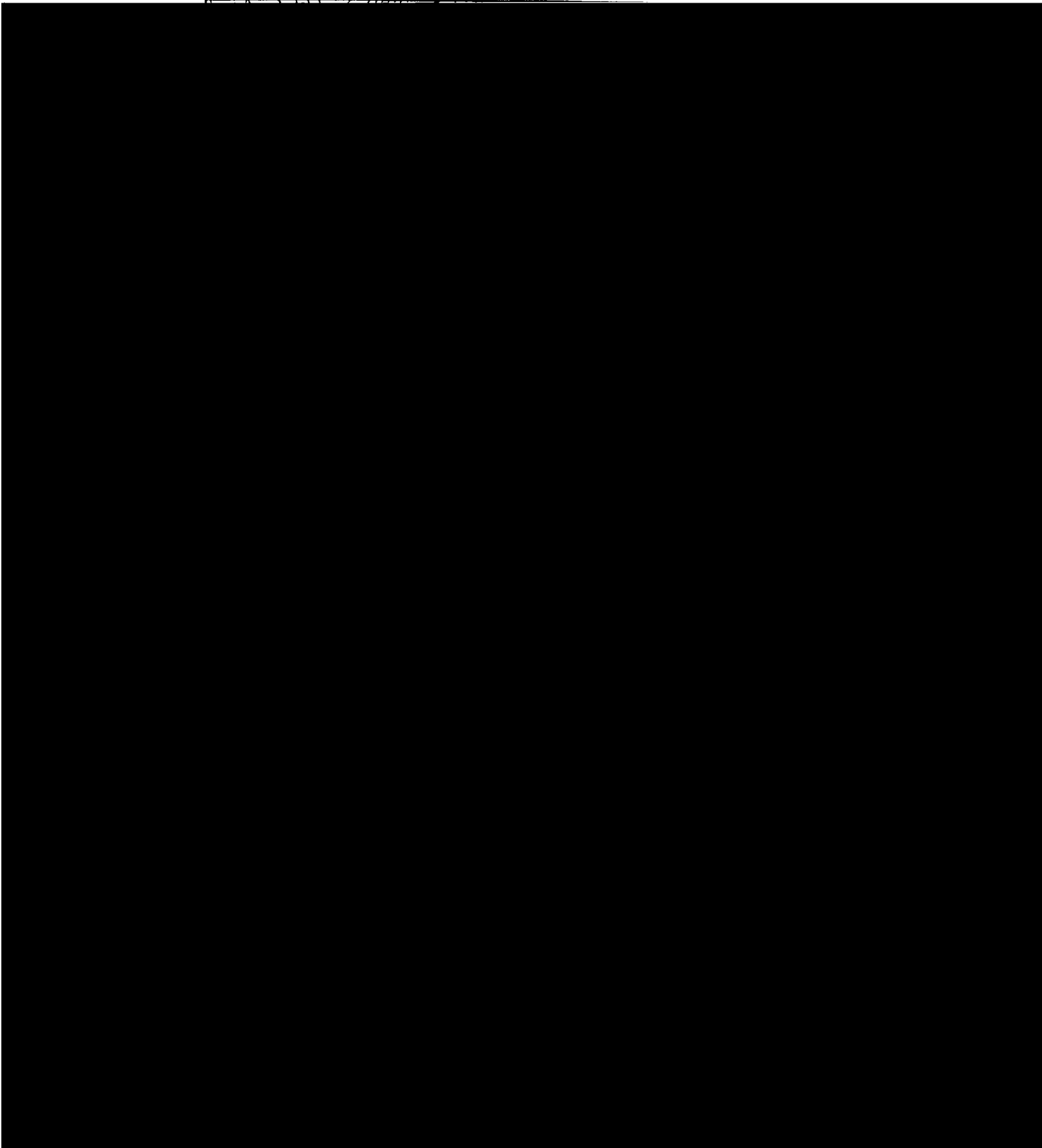


Figure 4-4-1. The "total-dry" potential temperature ( $^{\circ}\text{K}$ , top) and horizontal divergence ( $10^{-4} \text{ s}^{-1}$ , bottom) at 3 PM, on the XZ-cross section crossing the southern half of Lake Okeechobee. The two coasts are indicated as in Fig. 4-3-9.

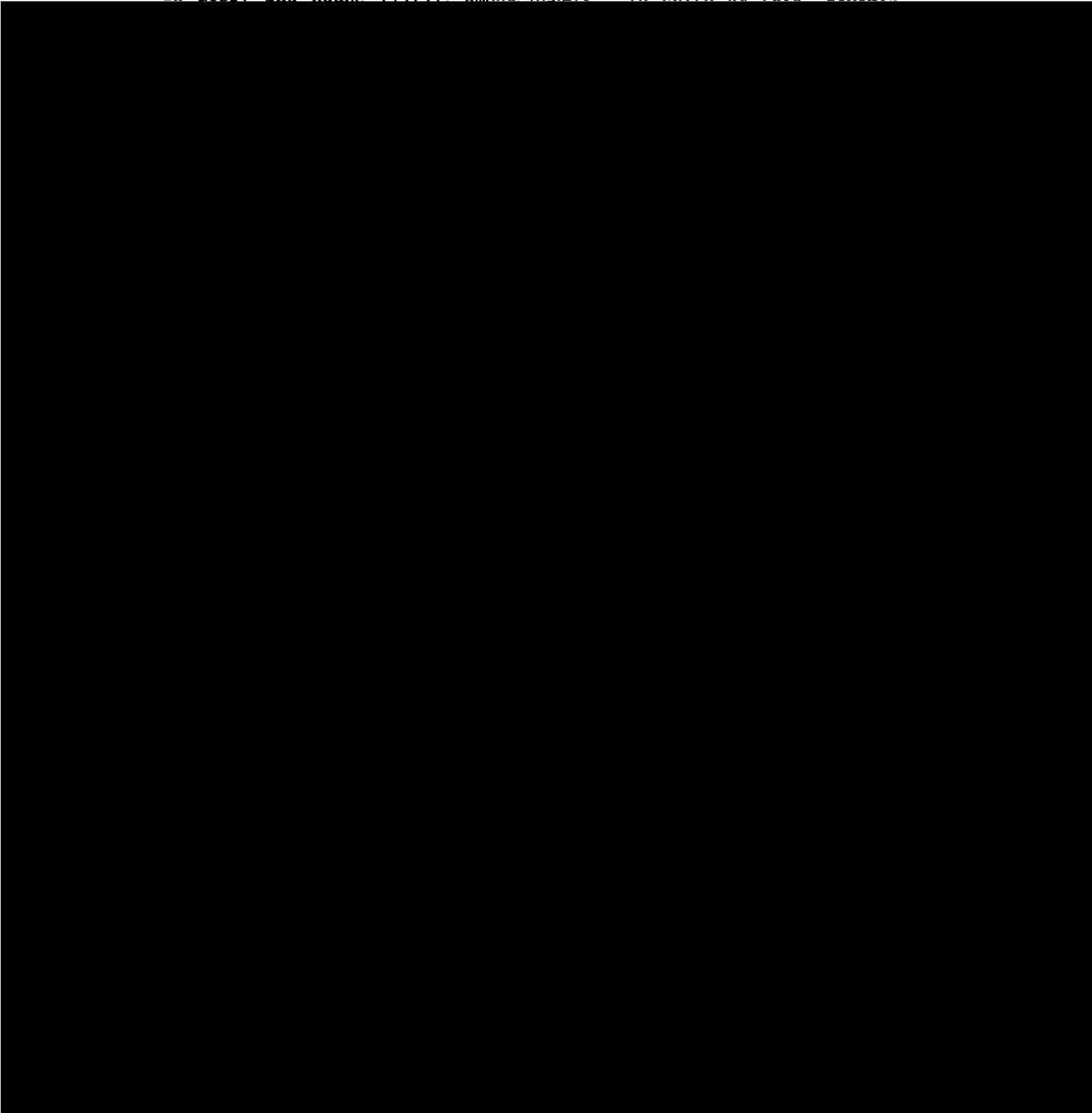
Due to the heating pattern shown above, a "four-cell" vertical solenoidal circulation pattern is evident in the horizontal u-velocity field (Fig. 4-4-2(a)) and the Y-direction vorticity field (Fig.

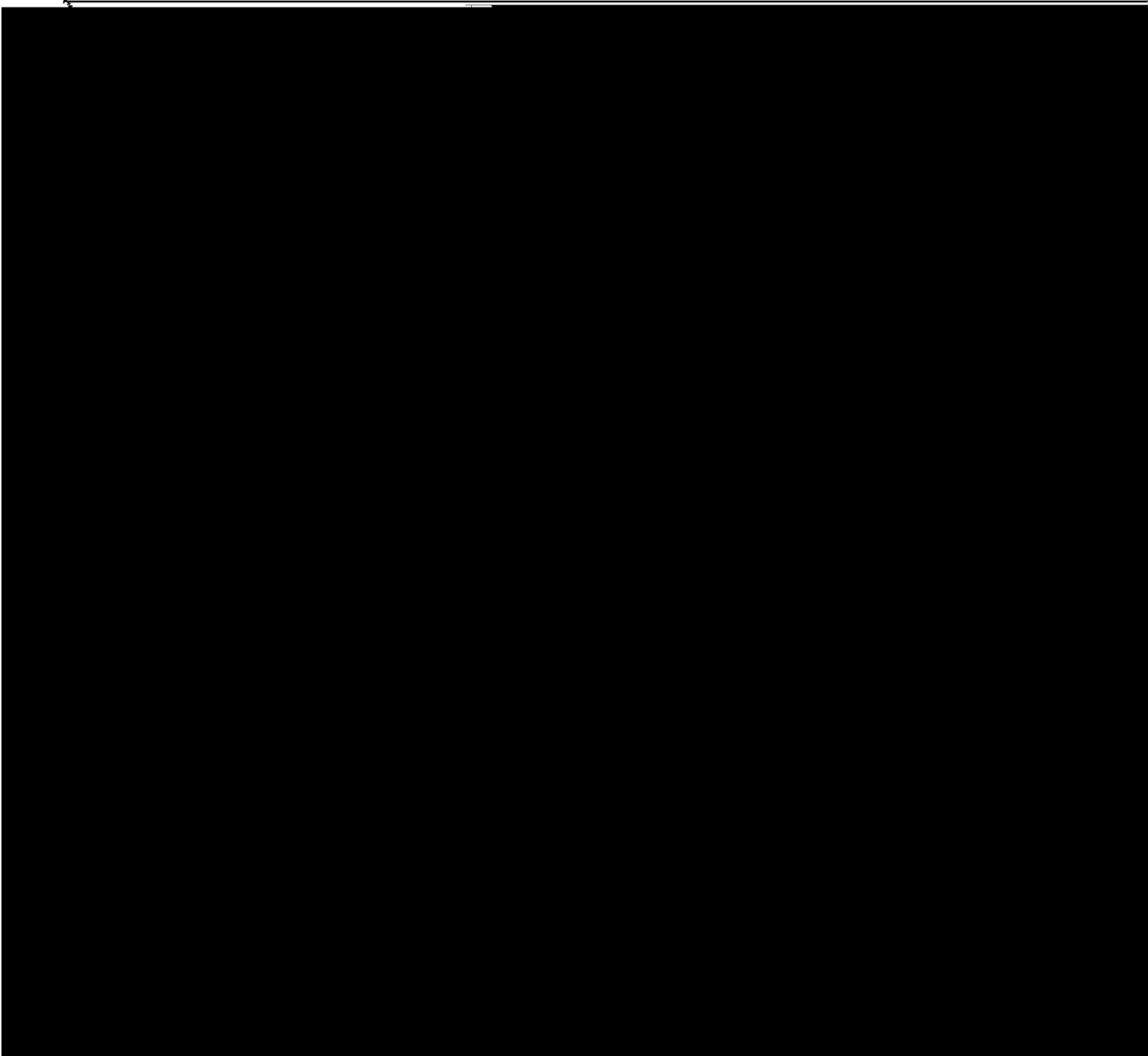
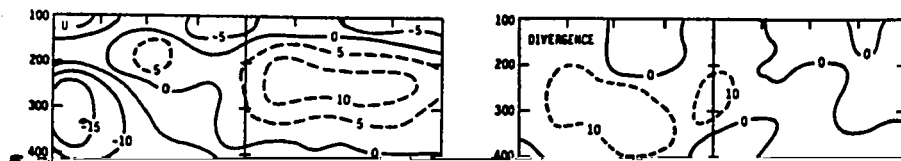






The mesoscale model used in the current study does not include latent heat release on the resolvable-scale field (i.e., all moist processes are produced in the convective parameterization). Therefore, this model does not generate the mesoscale updraft/downdraft introduced in Leary and Houze (1979), among others. In spite of this, however,



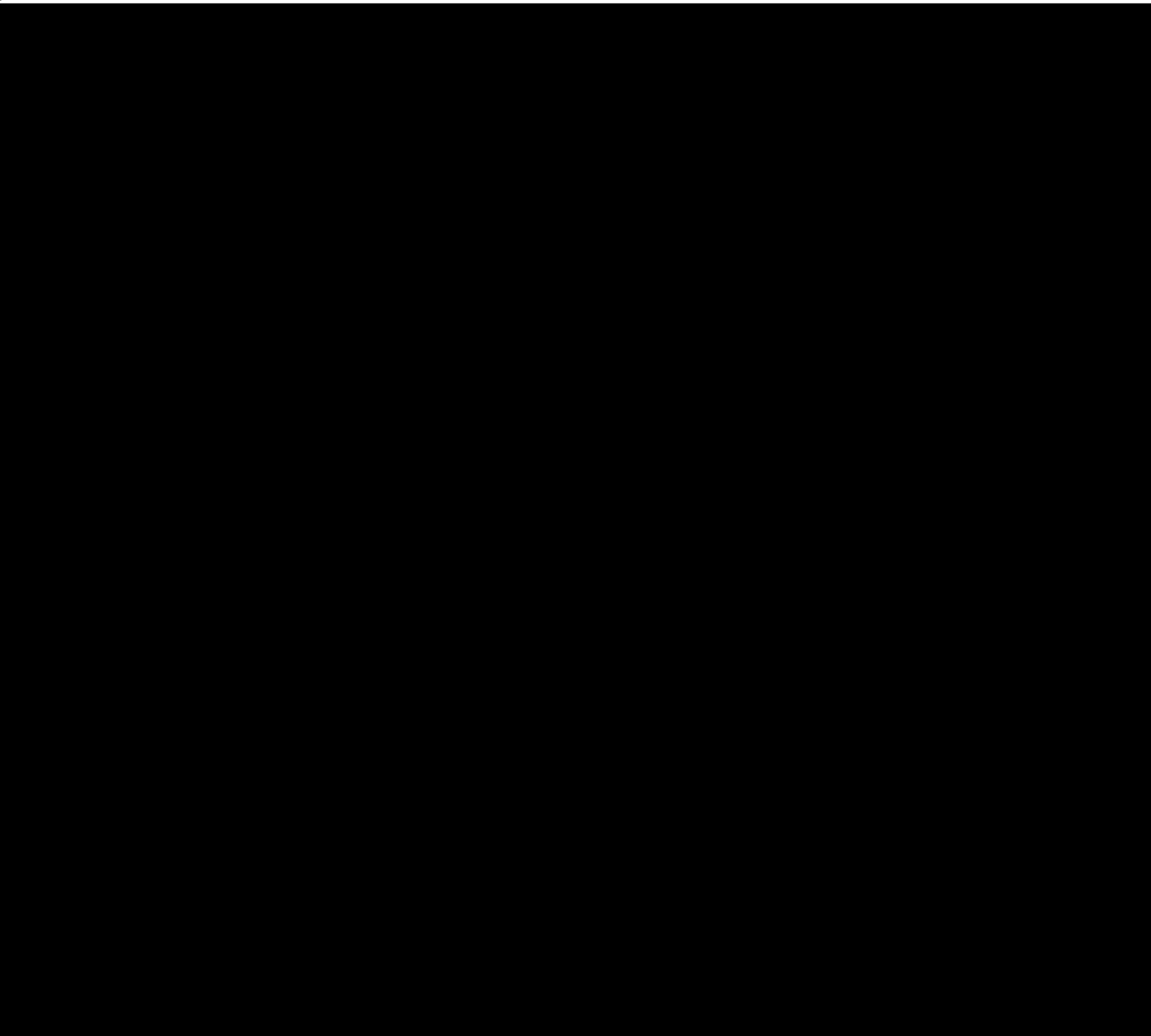


maximum in the upper troposphere with weaker easterly winds in the mid-and lower-troposphere. This wind structure is different from that in Ogura and Liou (1980) in which a westerly jet dominated the upper troposphere. In their study, it was stated that around the mid-troposphere (during the lifetime from mature stage to decaying stage), the westerly background momentum opposes the easterly momentum which is carried upward by the low-level jet.

---

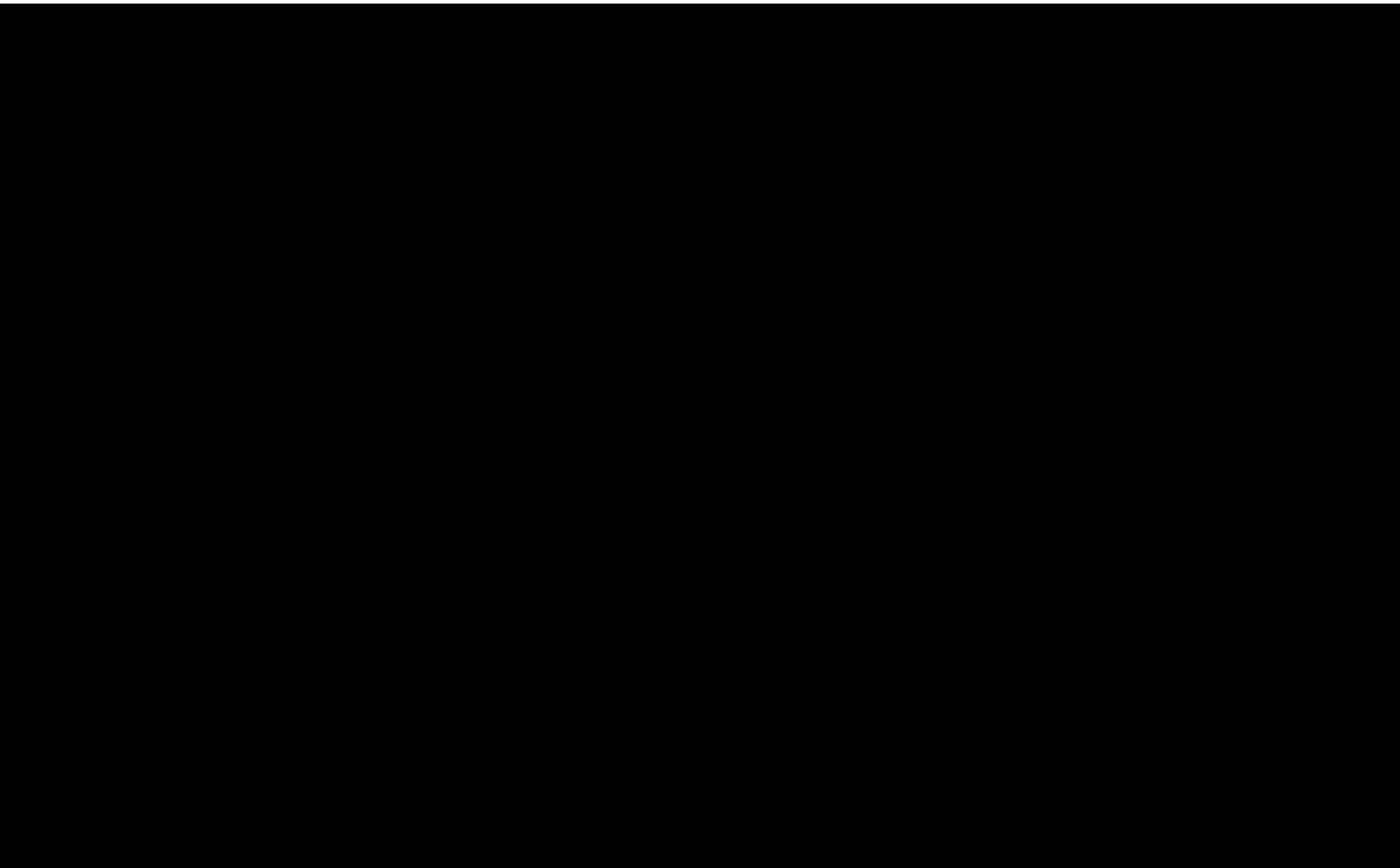
---

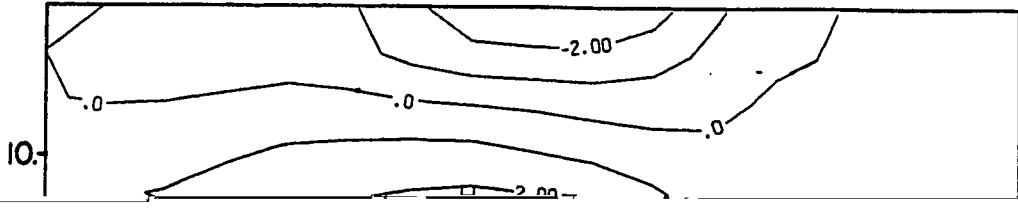
---

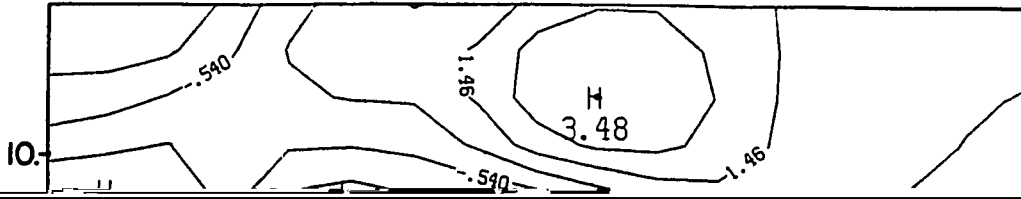


upper-troposphere, and because no explicit latent heating processes were represented on the grid-scale, the "total-dry" quantities should indicate the mesoscale responses due to pure cumulus convective forcing. Therefore, the mid-tropospheric convergence obtained in the current study, and the associated mesoscale upward and downward motions, are initiated and enhanced solely due to the convective heating in the upper troposphere and the convective-scale downdraft cooling in the lower troposphere. In their observational analysis of the Winter MONEX, Johnson and Kriete (1982) indicated that the convective-scale processes (melting and evaporation at low levels and condensation and freezing at upper levels) seemed to be able to drive a larger-than-cloud-scale circulation (mid-tropospheric convergence forced by vertically-divergence air streams) which, in turn, feeds

---







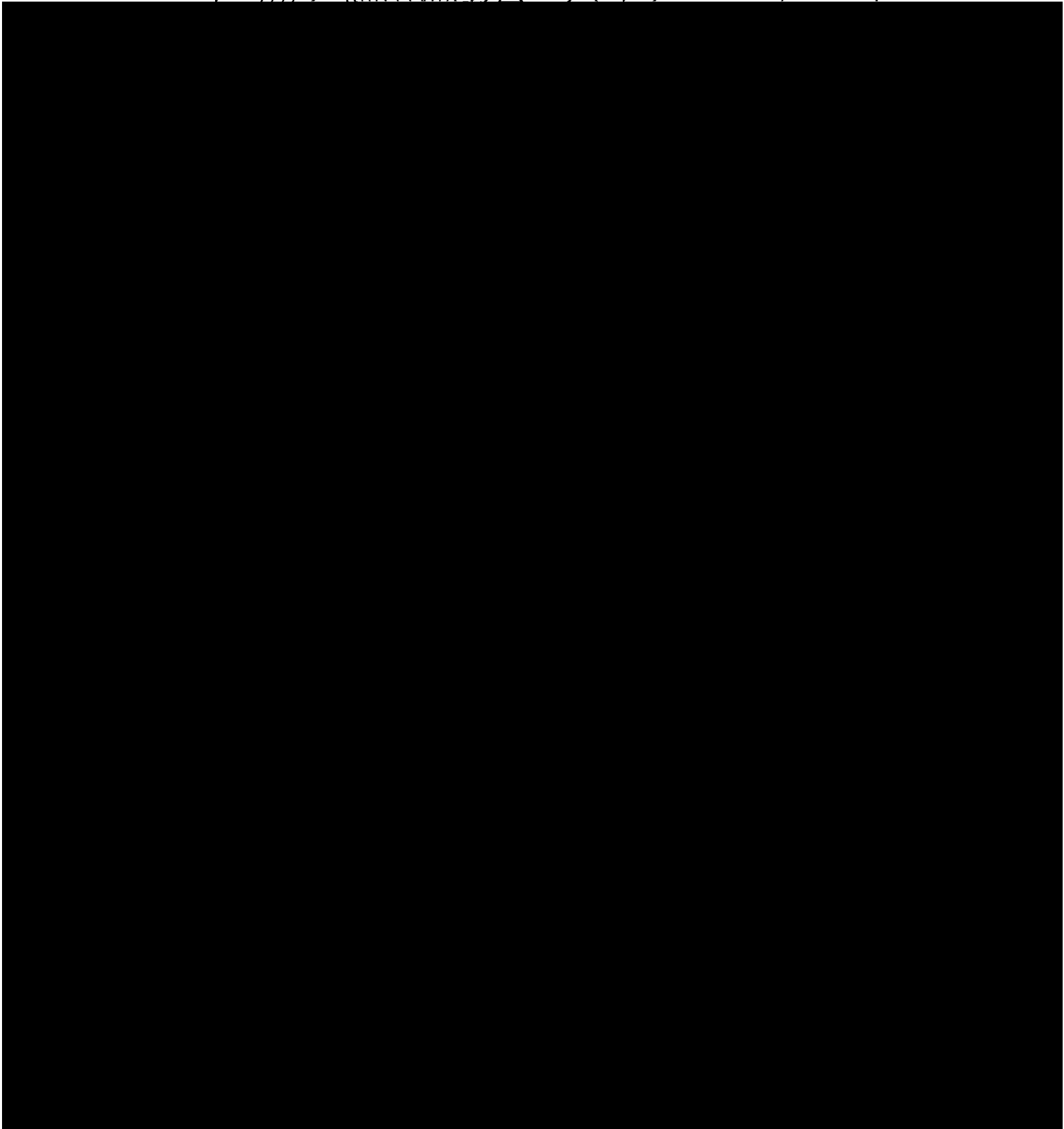
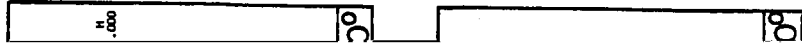


Figure 4-4-8 and Fig. 4-4-9, respectively, show the horizontal maps of the upper tropospheric (near 12 km) horizontal divergence and (the vertical component of) vorticity, for the time period of 11 AM-4 PM. The vorticity is associated with the atmospheric adjustment processes (toward geostrophic balance) due to the horizontal convergent/divergent motions. Comparing Fig. 4-4-8(a) through (f) with Fig. 4-4-9(a) through (f), we see that positive vorticity (i.e., cyclonic rotation) is related to the convergent flow field and negative vorticity to the divergent flow field.

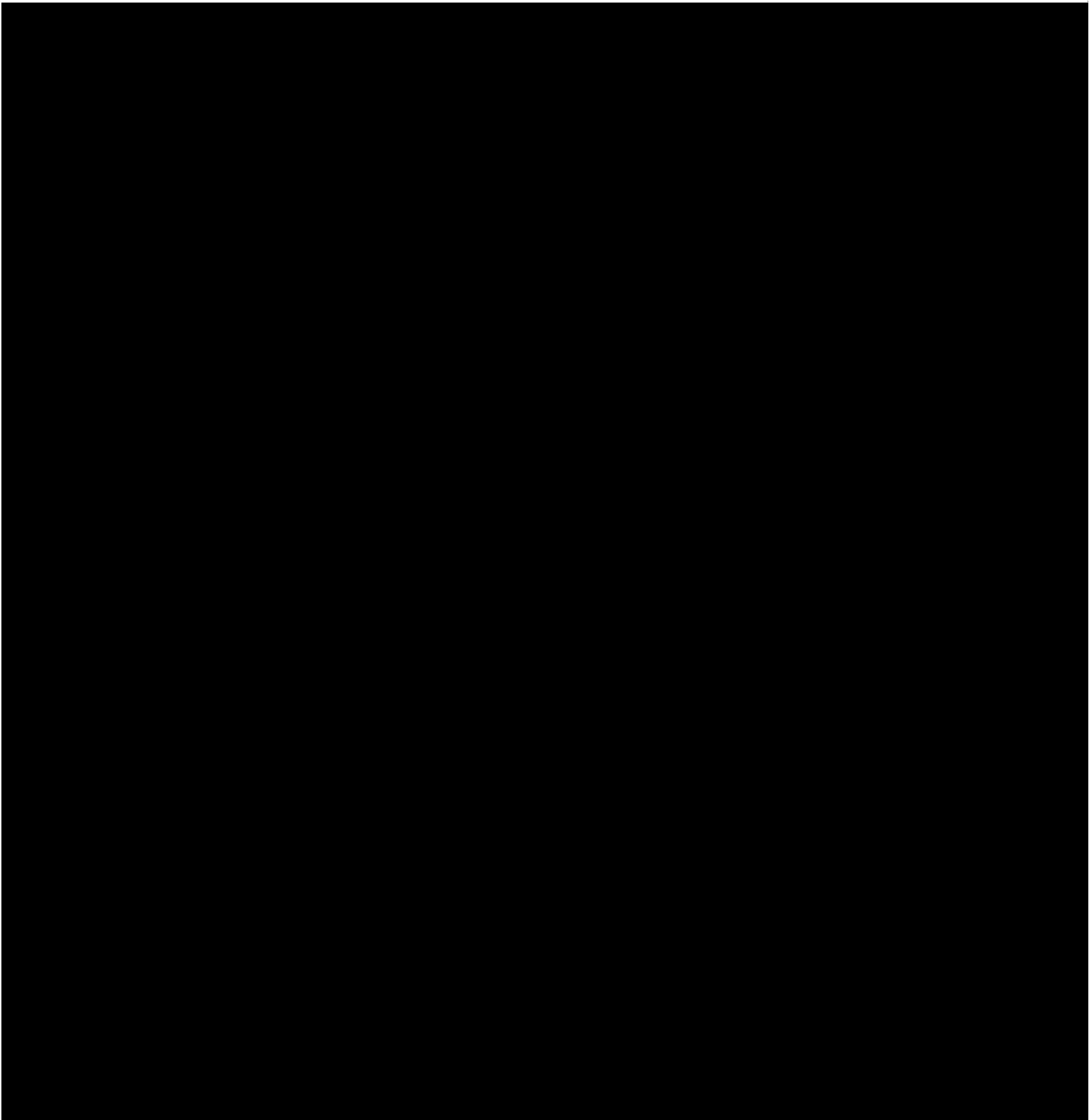
Summarizing various observational and numerical investigations of convective downdraft effects, we see that convective downdrafts typically have two distinct feedback effects upon the convective system from which the downdraft is initiated. The first is that surface stabilization by downdrafts such that convective development becomes weakened within the original convective area (Molinari and Corsetti, 1984). The second effect is that downdrafts are able to enhance subsequent convection through the surface outflow feedback mechanism (the "displacement instability" as described in Raymond, 1986).

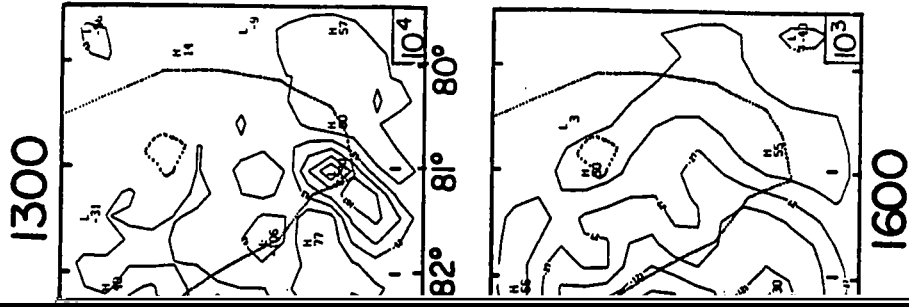
Molinari and Coresetti (1984), using a modified Kuo-type cumulus parameterization, indicated that without convective downdrafts the simulated rainfall significantly exceeded the observed amounts. Without the downdraft stabilization, in their model, there is an unrealistic positive feedback between convective-generated upper-level warming and lower-level convergence, which lead to overestimations of rainfall generation, as compared to observations.

Among the several existing convective parameterizations used for simulating mesoscale convective weather systems, Raymond (1986) introduced one which pays particular attention to the downdraft displacement



12 km) between  
included in each



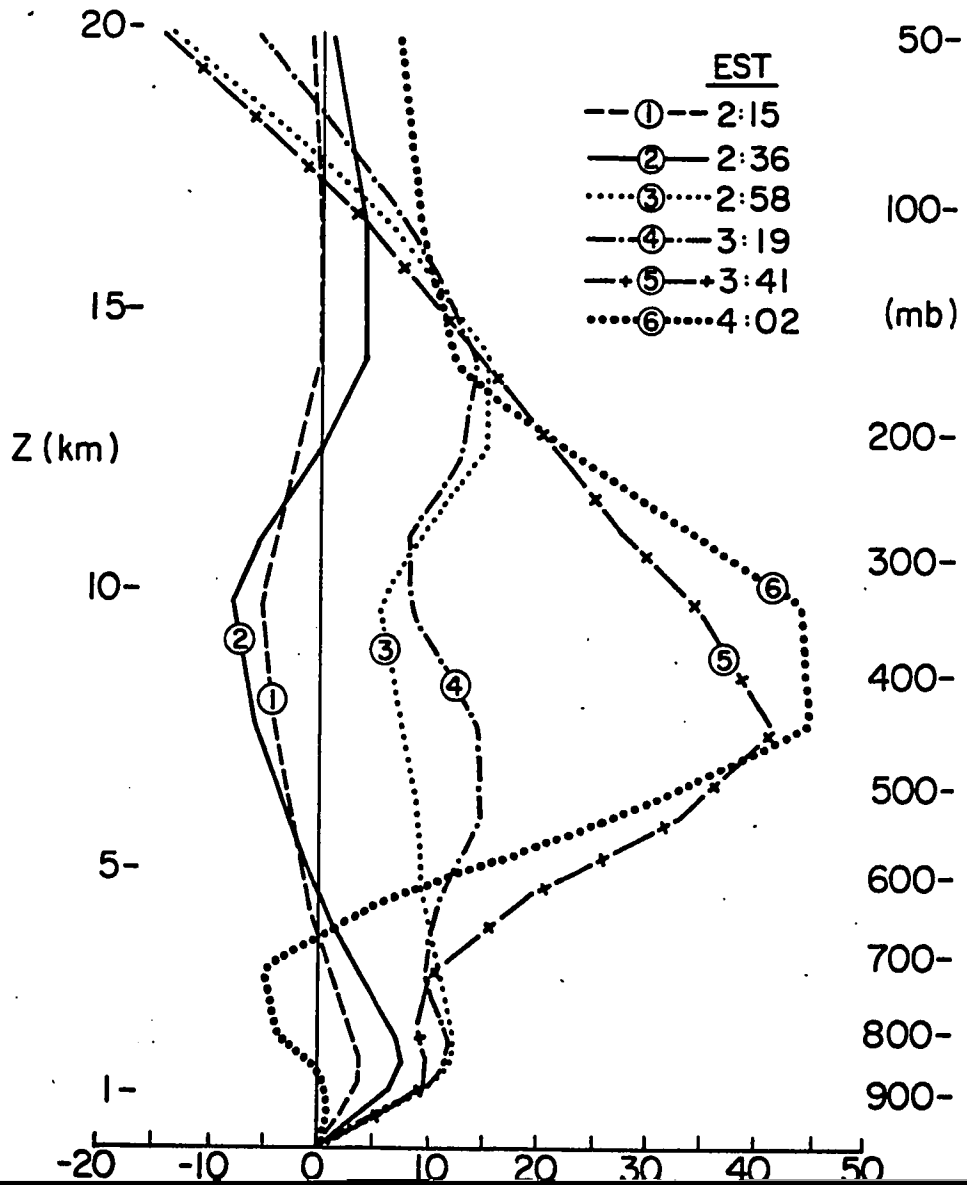


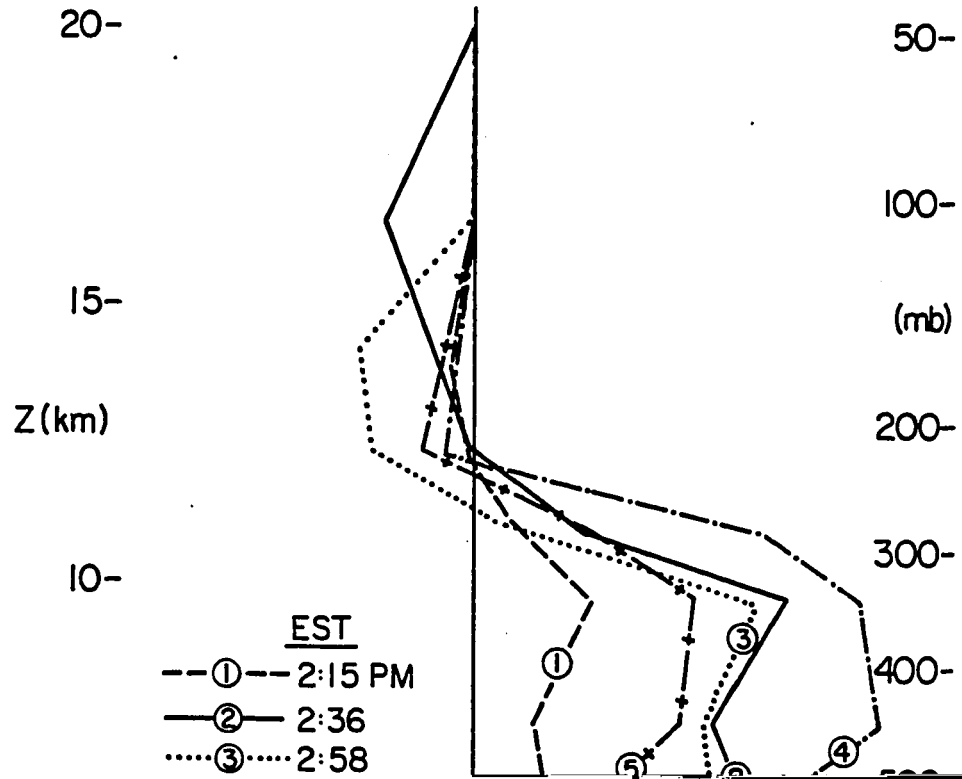
Contour interval is 1 km between 1100 EST  
Contours are included in each figure.

effect. By adding the downdraft effect into his simulation Raymond

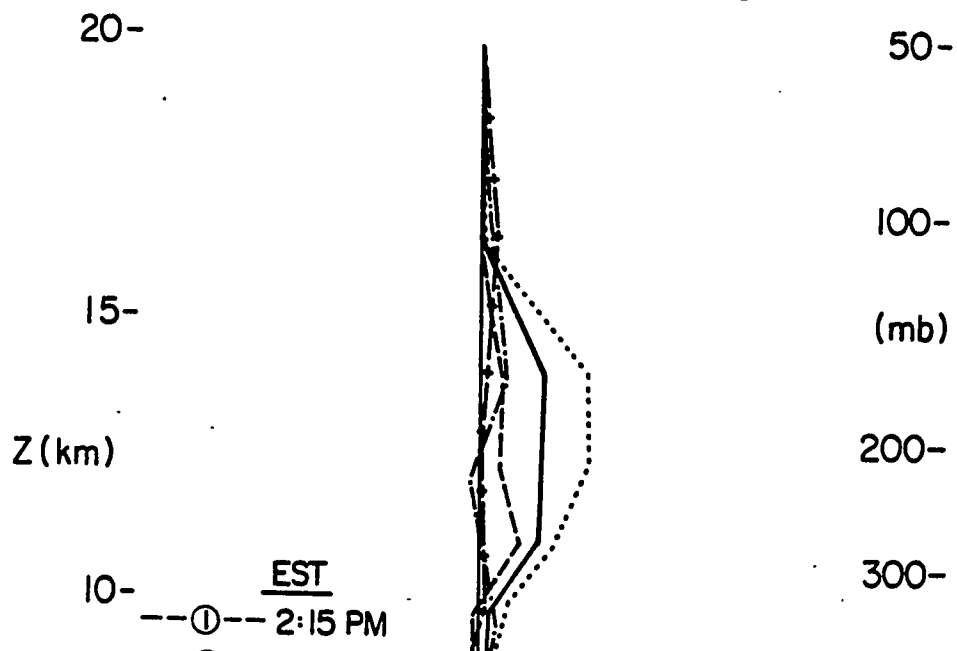


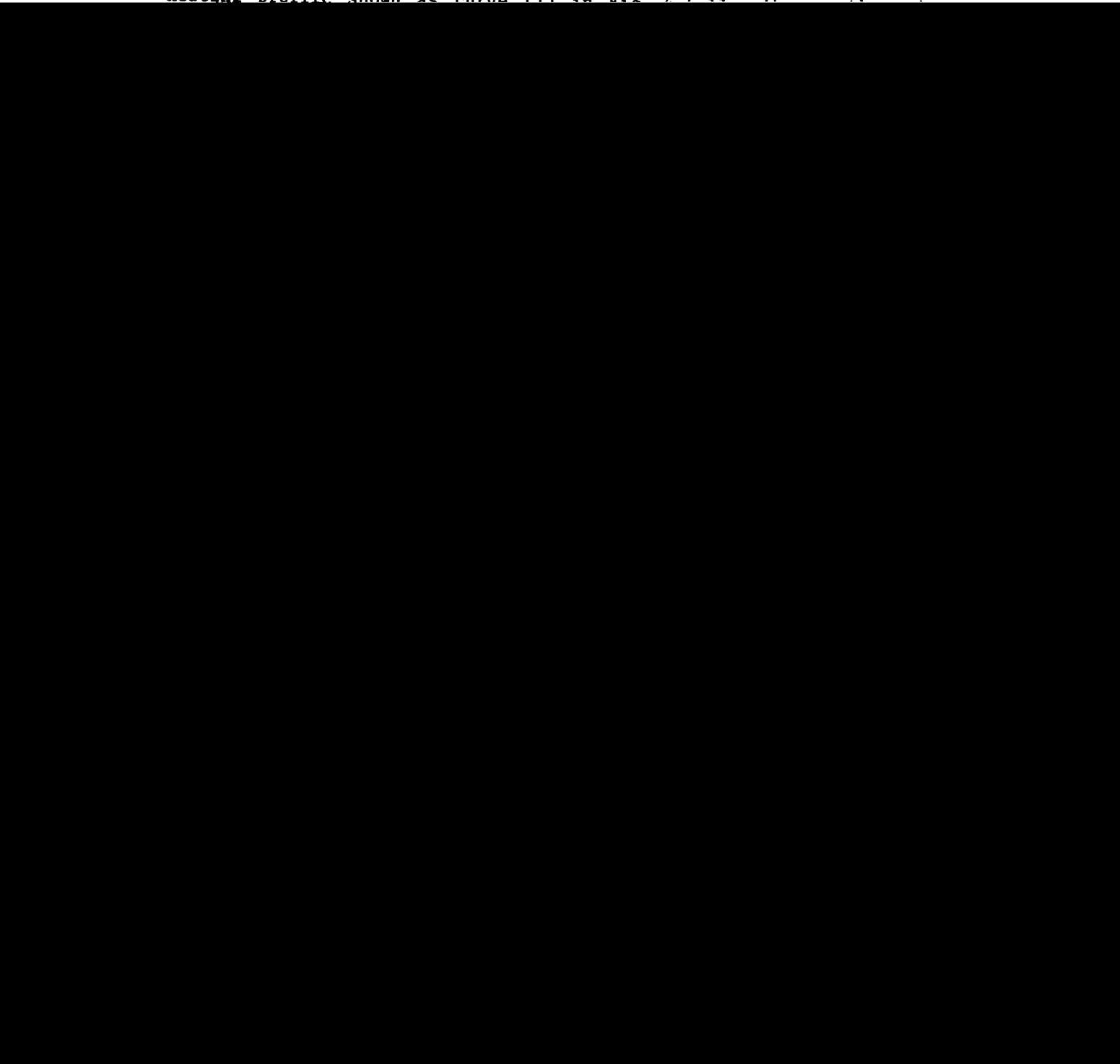
GRID SCALE VERTICAL VELOCITY (cm/s)



CONVECTIVE HEATING RATES ( $^{\circ}\text{C} / \text{DAY}$ )

CONVECTIVE MOISTENING RATES (G/KG/min)



Before 2:15, no cloud developed in this grid. Therefore, as seen in Fig. 4-4-10, curve (1) indicates there is weak downward motion throughout the mid and upper troposphere (presumably due to the compensating downward motion caused by neighboring convection) and weak upward motion in the lower troposphere due to sea breeze convergence. The first cloud is initiated at 2:15, which produces the convective heating profile shown as curve (1) in Fig. 4-4-11. 

downdraft cooling). Therefore, curve (6) in Fig. 4-4-10 already indicates downward motion in the lower troposphere (i.e., the system is in a decaying stage). Accordingly, there is no new cloud initiated at this grid.

Figure 4-4-12 shows that the deep convection provides important moistening over the layer between about 500 mb and 800 mb, and to a weaker degree around the tropopause (anvil evaporation). Subsidence motion produces drying between 800 mb and 900 mb, while downdraft evaporation acts as a moisture source in the subcloud layer.

The heating and moistening profiles obtained from the current scheme have been compared with various observational analyses both quantitatively and qualitatively - for mid-latitude: Ogura and Liou

(1980) ...

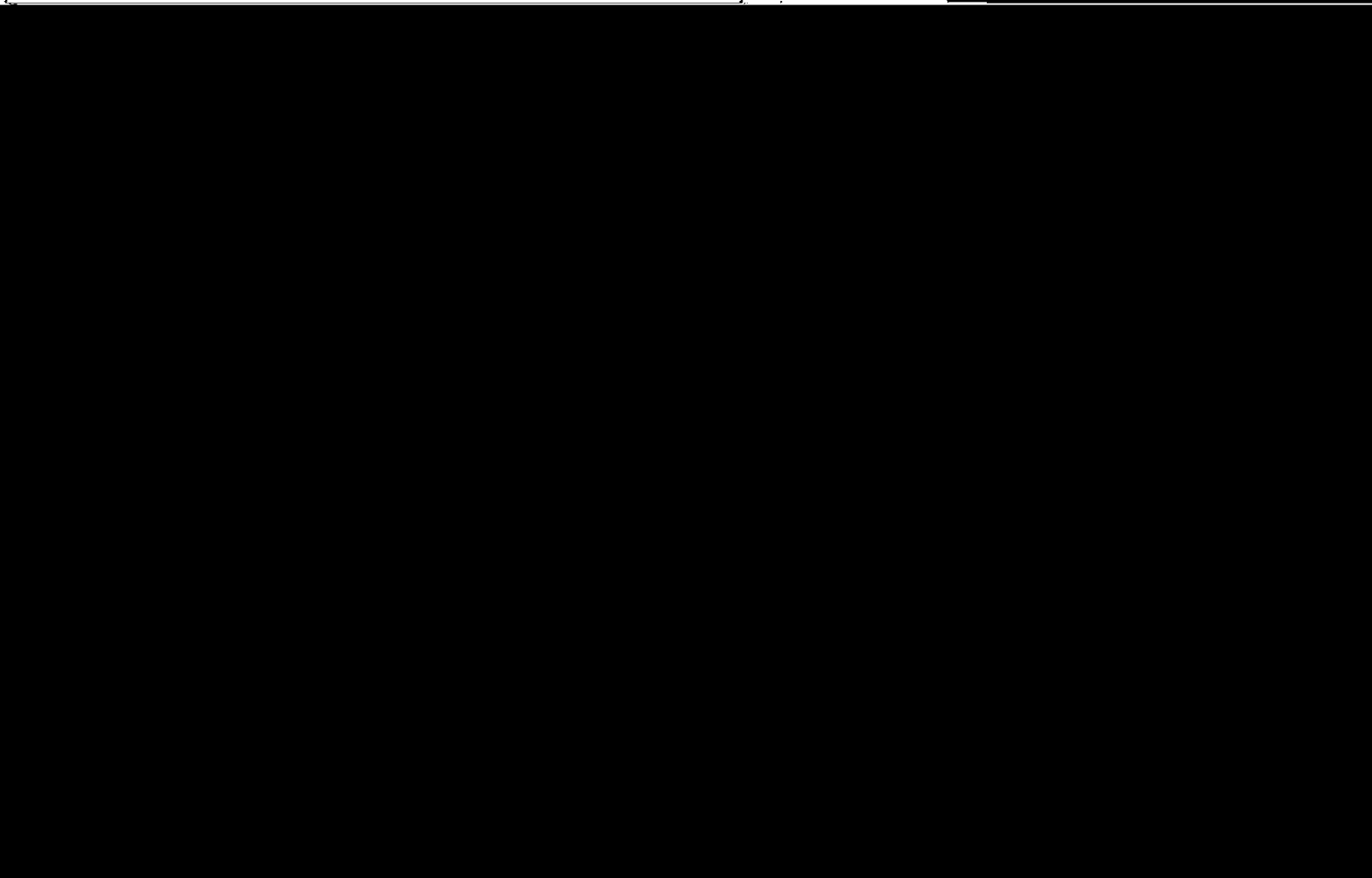
## Chapter 5

### PHYSICAL SENSITIVITY EXPERIMENTS

#### 5-1. Introduction

It was discussed in the last chapter that Florida's summertime deep cumulus convection is closely related to both the sea breeze circulation and mesoscale circulation caused in response to cooling of boundary layer air by deep cumulus-generated downdrafts. Boundary layer cooling produced by the downdrafts plays a major role in focusing subsequent deep convective development.

It is instructive to see how this mesoscale-convective interrelationship depends on various physical forcing mechanisms. In

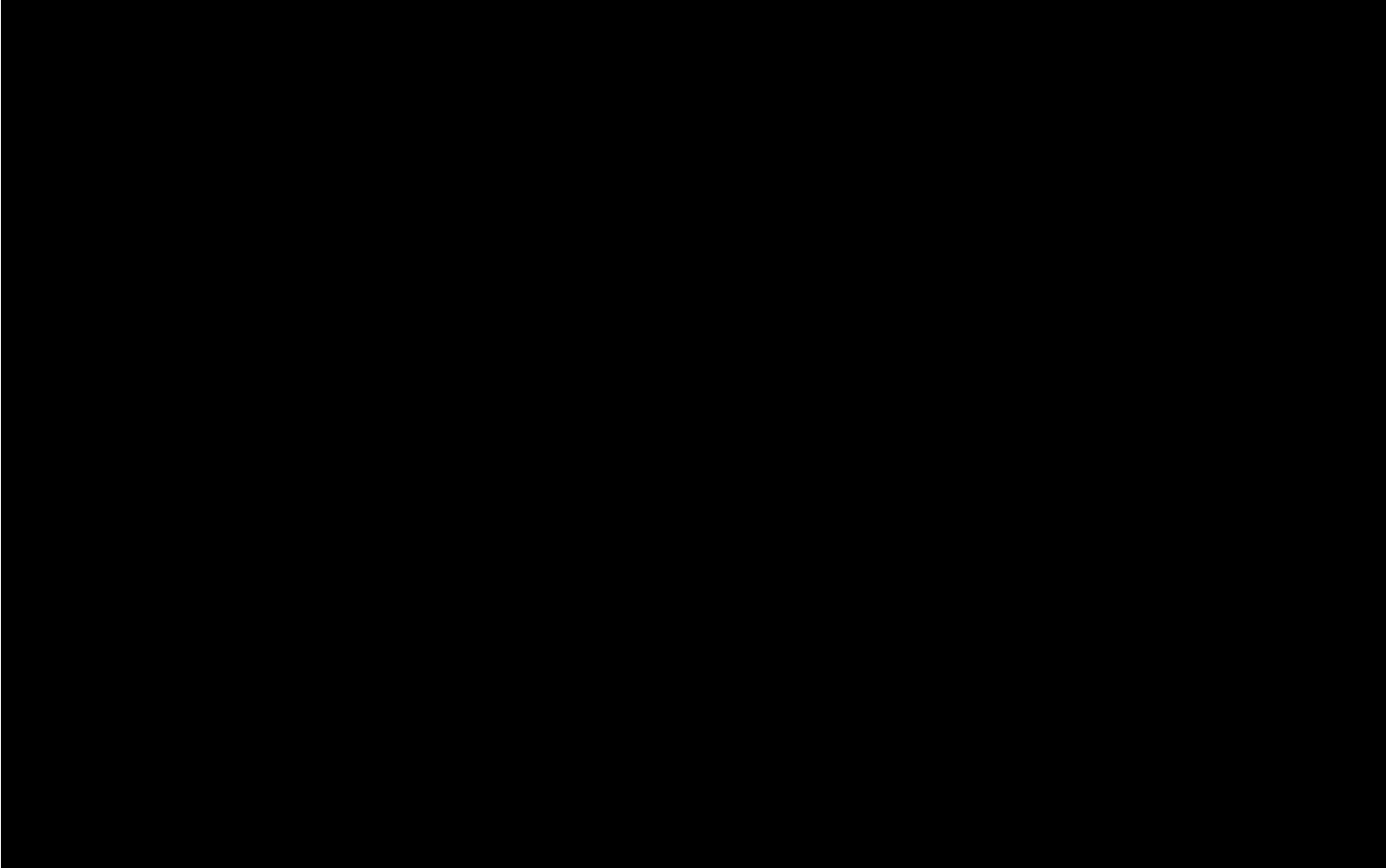


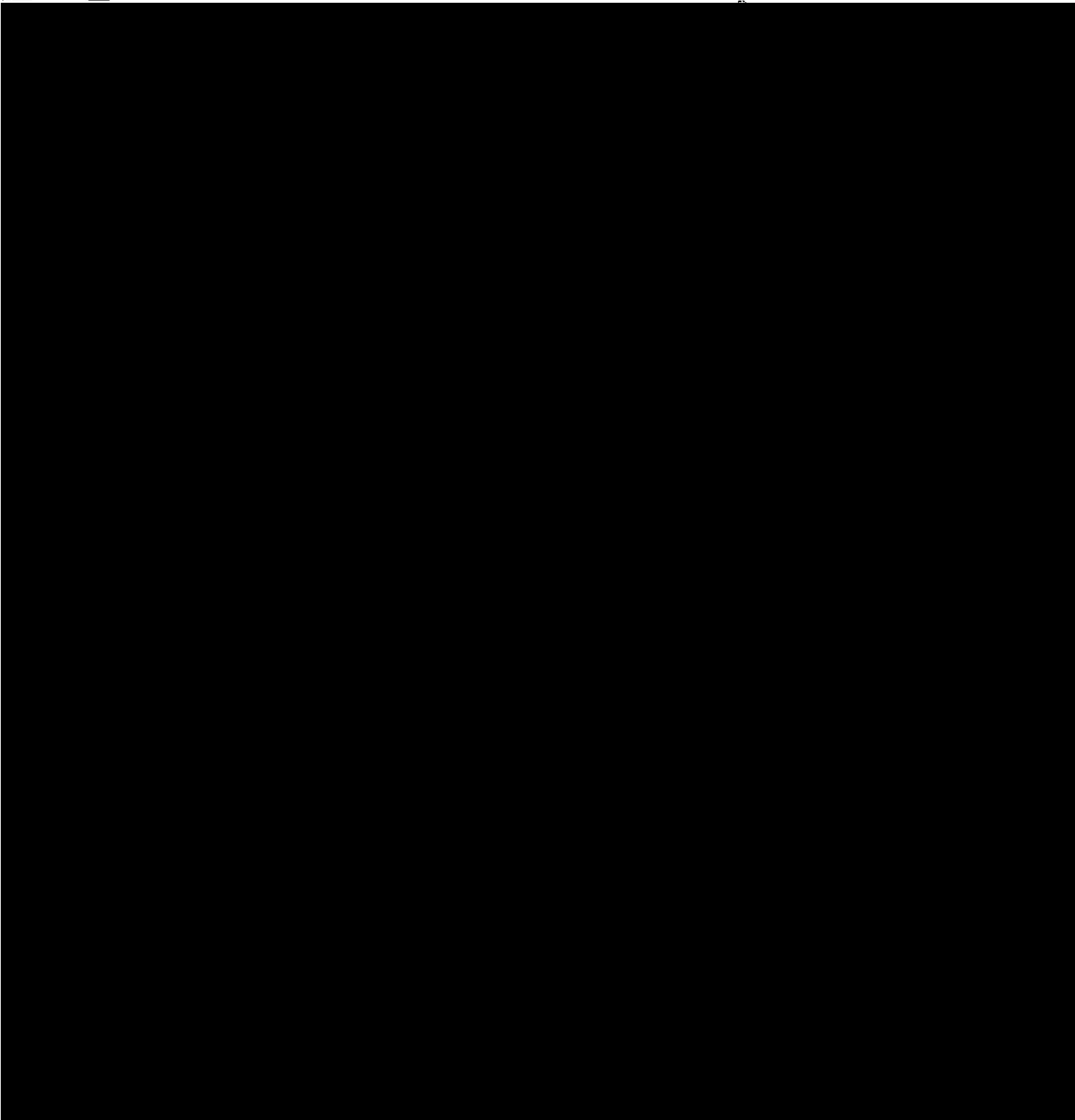
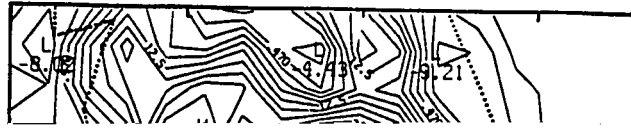
velocity field at 3 PM and 4 PM, and horizontal maps of the vertical velocities at 10 km and 1 km (for 4 PM only). Attention is paid primarily to the results which differ significantly from the control runs.

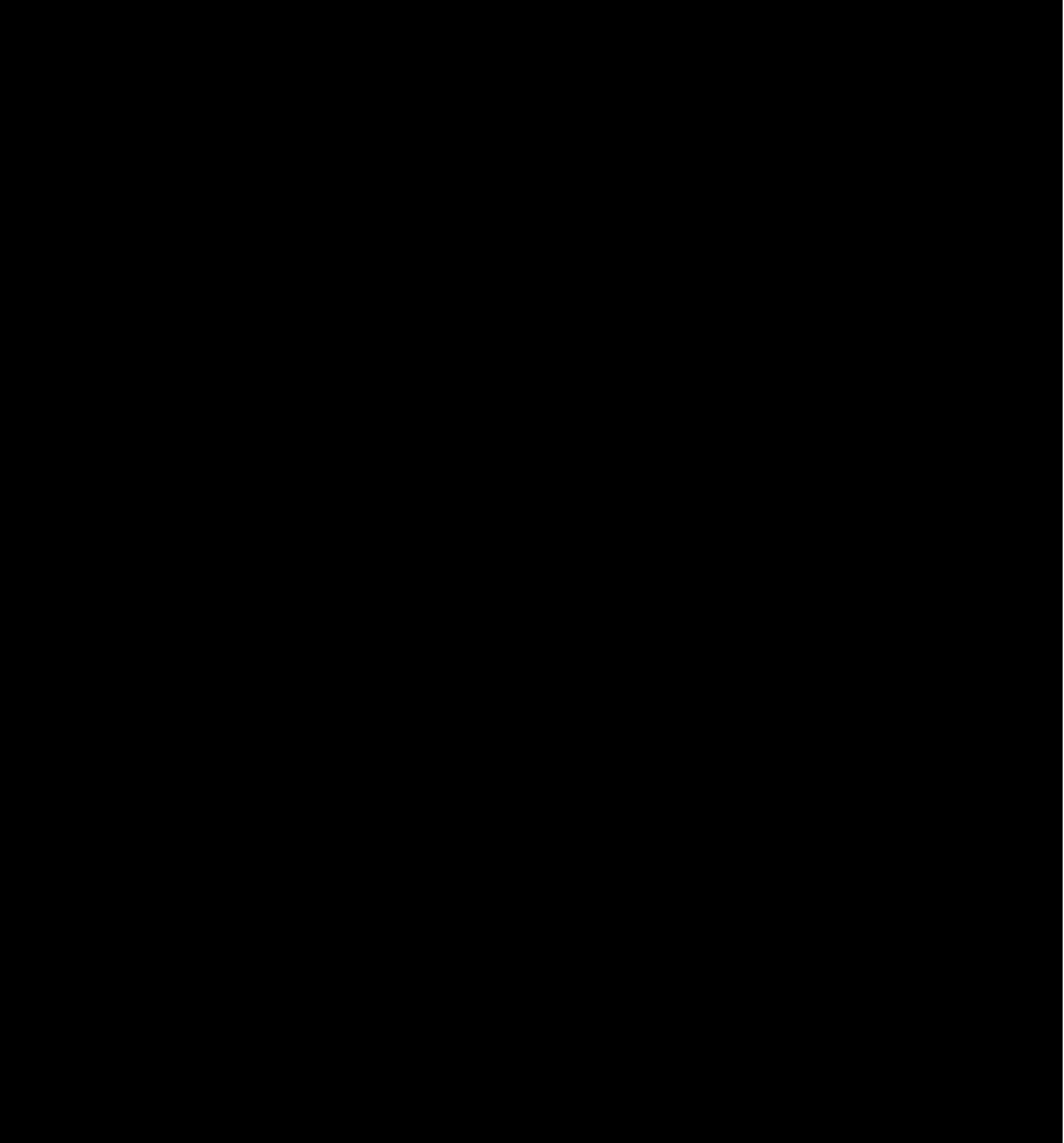
#### 5-2. Weak Southeasterly Experiment

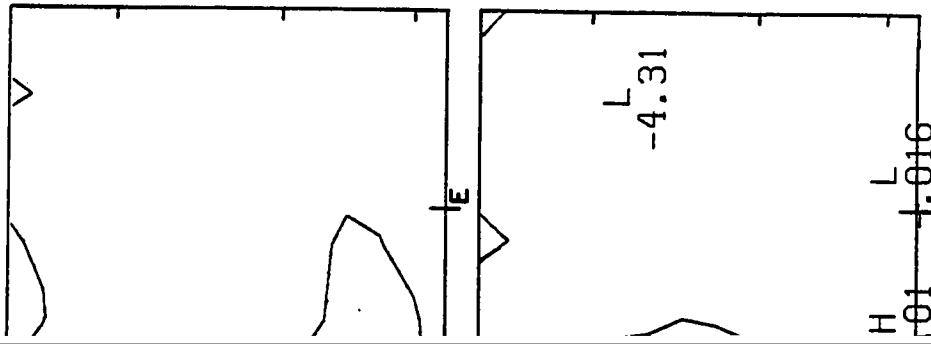
In terms of the initial surface wind, this experiment resembles the light and variable category included in McQueen and Pielke (1985), since both have weak wind near the surface in the early morning. This experiment, however, is initiated with the thermodynamic stratification of the control run, which has an initial environment that is moister than that associated with the light and variable category discussed in McQueen and Pielke (1985). Nevertheless, it is seen that the model has simulated deep convective developments at 4 PM (Fig. 5-1) around the

---





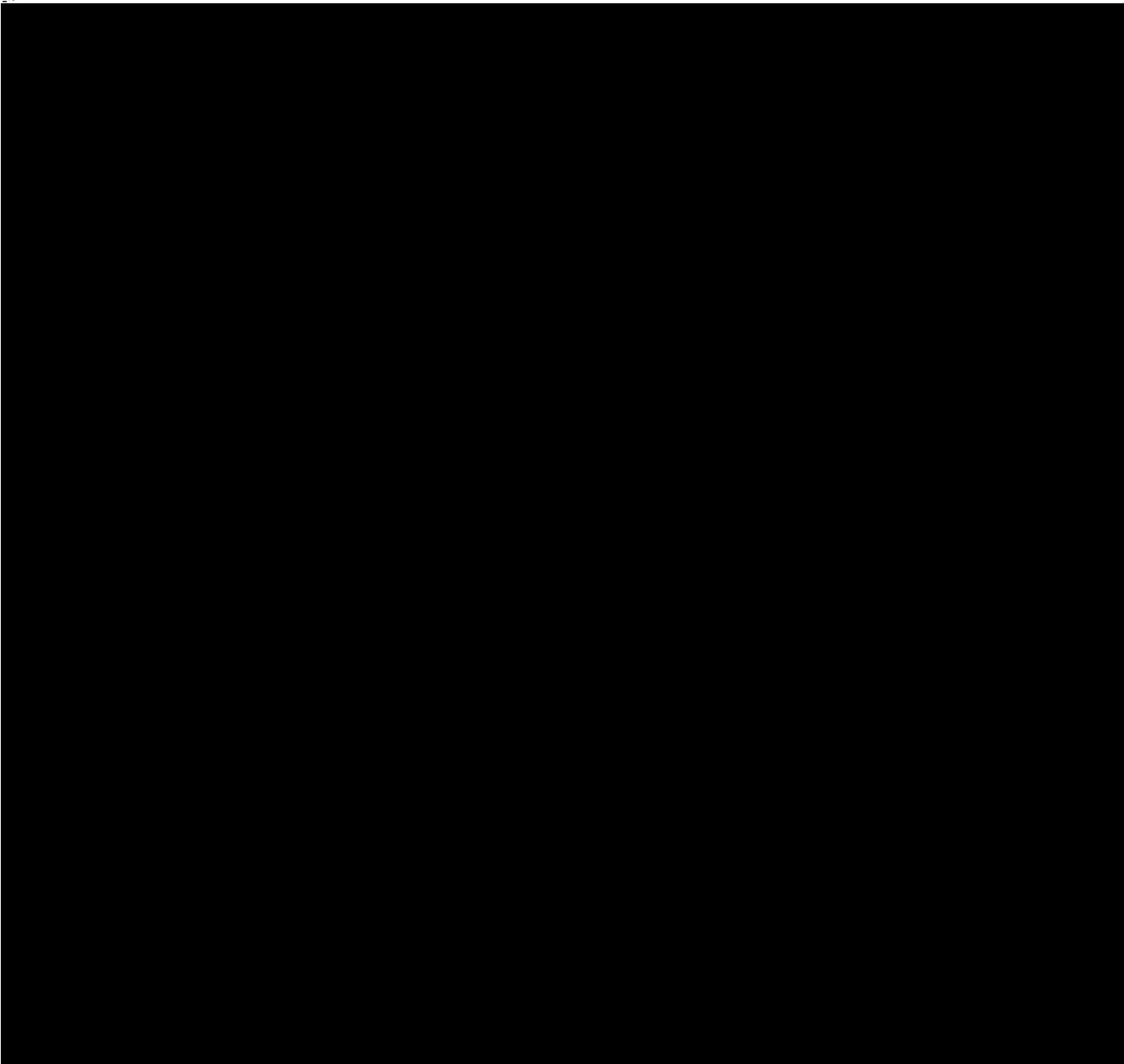
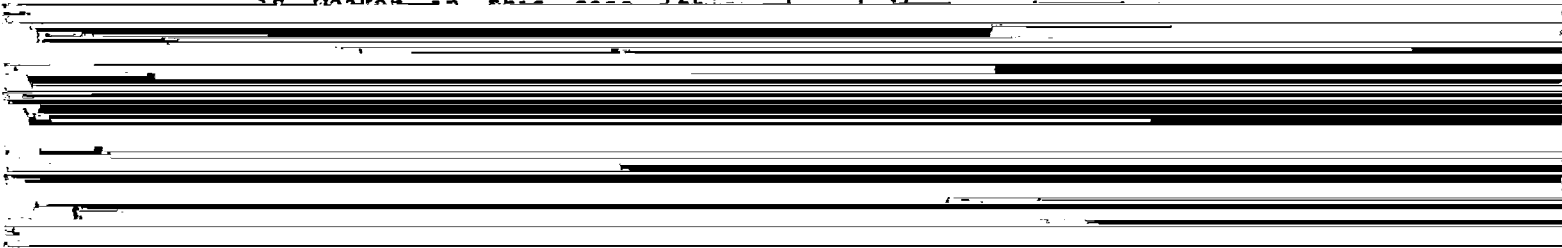


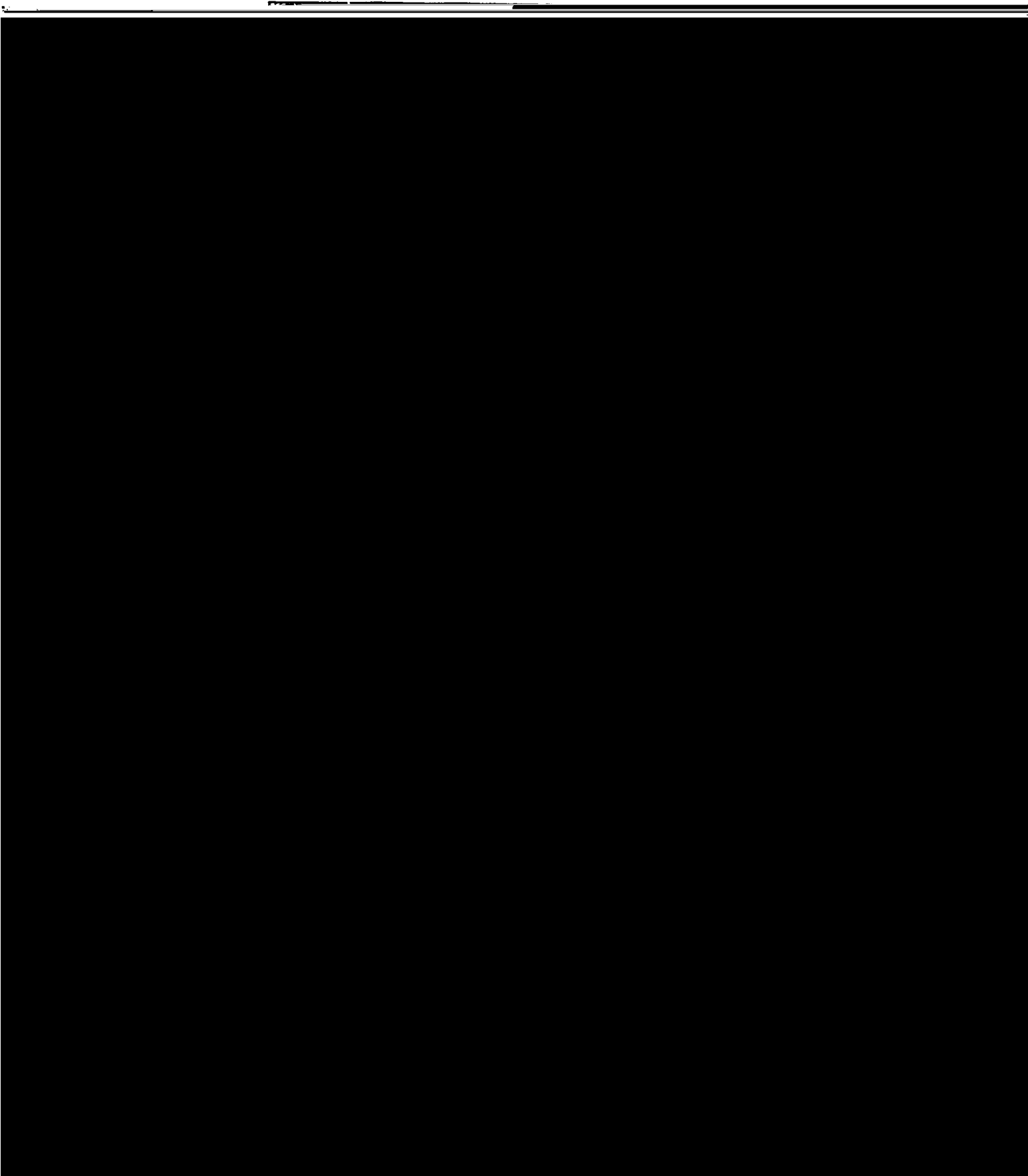


on the XZ-cross section for the

surface convergence in this experiment than in the control run. This weaker convergence occurs because the surface flow over the peninsula

is weaker in this case (this is the same as the control run).





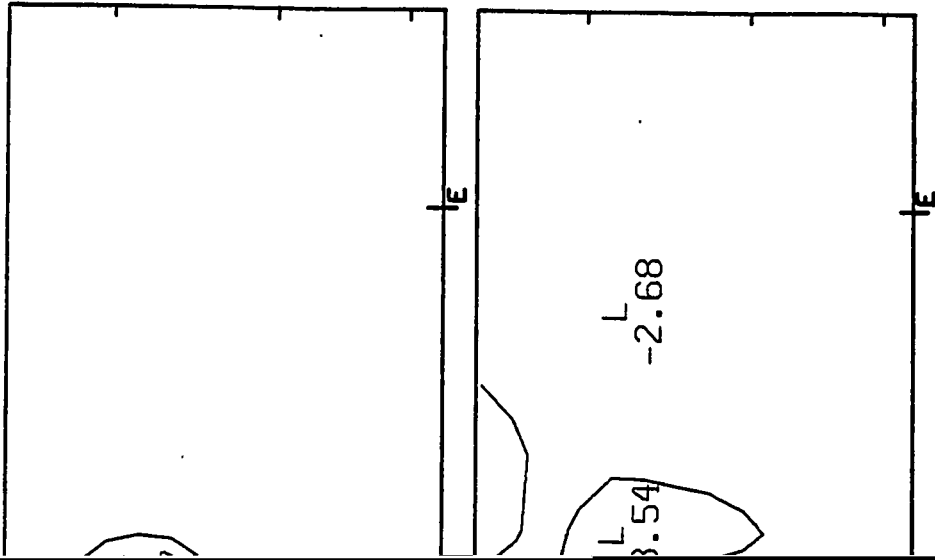
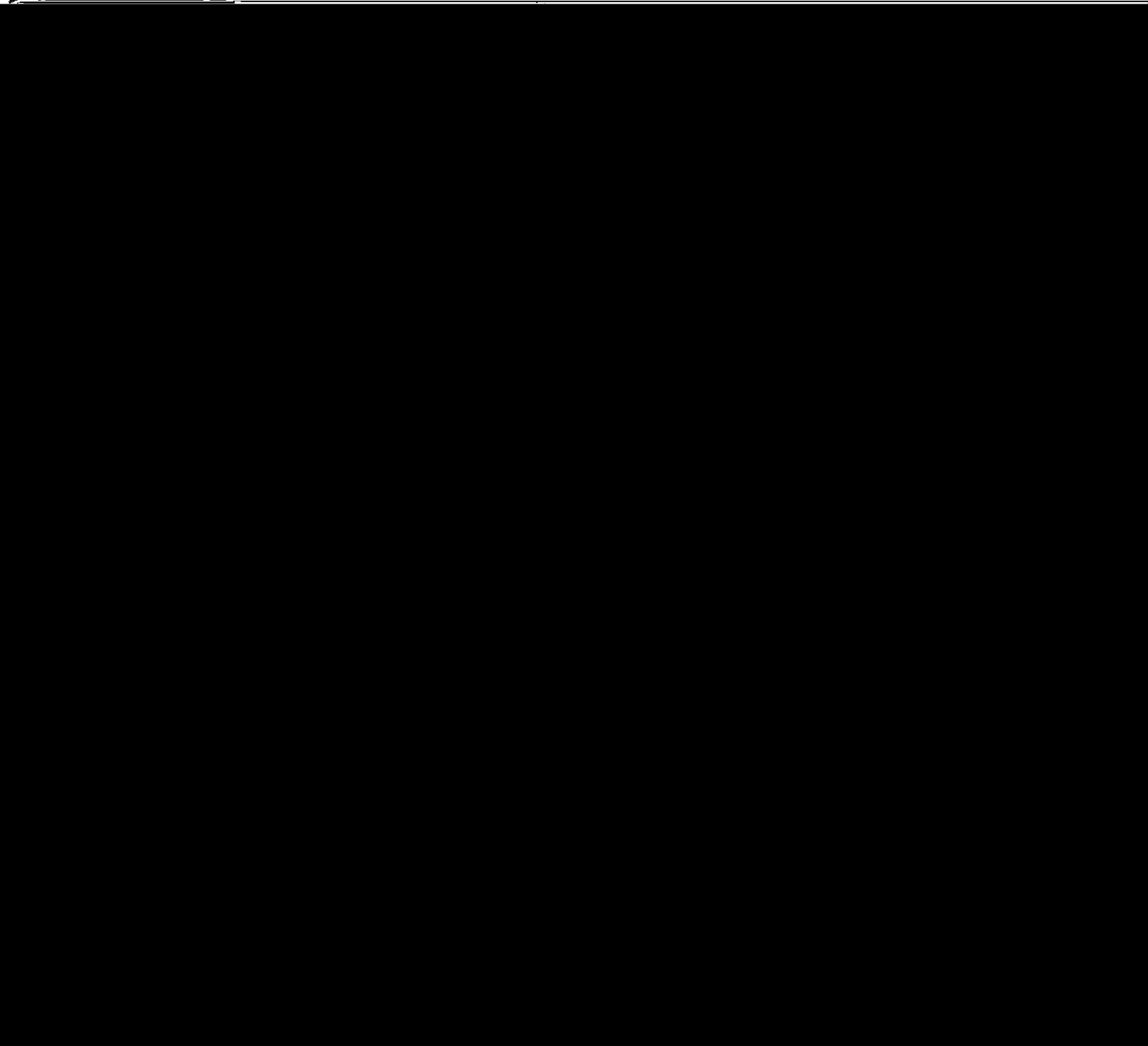
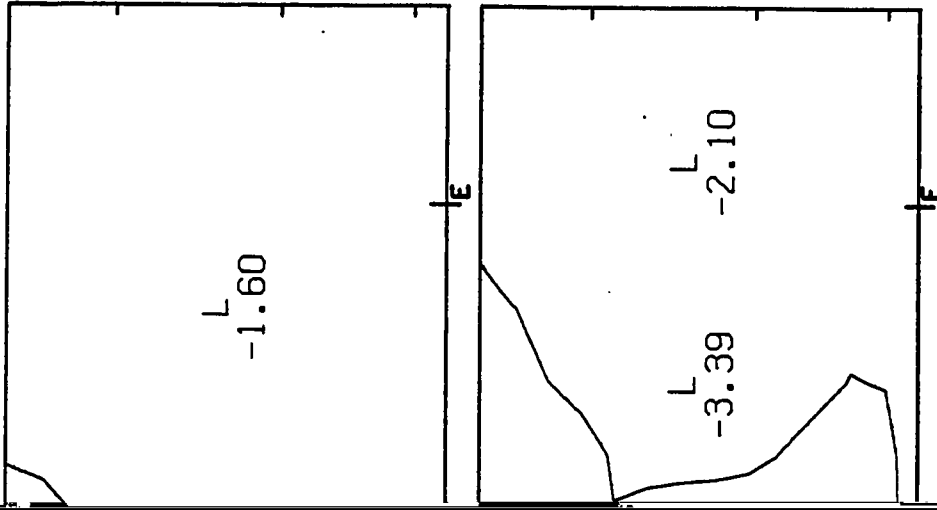


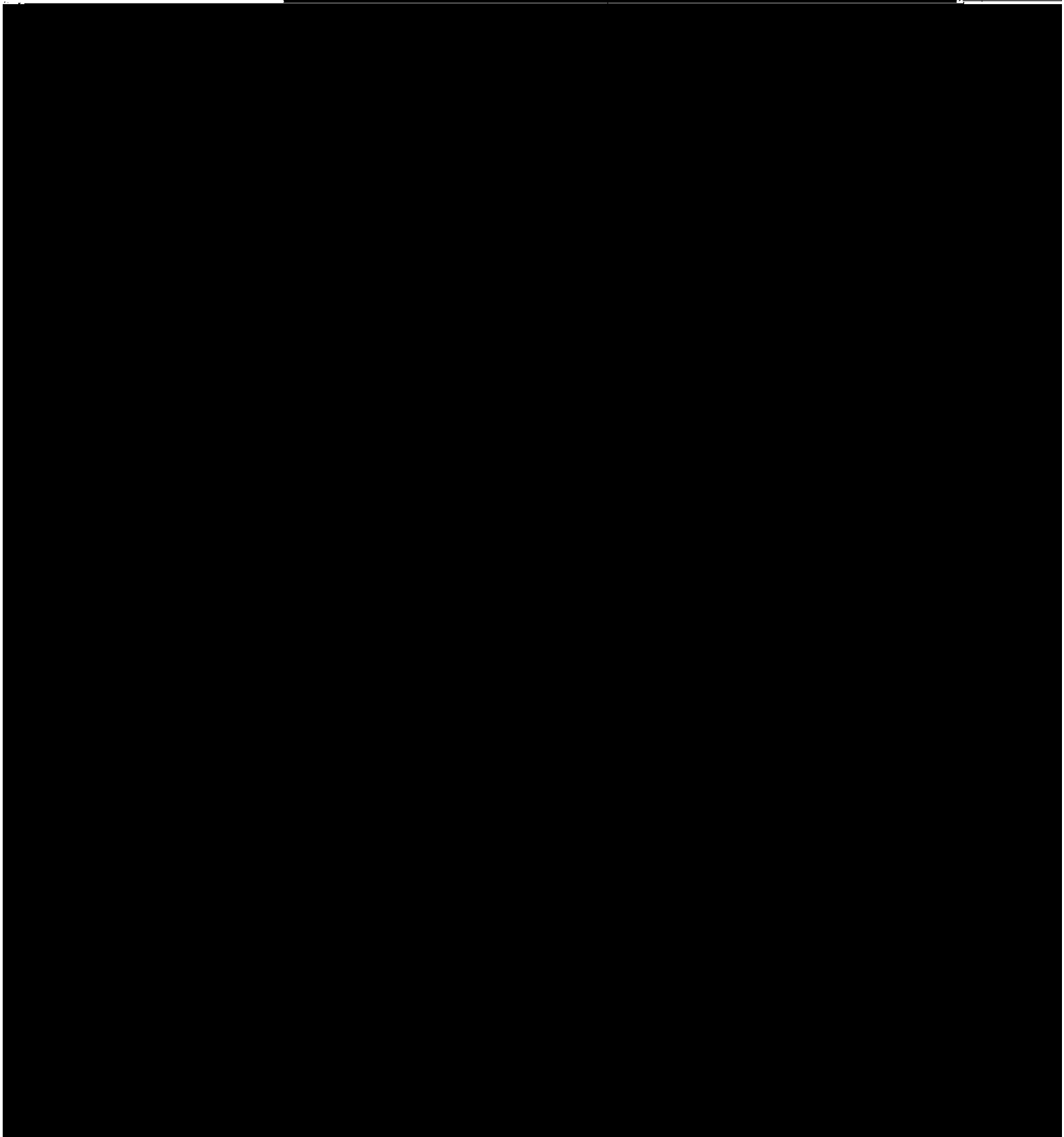
Figure 4 PM (bottom) on the XZ-cross section for the

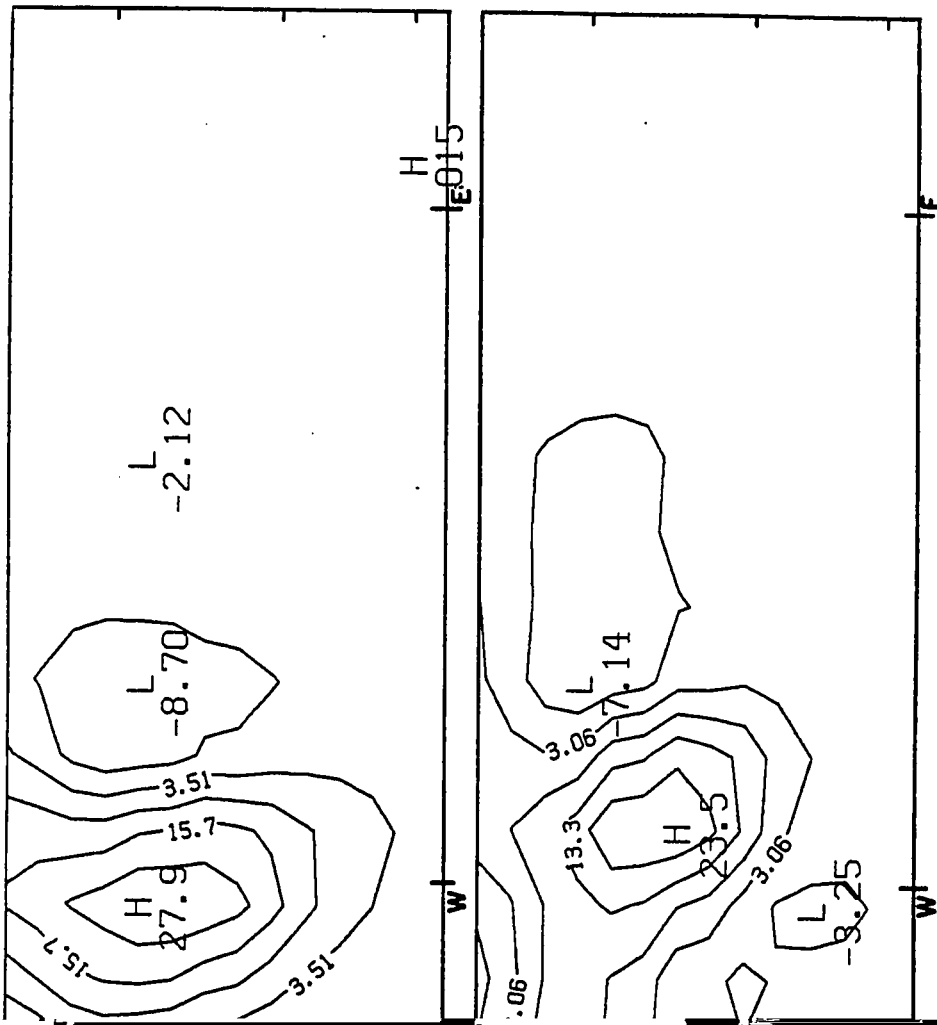
Due to the initial drier environment, the deep cumulus convective development is slower than the control run's during the earlier afternoon. However, during the late afternoon, convective downdraft cooling is generated which appears to be as strong, or in some occasions even stronger than, those of the control run. This implies that the drier environment is contributing, among other factors, to the generation of the strong downdrafts (Knupp, 1985). Therefore, we see from Fig. 5-6 that the maximum upward velocities at both 2 PM and 3 PM are





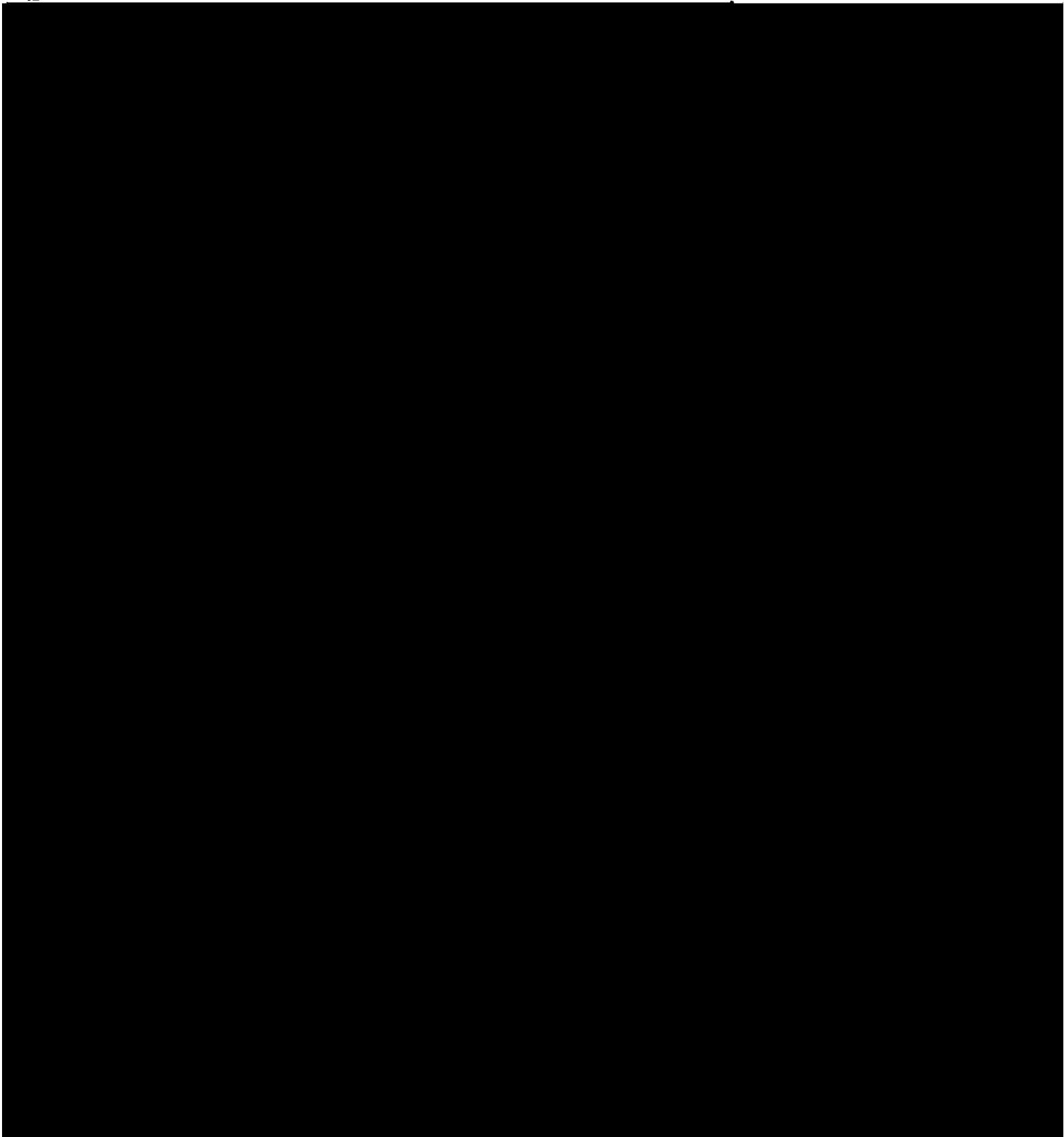
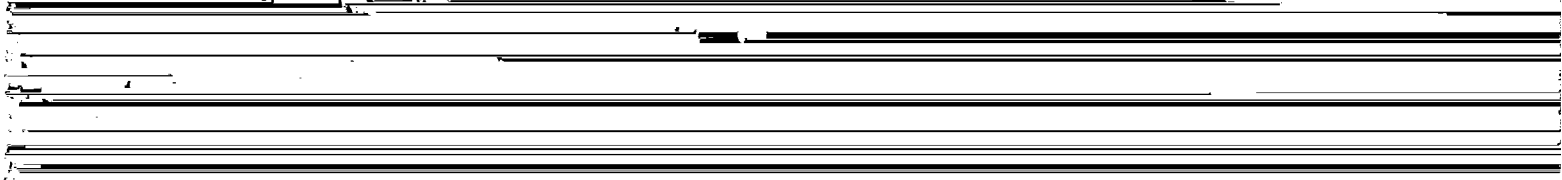
at 4 PM around 10 km (top) and 1 km (bottom)

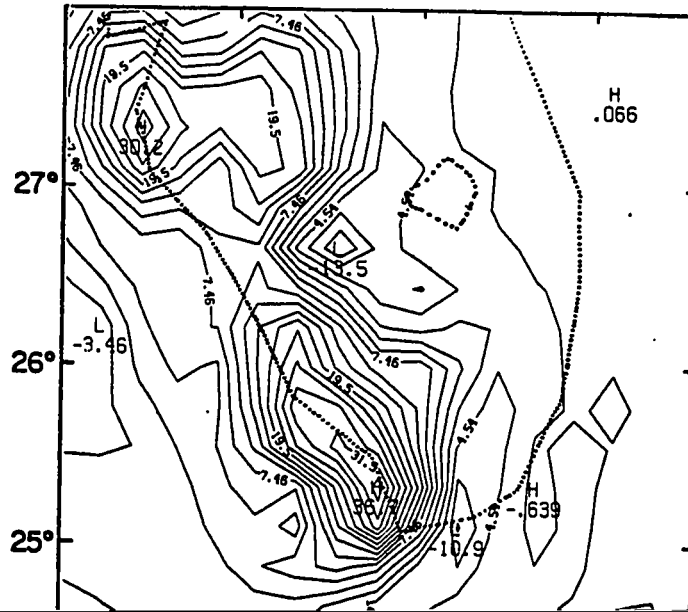




ies (cm/s) at 3 PM (top) and 4 PM (bottom) on the XZ-cross section for the experiment.

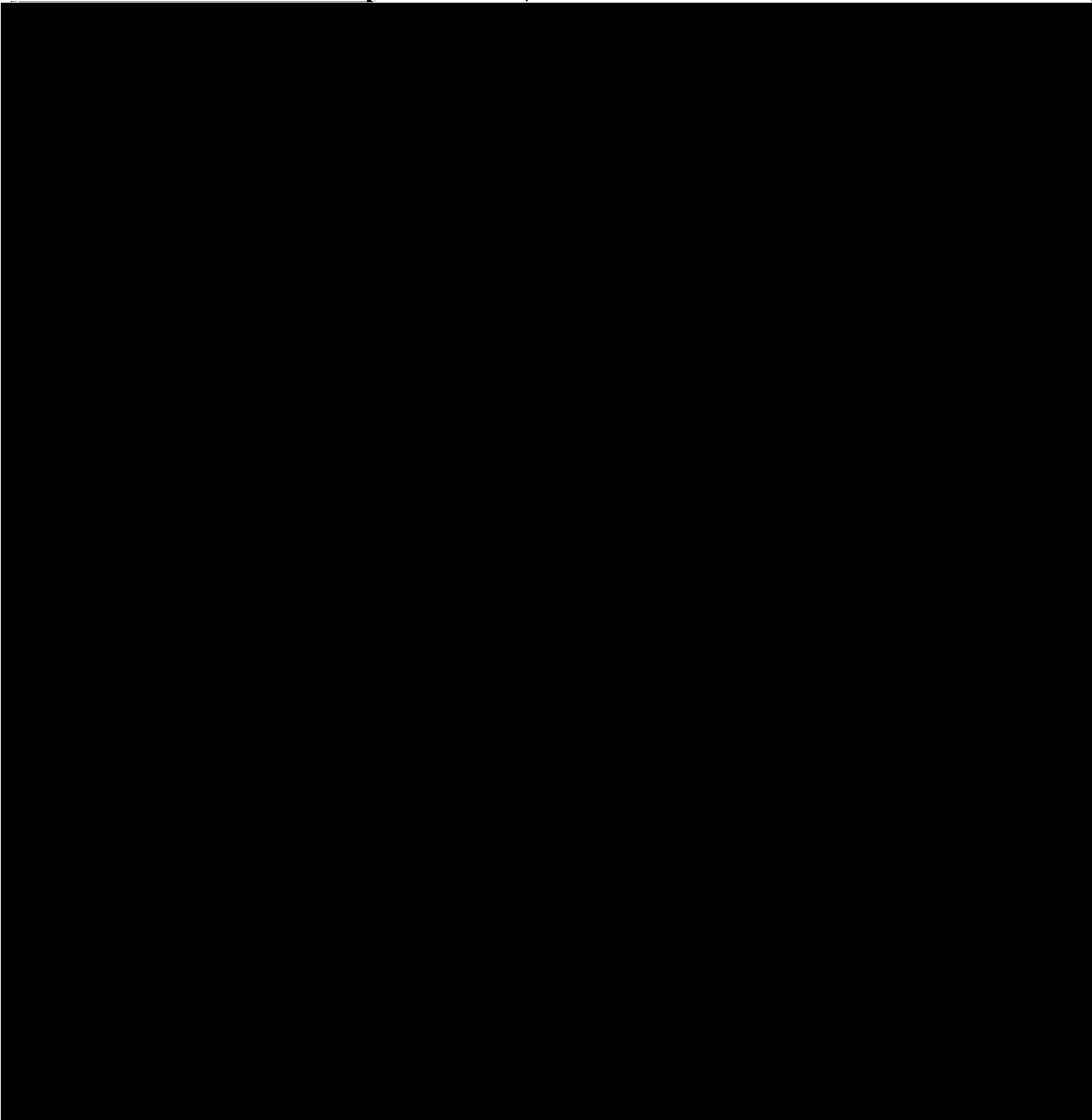
Figure 5-9 indicates that without the downdraft effect the





## Chapter 6

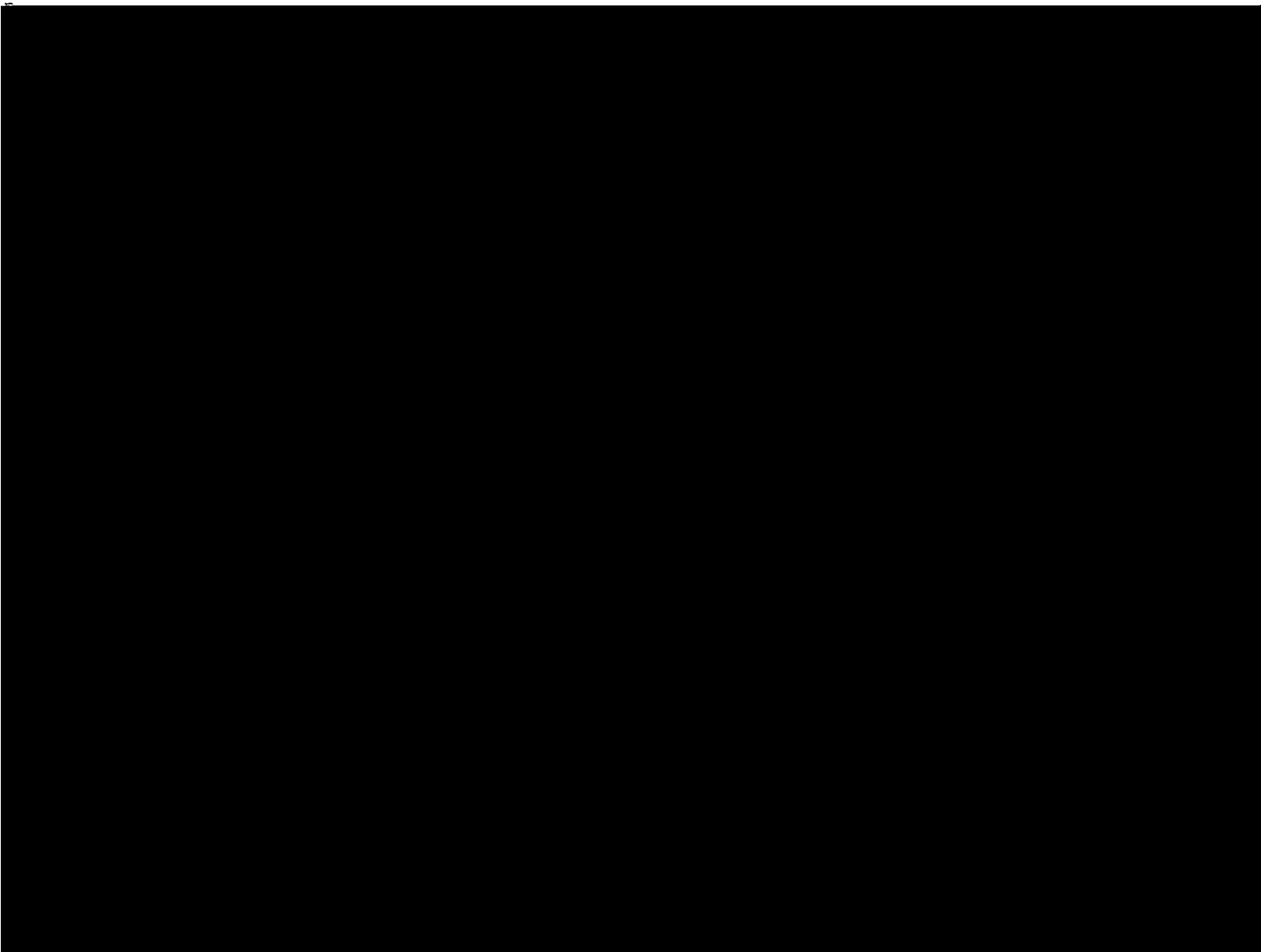
---



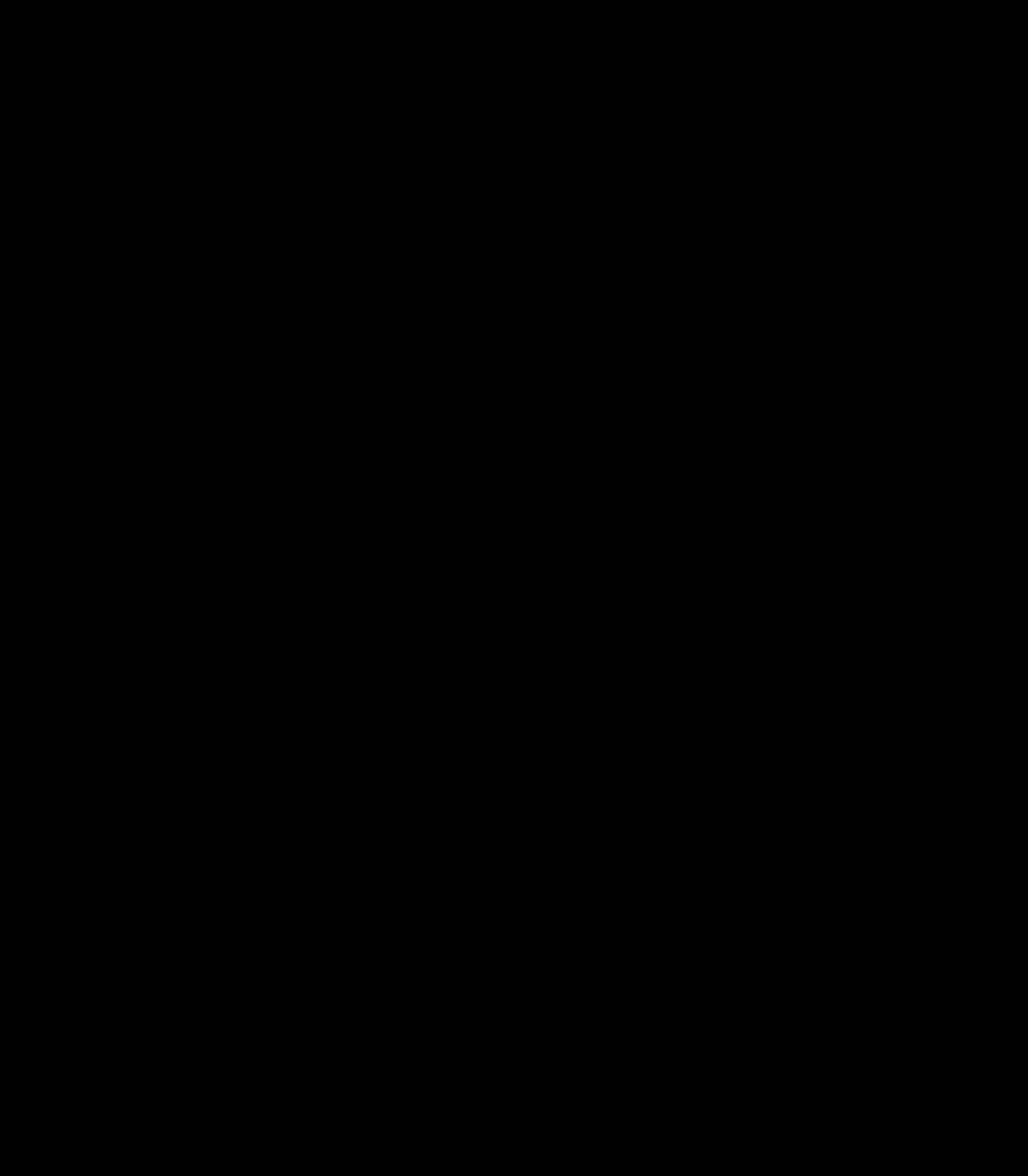
is a proper choice as the time separating the two stages: a sea breeze convergence stage; and a convective downdraft cooling stage.

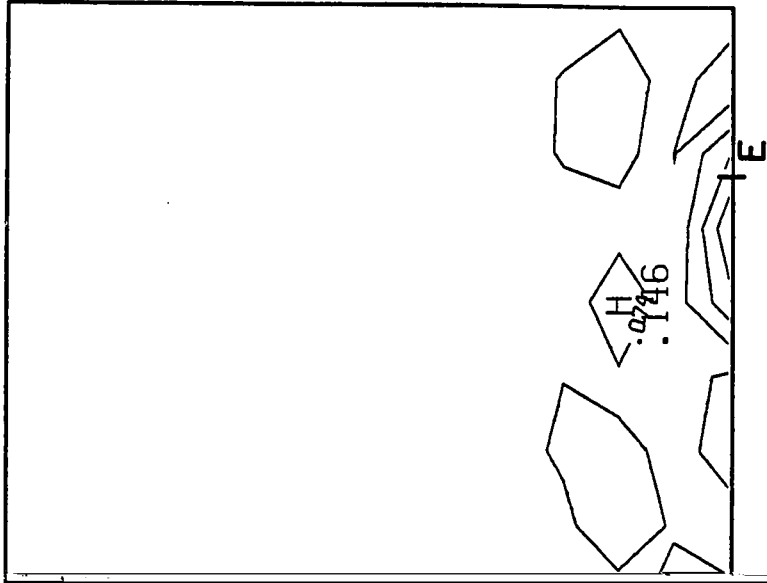
As discussed previously throughout this study, during the mature stage of the convective lifetime the downdraft cooling effect is seen to provide a positive feedback mechanism which enhances the subsequent convection by generating low-level upwind-side upward motion; meanwhile the downdraft tends to stabilize the original convective area by replacing the original boundary layer air with colder air. As discussed in section 4-4, the mid-tropospheric convergence is related to the mesoscale upward and downward motion during the late afternoon. The downward motion acts to decrease the low-level moisture supply from

---

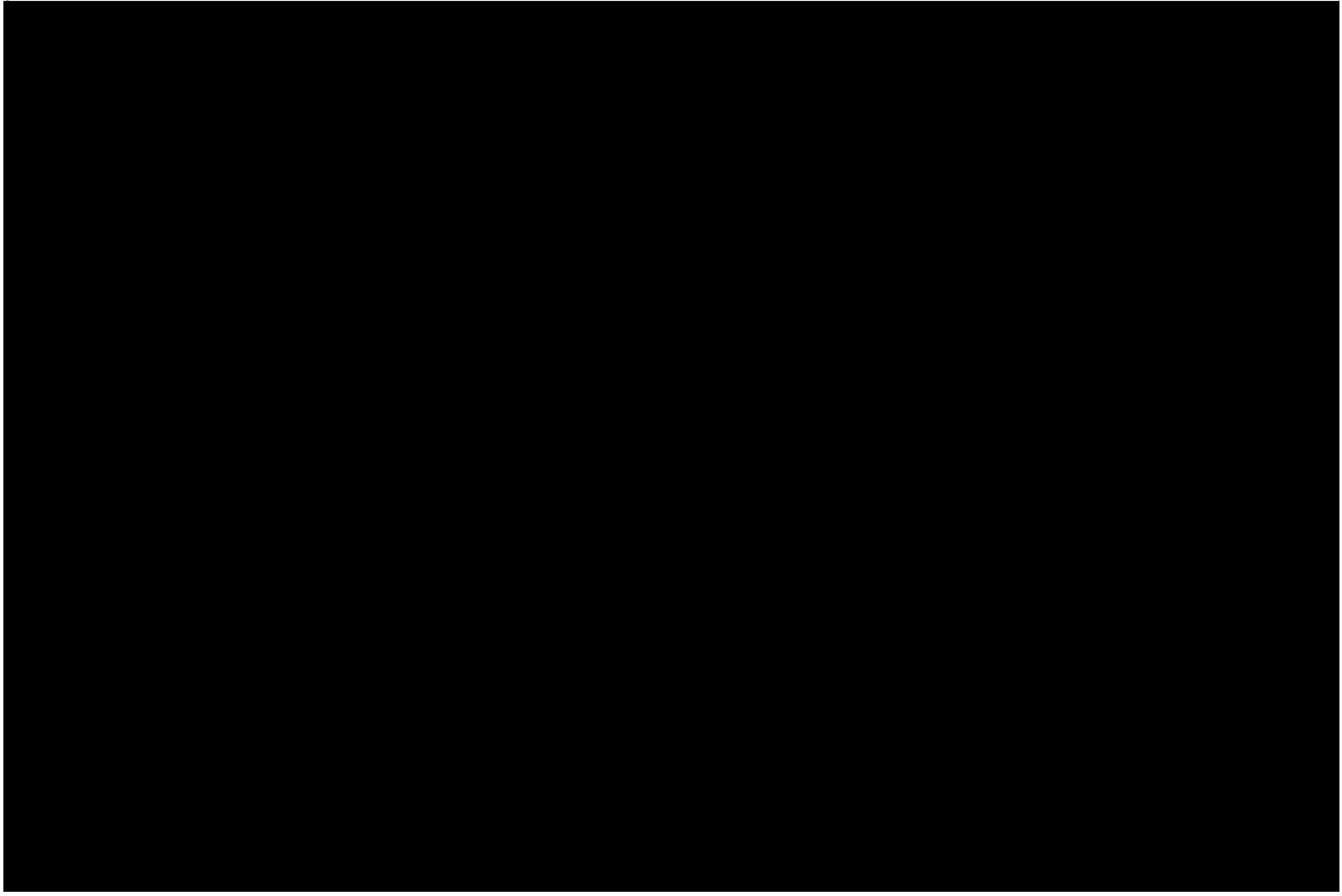


After a brief discussion of each stage, conceptual models will be used for each of the three stages, which are derived from the central model.





$10^{-4} \text{ s}^{-1}$ ) on the XZ-cross section for the Stage-1



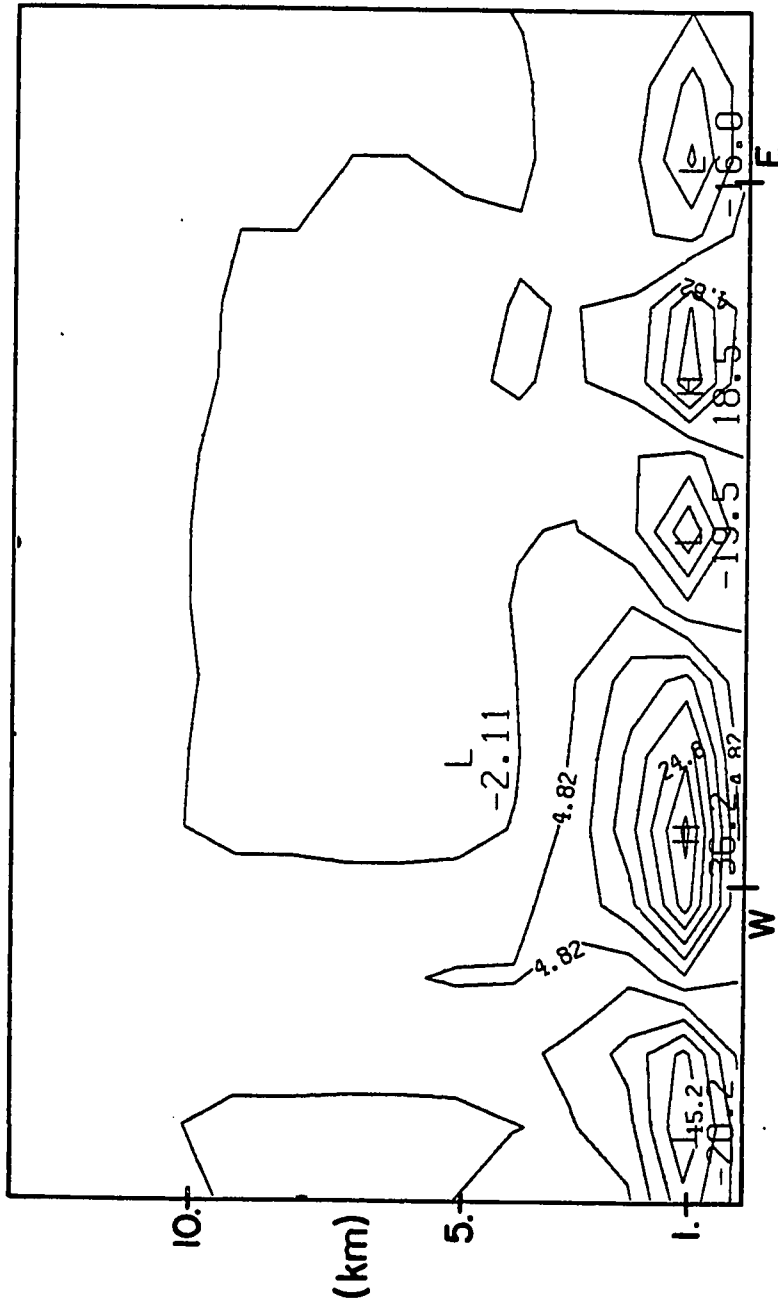
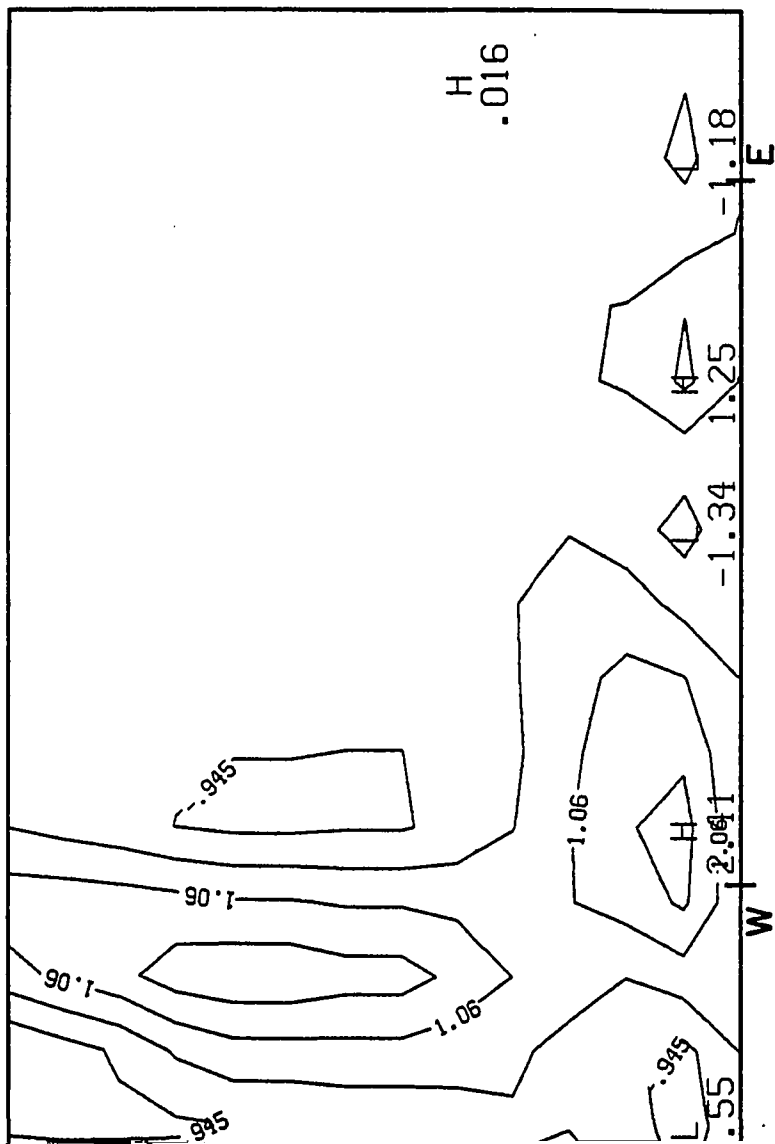
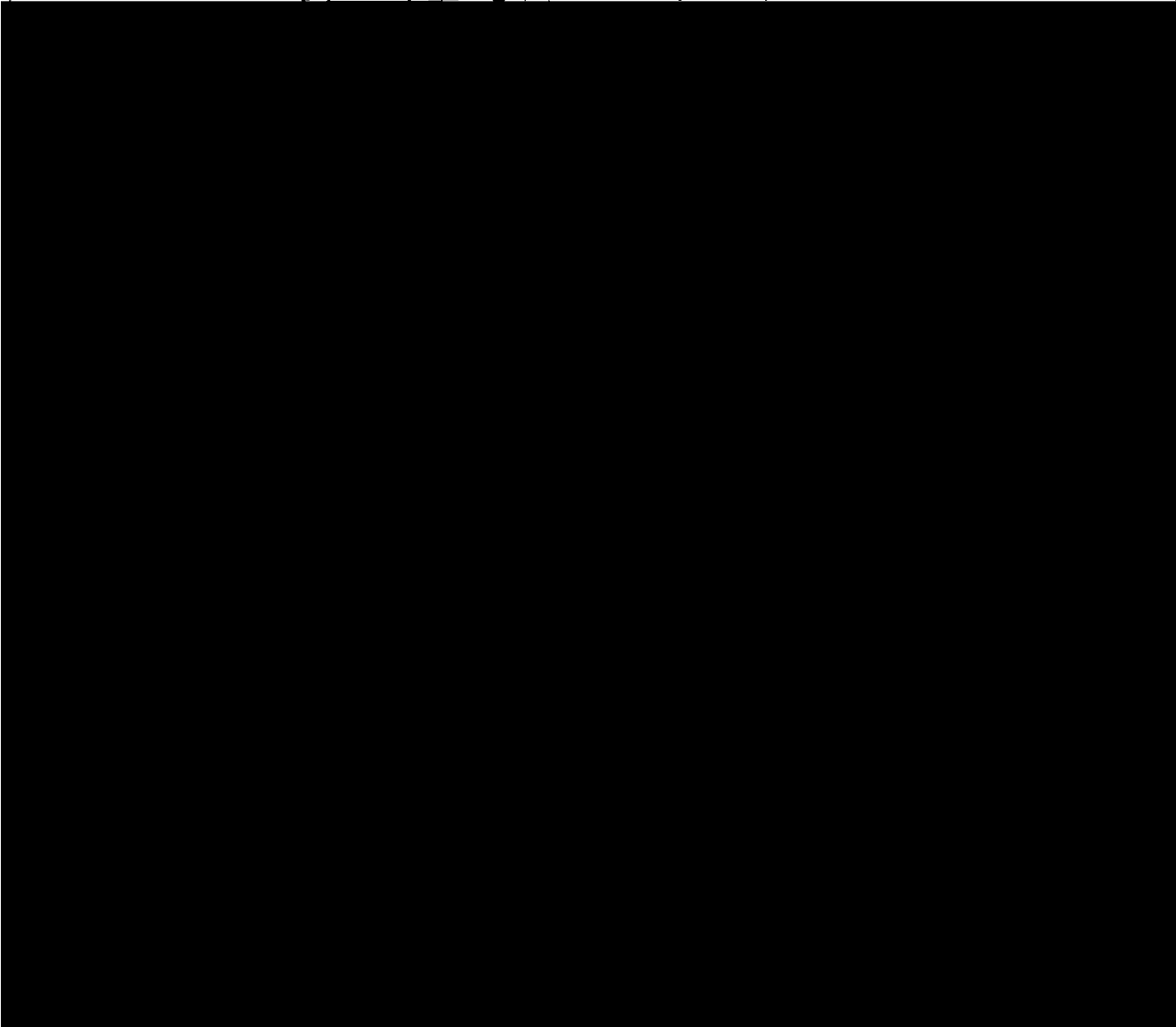
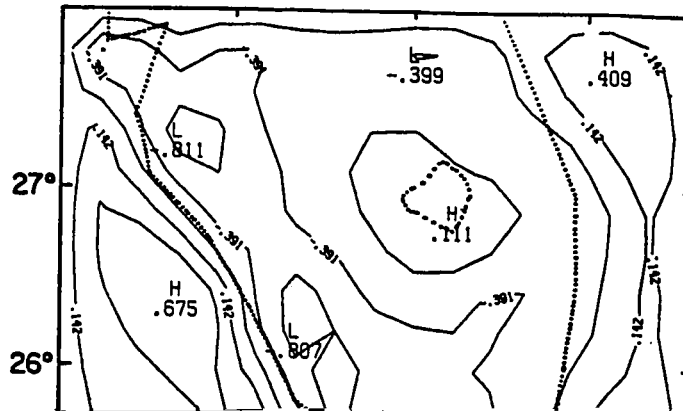
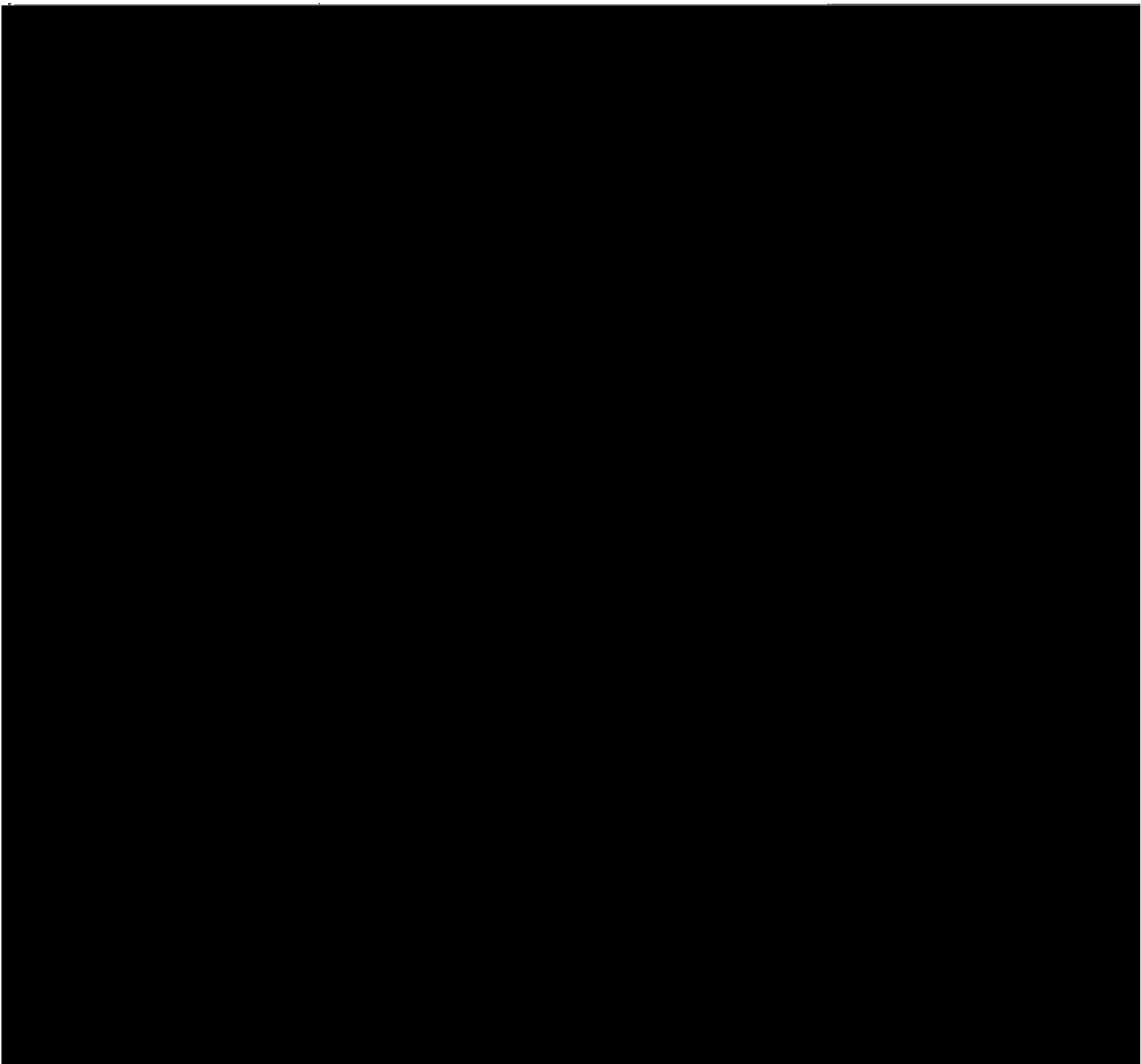


Figure 6-2. The time averaged moisture flux term (vertical velocity times specific humidity) on the XZ-cross section for the Stage-1 (over the time period of 1200-1400 EST).



me averaged vertical velocity (cm/s) on the XZ-cross section for the Stage-1 (over the period of 1200-1400 EST).





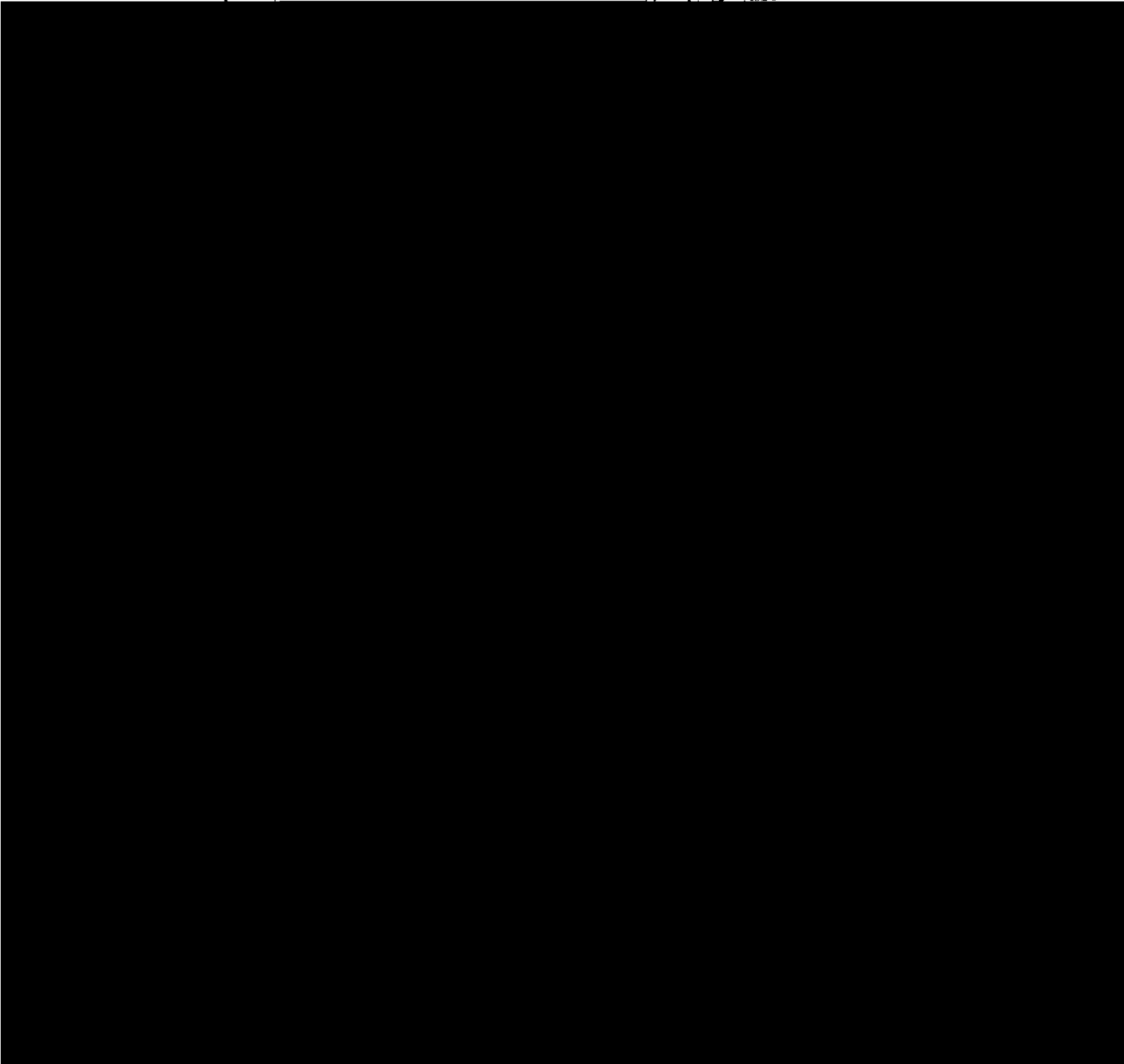
sea breeze circulation is enhanced and extended over a much thicker layer throughout the troposphere due to the convective effect.

6-2-b. Convective Downdraft Cooling Stage

Figure 6-6 shows the two-hour averaged horizontal divergence of



action for the Stage-2



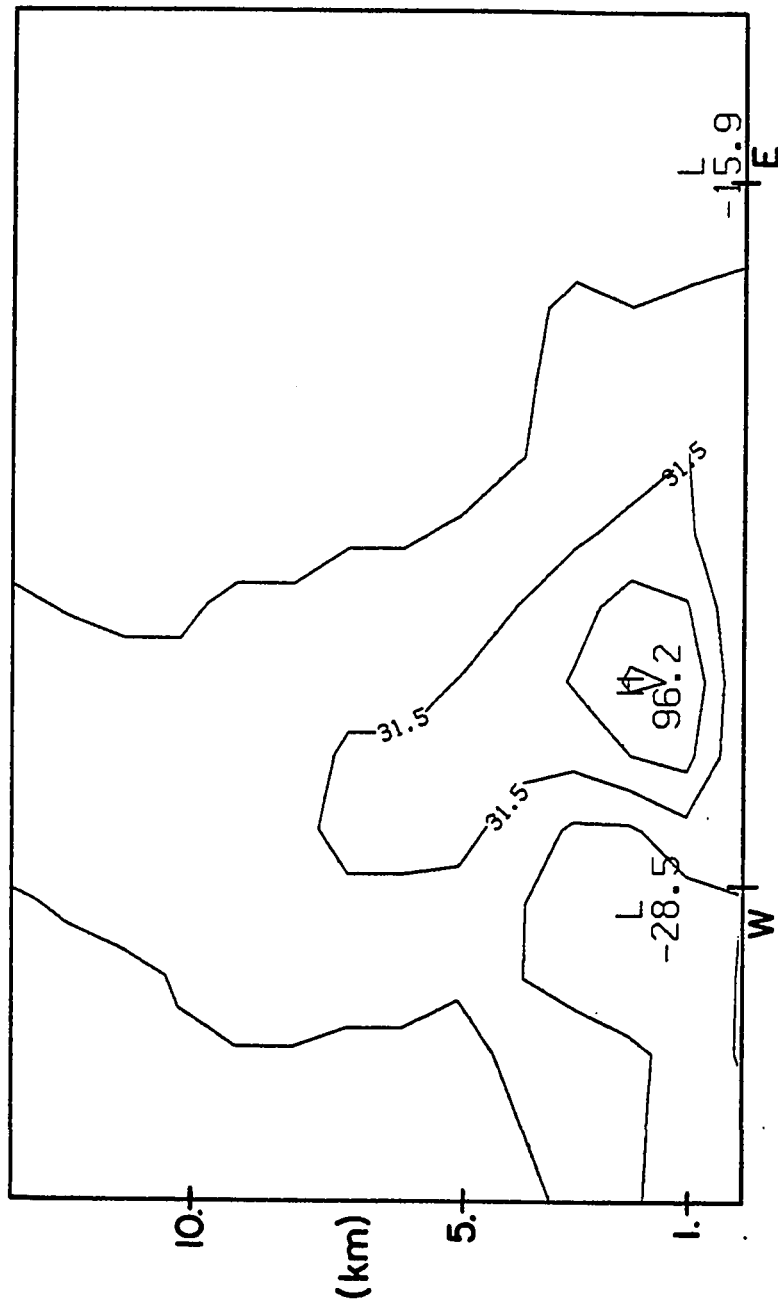
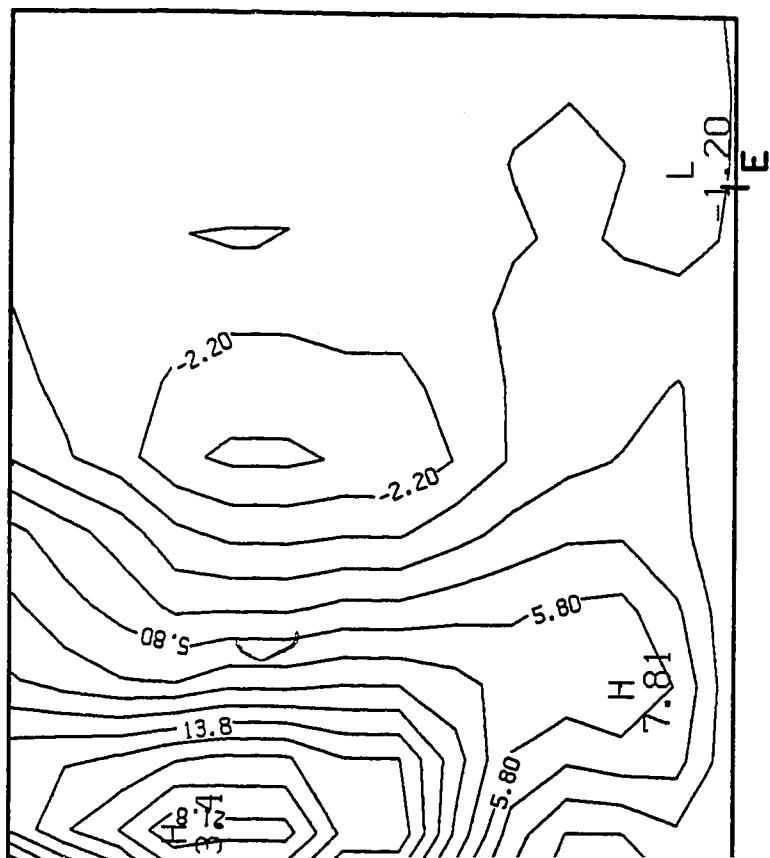
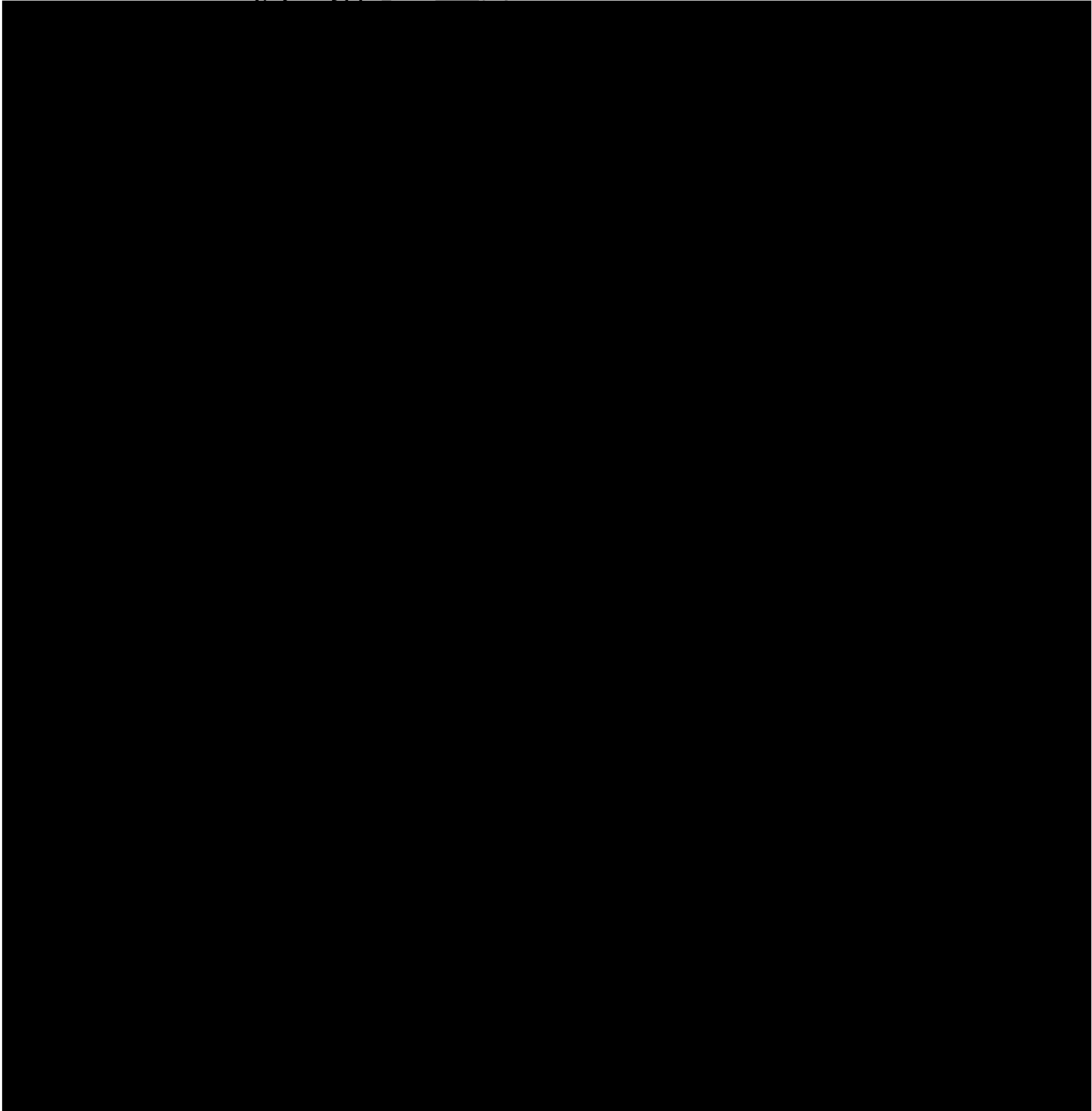
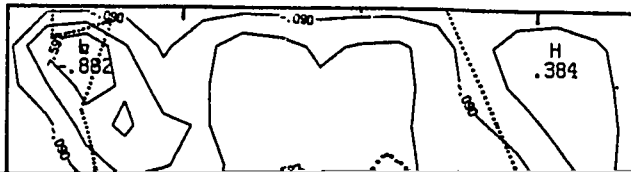


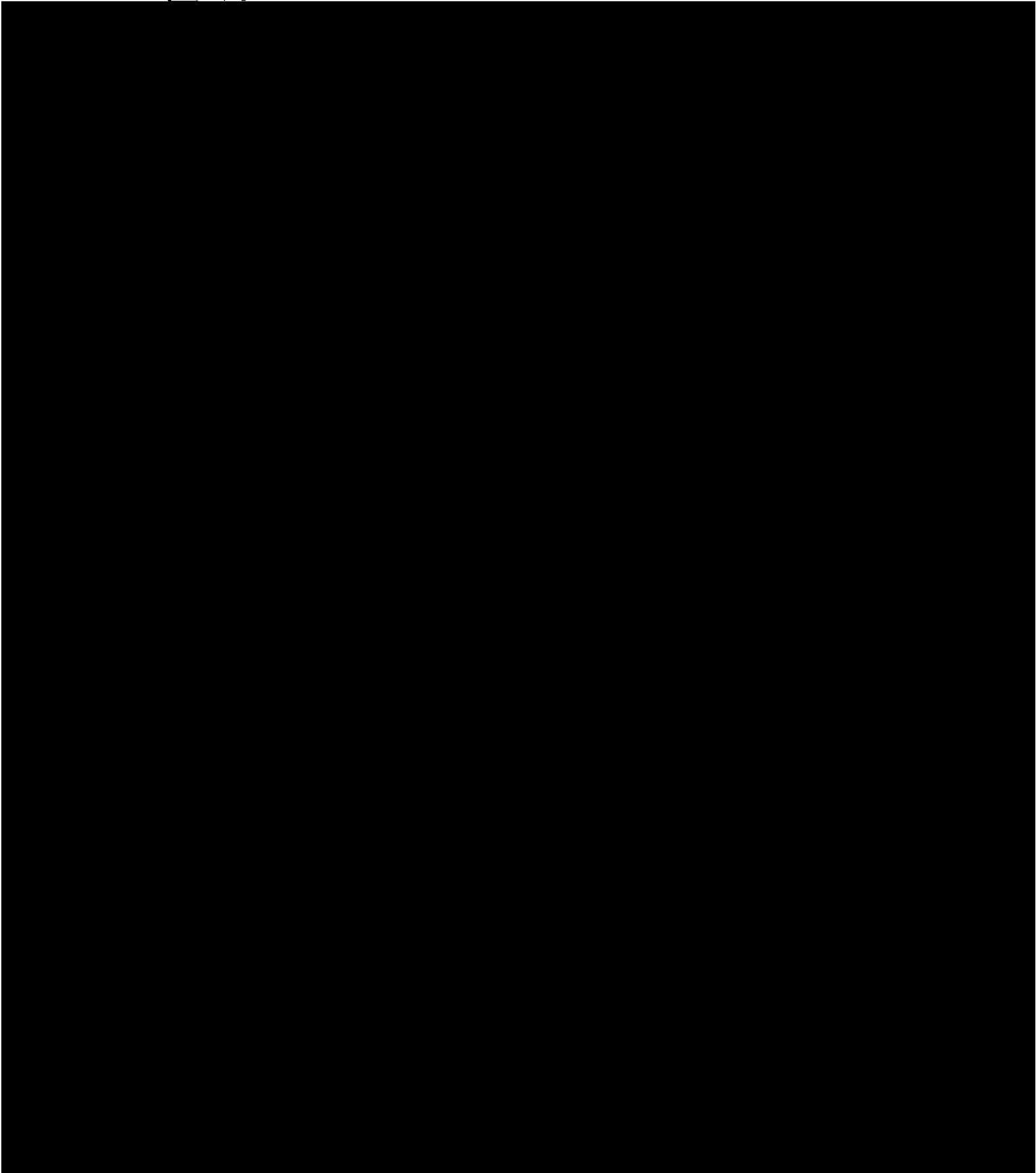
Figure 6-7. The time averaged moisture flux term (vertical velocity times specific humidity) on the XZ-cross section for the Stage-2 (over the time period of 1200-1400 EST).



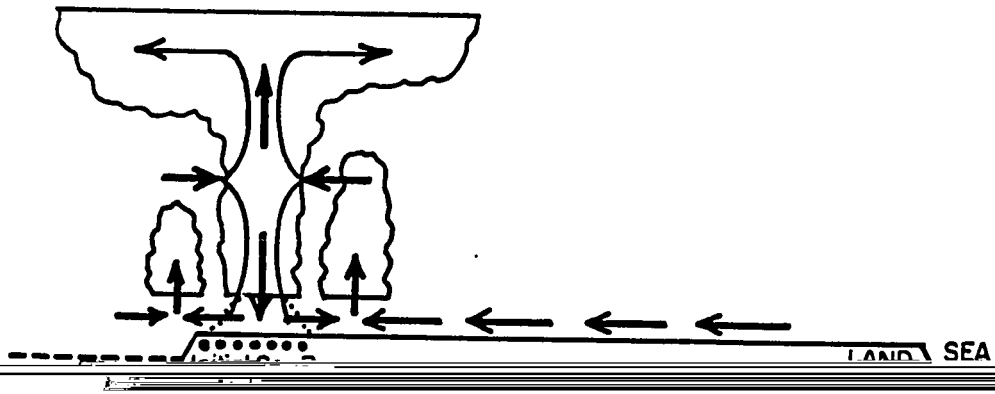
al velocity (cm/s) on the XZ-cross section for the Stage-2 (over the EST).



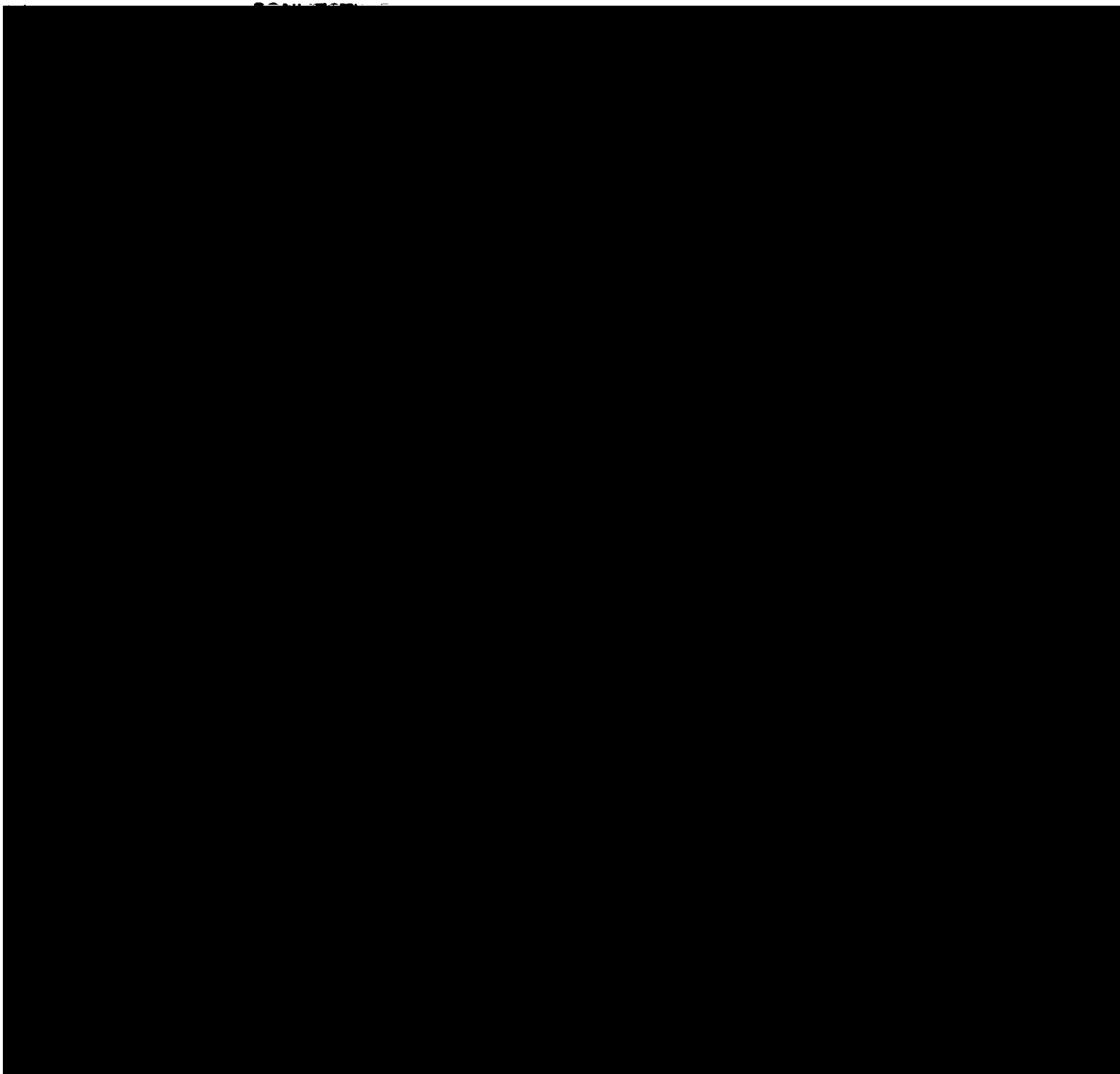
and surface vorticity maximum indicate that the convergence no longer acts to strengthen the original convective



STAGE-2 (1400-1600 EST) Part I  
CONVECTIVE DOWNDRAFT COOLING STAGE (I)



STAGE-2 (1400-1600 EST) Part II



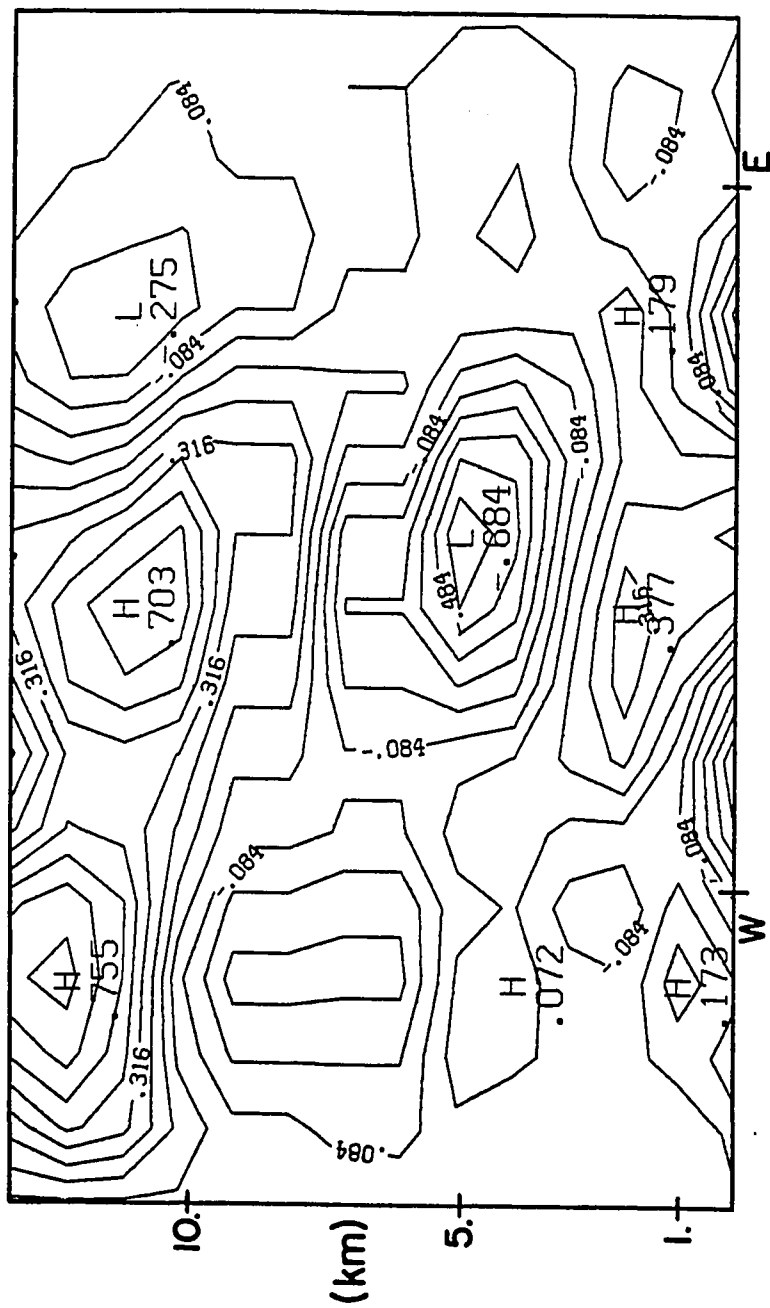


Figure 6-11. The time averaged horizontal divergence ( $10^{-4} \text{ s}^{-1}$ ) on the XZ-cross section for the Stage-3 (over the time period of 1200-1400 EST).

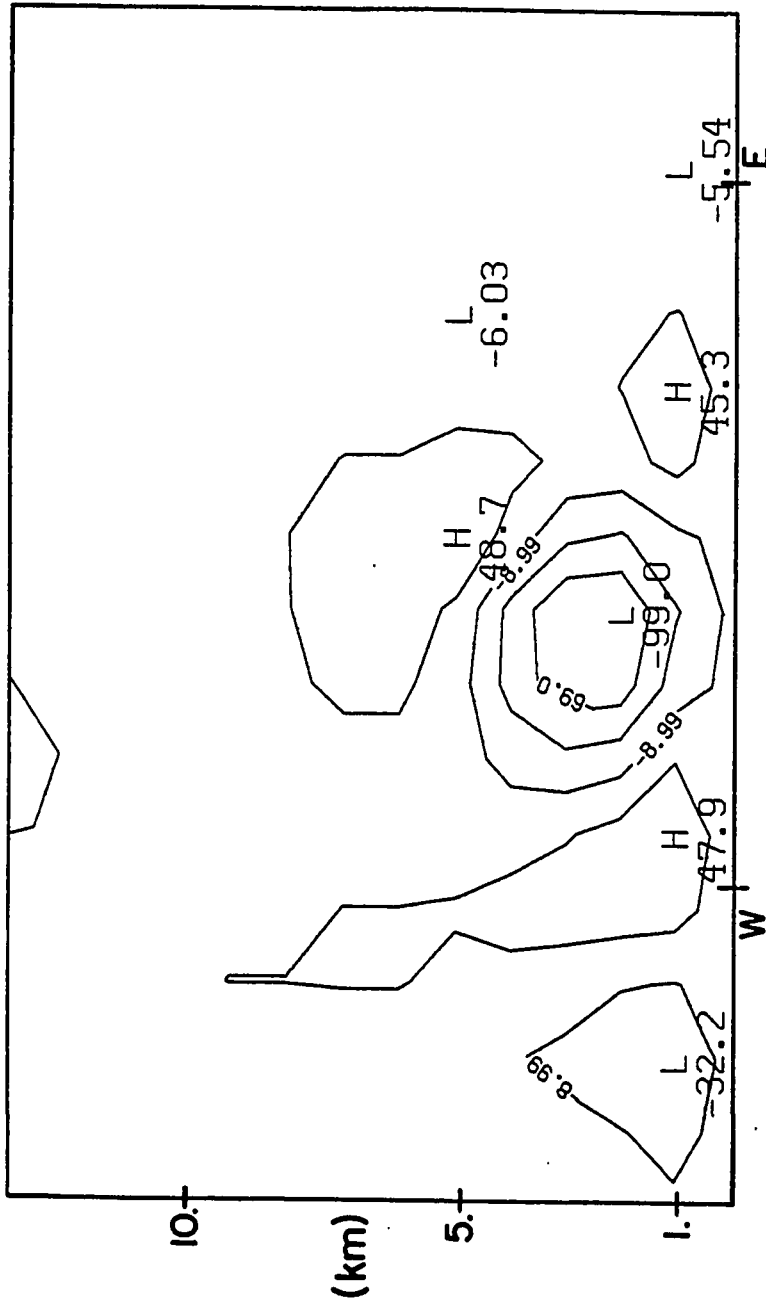
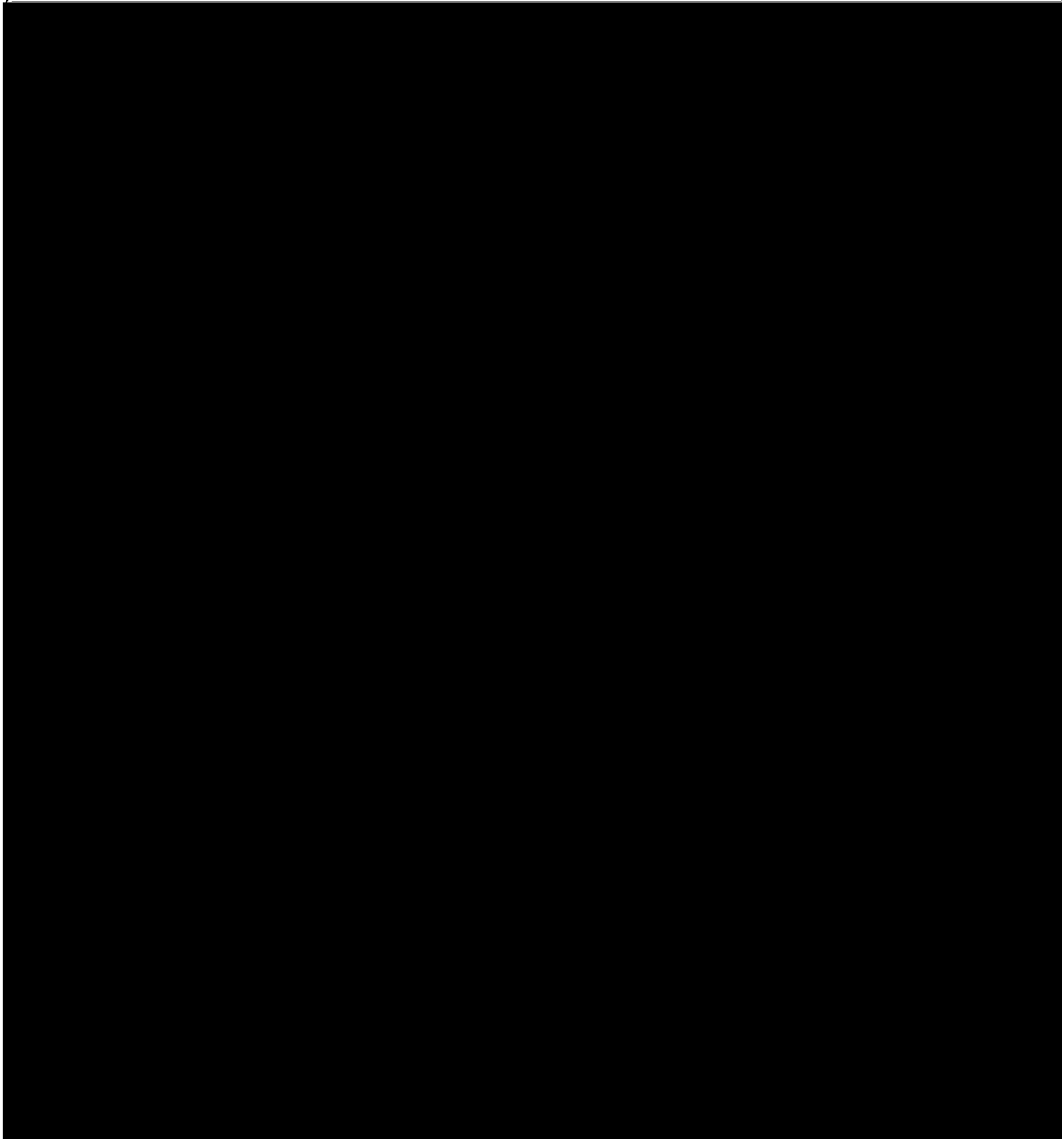


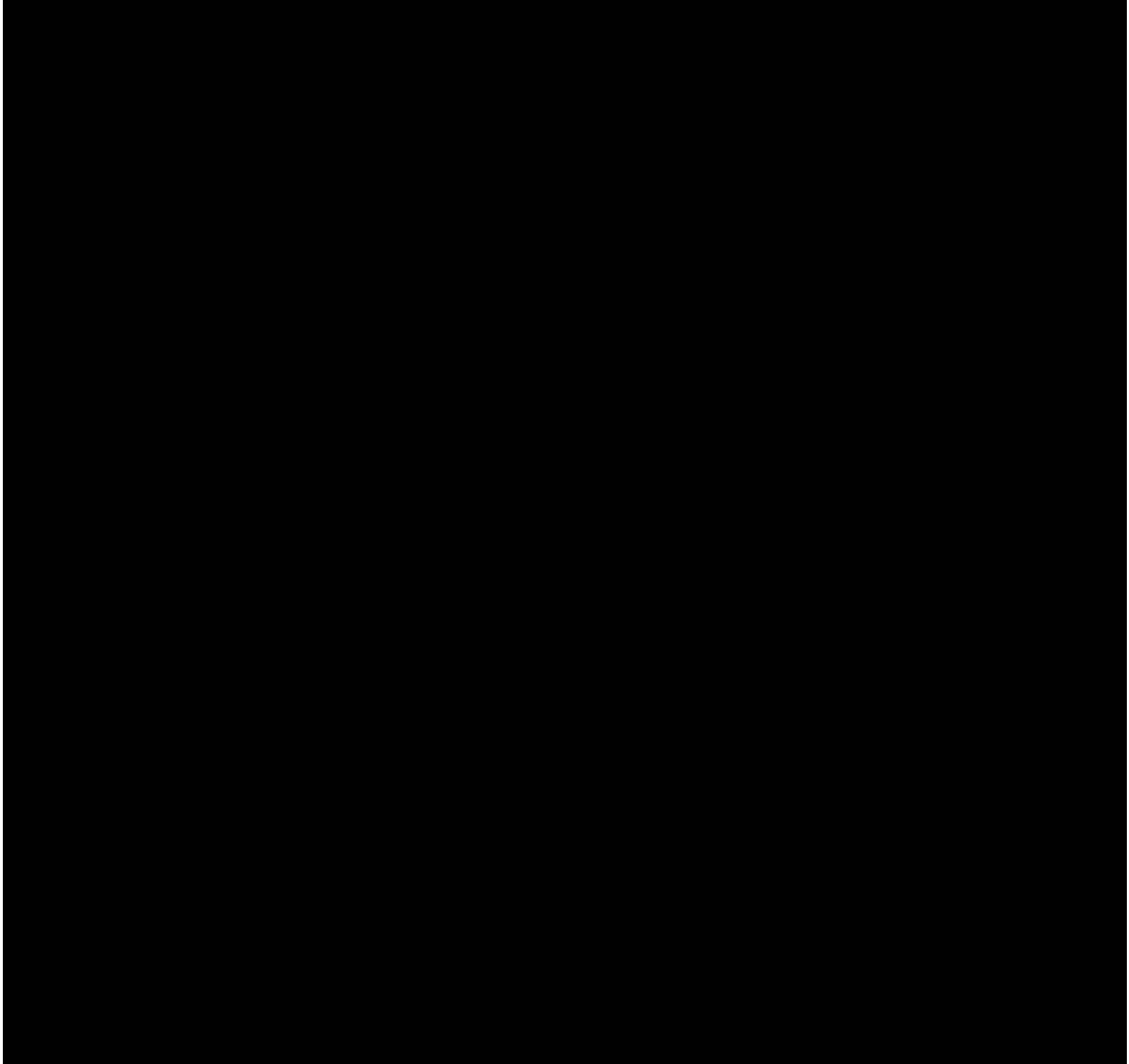
Figure 6-12. The time averaged moisture flux term (vertical velocity times specific humidity) on the XZ-cross section for the Stage-3 (over the time period of 1200-1400 EST).

-----





the Stage-3 (over the



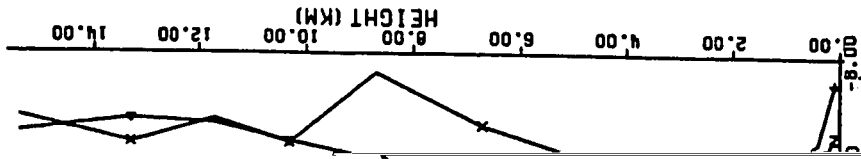
STAGE-3 (1600-1800 EST)

---

---

---



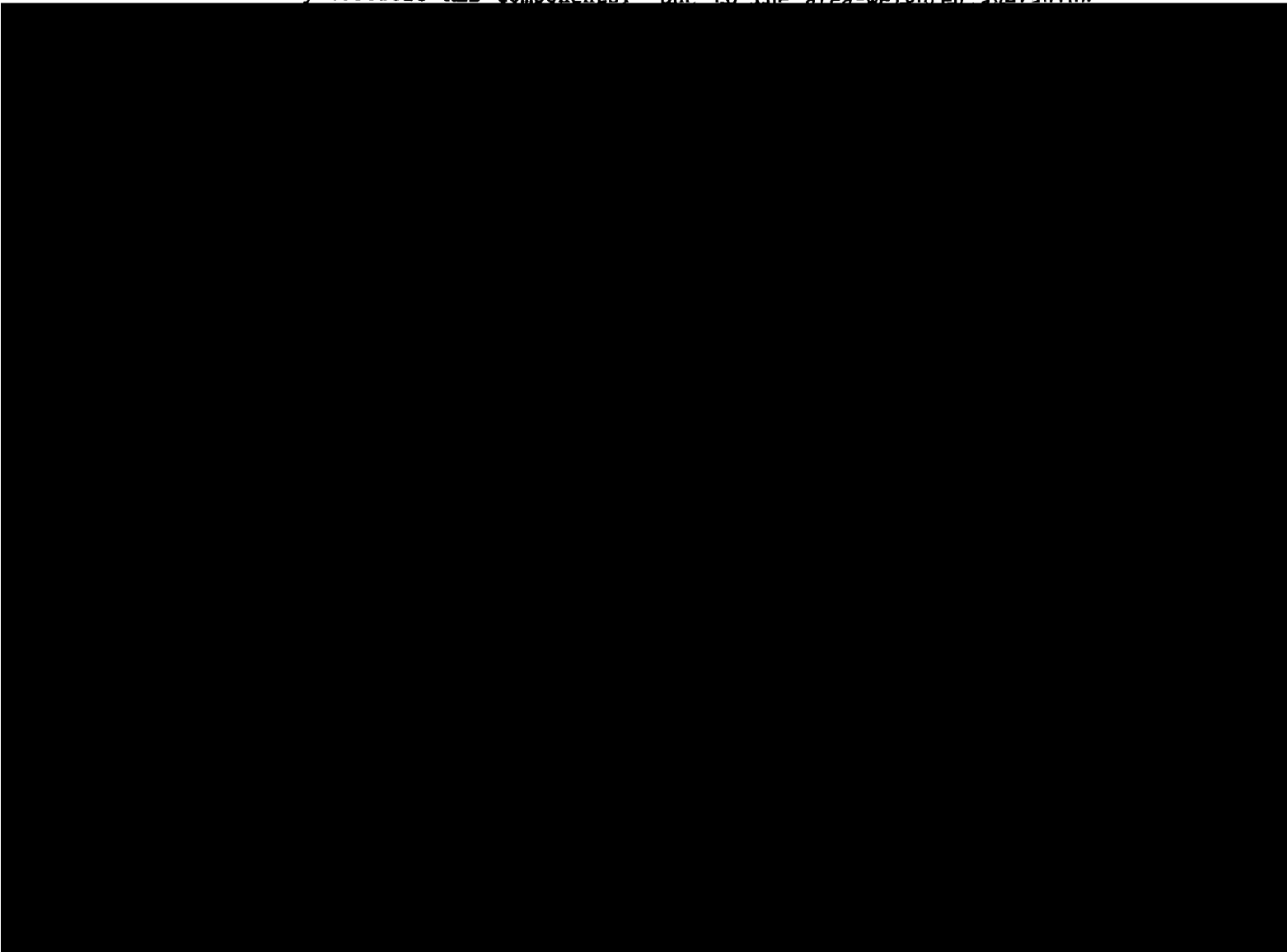


idget components (watt/m<sup>2</sup> /  
breeze run (right). The

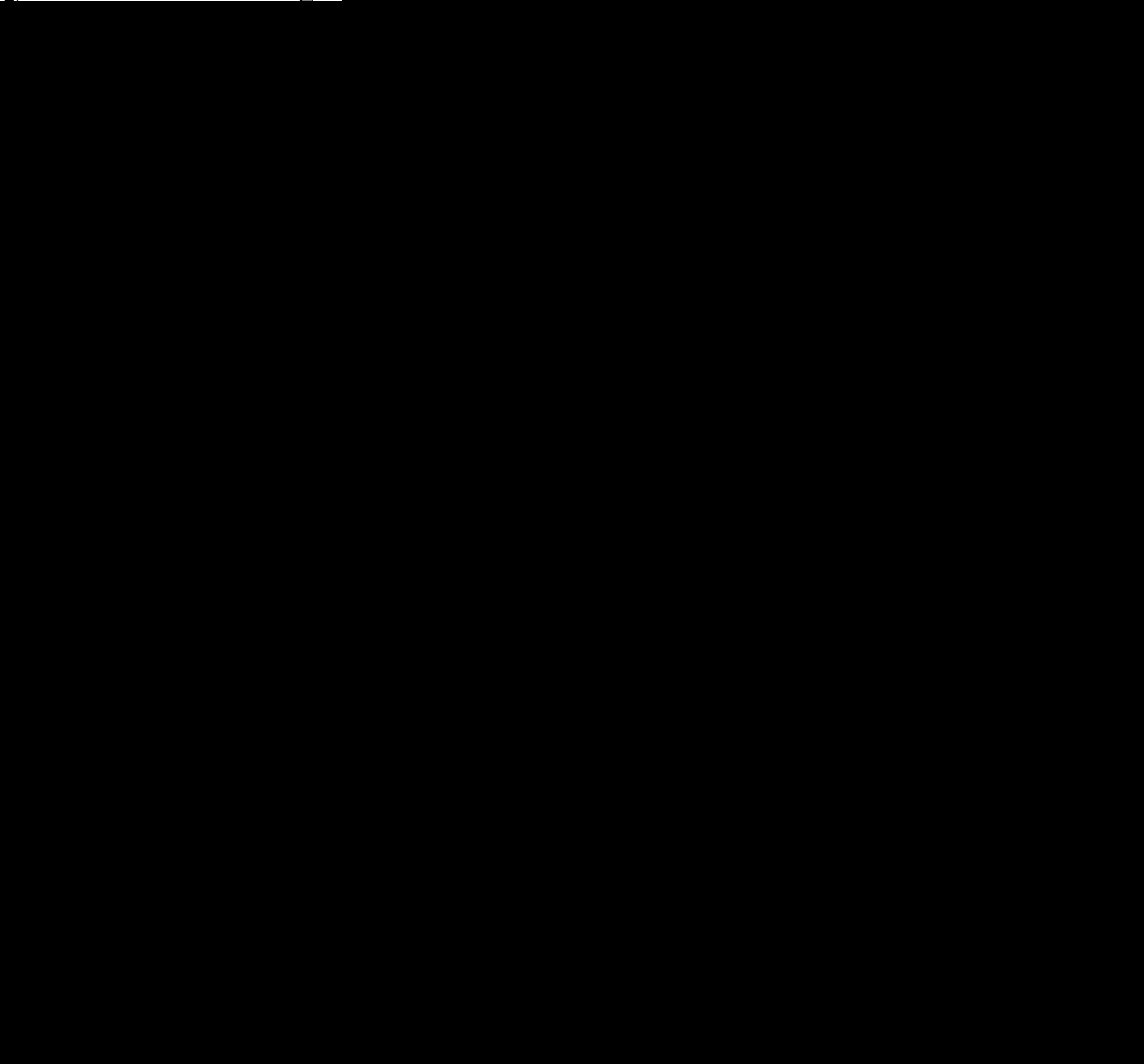
percent of the corresponding dry components' values) and a net KE sink at surface.

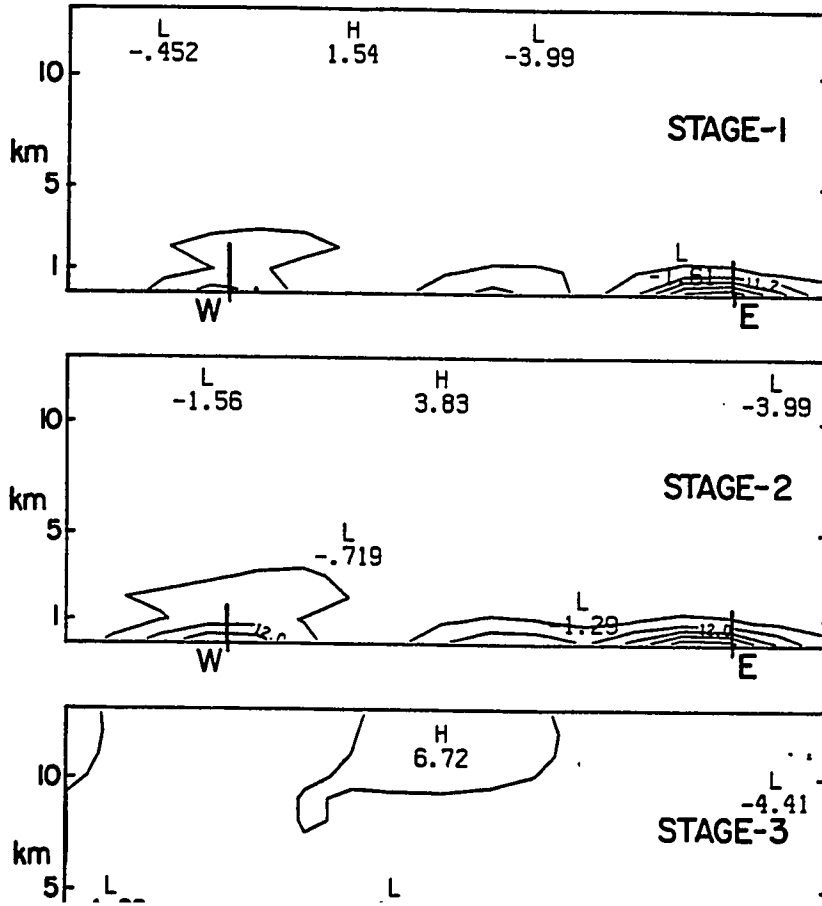
- The dry KEB components are negligible in the upper troposphere, while those of the moist case have relatively large values in the layer between about 8 km and 14 km (i.e., upper-level wind perturbations generated in response to the deep cumulus convection, around 12 km).

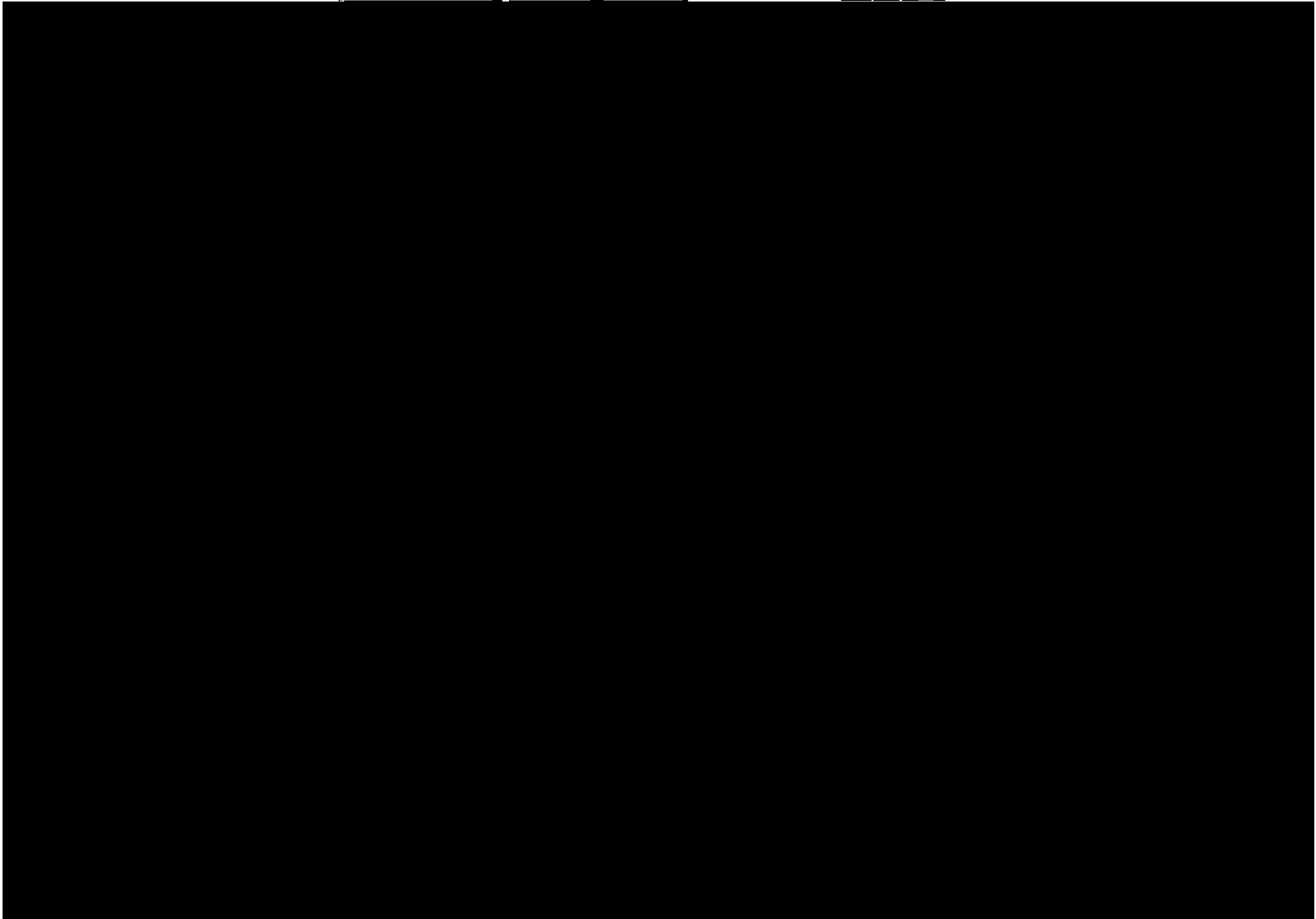
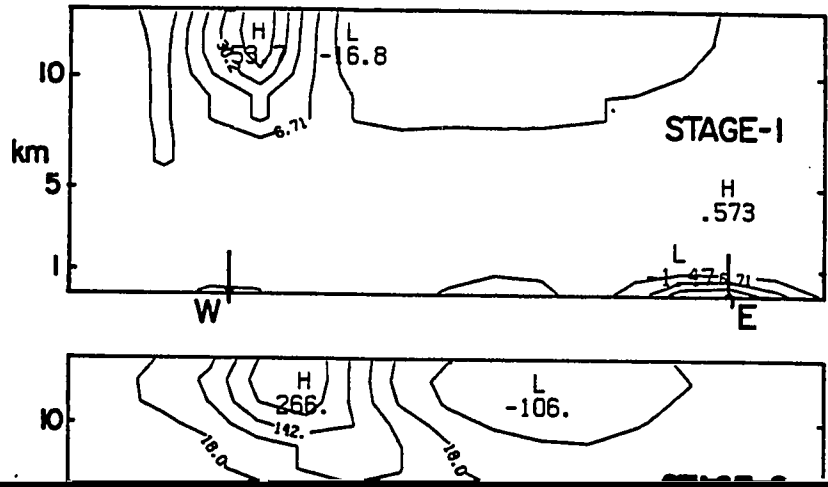
The direct contribution of deep cumulus convection upon the grid-scale horizontal kinetic energy budget is calculated using the procedure described in Section 3-6. The resultant vertical profile of this term is shown in Table 3-12, which can be directly compared with other hydrostatic KEB components. Due to the area-weighted averaging



Comparing Fig. 6-16 (dry sea breeze run) with Fig. 6-17 (moist sea breeze run), we see that the major difference between the dry and moist sea breeze energetics is that the deep convective effects produce significant horizontal pressure perturbations in the upper troposphere.



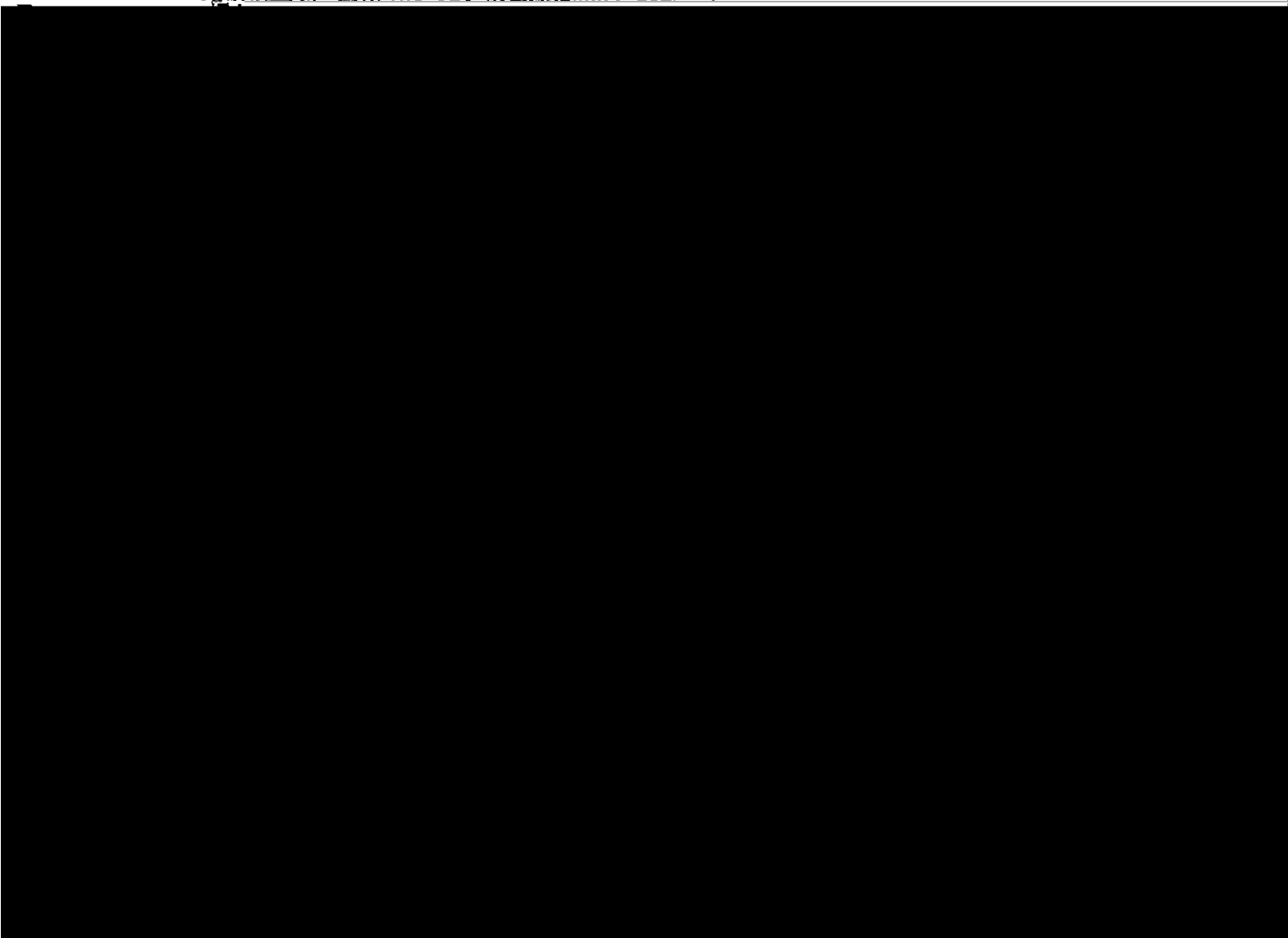




## Chapter 7

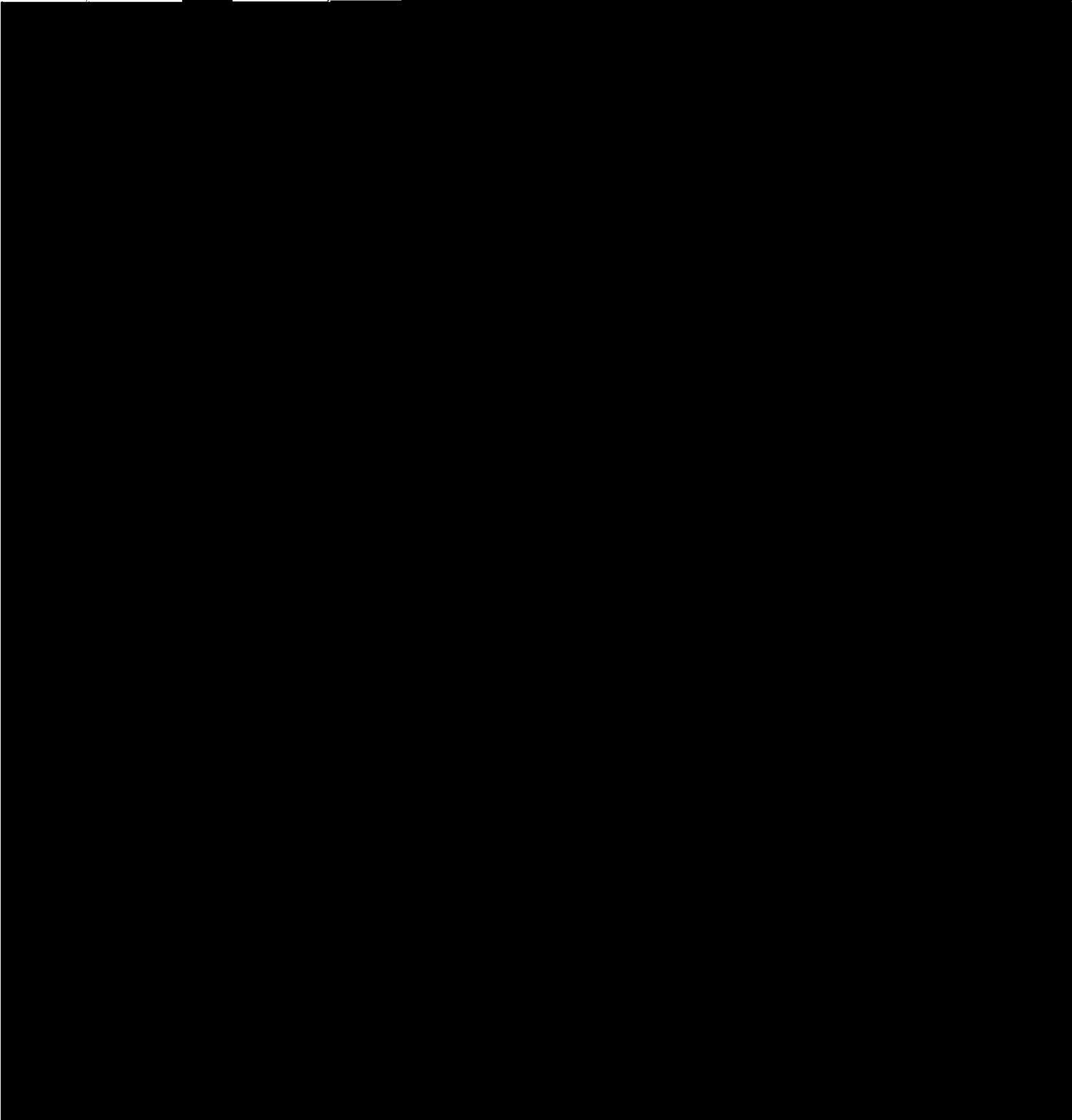
### SUMMARY AND CONCLUSIONS

Florida's deep cumulus convective effects upon the mesoscale sea breeze environment are investigated using a numerical approach validated by observations. The mesoscale hydrostatic primitive-equation model, originally developed by Pielke (1974) for simulating the Florida dry sea breeze circulation, is utilized together with a cumulus parameterization modified from that of Fritsch and Chappell (1980) for investigating the Florida sea breeze-deep convection interaction.



to synoptic categories; and surface radar rainfall hourly maps, for the southern Florida environment on a specific day.

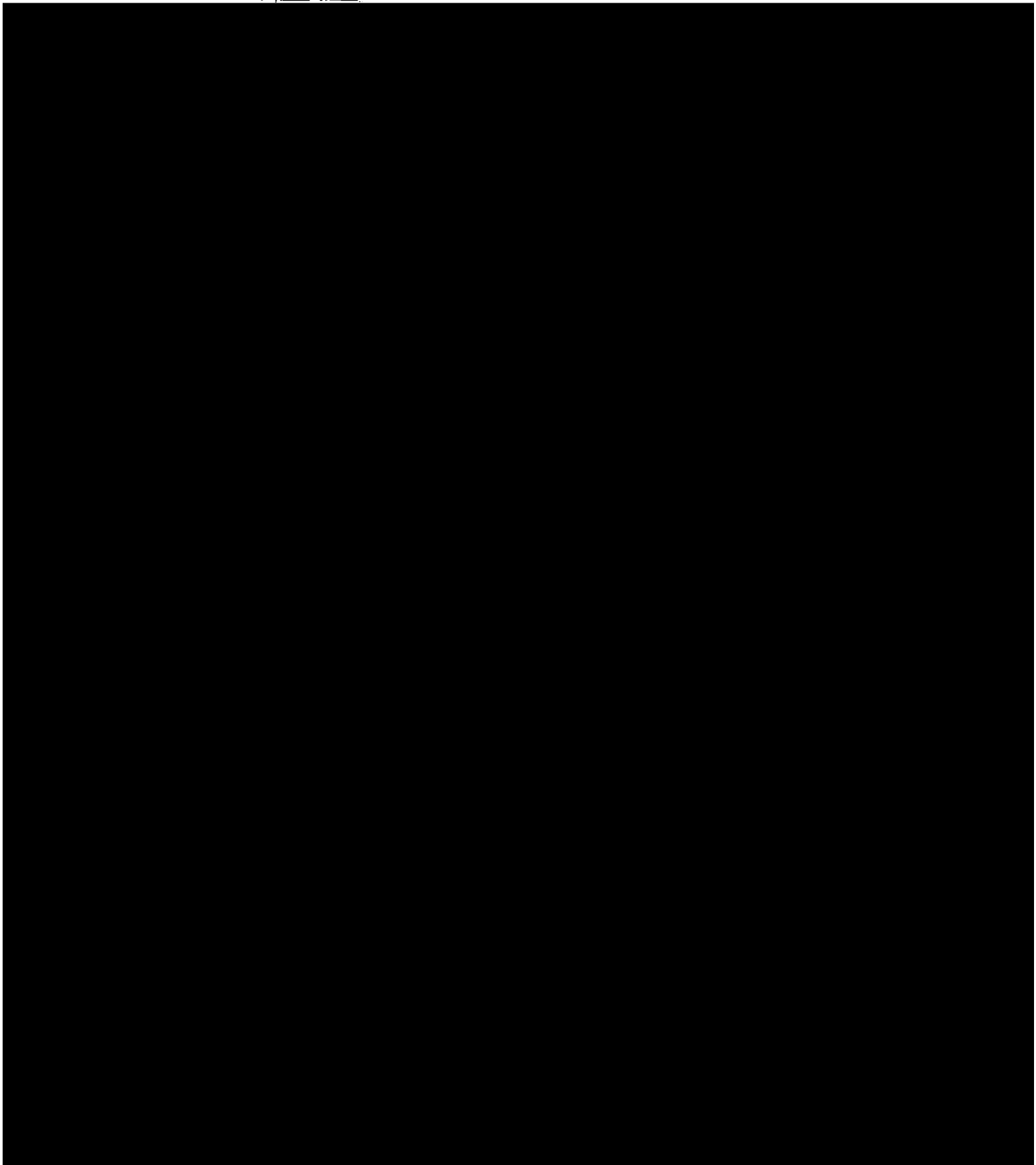
The simulation results are found to be able to produce in general the climatologically observed patterns of deep convection at

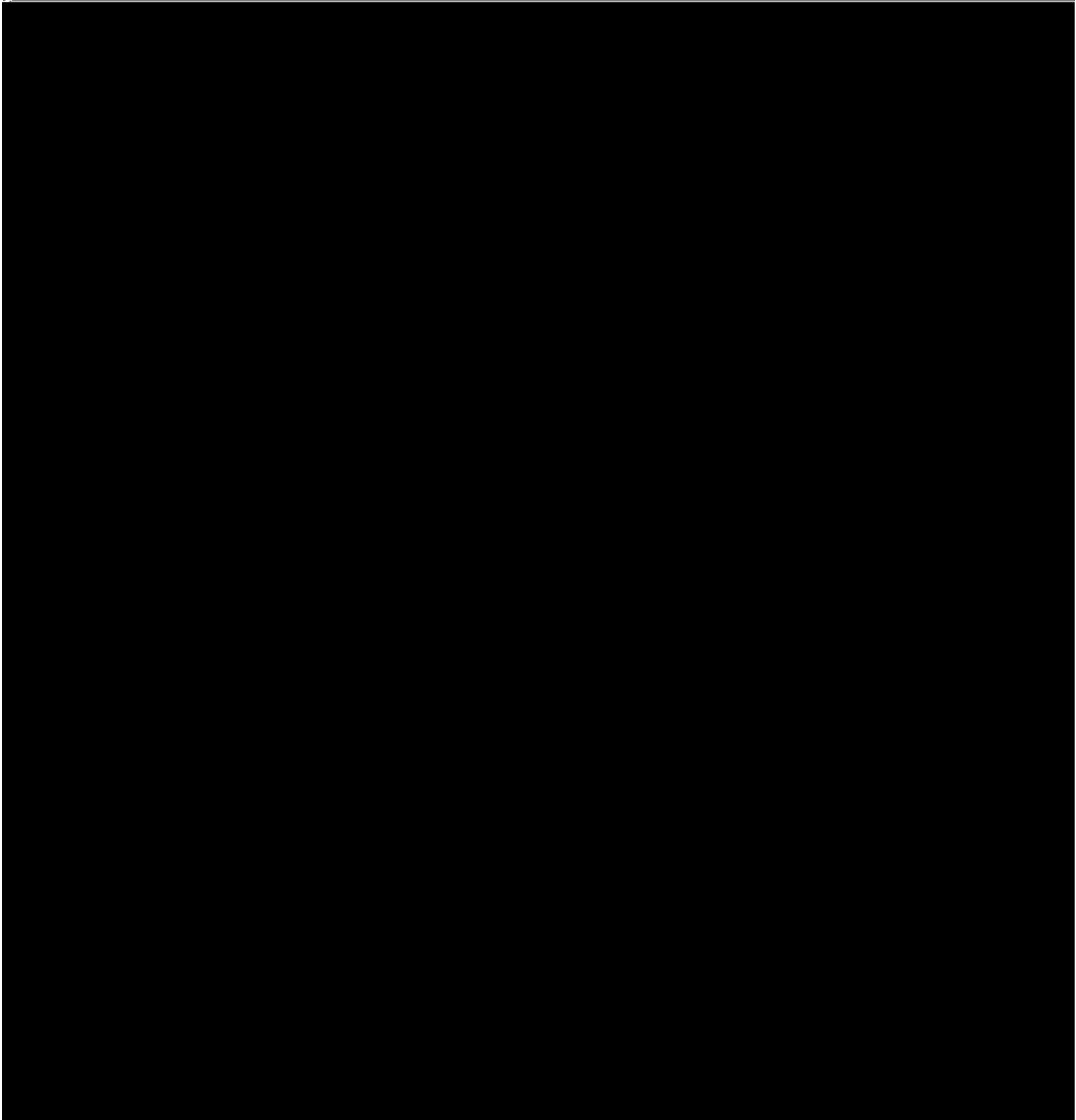


It is well known that deep convective downdrafts produce surface



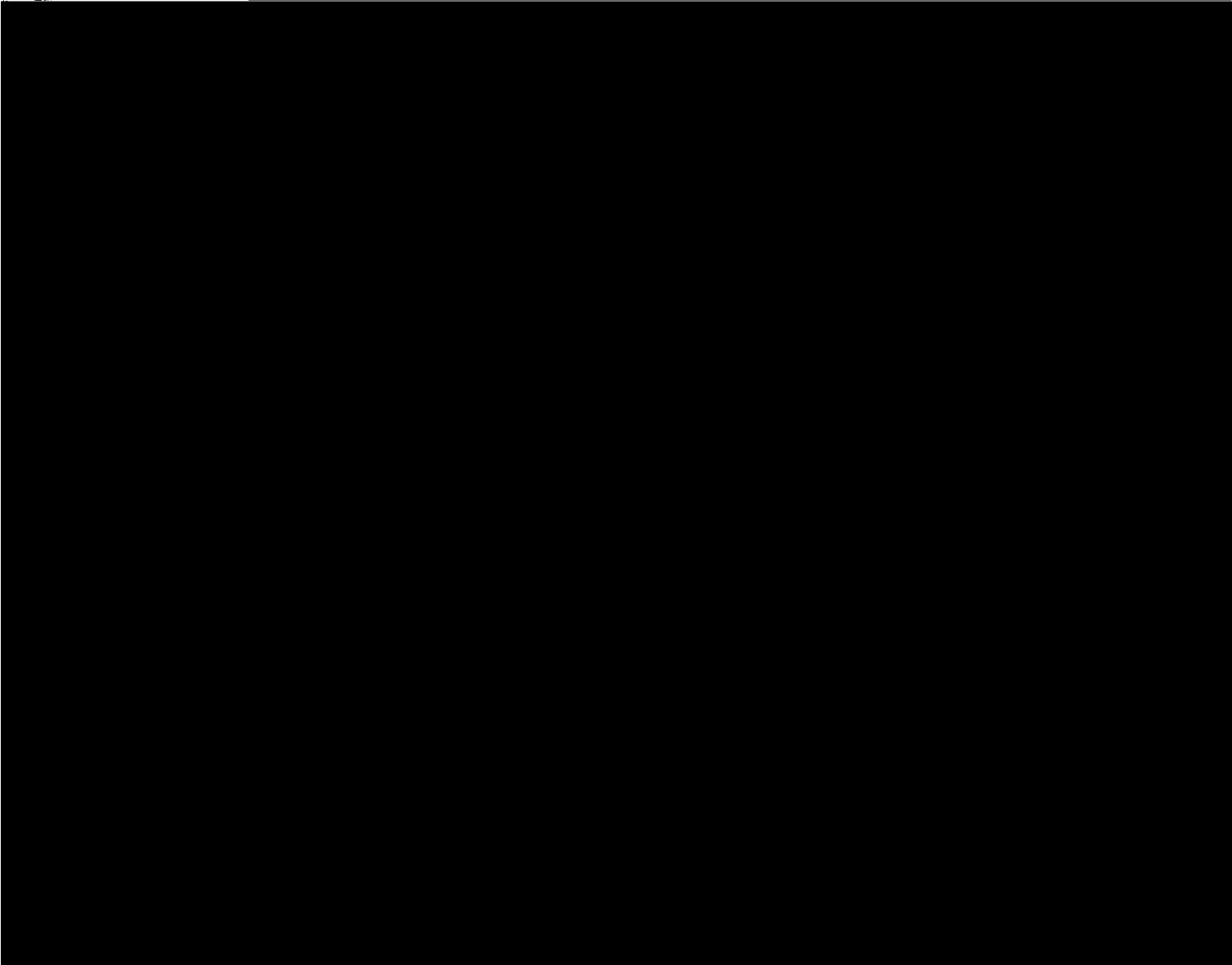
initiated by sea breeze convergence, remains located within  
the sea breeze convergence zone.



- (c) The decaying stage of the sea breeze-deep convective interaction is associated with both relatively significant mesoscale downward motion caused by the mid-tropospheric
- 

is associated with the establishment of coastal sea breeze convergence zones and embedded deep convection which vertically stretches the shallow solenoidal circulation (generated by the dry sea breeze) to much greater depths, thereby further enhancing the sea breeze convergence. Stage 2 (convective downdraft cooling stage) follows the onset of the relatively significant downdraft effects upon the peninsular-scale environment. The combination of the downdraft cooling effect and the sea breeze circulation, would

---



## REFERENCES

- Anthes, R. A., 1985: Cumulus Parameterization.<sup>1</sup>
- Anthes, R. A., and T. T. Warner, 1978: Development of hydrodynamic models suitable for air pollution and other mesometeorological studies. *MWR*, 106, 1045-1078.
- Anthes, R. A., 1977: A cumulus parameterization utilizing a one-dimensional cloud model. *Mon. Weather Rev.*, 105, 270-286.
- Arakawa, A., and W. H. Schubert, 1974: Interaction of a cumulus cloud ensemble with the large scale environment. Part I., *J. Atmos. Sci.* 31, 674-701.



Frank, W. M., 1983: A review of the cumulus parameterization problem. Mon. Wea. Rev., 111 (to appear).

Frank, W. M., and C. Cohen, 1983: A cumulus parameterization scheme incorporating subgrid-scale convective forcing. Submitted to the First Conference on Mesoscale Meteorology, May 31-June 3, 1983. Norman, Oklahoma.

Frank, W. M., and C. Cohen, 1983: A cumulus parameterization scheme incorporating subgrid-scale convective forcing. Submitted to the First Conference on Mesoscale Meteorology, May 31-June 3, 1983. Norman, Oklahoma.

- Hoxit, L. R., C. F. Chappell and J. M. Fritsch, 1976: Formation of mesolows or pressure troughs in advance of cumulonimbus clouds. Mon. Wea. Rev., 104, 1419-1428.
- Johnson, R. H., 1976: The role of convective-scale precipitation downdrafts in cumulus and synoptic-scale interactions. J. Atmos. Sci., 33, 1890-1910.
- Johnson, R. H., 1981: Large-scale effects of deep convection on the GATE tropical boundary layer. JAS, 38, 2399-2413.
- Johnson, R. H. and D. C. Kriete, 1982: Thermodynamic and circulation characteristics of winter monsoon typical mesoscale convection.

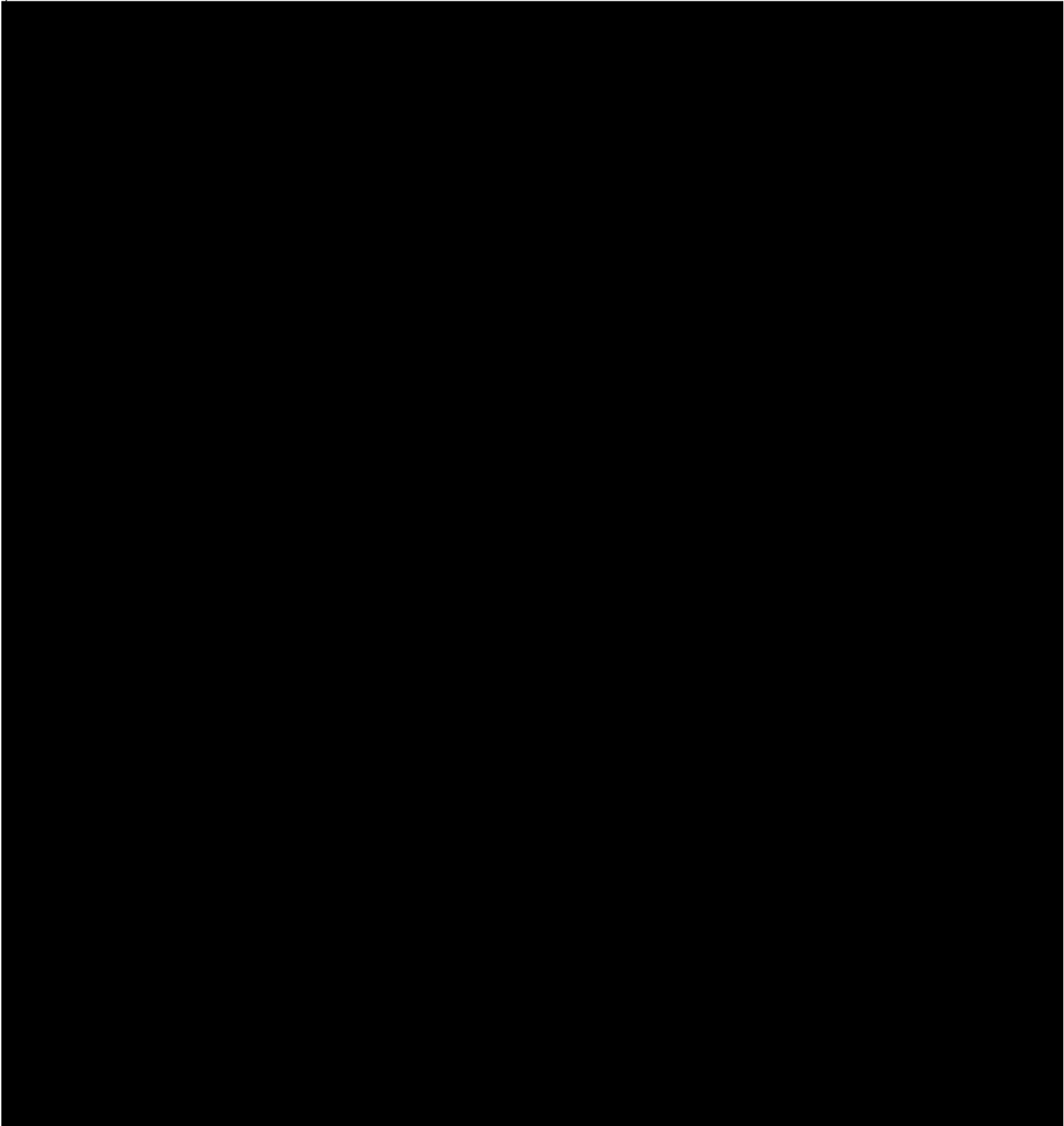
Lopez, P. E., D. O. Blanchard, R. Daniel, W. L. Hiscox, and M. J.



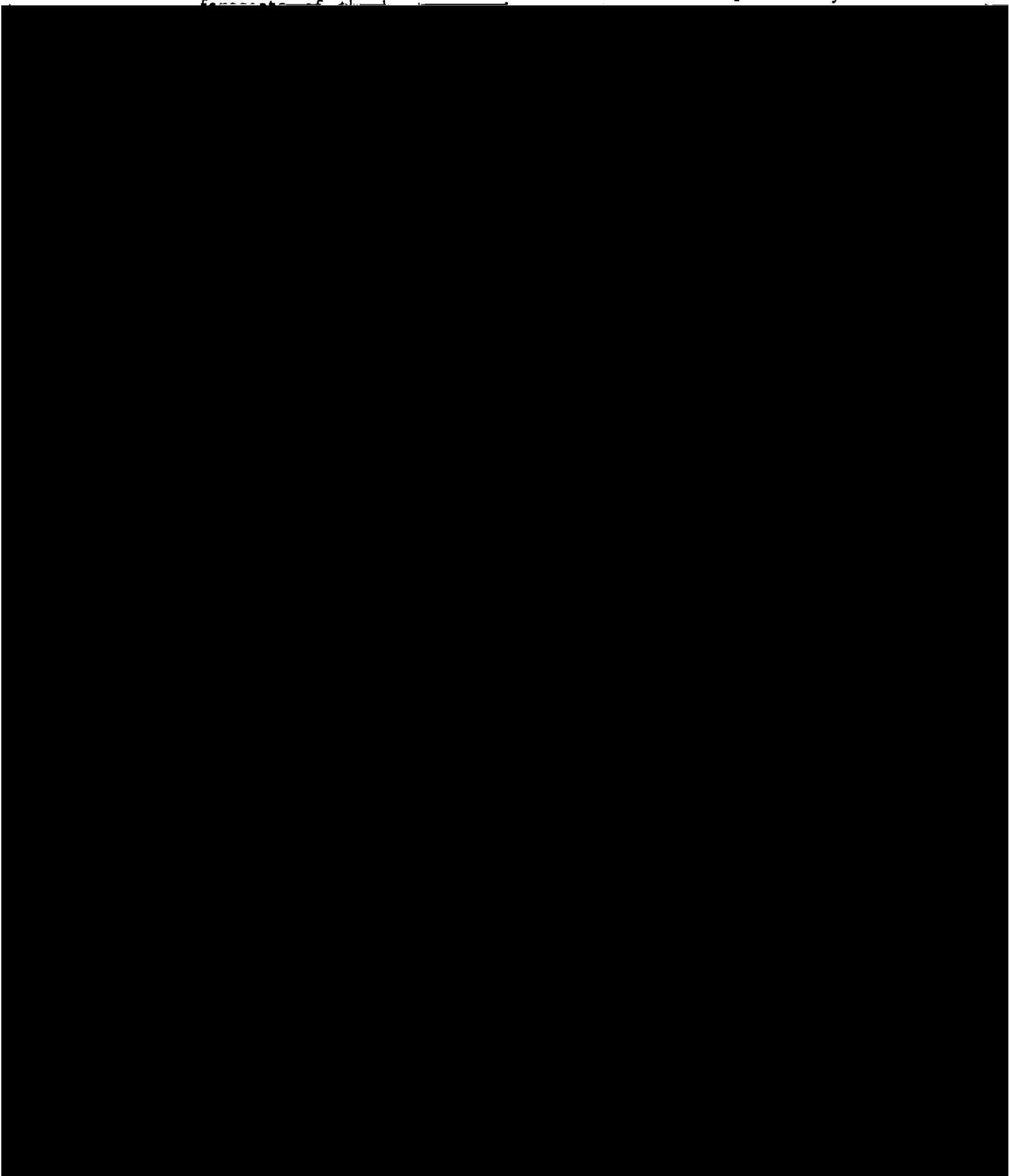
O'Brien, J. J., 1970: A note on the vertical structure of the eddy exchange coefficient in the planetary boundary layer. JAS, 27, 1213-1215.

Ogura, Y., and M. T. Liou, 1980: The structure of a mid-latitude squall line: A case study. J. of Atmos. Sci., Vol. 37, 553-567.

---

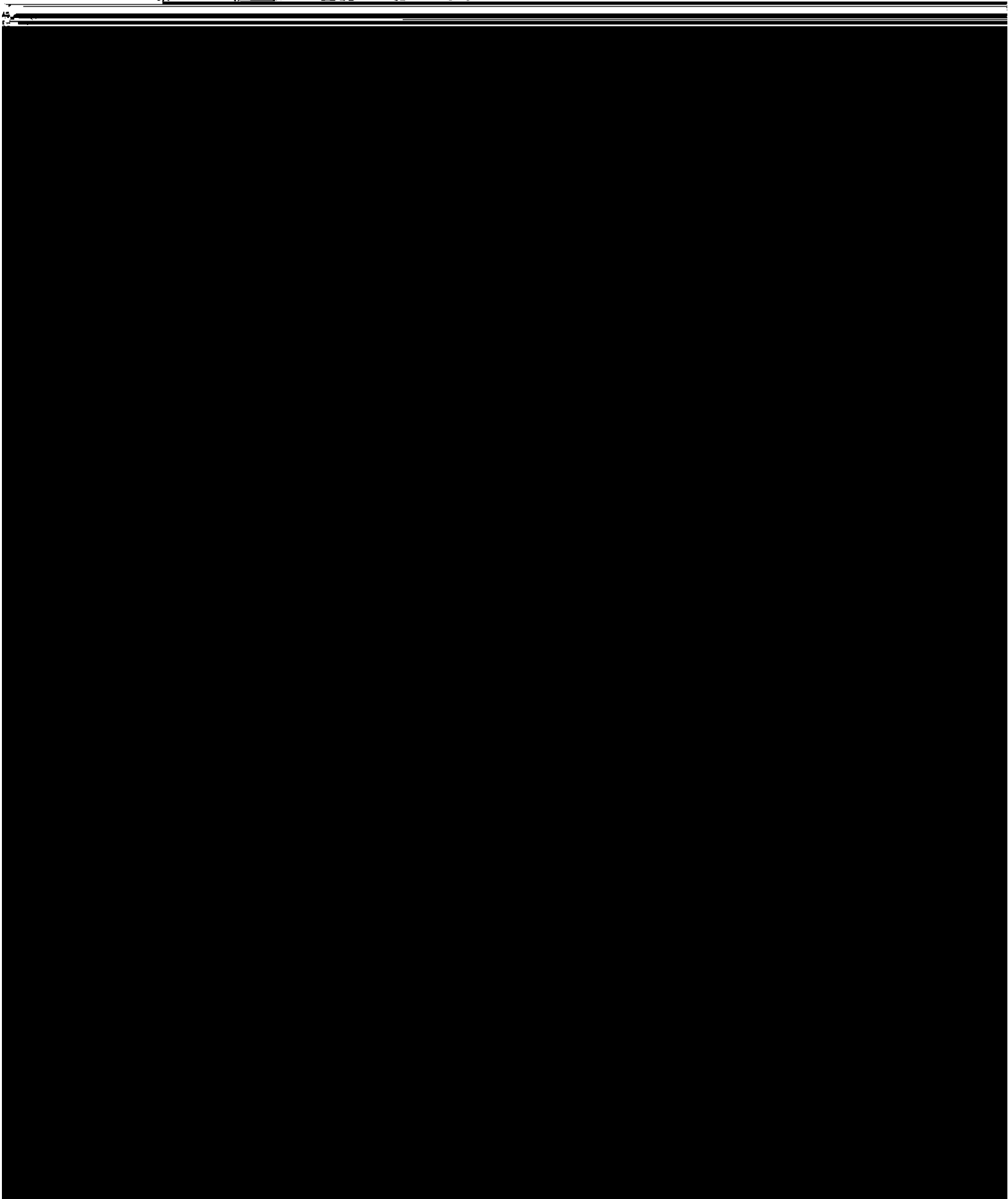


Reap, R. M., and D. S. Foster, 1979: Automated 12-36 hour probability



Song, J. L., R. A. Pielke, and M. Segal, 1985: Vectorizing a mesoscale





APPENDIX A

(A) BOUNDARY LAYER

The vertical exchange coefficients in the surface layer are given by

$$K_z^m(z^*) = k_o u_* z^* / \phi_m(\xi)$$

$$K_z^\theta(z^*) = K_z^q(z^*) = k_o u_* z^* / \phi_H(\xi)$$

where  $\xi = z^*/L_*$ , with  $L_* = \frac{\theta U_*^2}{k_o g \theta_*}$ .

The expression for the nondimensional wind and potential temperature profiles according to Businger (1973) are given below

$$\phi_m = \begin{cases} (1 - 15\xi)^{-1/4}, & \xi \leq 0. \\ 1 + 4.7\xi, & \xi > 0. \end{cases}$$

$$\phi_H = \begin{cases} .74(1 - 9\xi)^{-1/2}, & \xi \leq 0 \\ .74 + 4.7\xi, & \xi > 0 \end{cases}$$

where  $\phi_m = \frac{k_o z^*}{u_*} \frac{\partial u}{\partial z^*}$  and  $\phi_H = \frac{k_o z^*}{\theta_*} \frac{\partial \theta}{\partial z^*}$ .

The integrated version of the profiles are given by

$$u_* = k_o (u^2 + v^2)^{1/2} / (\ln(z/z_o) - \psi_1),$$

$$\theta_* = k_o (\theta - \theta(z_o)) / (.74(\ln(z/z_o) - \psi_2)).$$

$$q_* = k_o (q - g(z_o)) / (.74(\ln z/z_o) - \psi_2))$$

with  $\psi_1 = \begin{cases} 2 \ln[(1 + \phi_m^{-1})/2] + \ln[(1 + \phi_m^{-2})/2] - 2 \tan^{-1} \phi_m^{-1} + \pi/2 & \xi \leq 0 \\ -4.7\xi & \xi > 0 \end{cases}$

$$\text{and } \psi_2 = \begin{cases} 2 \ln[(1 + .74 \phi_H^{-1})/2] & \xi \leq 0 \\ -6.35 \xi & \xi > 0 \end{cases}$$

The functional form of the exchange coefficient above the surface layer

---

with the condition that

$$z_0 \geq 0.0015 \text{ cm.}$$

(B) SURFACE ENERGY BALANCE

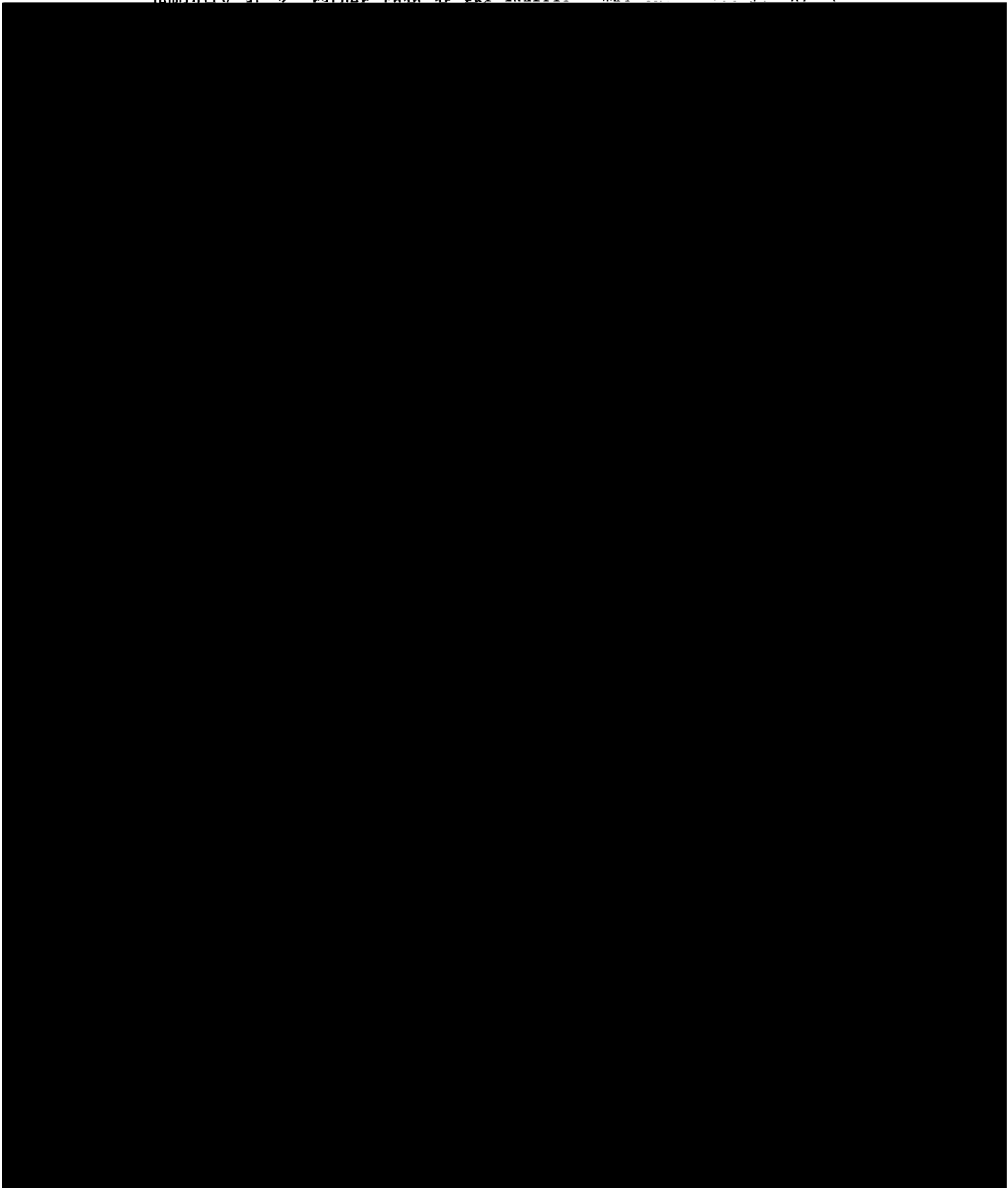
The land surface temperature is computed by a Newton-Raphson iteration solution to the heat balance equation

$$R_S + R_L + \rho L u_* q_* + \rho c_p u_* \theta_* - \rho_s c_s K_s \frac{\partial T}{\partial z}_G - \sigma T_G^4 = 0 \quad (2)$$

where

$R_S$  is the incoming solar radiation,

humidity at  $z$ , rather than at the surface. The equation for  $Q(z)$





length for water vapor ( $\Delta r_j$ ) is computed for each layer from the surface to the top of the model by

$$\Delta r_j = - \frac{(P_{j+1} - P_j)}{g} q_j .$$

The path length for  $\text{CO}_2$  ( $\Delta c_j$ ) is

$$\Delta c_j = - .4148239 (p_{j+1} - p_j) .$$

After these increments are obtained they are summed up from the first level to the  $i$ th level to give the total path length, given as

$$r_i = \sum_{j=1}^i \Delta r_j, \quad c_i = \sum_{j=1}^i \Delta c_j .$$

The emissivity for water vapor was derived from data of Kuhn (1963) and are given in Jacobs, et al. (1974).

Using the above emissivity functions we have for the downward and upward fluxes at a level N

$$R_d(N) = \sum_{j=N}^{\text{top}-1} \frac{\sigma}{2} (T_{j+1}^4 + T_j^4) [\varepsilon(N, j+1) - \varepsilon(N, j)] \\ + \sigma T_{\text{top}}^4 (1 - \varepsilon(n, \text{top}))$$

and

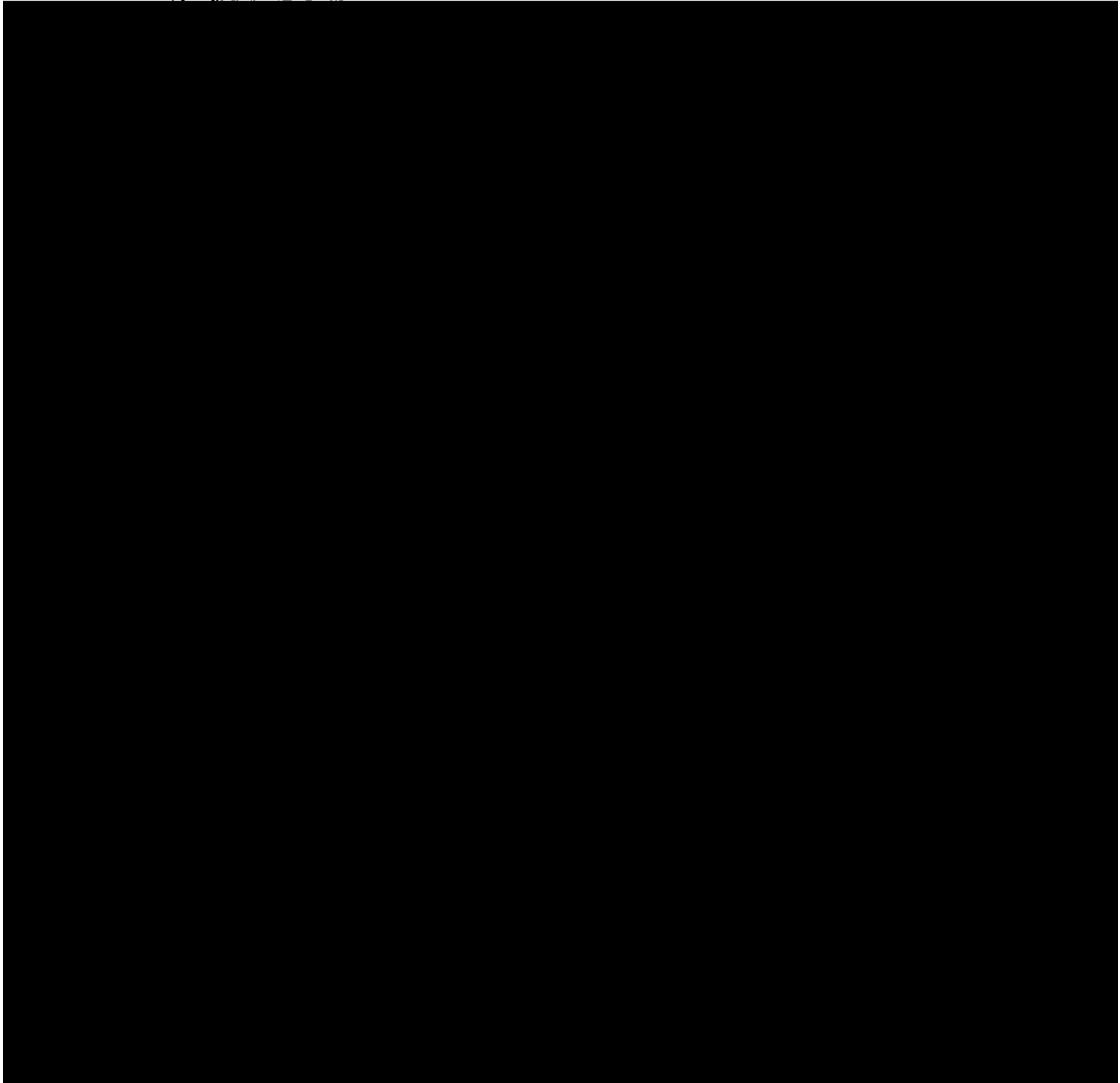
$$R_u(N) = \sum_{i=N}^{\text{top}-1} \frac{\sigma}{2} (T_{i+1}^4 + T_i^4) [\varepsilon(N, i) - \varepsilon(N, i+1)]$$

$$w_i^* \frac{\partial u}{\partial z^*} = w_i^* \frac{u_* |x| \phi_m}{k_o z^*}, \quad w_i^* \frac{\partial v}{\partial z^*} = w_i^* \frac{u_* |y| \phi_m}{k_o z^*}$$

$$w_i^* \frac{\partial \theta}{\partial z^*} = w_i^* \frac{\theta_* \phi_H}{k_o z^*}, \quad w_i^* \frac{\partial q}{\partial z^*} = w_i^* \frac{q_* \phi_H}{k_o z^*} .$$

This technique will result in a better estimate of the vertical advection terms near the ground since the standard finite difference

assumes that a linear relationship exists between the



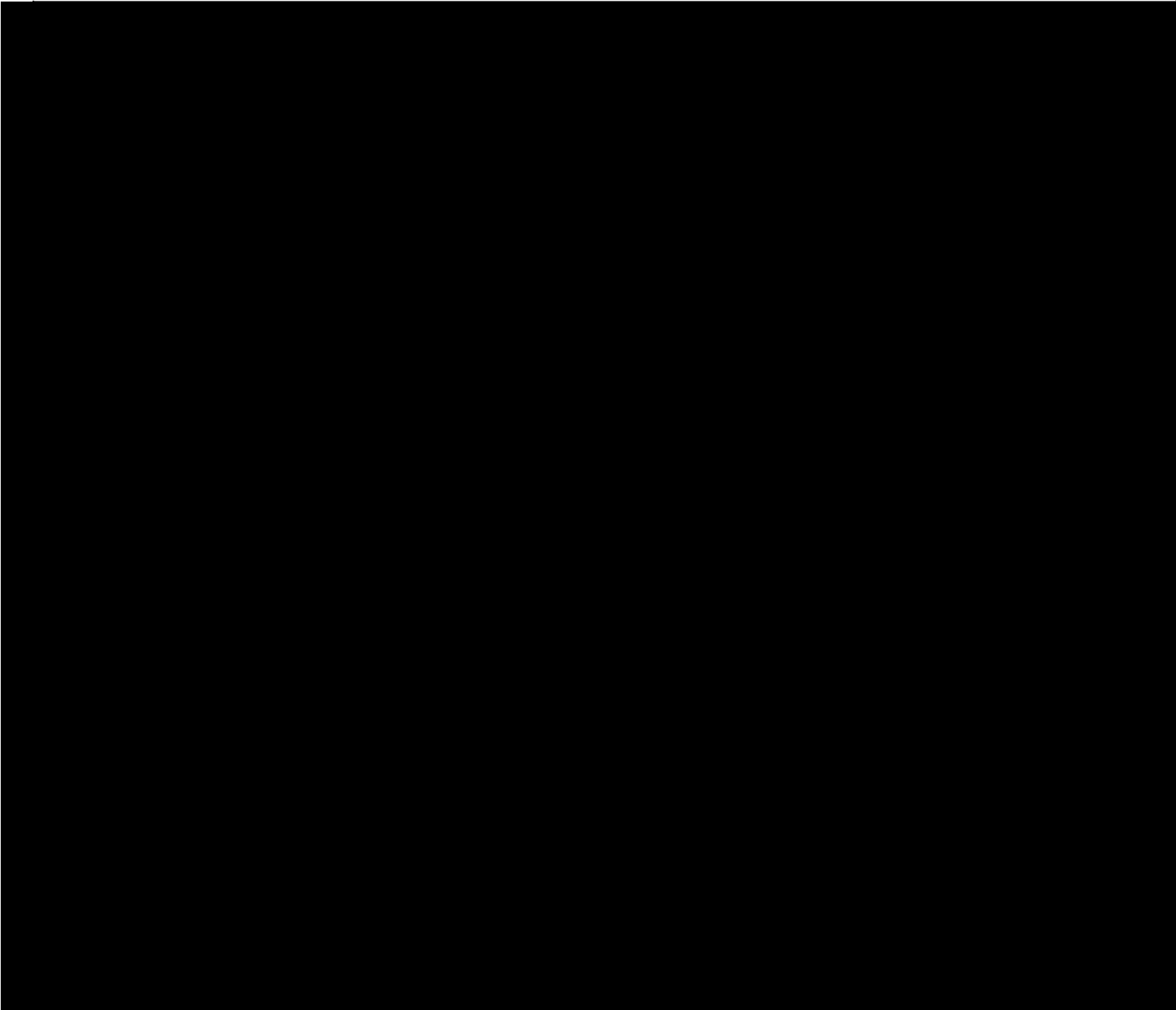
APPENDIX B

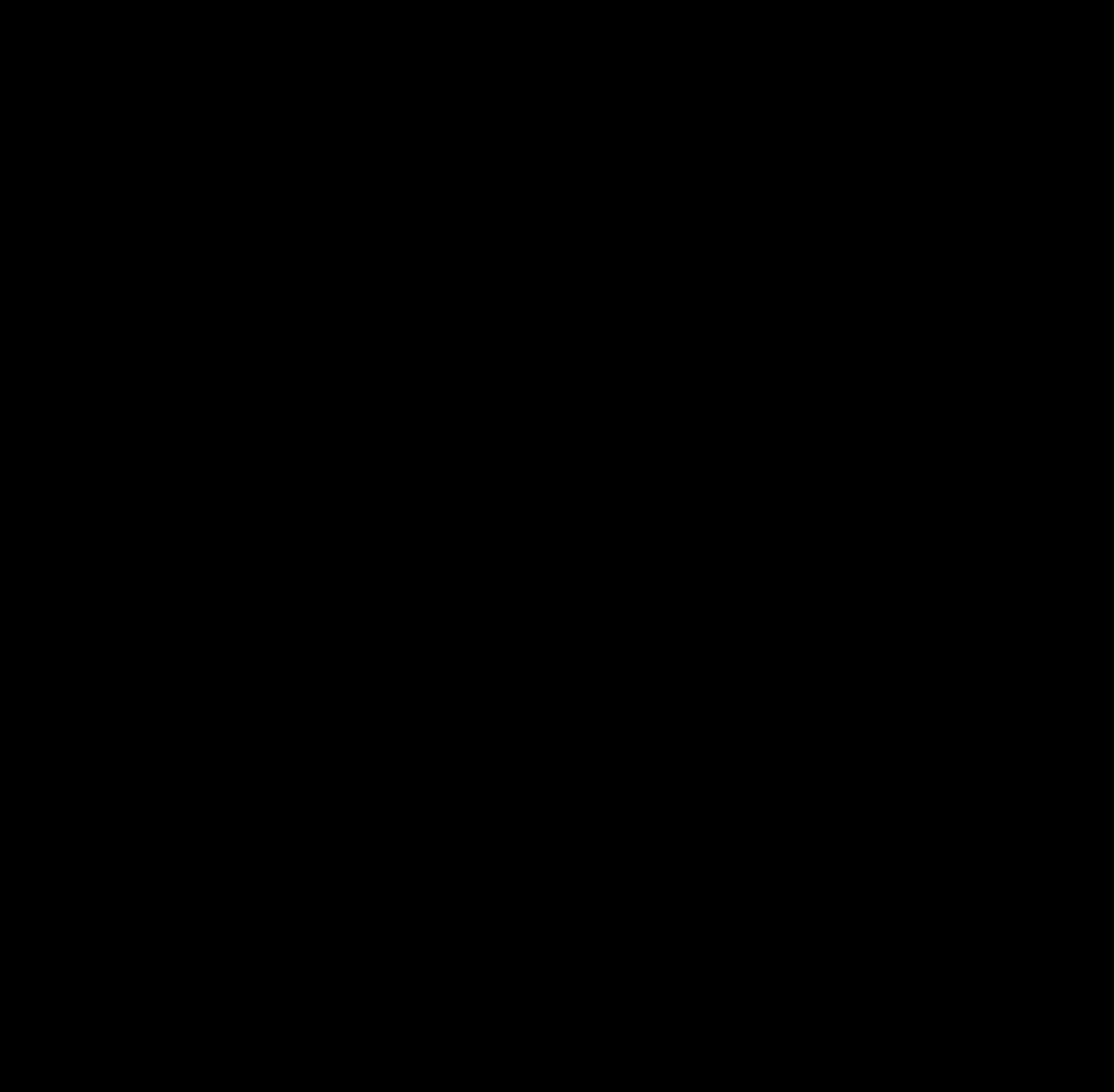
PROCEDURES OF THE CONVECTIVE PARAMETERIZATION

The step-by-step computational procedures of evaluating the convective updraft, downdraft, and grid-environmental effects are

---

---



- (3) Check if deep convection occur (as shown in the Steps (1)-(3) in Fig. 3-2). The parameterization proceeds only when the conditions are satisfied.
  - (4) Determine updraft massflux profile. The maximum updraft massflux is located at the height of the maximum temperature-excess term (for an undilute ascent of the convective plume).
- 
- 

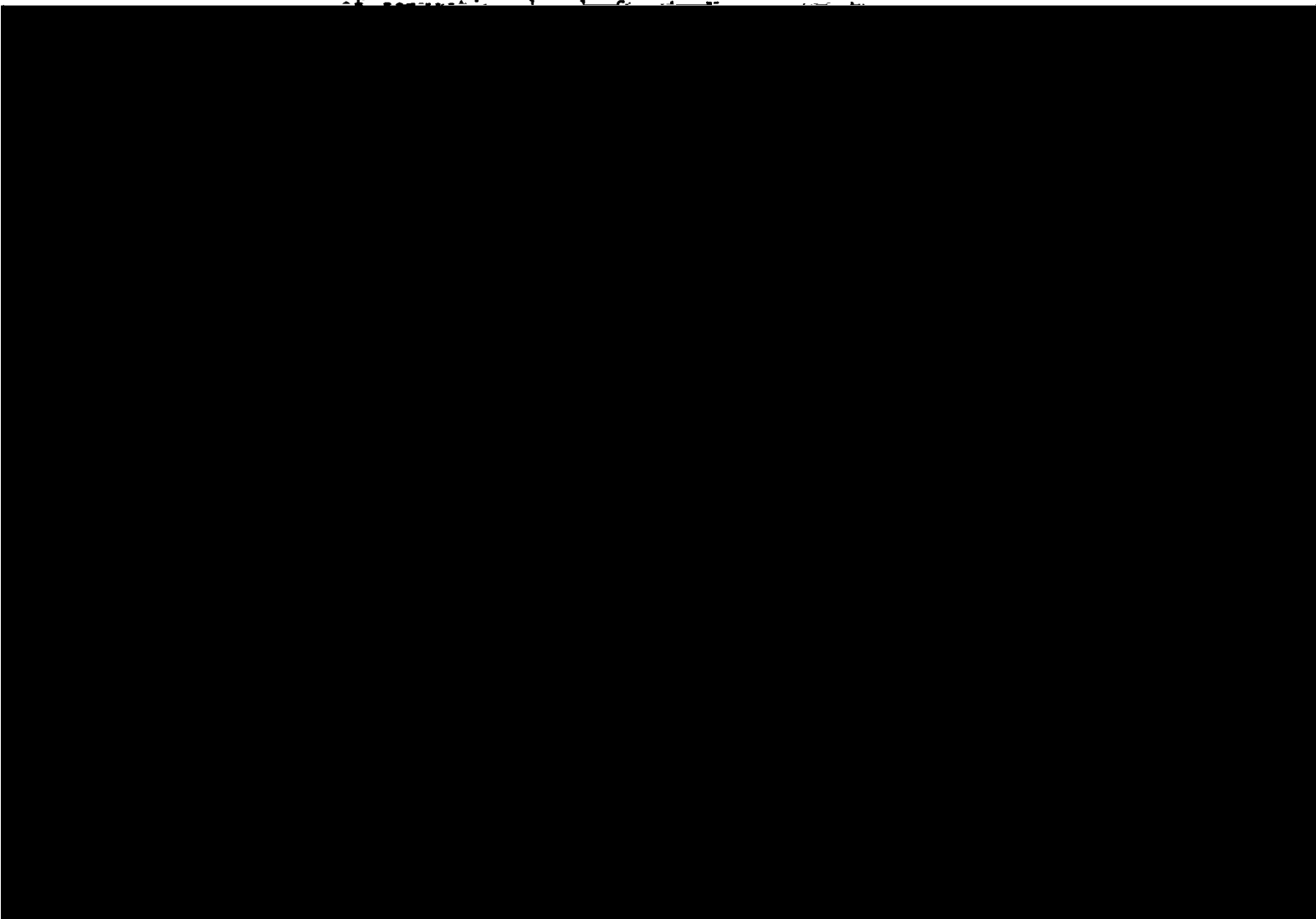
for the Florida summertime deep convection investigated in this study.

- (9) The freezing process of the updraft includes two parts. A specified fraction (FRACI) of the total accumulated liquid condensate produced below the  $-5^{\circ}\text{C}$  level is assumed to freeze, up to the  $-20^{\circ}\text{C}$  level (uniformly in the vertical). The "in situ" produced condensate above the  $-5^{\circ}\text{C}$  level is assumed to contain ice by percentages from 0 percent (at the  $-5^{\circ}\text{C}$  level) to 100 percent (at the  $-20^{\circ}\text{C}$  level).

#### B-2. Downdraft Calculation

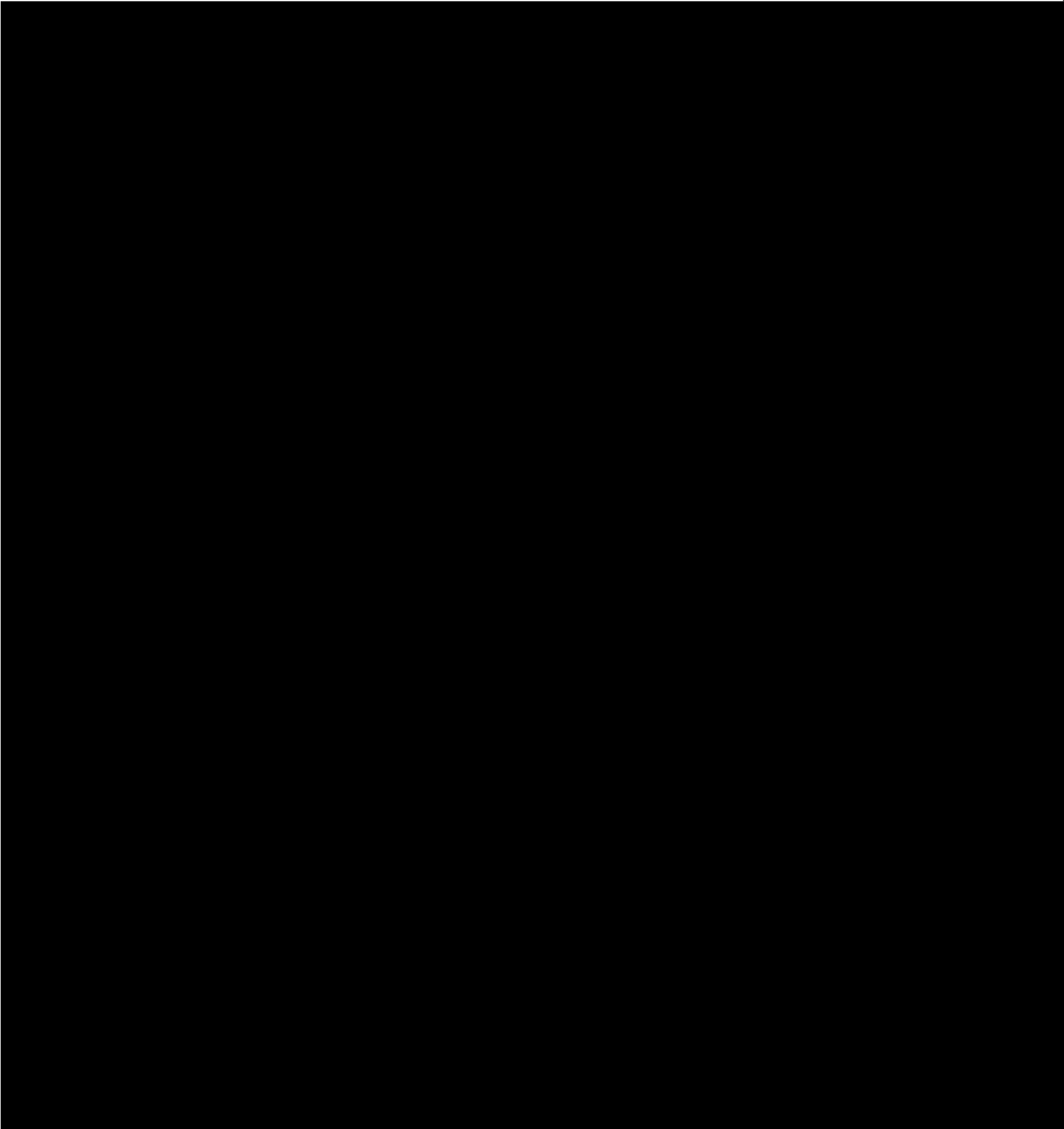
- (1) Downdraft is initiated at the level of minimum environmental equilibrium potential temperature (see a detailed discussion

of potential temperature in the appendix to the report.

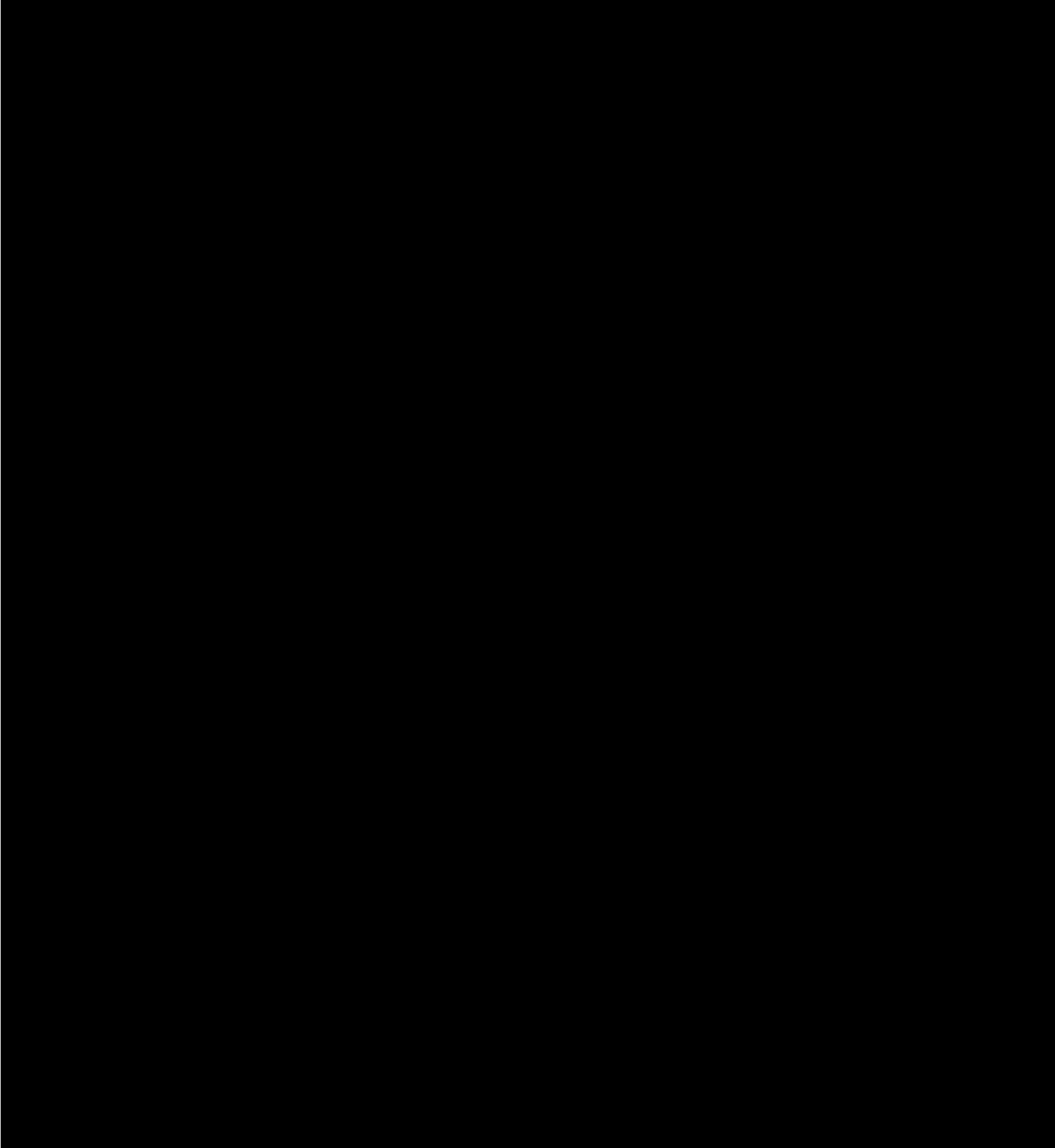


not thicker than 2 km is assumed to be immediately beneath the 0°C level. A small portion of the total ice (about 10 percent, as in Fritsch and Chappell, 1990) is assumed to

---



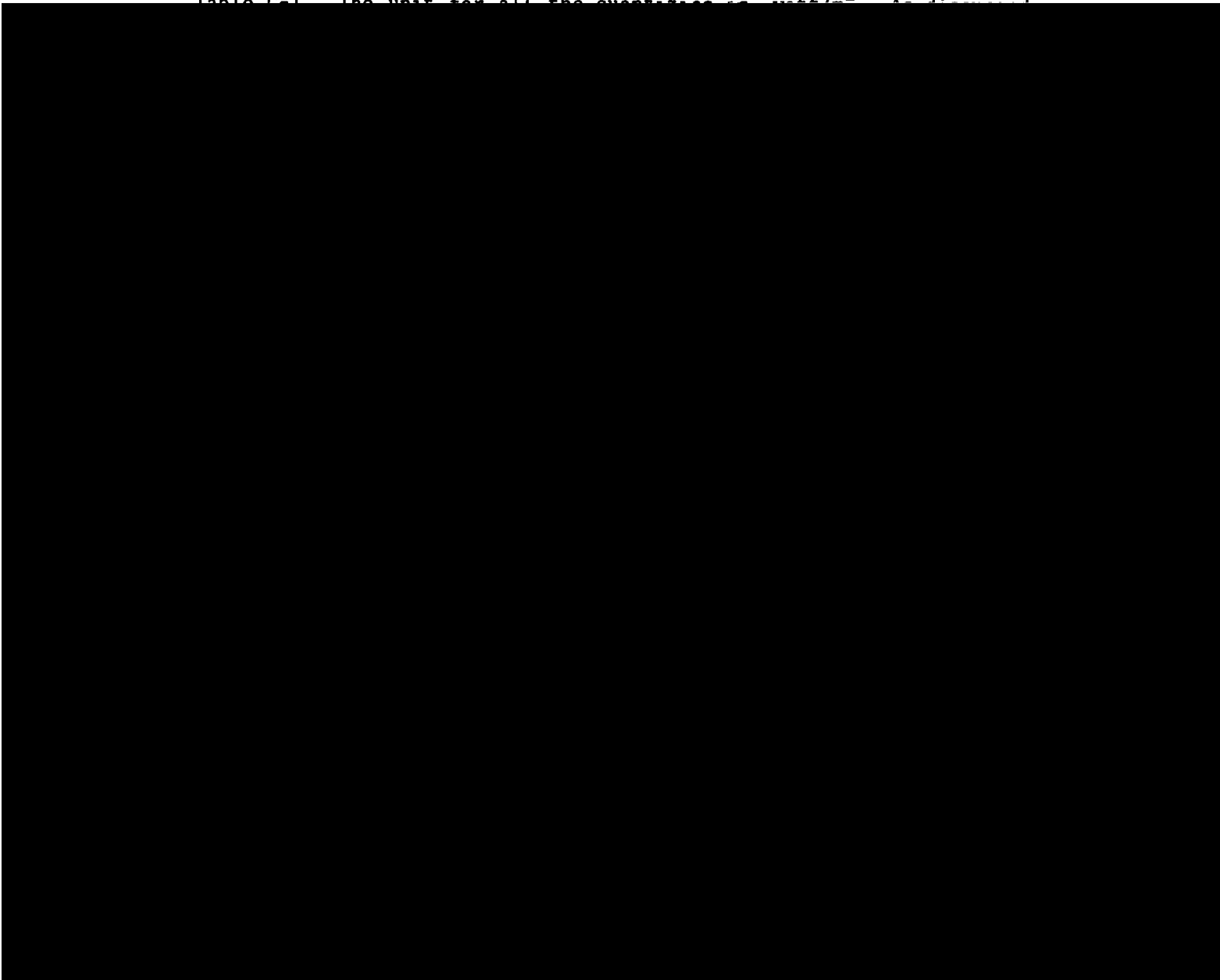
- (5) Near the surface, the downdraft replaces the unmodified air, thereby stabilizing the surface layer. The fractional area in which surface air is replaced is



## APPENDIX C

### DOMAIN-INTEGRATED KINETIC ENERGY BUDGET COMPONENTS OF THE MOIST SEA BREEZE SIMULATION

The domain-integrated kinetic energy budget components (introduced in Chapter 2) for the moist sea breeze simulation (i.e., the control run, as introduced in Chapter 4) are calculated and listed in Table C-1. The unit for all the quantities is  $\text{m}^2/\text{s}^2$ .



Horizontal Flux ID	Filter Term
572E-02	-.8192E-04
061E-01	-.3090E-03
026E-01	-.7458E-03
006E-01	-.2542E-02
34E-01	-.1035E-01
79E-01	-.2574E-01
69E-01	-.5678E-01
12E-01	-.1037E+00
56E-01	-.1357E+00
50E+00	-.1669E+00
99E-01	-.1938E+00
32E+00	-.2340E+00